GUIDE TO PROCESS BASED MODELING OF LAKES AND COASTAL SEAS

Anders Omstedt

Second Edition

$$\frac{\partial \phi}{\partial t} + W\frac{\partial \phi}{\partial z} = \frac{\partial}{\partial z}\left(\frac{\mu_{eff}}{\rho\sigma_{\phi eff}}\frac{\partial \phi}{\partial z}\right) + S_{\phi}$$

EXTRA MATERIALS
extras.springer.com

Springer

PRAXIS

Guide to Process Based Modeling of Lakes and Coastal Seas

Anders Omstedt

Guide to Process Based Modeling of Lakes and Coastal Seas

Second Edition

Springer

Published in association with
Praxis Publishing
Chichester, UK

PRAXIS

Professor Anders Omstedt
Department of Marine Sciences,
Oceanography
University of Gothenburg
Göteborg
Sweden

SPRINGER–PRAXIS BOOKS IN GEOPHYSICAL SCIENCES
SUBJECT *ADVISORY EDITOR*: Philippe Blondel, C.Geol., F.G.S., Ph.D., M.Sc., F.I.O.A., Senior Scientist, Department of Physics, University of Bath, Bath, UK

Additional material to this book can be downloaded from http://extras.springer.com

ISBN 978-3-319-17989-6 ISBN 978-3-319-17990-2 (eBook)
DOI 10.1007/978-3-319-17990-2

Library of Congress Control Number: 2015941138

Springer Cham Heidelberg New York Dordrecht London

Cover design: Jim Wilkie
Project management: OPS Ltd, Gt Yarmouth, Norfolk, UK

Printed on acid-free paper

Springer International Publishing AG Switzerland is part of Springer Science+Business Media (www.springer.com)

Foreword by Urban Svensson

(***Computer-aided Fluid Engineering AB***)

The Ekman spiral, the benthic boundary layer, and the wind-induced near-surface flow in a lake are all examples of environmental boundary layers. The atmospheric boundary layer is another member of this class of flows. As heat and matter are transported across these boundary layers, it is clear that all contributions to the understanding of the nature of these flows are of great value.

The computer code Program for Boundary Layers in the Environment (PROBE) is intended to be a tool for use in the study of these classes of flows. The history of PROBE goes back to 1975 when I was a student at Imperial College, London. Professor Brian Spalding supervised me in a number of small projects dealing with environmental flow and heat transfer. One of these considered the seasonal thermocline in lakes—a project that was later (1978) presented as my Ph.D. In 1982, I took up a position at the Swedish Meteorological and Hydrological Institute (SMHI). Together with my colleagues at SMHI, PROBE was further developed and also used in real-world problems. Among the major developments during the early 1980s, I would like to single out frazil ice dynamics (work done by Anders Omstedt), heat transfer in lakes including sediments (work done by Jörgen Sahlberg), and transport across the benthic boundary layer (work done by Lars-Arne Rahm). In 1986, I left SMHI, and soon thereafter, my involvement in PROBE ended. During the last 20 years, Anders Omstedt and Jörgen Sahlberg have successfully continued the development of PROBE and have linked biogeochemical variables to the code.

This book gives a detailed account of PROBE. Emphasis is placed on the basic equations (both physical and biogeochemical) and the methods for their solution. As the computer code and exercises are also included, the reader should be able to get a full understanding of (and be able to repeat) most of the simulations presented in the book.

Finally, I should like to say that it gives me great pleasure to see that the work I once initiated is now the subject of a book.

Foreword by Jörgen Sahlberg

(*Swedish Meteorological and Hydrological Institute*)

A large step was taken by Anders Omstedt in 1990 when he used PROBE to model the whole Baltic Sea as 13 sub-basins—including the Kattegat, the Belt Sea, and Öresund—and as a result achieved high vertical resolution in each basin. This was the first attempt to use PROBE on more than one coupled sub-basin. This model, called PROBE-Baltic, has been further developed during the last 20 years and has been used in many different applications: For example, it is capable of simulating the effect of climate change on salinity, temperature, and ice conditions in the Baltic. During the last 5–10 years, PROBE has also been used for solving biogeochemical equations in both the PROBE-Baltic model and the closely related Coastal Zone model. Anders has used the PROBE-Baltic model to investigate the uptake and release of carbon dioxide in the Baltic and bottom oxygen conditions as a result of different physical forcing.

My own contribution during the last ten years has been the development of the Coastal Zone model—an extension of the PROBE-Baltic model. It was developed mainly to describe the nitrogen, phosphorus, oxygen, and phytoplankton conditions in coastal waters around Sweden. Today, it covers the whole of the Swedish coast and is applied to more than 600 coupled sub-basins. The model has also been applied to Lake Mälaren (situated close to Stockholm).

SMHI has recently developed a database called "Vattenweb" where all the Coastal Zone model results may be found and extracted over the Internet. During the last 30 years, the PROBE model has been used in many different applications and in more than 100 scientific articles. In the future, we will probably see and use the PROBE model in cloud computing.

Finally, I would like to thank Urban Svensson and Anders Omstedt for all the valuable PROBE discussions we have had over the years. Anders deserves special thanks for his initiative in writing this book.

Preface to the Second Edition

The second edition was prepared some years after the first one. Interesting progress in modeling coastal seas was made during this period, and concern has increased as to the importance of considering multiple stressors acting on the seas. Coastal seas are under severe human-induced pressures, such as global climate change, excess nutrient release, pollution, ammunition dumping, overfishing, and various engineering-based modifications, including the strong growth of coastal settlement, hydro- and nuclear power plants, massive wind farms, and various bridge and tunnel crossings. At the same time, coastal areas are used for many purposes, such as intensive agriculture, shipping, and recreation.

Ocean acidification has emerged as a key research priority for marine science, and only recently, this has been addressed in coastal seas. The combination of acidification and increasing amounts of anoxic waters associated with eutrophication puts severe stress on the marine environment. The detection and attribution of anthropogenic changes in coastal seas are therefore crucial, and modeling tools are increasingly important.

In the second edition, the presentation of biogeochemical aspects has been rewritten and Sect. 4.8, "Modeling the Dynamics of CO_2 in Redox Environments," has been added. Modeling the marine CO_2–O_2 system makes climate change and eutrophication studies possible and is fundamental to understanding the Earth system. The second edition also includes new sections on detection and attribution and on modeling future changes, as well as improved exercises, updated software, and datasets.

March 2015 Anders Omstedt

Preface to First Edition

Guide to Process Based Modeling of Lakes and Coastal Seas is based on a series of lectures delivered to students at advanced and Ph.D. levels at the Department of Earth Sciences, University of Gothenburg. It is intended to provide the reader with a scientific understanding and well-tested computer code for successful aquatic studies. The intended reader should have some knowledge of geophysical fluid dynamics, numerical analysis, and computer programming. The structure of the *Guide* allows readers to develop their understanding gradually. Incorporating a range of exercises with solutions, the *Guide* is a comprehensive teaching aid. Learning via a combination of reading, analyzing observations, and building computer models is a very rewarding process. This approach also makes it possible for the learner to follow scientific developments, test new ideas, and evaluate research results.

The most characteristic feature of valid science is reproducibility. If scientists from different research groups cannot reproduce new results, they must conclude that they are invalid. This is the great strength of science, as it generates a system for self-correction. Earlier efforts and even some current research efforts have had problems in this area. Data and models are often gathered and developed at single institutions by scientists who are largely concerned with completing their research programs. The development of adding supplementary material to published articles represents a step forward. Quality-controlled shared databases are urgently needed, as are peer-reviewed data evaluations. Models introduce an even greater problem, as they are often undergoing development and are unavailable to the broader scientific community. The need to make model codes, model forcing data, and output data available to other groups is therefore fundamental. This *Guide* seeks to make aquatic modeling transparent and to share with the reader the joy of discovery inherent in scientific work.

January 2011 Anders Omstedt

Cover photograph: Observations and mathematical modeling are the two major tools for learning about aquatic systems. The photograph was taken during turbulence measurements under calm conditions in the Gullmar Fjord on the Swedish west coast (photograph courtesy of Christian Stranne).

Acknowledgments

This book started as a collection of lecture notes for students from the Department of Earth Sciences, Oceanography, University of Gothenburg, and from SMHI. Many people have contributed to the development of this material, including Leif Anderson, Lars Axell, Göran Björk, Ulf Cederlöf, Deliang Chen, Moa Edman (particularly in biogeochemical modeling), Christin Eriksson, Mattias Green, Bo Gustafsson, Erik Gustafsson, Daniel Hansson, Matti Leppäranta (who made many useful comments on this book), Helma Lindow, Christian Nohr, Leif Nyberg, Johan Rodhe, Anna Rutgersson-Owenius, Bernd Schneider, Hans von Storch, Christian Stranne, Artur Svansson, Karin Wesslander, and Anna Wåhlin. Special thanks are extended to the BALTEX Secretariat for their strong support of Baltic Sea research, to Jim Overland for many years of friendly discussions, to Urban Svensson for creating a really useful program, to Anders Stigebrandt for his bold approach to science, to Jörgen Sahlberg for his firm support, to Gösta Walin for his pure scientific spirit, and to Hans von Storch for inspiration regarding detection and attribution studies. Thanks are also due to Krister Boquist, Barry Broman, Phil Graham, Brian MacKenzie, Anders Moberg, and Jörgen Nilsson for making the data available. Agneta Malm is acknowledged for help with several figures and Stephen Sanborn at Proper English for editing the text.

Capable computer support from Martin Johnsson and Mats Olsson has made the work easier. The positive spirit at the Department of Earth Sciences and in the BALTEX research community has made my time working on modeling very productive and fun.

This work was partly financed by the University of Gothenburg, the Swedish Research Council, and the BONUS/Baltic-C program. Finally, the author wants to thank the PRAXIS team for their strong support in getting this book published.

Contents

Figures

Tables

Abbreviations and Acronyms

BALTEX	BALTic Sea EXperiment
BONUS	Baltic Organizations Network for fUnding Science
CFD	Computer Fluid Dynamics
FORTRAN	FORmula TRANslation
GOTM	General Ocean Turbulence Model
HIRLAM	HIgh-Resolution Limited Area Atmospheric Model
HYMEX	HYdrological cycle in the Mediterranean EXperiment
MIB	Maximum annual Ice extent in the Baltic Sea
NAO	North Atlantic Oscillation
NASA	National Aeronautics and Space Administration
PROBE	PROgram for Boundary Layers in the Environment
SeaWiFS	Sea-viewing Wide Field-of-View Sensor
T–S	Temperature–Salinity

Chapter 1
Introduction

The use of computational fluid dynamics to analyze and predict environmental changes has increased considerably in recent decades. Numerical models are now standard tools in research and in a wide range of practical applications. Intensifying concern about human influence on climatic and environmental conditions has increased the need for multidisciplinary modeling efforts, including the numerical modeling of oceans, lakes, land surfaces, ice, rivers, and the atmosphere. Scientists have traditionally developed specialized models limited to application within their own disciplines. Today, increasing efforts are being made to develop general equation solvers that allow users to create code applicable to a broad range of problems.

This book guides its reader through process-based modeling, using the PROBE general equation solver and building understanding step by step. The equation solver has been used in many applications, particularly in Sweden and Finland with their numerous lakes, archipelago seas, fjords, and coastal zones. It has also been used for process studies in the Arctic and in the Mediterranean Sea. The process-based approach, developed here, divides the studied water body into dynamically relevant parts or natural sub-basins and identifies major processes involved in the problem. Based on field observations and simplifications, the dynamics are expressed mathematically and tested carefully against relevant analytical solutions, extremes, and observations.

Lakes and coastal seas represent important human resources and are often under great human pressure. They have various geometries, ranging in size from small ponds to large sea areas, and are strongly influenced by their surrounding land areas. Water bodies are generally considered lakes when they are located inland and are not part of the ocean, which is why the Caspian Sea is regarded as the world's largest lake. At approximately 25 million years old, Lake Bajkal is probably the world's oldest lake; with depths of about 1700 m, it is certainly the deepest. Most lakes are much smaller and most lie in the Northern Hemisphere. Canada, the USA, the Nordic countries, and Russia, for example, have many lakes, which often become ice covered in winter.

Coastal seas are the water bodies that connect the land with the ocean, and their various types include open broad and flat continental shelf seas, semi-enclosed seas, fjords, estuaries, archipelago seas, and delta coasts. In the case of both lakes and

A. Omstedt, *Guide to Process Based Modeling of Lakes and Coastal Seas*,
Springer Praxis Books, DOI 10.1007/978-3-319-17990-2_1

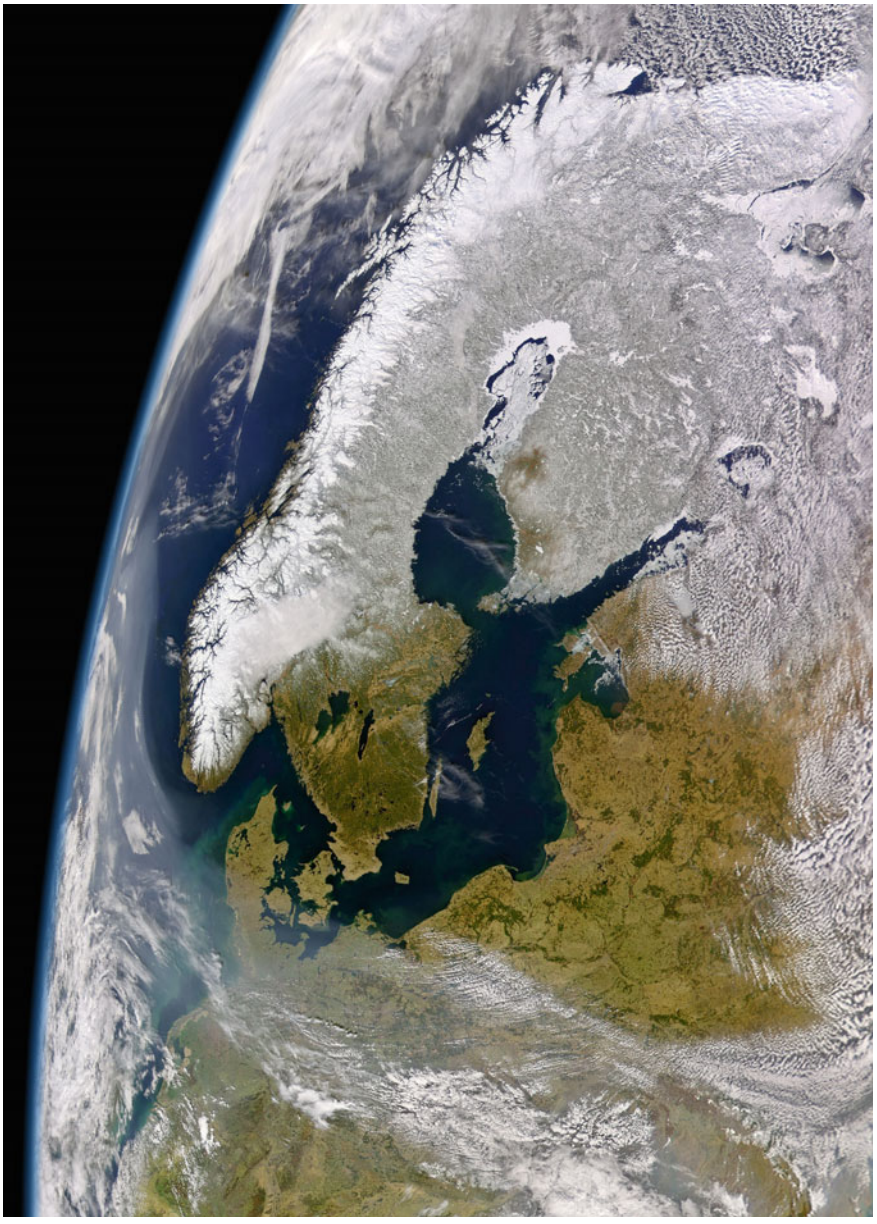

Fig. 1.1 Northern Europe on 1 April 2004, as seen from the SeaWiFS satellite (NASA/Goddard Space Flight Centre, http://visibleearth.nasa.gov/)

coastal seas, the geometries of the water bodies can be complex, involving geometric constrictions such as sounds, sills, islands, and coral reefs, and sub-basins such as bays and gulfs (Fig. 1.1). Bathymetric features, the surrounding hydrology,

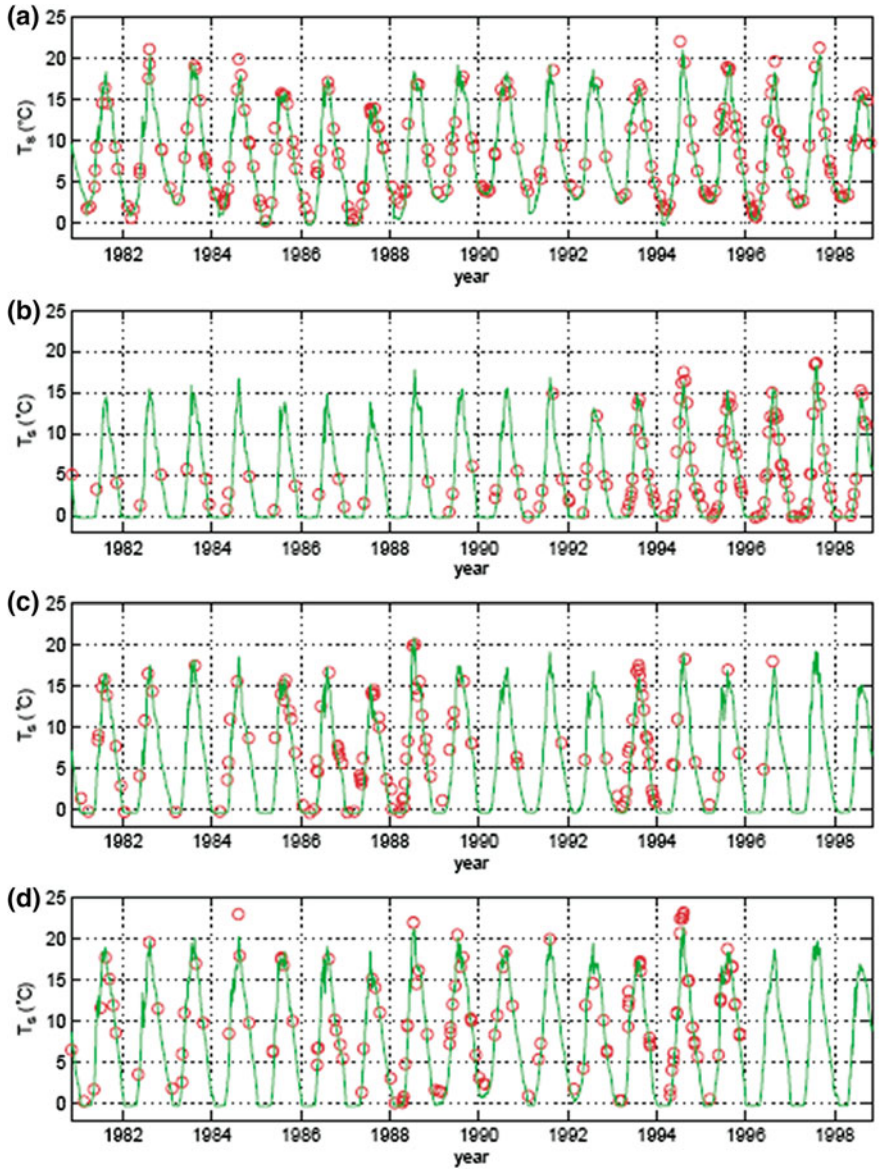

Fig. 1.2 Modeled (*fully plotted lines*) and observed (*circles*) sea surface temperatures in **a** Eastern Gotland Basin, **b** Bothnian Bay, **c** Gulf of Finland, and **d** Gulf of Riga (Omstedt and Axell 2003)

and climate strongly influence the dynamic and thermohaline processes in these aquatic systems. The Baltic Sea, for example, is a non-tidal coastal sea affected by climate change, eutrophication, and nutrient recycling. Both the White and North Seas are strongly influenced by tides and by small and large human populations,

respectively. The Caspian Sea and the North American Great Lakes are examples of closed inland seas. The Mediterranean Sea, the Black Sea, Hudson's Bay, and the Baltic Sea, on the other hand, are seas having limited exchange with surrounding coastal zones due to narrow straits and sills.

We often lack complete data series of temperature and other properties for various water bodies. Figure 1.2 shows how the results of a coastal sea model can reproduce the surface temperatures in various parts of the Baltic Sea. The model can be validated over periods and regions for which measurements are available. Over periods when measurements are sparser—for example, Bothnian Bay in the 1980–1992 period—we are presented with only a modeled approximation of the environmental conditions. A combination of models and observations is needed both to detect changes in observations and to attribute causes to the changes by using models.

Another example related to the water balance will illustrate model extrapolation. Over the last hundred years, freshwater inflow to the Baltic Sea has hovered around a mean of 15,000 $m^3\ s^{-1}$. What would happen if the freshwater supply increased? The curves in Fig. 1.3 indicate that, if the freshwater inflow were tripled, the Baltic Sea would be transformed into a freshwater sea. Can one rely on that result, and how is one supposed to know? The calculations indicate that the sea is sensitive to variations in freshwater inflow, though it is highly unrealistic to conceive of an

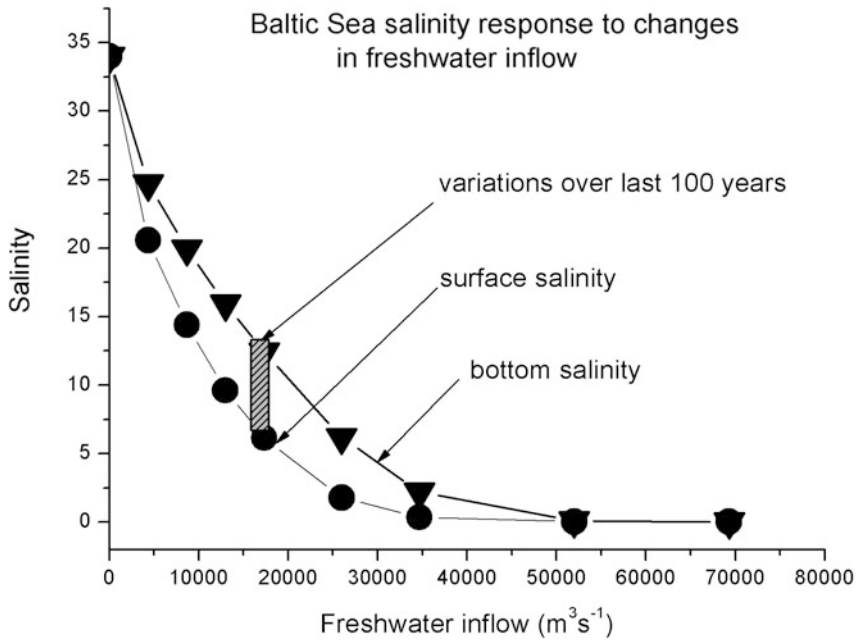

Fig. 1.3 Model calculations indicating how salinity in the central Baltic Sea can vary with variations in freshwater inflow from rivers and precipitation. The *hatched field* represents observed variation over the last hundred years (redrawn from Omstedt and Hansson 2006a)

increase of several hundred percent. The calculations indicate that the Baltic Sea will remain brackish in the future. This example has interesting implications for that part of the model results that lies outside the observed range. When using models, we of course must be careful with extrapolations as they are unsupported by direct validation data. However, the potential to extrapolate is much of the reason why we develop models, as extrapolations can teach about things outside present observational knowledge.

A third example is how process-based modeling can yield important knowledge of marine system dynamics. Björk (1997) and Björk and Söderkvist (2002) investigated ice thickness in the Arctic Ocean. The basic processes considered in the modeling are depicted in Fig. 1.4. The modeling resolves only the vertical dimension, whereas the processes working in horizontal directions are parameterized. The approach explains many of the observed characteristics of the Arctic

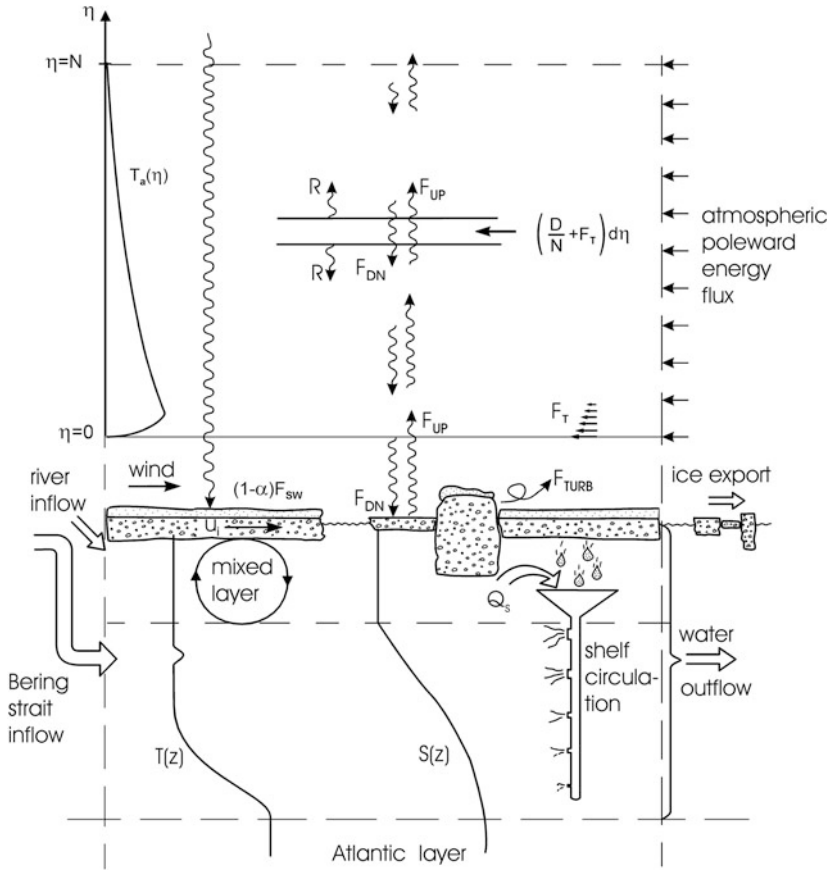

Fig. 1.4 A process-based modeling view of the Arctic Ocean climate system (from Björk and Söderkvist 2002)

Ocean, such as stratification, ice thickness distribution, and sensitivity to climate change.

The aim of the book is to guide the reader into the process-based numerical modeling of lakes and coastal seas, using the PROBE equation solver. In the book, we mostly use the Baltic Sea as an illustration, but the method is general and could be applied to many other aquatic systems. After an introduction to background physics and biogeochemistry (Chap. 2), the main foundations are laid for physical modeling (Chap. 3) and biogeochemical modeling (Chap. 4). The construction of nets of sub-basins is then presented, together with a discussion of the detection and attribution of anthropogenic changes and scenarios (Chap. 5). The book incorporates several exercises, whose solutions are fully worked through (Chap. 6). Finally, a summary with conclusions is presented (Chap. 7). Appendices follow, treating matters such as an introduction to FORTRAN programming (Appendix A), nomenclature (Appendix B), a description of the programs and data needed to solve the exercises (Appendix C), which can be downloaded from http://extras.springer.com, the PROBE *Manual* (Appendix D), and a discussion of how to go about historical reconstructions when extending our knowledge back in time to periods for which instrumental data are not available (Appendix E).

Chapter 2
Background Physics and Biogeochemistry

2.1 Conservation Principles and Governing Equations

Conservation equations can be formulated for most aquatic properties (ϕ). For transient three-dimensional problems, the general differential equation is:

$$\frac{\partial}{\partial t}\phi + U_i\frac{\partial \phi}{\partial x_i} = S_\phi \quad where\ i = x, y, z \tag{2.1}$$

where ϕ could be, for example, momentum, temperature, salinity, or oxygen, U_i is the velocity, where the index indicates velocity components in the horizontal and vertical directions, and S_ϕ is the source/sink term related to the properties considered. The coordinates in space are denoted x, y, and z, while t is the coordinate in time. As geophysical flows are not only typically turbulent, but also include waves, their properties can be divided into mean, wave, and fluctuation or turbulent parts and simplifications can then be made based on scale analysis. If we neglect the wave motion, division can be formulated as:

$$\begin{aligned} U_i &= \overline{U_i} + U_i' \\ \phi_i &= \overline{\phi_i} + \phi_i' \end{aligned} \tag{2.2}$$

where $\overline{U_i}$ and $\overline{\phi_i}$ represent the mean velocity and mean property, and U_i' and ϕ_i' represent the corresponding fluctuating parts. Equations derived from the conservation principles using the Reynolds method of averaging and the eddy viscosity concept read:

$$\begin{aligned} \frac{\partial}{\partial t}\overline{\phi} + \overline{U_i}\frac{\partial \overline{\phi}}{\partial x_i} &= \frac{\partial}{\partial x_i}\left(\Gamma_\phi \frac{\partial}{\partial x_i}\overline{\phi}\right) + \overline{S_\phi} \\ \Gamma_\phi &= \frac{\mu}{\rho\sigma_\phi} + \frac{\mu_T}{\rho\sigma_{\phi T}} \end{aligned} \tag{2.3}$$

A. Omstedt, *Guide to Process Based Modeling of Lakes and Coastal Seas*,
Springer Praxis Books, DOI 10.1007/978-3-319-17990-2_2

where Γ_ϕ includes the sum of molecular and turbulent diffusion processes; μ denotes the dynamic viscosity, μ_T the turbulent viscosity, ρ density, σ the Prandtl/Schmidt number, and $\sigma_{\phi T}$ the turbulent Prandtl/Schmidt number. The terms of the conservation equation, from left to right, represent property changes: in time, due to advection, due to turbulent diffusion, and due to sources/sinks. The geophysical flow equations are described in detail by Cushman-Roisin and Becker (2011).

The source/sink terms in the momentum equation are pressure, gravity, and the Coriolis term; the last term is part of acceleration but can also be treated as a source term. The source term in the temperature equation is the sun radiation that penetrates the water body.

An important aspect of the general conservation equation (Eq. 2.1) is that it can form the basis for developing general equation solvers. Based on this equation, one can derive the corresponding discretized equation through integration over a control volume. The general discretization equation can then be formulated as:

$$a_P\theta_P = a_W\theta_W + a_E\theta_E + a_S\theta_S + a_N\theta_N + a_B\theta_B + a_T\theta_T + S_\theta \tag{2.4}$$

where we now use θ to represent the finite volume form of ϕ. The indices represent the calculations in position P determined from information from the west (W), east (E), south (S), north (N), bottom (B), and top (T) nodal points. This type of equation forms the basis of several general equation solvers (Versteeg and Malalasekera 1995).

Exercise 2.1
The mean depth of the Baltic Sea is 54 m and its surface area is 3.9×10^5 km^2. How much would the level of the Baltic Sea increase over a year with river water inflow of 15,000 m^3 s^{-1} and no outflows? If the outflowing volume flow were 30,000 m^3 s^{-1}, how large would the inflowing volume flow need to be to keep the sea level unchanged? If the salinity of the inflowing water were 17 salinity units, what would the salinity be in the basin?

2.2 Physical Aspects

A description of a fluid should relate the fluid's density to its state variables, a relationship called the equation of state. For natural waters, this equation is generally a function of temperature, salinity, and pressure (Gill 1982, App. 3); for coastal seas, however, one can often neglect pressure and use the following approximation:

$$\begin{aligned} \rho &= \rho_0\left(1-\alpha_1\left(T-T_{\rho m}\right)^2+\alpha_2\left(S-S_{ref}\right)\right) \\ T_{\rho m} &= 3.98-0.22S \end{aligned} \tag{2.5}$$

where T and S are temperature and salinity, ρ_0 the reference density, $T_{\rho m}$ the temperature of maximum density, S_{ref} reference salinity, and α_1 and α_2 the thermal and salinity expansion/contraction coefficients, respectively. Typical values for brackish water are $\rho_0 = 1000$ (kg m^{-3}), $S_{ref} = 0$, $\alpha_1 = 5.10^{-6}$ (°C^{-2}), and $\alpha_2 = 8.10^{-4}$.

The freezing temperature of seawater is:

$$T_f = -0.0575S + 0.0017S^{1.5} - 0.0002S^2 - 0.00753P_w \tag{2.6}$$

where P_w is the water pressure in bars (we can neglect the pressure term for shallow lakes and seas). Brackish water is often defined as saline water that has a freezing point below the temperature of maximum density. The upper salinity limit is thus 24.7 and the lower limit is estimated to be 0.5 (Leppäranta and Myrberg 2009).

In the case of freezing water, ice needs to be considered. Ice forms a thin, rigid but fragile layer over the water body that dramatically changes the heat, momentum, and gas exchanges between atmosphere and water. In nature, ice forms in two ways: (1) under calm conditions when the water surface is slightly supercooled and (2) after atmospheric seeding, when ice crystals start growing horizontally into large crystals. When the horizontal space is occupied, the crystals then grow vertically (in seawater, ice crystals form from pure water, the salinity leaking out along the crystal boundaries). These ice crystals grow, forming columnar ice that, together with snow, is often seen in sheltered lakes and inland waters. Under windy conditions accompanied by supercooling, small ice crystals get mixed into the water column and form frazil ice. Under open water conditions, all the heat that escapes the cold water surface is used for ice production, resulting in huge amounts of frazil ice. Frazil ice is later transformed into grease ice and pancake ice, which often constitutes the base for sea ice formation.

When a thin ice layer has formed, winds and currents cause it to drift. During free ice drift, the ice moves at approximately 2–3 % of the 10-m wind velocity and 20–30° to the right (in the Northern Hemisphere) of the wind direction, due to the Coriolis effect. Under the influence of onshore winds or when the ice concentration is high, the plastic behavior of ice starts to influence the drift. This reduces the ice velocity, but at a certain ice pressure, the ice breaks and starts forming ridged ice.

Exercise 2.2
Investigate the equation of state by plotting Eq. 2.5 for different temperatures and salinities. What are the typical densities in the Baltic and Mediterranean seas? What are the dominant factors that control density in coastal seas? Compare Eq. 2.5 with the full equation of state given by Gill (1982, App. 3).

2.3 Simplifications

The conservation equations are nonlinear, and it is often impossible to find analytical solutions except in simple flow cases. Instead, we must rely on numerical methods to solve the equations. Before making any calculations, we must systematically reduce the problem complexity by making proper simplifications. We begin a process-based approach by carefully identifying the problem. The first step is to identify the water volume and divide it, guided by observation, into dynamically relevant processes. Hypsographic curves yield important information about the water volumes available at various depths, while bathymetric charts tell us where narrow straits, channels, and canyons are and where natural sub-basins occur (Fig. 2.1). Knowledge of forcing functions (i.e., meteorological, hydrological, and ocean conditions outside the coastal sea) also provides a good basis for modeling design. As water circulation is often crucial, hydrodynamic equations could be simplified by identifying the scales of motion.

The use of dimensionless numbers can help with the scaling. Important dimensionless numbers in geophysical flow dynamics are the temporal Rossby number, $Ro_t = \frac{1}{\Omega T}$, and the Rossby number, $Ro = \frac{U}{\Omega L}$, where $\Omega = \frac{2\pi}{time\ of\ one\ revolution}$ is Earth's

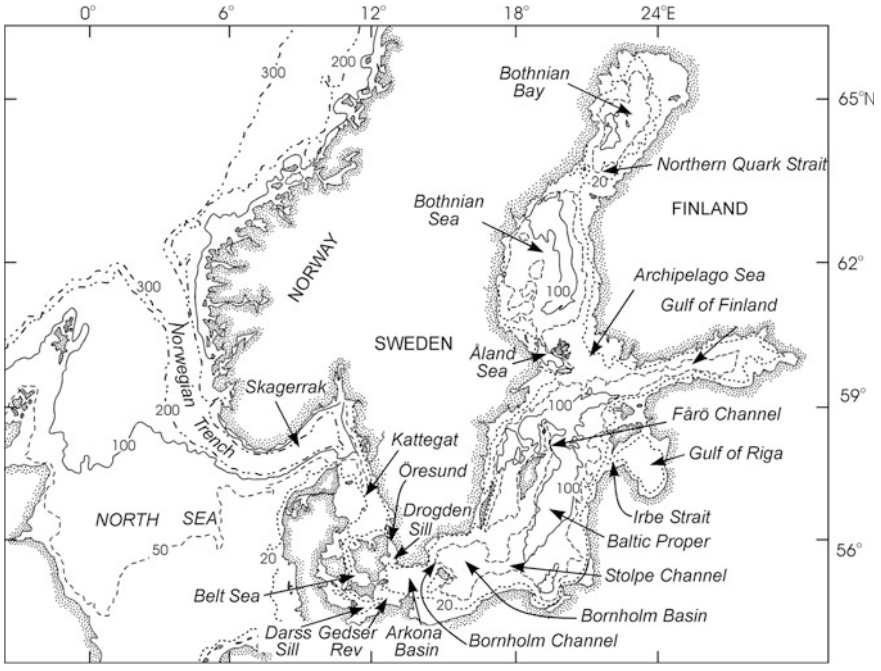

Fig. 2.1 The Baltic Sea–North Sea region with depth contours indicated (from Omstedt et al. 2004)

rotation frequency, equal to 7.29×10^{-5} (s^{-1}), and L, T, and U represent the typical scales of length, time, and speed, respectively. In large-scale flows, these dimensionless numbers are often small, implying that the acceleration terms are small.

The importance of friction can be estimated from the horizontal, $Ek_h = \frac{\mu_T}{\rho \Omega L^2}$, and vertical, $Ek_v = \frac{\mu_T}{\rho \Omega H^2}$, Ekman numbers. Outside boundary layers, the Ekman numbers are small and friction effects can be neglected. The implications of these numbers can be easily understood if we examine the governing geophysical equations (Cushman-Roisin and Becker 2011), considering the x and y dimensions first and then estimating scales under the various terms:

$$\begin{array}{cccccccc} \frac{\partial}{\partial t}\overline{U} + \overline{U}\frac{\partial \overline{U}}{\partial x} + \overline{V}\frac{\partial \overline{U}}{\partial y} + \overline{W}\frac{\partial \overline{U}}{\partial z} - f\overline{V} = -\frac{1}{\rho_0}\frac{\partial P_w}{\partial x} + \frac{\partial}{\partial x}\left(\Gamma_h \frac{\partial \overline{U}}{\partial x}\right) + \frac{\partial}{\partial y}\left(\Gamma_h \frac{\partial \overline{U}}{\partial y}\right) + \frac{\partial}{\partial z}\left(\Gamma_z \frac{\partial \overline{U}}{\partial z}\right) \\ \frac{U}{T} \quad \frac{U^2}{L} \quad \frac{U^2}{L} \quad \frac{WU}{L} \quad \Omega U \quad \frac{P_w}{\rho_0 L} \quad \frac{\mu_h U}{\rho_0 L^2} \quad \frac{\mu_h U}{\rho_0 L^2} \quad \frac{\mu_v U}{\rho_0 H^2} \end{array} \tag{2.7}$$

$$\begin{array}{cccccccc} \frac{\partial}{\partial t}\overline{V} + \overline{U}\frac{\partial \overline{V}}{\partial x} + \overline{V}\frac{\partial \overline{V}}{\partial y} + \overline{W}\frac{\partial \overline{V}}{\partial z} + f\overline{U} = -\frac{1}{\rho_0}\frac{\partial P_w}{\partial y} + \frac{\partial}{\partial x}\left(\Gamma_h \frac{\partial \overline{V}}{\partial x}\right) + \frac{\partial}{\partial y}\left(\Gamma_h \frac{\partial \overline{V}}{\partial y}\right) + \frac{\partial}{\partial z}\left(\Gamma_z \frac{\partial \overline{V}}{\partial z}\right) \\ \frac{U}{T} \quad \frac{U^2}{L} \quad \frac{U^2}{L} \quad \frac{WU}{L} \quad \Omega U \quad \frac{P_w}{\rho_0 L} \quad \frac{\mu_h U}{\rho_0 L^2} \quad \frac{\mu_h U}{\rho_0 L^2} \quad \frac{\mu_v U}{\rho_0 H^2} \end{array} \tag{2.8}$$

where $f = 2\Omega \sin \varphi$ is the Coriolis parameter and φ the latitude.

By dividing the estimated sizes beneath the equation by ΩU, we can easily identify the various dimensionless numbers given above. For example, if $Ro_t \ll 1$, the transient term can be neglected relative to the rotation part.

The incompressible approximation for water leads to the implication of divergence-free motion (represented by the continuity equation, Eq. 2.9). That is, if the density fluctuations are small relative to the density itself, any imbalance in horizontal motion will be reflected in the vertical motion:

$$\frac{\partial \overline{U}}{\partial x} + \frac{\partial \overline{V}}{\partial y} + \frac{\partial \overline{W}}{\partial z} = 0 \tag{2.9}$$

By scaling the continuity equation, we learn that $\frac{U}{L}$ must be of the same order as $\frac{W}{H}$, and as the horizontal dimension is often much larger than the depth (i.e., $\frac{H}{L} \ll 1$), the vertical velocity must be much less than the horizontal velocity (i.e., $\frac{W}{U} \ll 1$). In addition, as geophysical flows often have time scales larger than the rotation scale (i.e., $T \geq \frac{1}{\Omega}$ and $\frac{U}{L} \leq \Omega$), we can simplify the vertical equation by analyzing the various terms one by one. The equation for the vertical velocity component with estimated scales reads:

$$\frac{\partial}{\partial t}\overline{W}+\overline{U}\frac{\partial \overline{W}}{\partial x}+\overline{V}\frac{\partial \overline{W}}{\partial y}+\overline{W}\frac{\partial \overline{W}}{\partial z}-f_*\overline{U}=-\frac{1}{\rho_0}\frac{\partial P_w}{\partial z}-\frac{g\rho}{\rho_0}+\frac{\partial}{\partial x}\left(\Gamma_h\frac{\partial \overline{W}}{\partial x}\right)+\frac{\partial}{\partial y}\left(\Gamma_h\frac{\partial \overline{W}}{\partial y}\right)+\frac{\partial}{\partial z}\left(\Gamma_z\frac{\partial \overline{W}}{\partial z}\right)$$

$$\frac{W}{T}\quad \frac{UW}{L}\quad \frac{UW}{L}\quad \frac{W^2}{H}\quad \Omega U\quad \frac{P_w}{\rho_0 H}\quad \frac{g\Delta\rho}{\rho_0}\quad \frac{\mu_h W}{\rho_0 L^2}\quad \frac{\mu_h W}{\rho_0 L^2}\quad \frac{\mu_v W}{\rho_0 H^2}$$

where $f_* = 2\Omega\cos\varphi$ is the reciprocal Coriolis parameter.

From the scaling conditions given, we conclude that the first term in this equation can be neglected. The next three terms are also much less than ΩU and could therefore be neglected. If we now compare the fifth term with the first pressure term on the left side of the equation, one finds that $\frac{\rho_0 \Omega H U}{P} \sim \frac{H}{L}$, so even the fifth term can be neglected. Finally, we realize that the last three terms are small and can be neglected. The scaling thus illustrates that in geophysical flows we may often only need to consider hydrostatic balance or:

$$0 = -\frac{1}{\rho_0}\frac{\partial P_w}{\partial z}-\frac{g\rho}{\rho_0} \tag{2.10}$$

Other important simplifications are that large-scale circulation is often in geostrophic and hydrostatic balance, implying a balance in the horizontal dimensions between Earth's rotation and the horizontal pressure gradients and in the vertical dimension between gravity and the vertical pressure gradient. In this case, the dimensionless numbers $Ro_t, Ro, Ek_h,$ and Ek_v are all much less than one.

At the surface and bottom boundary layers (i.e., $Ek_v \sim 1$), one can find analytical solutions to the boundary equations. For the surface boundary layer, the net mass transport is perpendicular to the wind direction and to the right in the Northern Hemisphere. The analytical solution for the mass transport in the bottom boundary layer indicates transport to the left of the geostrophic flow direction.

If $Ro_t, Ro,$ and $Ek_v \ll 1$, several important analytical aspects of the fluid flow can be derived. For example, the flow is geostrophic. The Taylor–Proudman theorem states that the horizontal velocity field has no vertical shear and that the flow cannot proceed across changes in bottom topography; instead, all motions follow depth contours. Bathymetric charts then give us important information about circulation, information that has implications for how to divide the water body into dynamic regions.

For time-dependent frictionless geostrophic flow, one can derive useful expressions for the vorticity dynamics; with Ro and $Ek_v \ll 1$ and $Ro_t \leq 1$, the change in relative vorticity needs to be conserved, as follows:

$$\frac{d}{dt}\left(\frac{f+\frac{\partial V}{\partial x}-\frac{\partial U}{\partial y}}{H}\right)=0 \tag{2.11}$$

For a change in the bottom topography, this equation means that the fluid flow will change its vorticity.

In stratified fluids, the Froude number, $Fr = \frac{U}{NH}$, where N is the stratification frequency or the Brunt–Väisälä frequency (i.e., $N^2 = -\frac{g}{\rho_0}\frac{d\rho}{dz}$), also yields useful information. The rule is that if $Fr \leq 1$, then the stratification effects are important. The length scale at which stratification and rotation become equally important is called the internal Rossby radius of deformation, i.e., $L_{Ro} = \frac{NH}{\Omega}$.

When fluids are stratified (or non-stratified), we can simplify the equations by assuming wave solutions. Assuming a wave solution with no space limitation, i.e., $W = W_0 e^{i(lx+my+nz-\omega t)}$ (note that $e^{i\phi} = \cos\phi + i\sin\phi$), one can demonstrate that the internal wave frequency is limited by the Coriolis frequency and the stratification frequency (i.e., $f \prec \omega \prec N$). Such waves, called inertia–gravity waves, are oscillating in nature and typical of open sea conditions. The wave number and frequency are denoted by $n = \frac{2\pi}{L_x}$, $m = \frac{2\pi}{L_y}$, $n = \frac{2\pi}{L_z}$, and $\omega = \frac{2\pi}{T}$, respectively.

If we instead assume a wave solution (i.e., $w = w_0 e^{i(my+nz-\omega t)-lx}$) with one coast along $x = 0$ and a normal velocity of zero at the coast, the results indicate that the waves have no lower frequency limit (i.e., $\omega \prec N$). These waves, called coastal-trapped waves, move along the coast with the coast to the right of the wave propagation and often at a low frequency. In semi-enclosed basins, one may thus expect to have coastal-trapped waves along coastlines without lower wave frequency limits; in the open parts of such basins, one may encounter oscillating currents bounded by the stratification and Coriolis frequencies.

Analytical solutions have important implications for any model design. From analytical solutions, we learn the basic processes involved, and solutions can be used to test the accuracy of numerical modeling. However, we must eventually face the fact that we must solve equations using numerical methods. Numerical models are based on grids in which one can solve equations at a limited resolution. Dynamic features larger than the grid domain must then be prescribed, while features smaller than the grid size must be parameterized. If we were to construct a numerical model of, for example, coastal upwelling (with typical spatial and time scales of L = 10 km, H = 100 m, and T = 10 days), we would need a domain at least 10 times larger than the upwelling in both space and time. To resolve the motions, we often need a grid size less than 1/10 of the typical spatial and time scales we wish to resolve. Given these considerations, we need to prescribe motion on a horizontal scale of 100 km and a vertical scale of 1000 m, as well as computer time of 100 days. Processes such as geostrophic eddies, thermohaline circulation, tides, and climate effects (Fig. 2.2) must therefore be prescribed. The resolved motion includes front dynamics, but we should be aware that errors in numerical models could be of several types, such as discretization, iteration, and rounding errors. Numerical tests, conservation checks, and validation using observations are therefore needed. Parameterized motions are those at grid scales less than the resolved one, in this case, at a horizontal scale of 1 km, a vertical scale of 10 m, and a time interval of 1 day. All motions at these spatial and time scales must therefore be parameterized, which in our example includes turbulence, surface waves, Langmuir circulation, swell, shipping effects, and breaking waves.

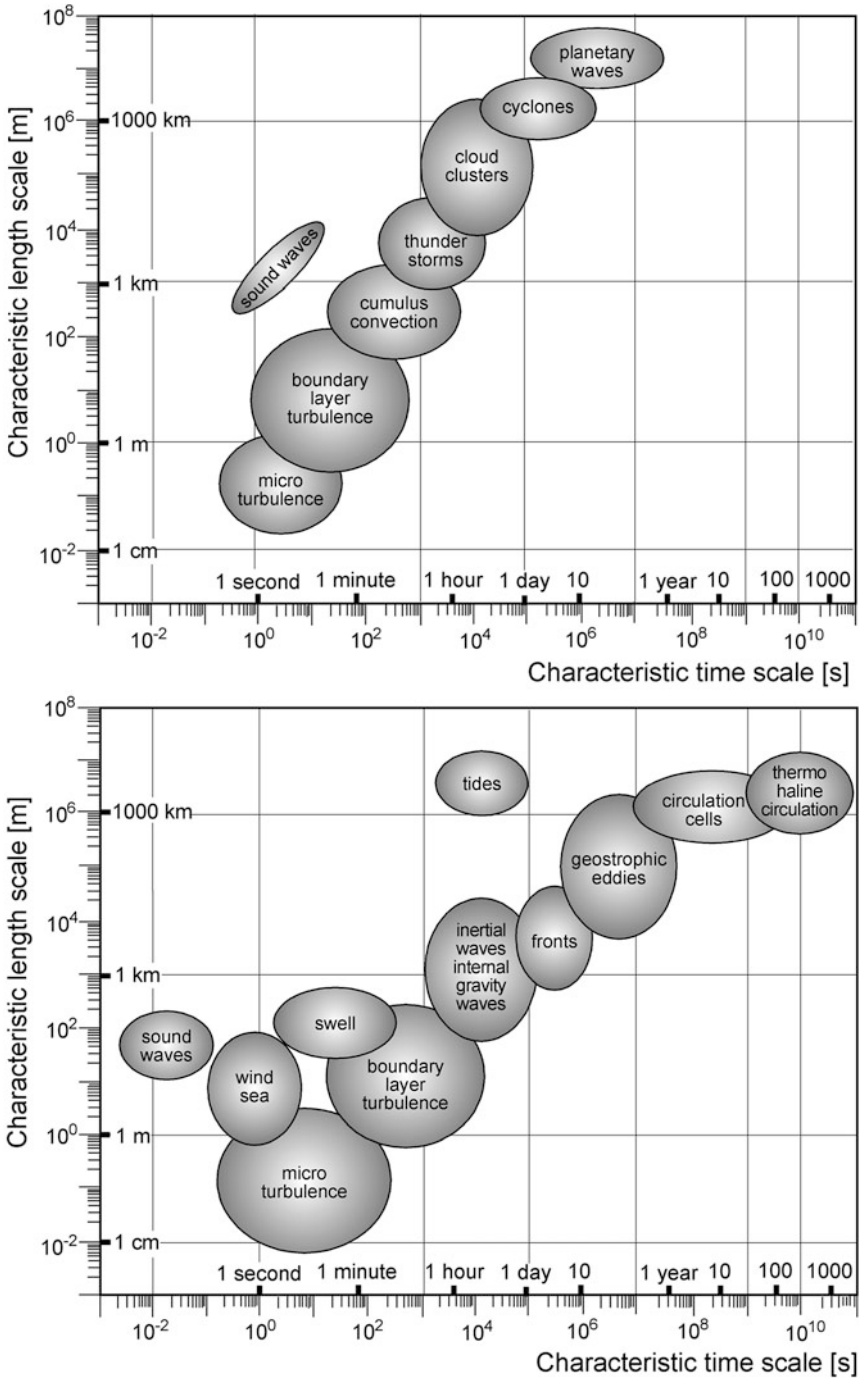

Fig. 2.2 Spatial and temporal scales of some atmospheric and ocean processes (*courtesy* of Hans von Storch)

Exercise 2.3
Some oceanographers imagine studying Earth's rotation by sitting in a bathtub and letting the water drain while they are passing over the Equator. Would Earth's rotation significantly affect the water flow when emptying a bathtub? Assume a horizontal scale of 1 m, a drainage rate in the order of 0.01 m s^{-1}, a motion time scale of 1000 s, and an ambient rotation rate of 7.3×10^{-5}.

Exercise 2.4
A 60-m-deep surface layer with a salinity of approximately 7 characterizes the central Baltic Sea. Below the halocline, salinity is approximately 10. Using a value of 8×10^{-4} for the coefficient of salinity expansion, calculate the stratification or Brunt–Väisälä frequency. What is the horizontal scale at which rotation and stratification play comparable roles? *Hint*: Use the equation of state, i.e., $\rho = \rho_0(1 + \alpha_2 S)$, and assume that the density change takes place over 60 m.

Exercise 2.5
Examine vorticity dynamics by assuming that the outflow from the Baltic Sea into the Kattegat conserves potential vorticity. What happens to the flow when the outflow enters the much deeper Skagerrak? Demonstrate how the relative vorticity might change.

2.4 Water Masses and Water Pools

Water mass and tracer analysis are the two basic methods for determining ocean circulation (e.g., Aken 2007). Based on temperature (T) and salinity (S) measurements and on plotting these variables in a T–S diagram, we can obtain important information about coastal sea circulation and mixing processes. Figure 2.3 depicts the T–S structure of some sub-basins of the Baltic Sea. Starting from the deep Northwestern Gotland Basin, the T–S structure indicates three different water masses: (1) the surface layer, with large temperature and small salinity variations, (2) the halocline layer, with quite small temperature and salinity variations, and (3) the deep water layer, with small temperature but larger salinity variations. In the other sub-basins, the surface water is diluted by river runoff and the deep water masses are influenced by inflow from surrounding basins and the presence of sills.

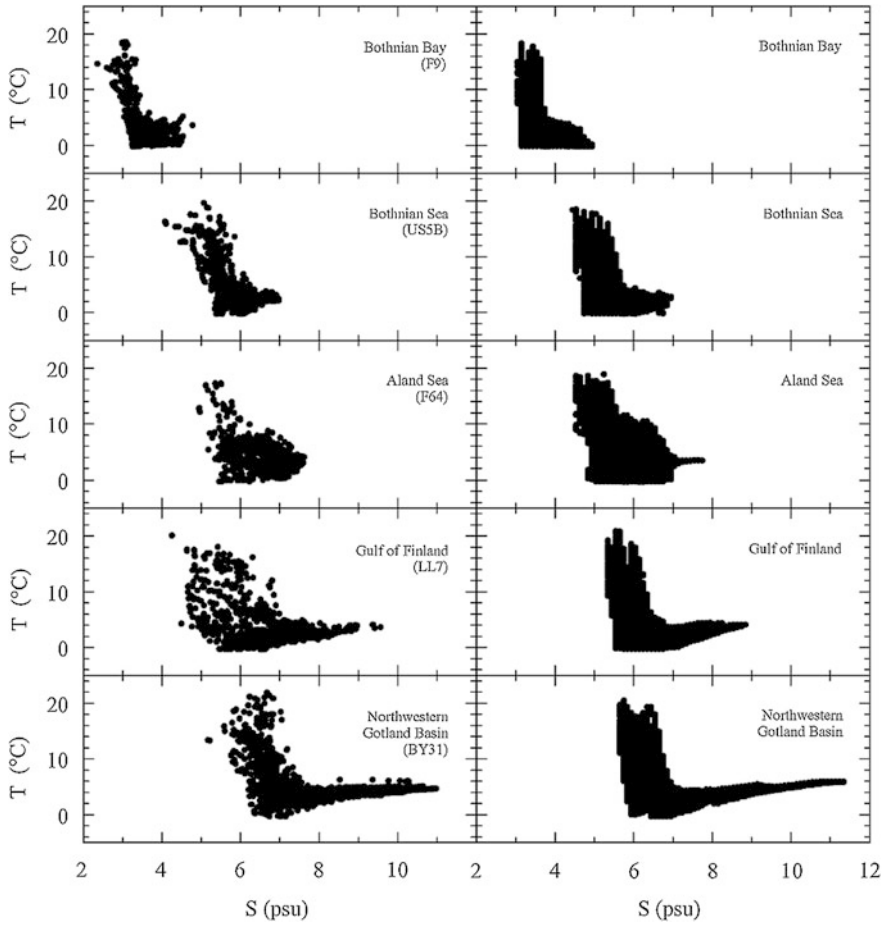

Fig. 2.3 Observed long-term T–S structure in the Northern Baltic Sea (from Omstedt and Axell 2003)

Water masses often form pools of water under specific dynamic control mechanisms; for example, we can speak of the Arctic Ocean surface water pool or the Bornholm Basin deep water pool. Analyzing the dynamics underlying the filling and emptying of such pools can often lead to new insights and interesting model simplifications (Stigebrandt 2001).

When water leaves a water mass, it may form surface brackish layers, as in the Kattegat, or dense bottom layers, as in the Baltic Proper (Fig. 2.4). These surface or bottom water masses are filled with currents transporting dense or light water and influenced by mixing processes. Sometimes the dynamics are very transient, with the formation of pulses and eddies indicating transient dynamics and strong mixing (Piechura and Beszczynska-Möller 2004).

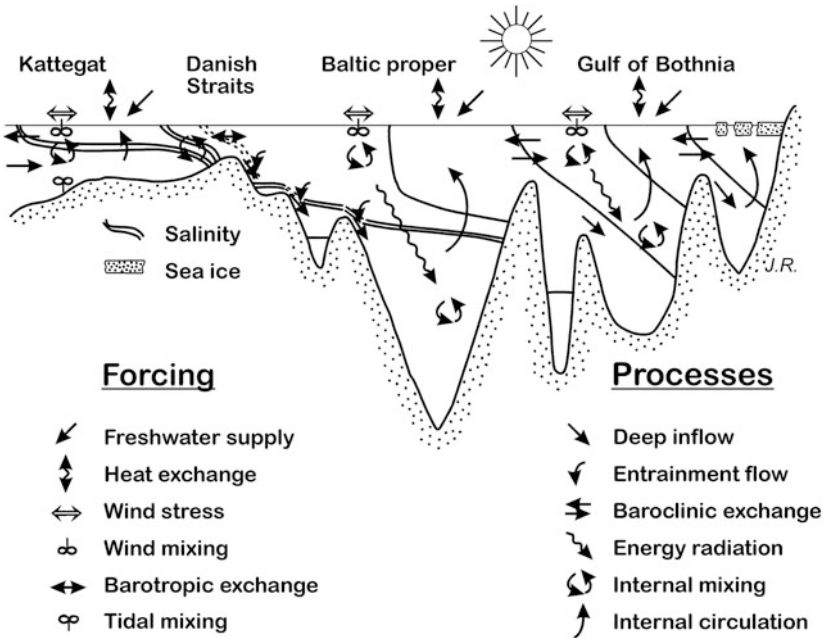

Fig. 2.4 Schematic of processes and forcing mechanisms in the Baltic Sea (redrawn from Winsor et al. 2001, 2003)

The level at which water is drawn when passing over a sill depends on the dynamics. When the water is drawn from a layer in a stratified fluid, several processes may take place, such as fluid acceleration, wave generation, and turbulence. Selected withdrawal dynamics may therefore need to be considered when examining outflow levels. One such example is the Sound, for which Mattsson (1996) estimated that the water flowing into the Baltic Sea comes from levels below the Drogden Sill depth.

2.5 Strait Flows

Inshore–offshore water exchange and exchange between sub-basins are often controlled by geometric constrictions such as sills and straits (Fig. 2.5). Straits are often narrow, shallow regions, and a basic understanding of strait flow dynamics (including mixing) is needed to facilitate modeling. In this context, we generally speak of barotropic and baroclinic flows being associated with sea level changes and density changes, respectively.

The flow dynamics through the Baltic Sea entrance area are transient, with volume flows changing from 0 to 100,000 $m^3\ s^{-1}$ in both directions, so direct

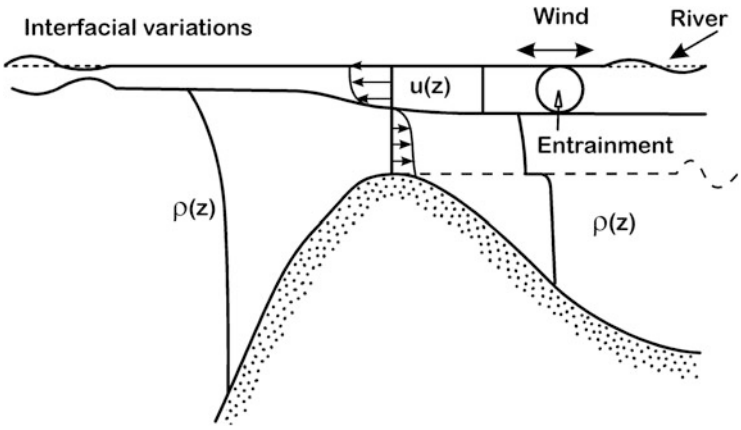

Fig. 2.5 Exchange in an inshore–offshore region with a sill (redrawn from Green 2004)

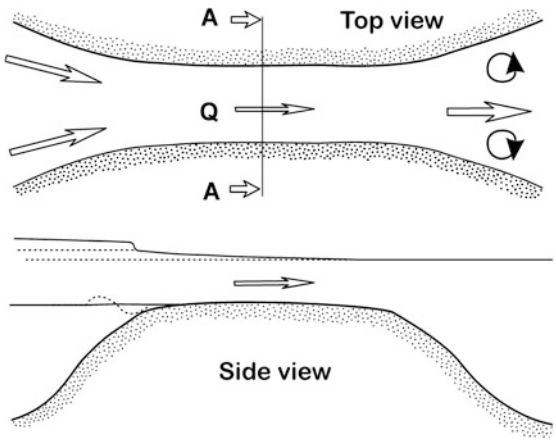

Fig. 2.6 Barotropic exchange through a shallow channel (redrawn from Green 2004)

measurements are quite difficult to make. As these strait flows are driven mainly by the differences in sea level across the entrance area, inflows and outflows have so far mainly been calculated from sea level observations or from models (Fig. 2.6). This complex exchange can be modeled according to the volume conservation principle and a simple barotropic strait model (Stigebrandt 2001):

$$\begin{aligned} A_s \frac{dz_s}{dt} &= Q_b + (P - E)A_s + Q_r \\ Q_b^2 &= \frac{1}{c_s}\Delta z \end{aligned} \tag{2.12}$$

where A_s is the surface area of the Baltic Sea, z_s the water level of the Baltic Sea, Δz the sea level difference between the two basins, Q_b the barotropic inflows and

outflows through the Baltic Sea entrance area, c_s a strait-specific constant, P and E the precipitation and evaporation rates, and Q_r river runoff.

Freshwater exchange from land often results in surface layers that mix with the surrounding coastal waters and denser, deeper waters that flow inshore. In straits wider than the internal Rossby radius of deformation, we often assume a geostrophic baroclinic flow formulated as follows (Stigebrandt 2001):

$$Q_g = \frac{g\left(\frac{\rho_2 - \rho_1}{\rho_0}\right) H_1^2}{2f} \tag{2.13}$$

where H_1 represents a mixed surface layer of density ρ_1 overlying a deeper layer of density ρ_2.

In narrow straits, the concept of baroclinic controls can be used. If freshwater runoff from land causes the surface layer to be thicker inshore than offshore, then its thickness must be adjusted as it approaches the offshore basin. A two-layer flow can then become hydraulically controlled, establishing a well-defined condition for the properties of the flow at the mouth (Stommel and Farmer 1953). Of special interest is the concept of maximum baroclinic transport capability applied in the Northern Kvark Strait, connecting Bothnian Bay to the Bothnian Sea, as suggested by Stigebrandt (2001) and later validated through model simulations by Omstedt and Axell (2003) and studied in the field by Green et al. (2006).

Exercise 2.6
Calculate mean sea level variation in the Baltic Sea by examining the barotropic strait model given in Eq. 2.12. Assume that river runoff and net precipitation are constant and equal 15,000 and 1000 $m^3\ s^{-1}$, respectively. In addition, assume that the surface area is 3.9×10^5 km^2 and that the strait-specific constant, c_s, is typically 0.3×10^{-5} ($s^2\ m^{-5}$). Use sea level data from the Kattegat to force the model and compare the mean sea level with sea level variation in Stockholm (for the data needed, see Appendix C).

2.6 Turbulence

All flows become unstable above a certain Reynolds number (i.e., $\mathrm{Re} = \frac{UL}{\nu}$). Flow is laminar at low Reynolds numbers but turbulent at high numbers. Turbulent flow is chaotic and random, including a whole spectrum of eddies of various sizes. From the energy-containing part of this spectrum, the kinetic energy of eddies is transformed into smaller eddies, through the inertial sub-range and into the dissipative range in which the kinetic energy is dissipated into heat. The energy to feed the turbulence comes from the shear currents or from convection, and the size of these energy-containing eddies is often determined by flow geometry. In our

mathematical formulation, Eq. 2.3, we represent the turbulent processes using effective eddy momentum diffusion as follows:

$$\Gamma_{\rho u} = \frac{\mu}{\rho} + \frac{\mu_T}{\rho} \tag{2.14}$$

where μ and $\frac{\mu}{\rho}$ represent the dynamic and kinematic viscosities, respectively, and μ_T is the turbulent dynamic viscosity. The unit of kinematic viscosity is square meters per second, which incorporates the velocity dimension times length. Solving eddy viscosity therefore requires two equations for turbulent quantities. Here we take one equation for the turbulent velocity scale and another for the turbulent length scale. Two-equation turbulent models describe processes that both generate and damp these two scales. Typical processes that generate turbulence are current shear (due to winds and tides), buoyancy (due to the cooling of surface water above the temperature of maximum density), evaporation, ice formation, and the breaking of surface or internal waves. Damping effects include stable stratification, precipitation or melting ice, interfaces (the air–water, ice–water, and water–bottom interfaces), and dissipation.

2.7 Water and Salt Balances

The water and heat cycles are the heart of the climate system. It is impossible to understand the expected processes of change in the climate system without understanding these cycles and the interconnections between them. For example, we cannot understand changes in ocean salinity and sea level if we do not understand changes in the water balance. Likewise, we cannot understand changes in sea ice cover and water temperature if we do not understand changes in the heat balance. Estimating the various components of the water and heat cycles is therefore crucial (Fig. 2.7) and is the main objective of research programs such as BALTEX (the Baltic Sea Experiment) and HYMEX (the HYdrological cycle in the Mediterranean EXperiment).

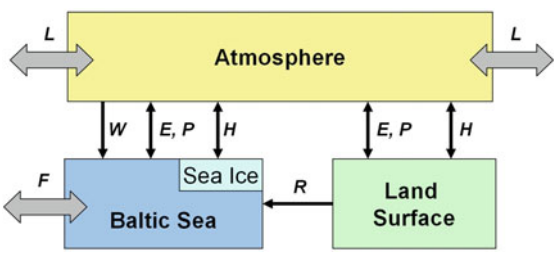

Fig. 2.7 The BALTEX box during Phase I (1993–2002) when water and heat balances were included: *L* denotes lateral exchange with the atmosphere outside the region, *W* wind stress, *E* evaporation rate, *P* precipitation rate, *H* heat and energy fluxes, *R* river runoff, and *F* inflows and outflows through the entrance area (*courtesy* of Marcus Reckermann)

Starting from the volume conservation principle, we can formulate the water balance equation as follows:

$$A_s \frac{dz_s}{dt} = Q_{in} - Q_{out} + (P - E)A_s + Q_r + Q_g \tag{2.15}$$

where A_s is the surface area of the sea, z_s the water level of the sea, Q_{in} and Q_{out} the inflows and outflows through the entrance area, P and E the precipitation and evaporation rates (the difference is called net precipitation), Q_r river runoff, and Q_g groundwater inflow. The left term in Eq. 2.15 is the change in water storage, which can be important for short-term estimations of the water balance. This term also includes volume changes due to thermal expansion and salt contraction. The major water balance components of the Baltic Sea are inflows and outflows at the entrance area, river runoff, and net precipitation (Omstedt et al. 2004) (Fig. 2.8).

If we know the water balance, we can calculate the salt balance, which, based on the conservation principles, reads as follows:

$$\frac{dV_0 S}{dt} = S_{in} Q_{in} - S Q_{out} - S((P - E)A_s + Q_r) \tag{2.16}$$

where V_0 and S are the water volume and salinity of the semi-enclosed basin and S_{in} is the salinity of the inflowing water. Salinity is thus closely linked to the water balance and forms the basis of many budget calculations. A useful integral property is the mean salinity (vertically and horizontally integrated) or freshwater content. The annual mean salinity of the Baltic Sea has varied around 7.6 over the last century, with a variability of approximately ±0.5 (Winsor et al. 2001, 2003).

2.8 Heat Balance

From conservation principles, we can formulate the heat balance equation for a semi-enclosed sea area, according to Omstedt and Rutgersson (2000), as follows:

$$\frac{dH}{dt} = (F_i - F_o - F_{loss})A_s \tag{2.17}$$

where $H = \int\int \rho c_p T dz dA$ is the total heat content of the sea, F_i and F_o the heat fluxes associated with in- and outflows, and F_{loss} the total heat loss to the atmosphere (note that the fluxes are positive when going from the water to the atmosphere). F_{loss} is formulated as follows:

$$F_{loss} = (1 - A_i)(F_n + F_s^w) + A_i(F_w^i + F_s^i) - F_{ice} + F_r + F_g \tag{2.18}$$

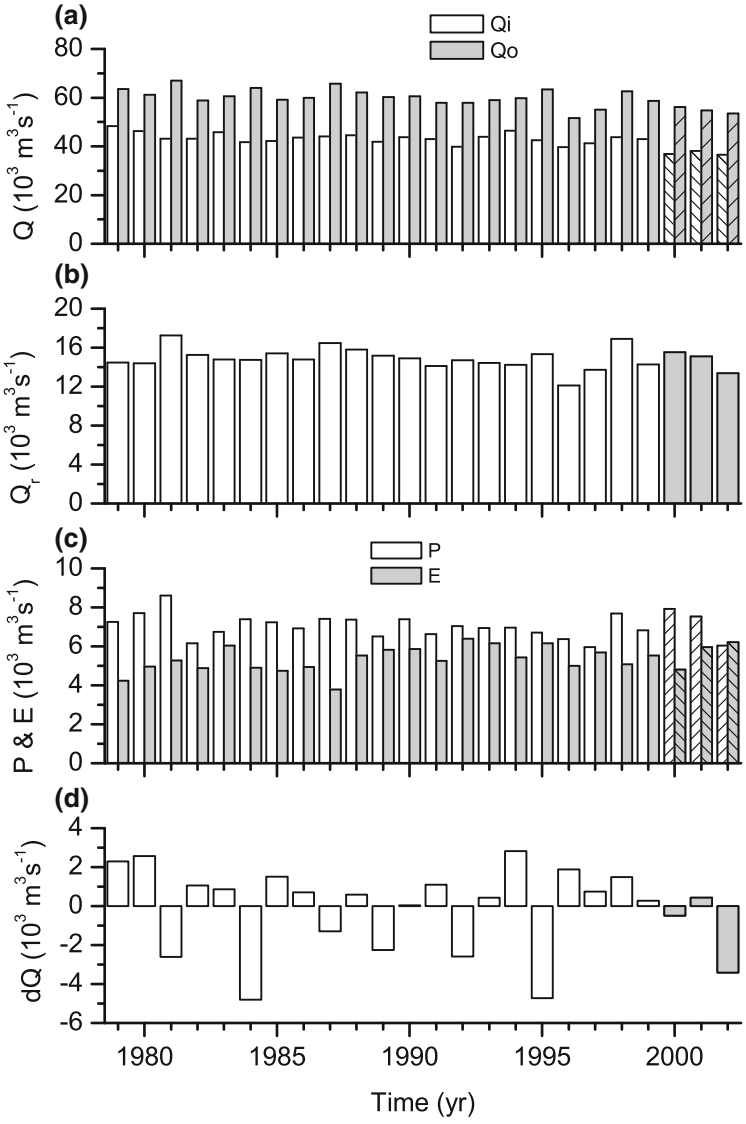

Fig. 2.8 Baltic Sea (excluding the Kattegat and the Belt Sea) annual mean **a** inflows and outflows, **b** river runoff, **c** net precipitation, and **d** net volume change (Omstedt and Nohr 2004)

where

$$F_n = F_h + F_e + F_l + F_{prec} \tag{2.19}$$

The various terms of the equations are denoted as follows: A_i is ice concentration, F_h sensible heat flux, F_e latent heat flux, F_l net long-wave radiation, F_prec heat

fluxes associated with precipitation in the form of rain and snow, F_s^w sun radiation to the open water surface, F_w^i heat flux from water to ice, F_s^i sun radiation through the ice, and F_r and F_g heat flows associated with river runoff and groundwater flow, respectively. In terms of long-term mean, the Baltic Sea is almost in thermodynamic balance with the atmosphere and only 1 Wm^{-2} is needed to compensate for the heat loss due to a net outflow from the Baltic Sea (Omstedt and Nohr 2004). Dominant fluxes, in terms of annual means, are sensible heat, latent heat, net long-wave radiation, solar radiation to the open water, and the heat flux between water and ice (Fig. 2.9).

A useful integral property is the heat content of water (or the vertically and horizontally integrated water temperature), in particular, the change of heat content directly connected to heat fluxes (Eq. 2.17). Surface temperatures are often a poor measure of heat content and may even be unable to measure the accumulation of heat in the water, as other fluxes may compensate for the net effect (Omstedt and Nohr 2004). Pielke (2003) therefore suggested that stored heat content and its change over time should be the focus of international climate-monitoring programs, as change in heat content is a much better measure of climate change than is surface temperature.

Exercise 2.7
Consider the Baltic Sea and its surface area of 3.9×10^5 km^2. Assume that the volume and heat content of the Baltic Sea do not change over time and that the exchange through the entrance area occurs via a two-layer flow. Assume that inflowing water and river water both equal 15,000 m^3 s^{-1} and that the inflowing and outflowing water temperatures both equal 8 °C. If the river runoff temperature is 1 °C colder/warmer than the Baltic Sea surface temperature, what is the estimated heat exchange with the atmosphere?

2.9 Nutrient Balance and Primary Production

Water and energy balances form the basis of the physical state of lakes or coastal seas. The balances of nutrients—including nitrogen, phosphorus, and silicon, together with the carbon balance—form the basis for the chemical and biological state of the water body under study. These balances actively interact and involve many interesting modeling considerations, such as knowledge of human activity (Fig. 2.10). In addition, reliable datasets incorporating marine and atmospheric data, biochemical variables, atmospheric deposition, and river load are needed in modeling efforts (Omstedt et al. 2014).

Biogeochemical modeling often starts from simple stoichiometric considerations and links the water, salinity, and nutrient budgets in which, for example, carbon (C), nitrogen (N), and phosphorus (P) are considered. The first step is often to establish

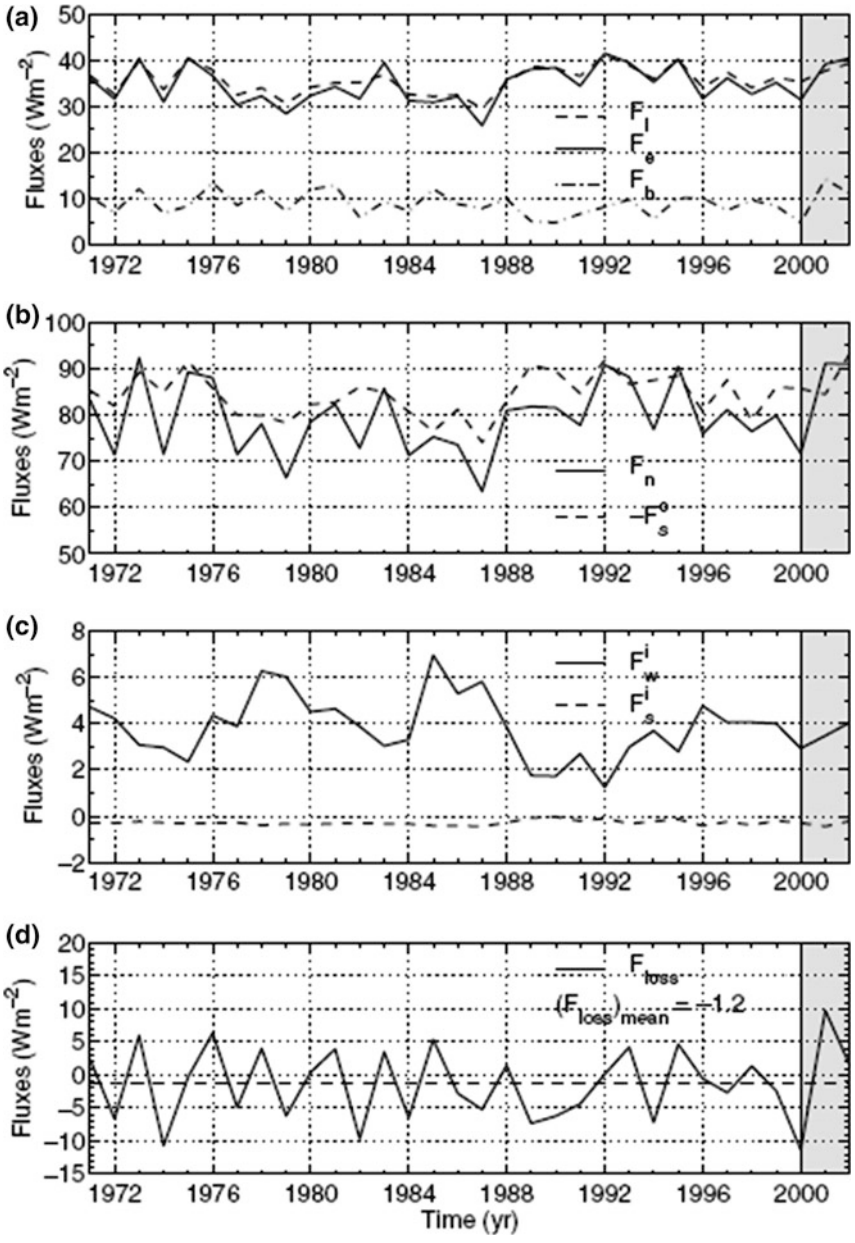

Fig. 2.9 Annual means of: sensible heat (F_h), latent heat (F_e), net long-wave radiation (F_l), net heat flux ($F_n = F_h + F_e + F_l$), sun radiation to the open water surface (F_s^o), sun radiation through ice (F_s^i), heat flow from water to ice (F_w^i), and net Baltic Sea heat loss, i.e., $F_{loss} = (1–A_i)(F_s^o + F_h + F_e + F_l) + A_i(F_s^i + F_w^i)$, where A_i is the ice concentration (Omstedt and Nohr 2004)

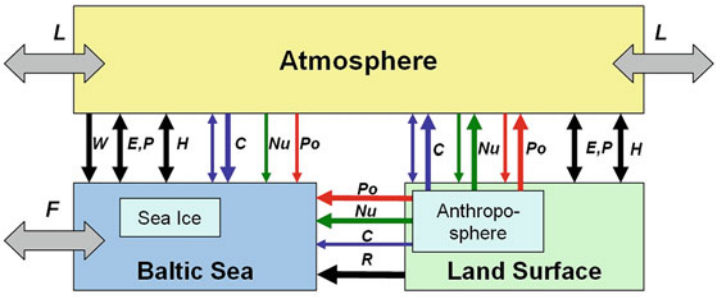

Fig. 2.10 The BALTEX box during Phase II (2013–2012) when water, heat balances, nutrients, and carbon cycles were included: *L* denotes lateral exchange with the atmosphere outside the region, *W* wind stress, *E* evaporation rate, *P* precipitation rate, *H* heat and energy fluxes, *R* river runoff, *F* inflows and outflows through the entrance area, *C* carbon fluxes, *Nu* nutrient fluxes, and *Po* pollutant fluxes (*courtesy* of Marcus Reckermann)

the steady state of the water and salt balances; based on these two equations, the various water flows can then be calculated. Salinity is a conservative property suitable for establishing the exchange of water between the system and adjacent seas. Total alkalinity can sometimes also be used as a conservative property and supplies additional information on the total alkalinity of river water entering the system and water circulation (Hjalmarsson et al. 2008). The next step is to establish budgets for non-conservative materials (Gordon et al. 1996), as follows:

$$\frac{dV_0^{\phi}C}{dt} =^{\phi} C_{in}Q_{in} -^{\phi} CQ_{out} + \Delta^{\phi}C \tag{2.20}$$

where ${}^{\phi}C$ is the concentration of the non-conservative material (mol kg^{-1}) and $\Delta^{\phi}C$ the sum of all non-conservative fluxes. The results of Eq. 2.20 let us quantify the net non-conservative reaction of the material in the system.

Stoichiometric relationships and chemical reaction formulas are used to describe the proportions of the compounds involved in chemical reactions. The expression to the left of the arrow represents the elements before the reaction. The products of the reaction are described by the expression to the right of the arrow. For example, the carbon cycle can be related to organic material due to primary production, as follows:

$$\begin{aligned} &aCO_2 + bHNO_3 + cH_3PO_4 + (a+b)H_2O \\ &\quad \Leftrightarrow (CH_2O)_a(NH_3)_b(H_3PO_4)_c + (a+2b)O_2 \end{aligned} \tag{2.21}$$

where (a:b:c) = (106:16:1) are the standard Redfield values. The expression illustrates how carbon dioxide, water, and nutrients may form plankton in its simplest form (i.e., $(CH_2)_a(NH_3)_b(H_3PO_4)_c$) and oxygen. For a discussion of the

Redfield concept and marine biogeochemistry, the reader should consult Sarmiento and Gruber (2006).

The presence of many strongly nonlinear relationships and the frequent absence of clear basic laws make marine ecosystems difficult to describe (i.e., measure and model) quantitatively. Included in these variables are many kinds of marine organisms that transform nutrients and inorganic carbon into organic material. The primary production of the world's oceans is based on diatoms, dinoflagellates, coccolithophorids, silicoflagellates, and blue–green and other bacteria, all of which need to be understood quantitatively. Regional and species distributions vary considerably, as do light and nutrient limitations.

Figure 2.11 depicts some processes related to modeling Baltic Sea eutrophication, based on the approach of Savchuk and Wulff (2007). The importance of the oxygen dynamics for the phosphate dynamics is depicted in Fig. 2.12. At low oxygen concentrations, the sediments start to leak phosphate. From observations, Conley et al. (2002) demonstrated that the annual change in dissolved inorganic phosphate was positively correlated with the area of sea bottom depleted of oxygen. The figure also indicates that, in oxic water, the sediments may bind phosphate. However, the nitrate dynamics are also influenced and, if the water volume becomes anoxic, this will result in a nitrogen sink, as the NO_3 in the water is reduced to N_2. Oxygen depletion may also increase the total alkalinity (Edman and Omstedt 2013). The modeling of eutrophication must therefore consider how low oxygen concentrations influence the nutrient and carbon dynamics.

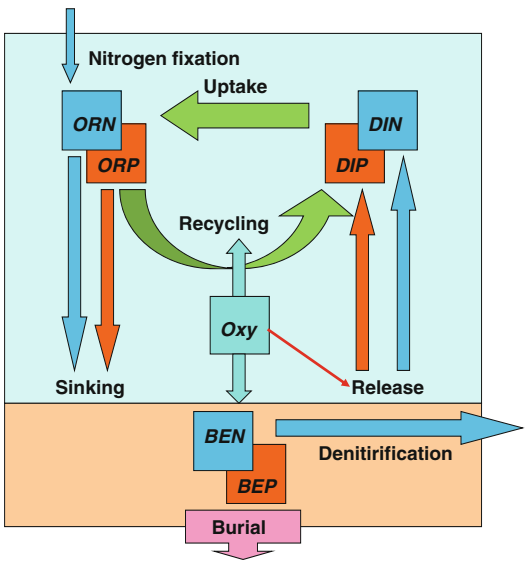

Fig. 2.11 Processes related to modeling the eutrophication in the Baltic Sea based on the modeling approach of Savchuk and Wulff (2007). The organic nitrogen and phosphate parts are denoted by ORN and ORP, the inorganic parts by DIN and DIP, and the benthic parts by BEN and BEP, respectively

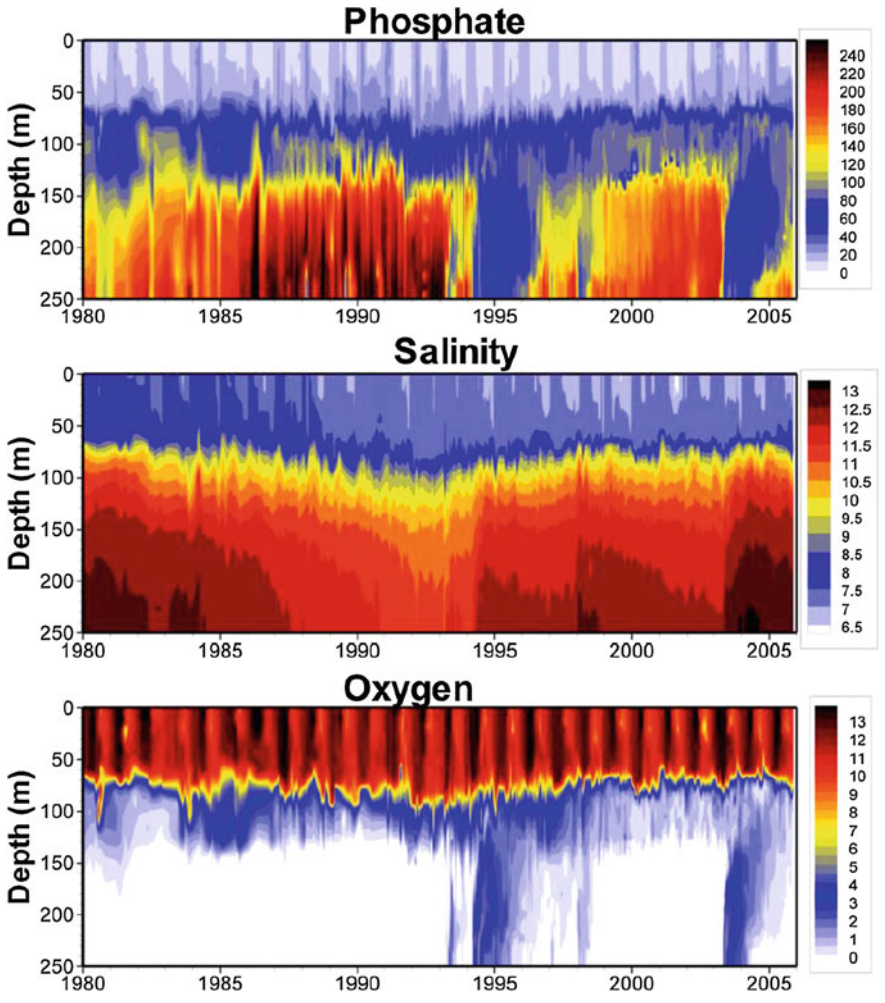

Fig. 2.12 Measurements from the Gotland Deep in the Baltic Sea (Stigebrandt and Gustafsson 2007)

Exercise 2.8
Use `P` and `N` observations from the Baltic Sea and plot the surface properties of PO_4 and NO_3 for the last five years. Discuss the dynamics and discover what is controlling the primary production (for the data needed, see Appendix C).

2.10 Acid–Base (pH) Balances

Water and heat balances are at the heart of climate research and the carbon cycle lies at the heart of biogeochemical modeling. Great efforts are being made to link climate and biogeochemical models and to include them in Earth System Modeling. For anthropogenic climate change due to increased carbon dioxide, the connection between eutrophication and climate change, including ocean acidification, relies on the correct modeling of the CO_2–O_2 marine system, which requires a full understanding of the carbon system.

The seawater acid–base (pH) balance is characterized by the total alkalinity, A_T, which is defined as the excess of proton acceptors (anions of weak bases) over proton donors (strong acids). The major proton acceptors in seawater are hydrogen carbonate (HCO_3^-, 95.5 %), carbonate (CO_3^{2-}, 4 %), and borate ($B(OH)_4^-$, 0.5 %) ions, whereas hydrogen ions (H^+) and hydrogen sulfate ions (HSO_4^-) act as proton donors. A_T is influenced by, for example, limestone dissolution through the increase in carbonate ions. This addition of carbonate ions strengthens the buffering capacity (A_T) and increases the pH. The addition of weak acids such as CO_2 lowers the pH. However, the effect is small because most of the added CO_2 reacts with CO_3^{2-} and only a small fraction of the CO_2 adds hydrogen ions to the system by dissociation of H_2CO_3 to HCO_3^- and H^+. The problem is that when enough carbonic acid has been added, not enough carbonate and bicarbonate ions remain, so pH decreases more rapidly with further additions (Fig. 2.13). This has been observed in freshwater systems exposed to airborne sulfuric acid, though freshwater systems generally have much weaker buffering capacities than do marine systems. In addition, primary production (i.e., carbon dioxide uptake) and mineralization (i.e., carbon dioxide release) greatly influence the acid–base (pH) balance with daily, seasonal, interannual, and regional variations being observed in coastal regions (Wesslander et al. 2010; Wotton et al. 2008).

To estimate the pH of the water, one must consider the concentration of dissolved inorganic carbon, which includes the following components: carbon dioxide (CO_2), carbonic acid (H_2CO_{3aq}), bicarbonate (HCO_{3aq}^-), and carbonate (CO_{3aq}^{2-}), the sum of which is referred to as the total dissolved inorganic carbon (C_T). The state variables for the dissolved inorganic carbon system are C_T and A_T, defined as follows:

$$\begin{aligned} C_T &= [CO_2] + \left[HCO_3^-\right] + \left[CO_3^{2-}\right] \\ A_T &\approx \left[HCO_3^-\right] + 2\left[CO_3^{2-}\right] + \left[B(OH)_4^-\right] + [OH^-] - [H^+] \end{aligned} \tag{2.22}$$

If the total inorganic carbon and total alkalinity are known, we can derive a simplified relationship for the pH by ignoring the presence of boric acid. This simplified analytical relationship is as follows:

$$[H^+] \approx \frac{K_2(2C_T - A_T)}{A_T - C_T} \tag{2.23}$$

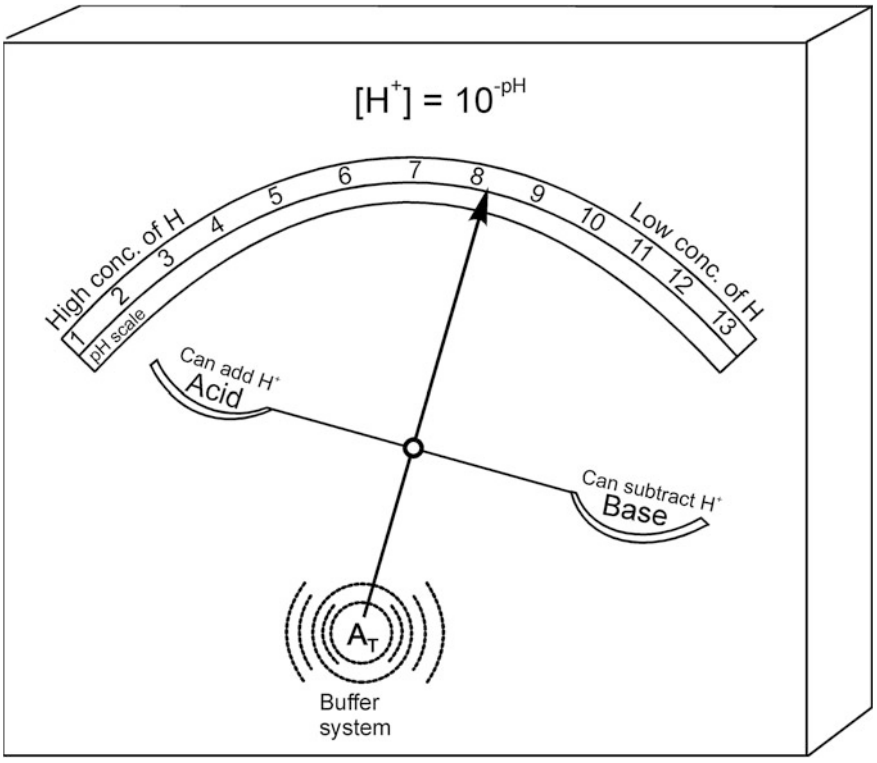

Fig. 2.13 The acid–base (pH) balance depicted as a balance between the concentrations of proton donors and proton acceptors, damped by the buffer system represented by the total alkalinity (A_T)

where K_2 is a solubility constant, which is temperature and salinity dependent. An important aspect of this simplified equation is that the pH ($[H^+] = 10^{-pH}$) of water is dependent on the difference between total alkalinity and total inorganic carbon. For seawater with a temperature of 10 °C and salinity of 10, K_2 is 2.94×10^{-10}. With a total alkalinity of 1600 µmol kg^{-1} and total inorganic carbon of 1500 µmol kg^{-1}, the pH equals 8.4. The mathematical behavior of Eq. 2.23 indicates that pH is mainly dependent on the difference between total alkalinity and total inorganic carbon. In addition, small differences between these parameters can drastically reduce the pH.

Using calculations based on the marine carbon system, the sensitivity of Baltic Sea surface pH was examined by Omstedt et al. (2010). Figure 2.14 illustrates how pH varies with changes in A_T and in the partial pressure of CO_2 in water, pCO_2^W. pH sensitivity to change in A_T varies throughout the Baltic Sea, the greatest impact being anticipated in the north where A_T is the lowest. The buffer effect is illustrated by pH curves becoming less steep at high A_T values.

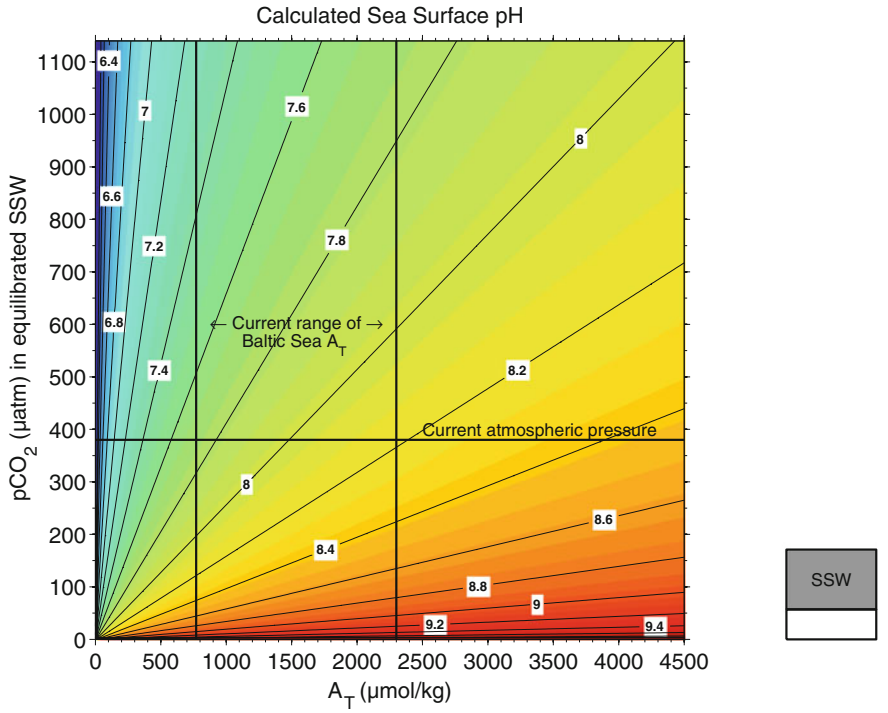

Fig. 2.14 Change of pH with variation in water carbon dioxide pressure and A_T. Salinity is kept at 8 and temperature at 0 °C throughout the calculations. Indicator lines show the current status of the area with regard to A_T (Hjalmarsson et al. 2008) and atmospheric carbon dioxide pressure (Omstedt et al. 2010)

Exercise 2.9
Use pH observations from the Baltic Sea and plot the surface values. Discuss what controls seasonal and long-term variations of the acid–base balance (for the data needed, see Appendix C).

2.11 Some Comments Related to Climate Change

Observations of climate parameters constitute the basis of our understanding of climate and climate change. However, what we subjectively see from data depends greatly on what we are expecting and on our scientific training (BACC I Author Team 2008). Figure 2.15 presents a time series as both original and normalized data. In the figure, the same time series is interpreted in three ways. The original

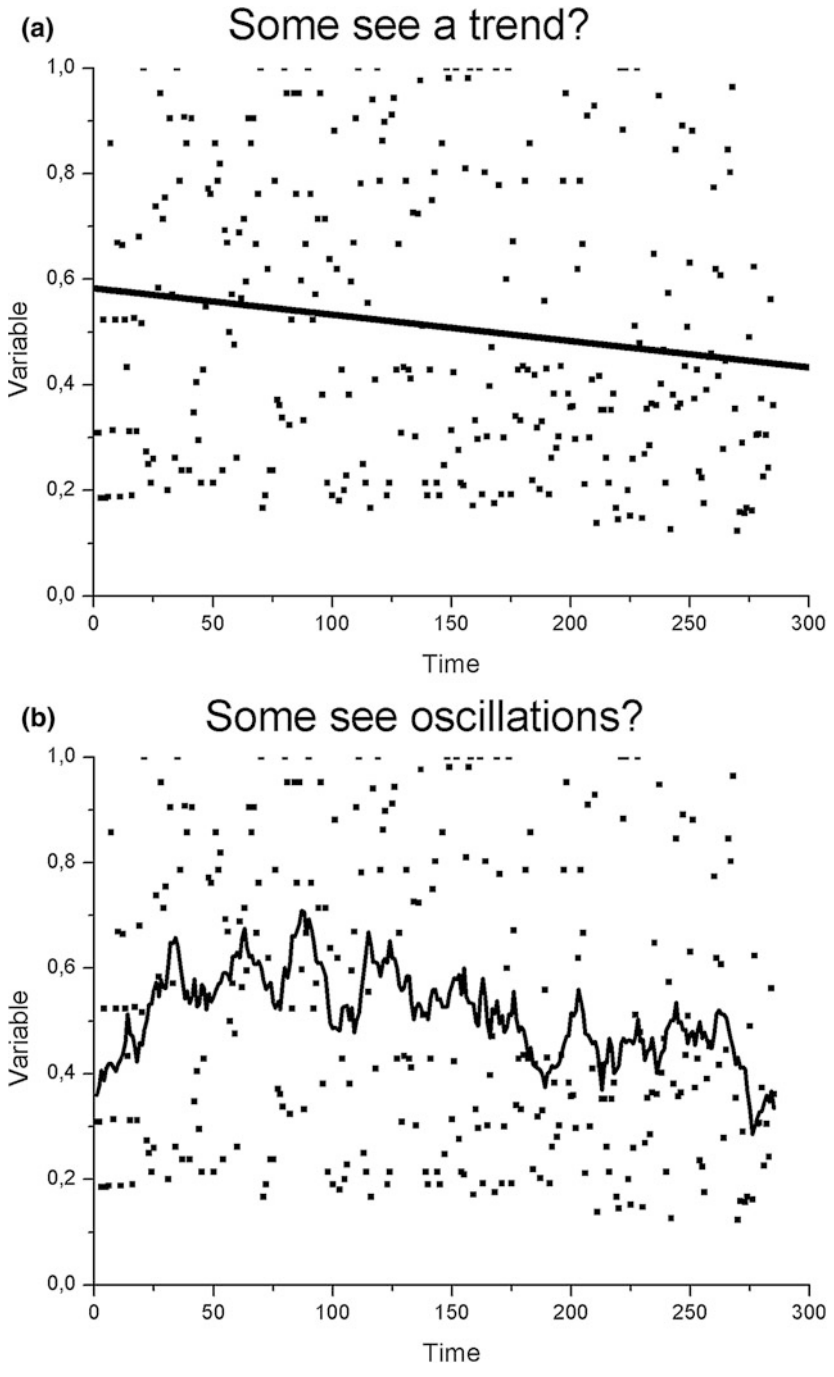

Fig. 2.15 Climate change can be detected in terms of **a** trends, **b** oscillations, and **c** jumps or regime shifts. In this figure, the same data are used and normalized (**a–c**); the original dataset is presented in (**d**) (redrawn from BACC Author Team 2008)

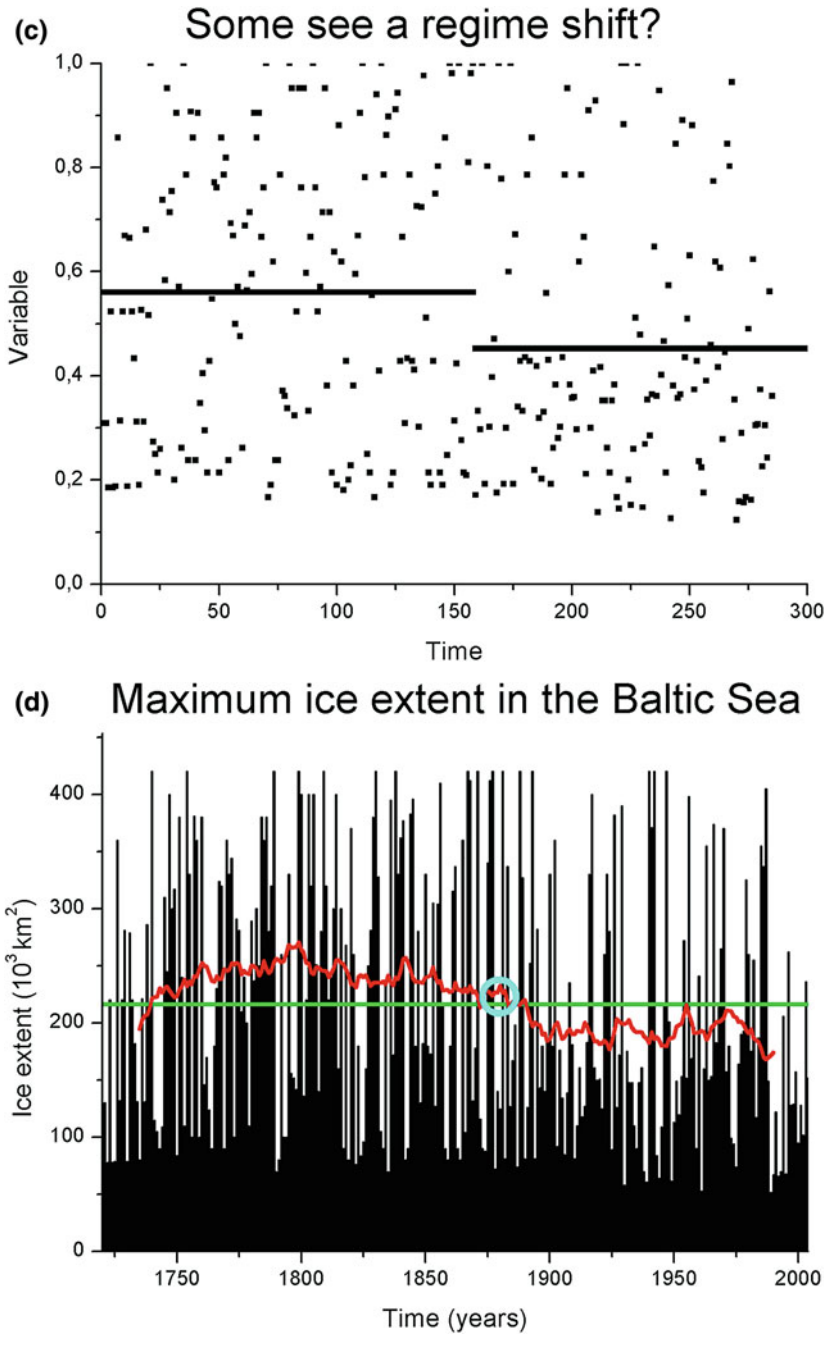

Fig. 2.15 (continued)

dataset captures how the maximum annual ice extent in the Baltic Sea (MIB) has varied from 1720 up to now. Obviously, the data are very noisy. When scientists communicate their results to decision makers or the public, the message is often given political implications. Presenting a trend, the message implies that society must do something. When we present oscillation, the message is that society does not need to take any action. Finally, when we are speaking about regime shifts, the message to the public is that we have found something that will not be able to change back to earlier conditions. How scientists address their messages to the public sends strong implicit signals regarding various potential actions; thus, there is a need for scientists to improve the way in which they convey science in lay terms (e.g., Pielke 2007). Often we need to define terms such as climate variability, climate change, and anthropogenic climate change, as the public understands these terms differently from the way scientists do (BACC I Author Team 2008).

The MIB time series is a key data source for understanding the Baltic Sea climate, and has recently been extended back to AD 1500 (Hansson and Omstedt 2008). While MIB is only an estimated number for each year, it represents an integrated measure of the severity of winter ice. Proxy information about climate change based on MIB, the North Atlantic Oscillation (NAO) index, and Stockholm sea level data gives us a preliminary simplified view of climate change and variability. Using such proxy information together with other long-term datasets, Eriksson et al. (2007) have characterized the last 500 years of climate in northern Europe, illustrating event-type conceptual behavior in 15 different periods.

Climate and weather display stochastic and periodic behavior; to understand such behavior, we must look far into the past. A rule of thumb is that we must understand at least ten 100-year periods in the past, taking us back to AD 1000, to understand the coming 100 years. From the record of the past 500 years, it seems as though the change from the warm 1730s to the extremely cold year 1740 spans the climate variability range in the Baltic Sea region for the last 500 years (Jones and Briffa 2006). Another interesting consideration comes from studies of the Greenland ice and Baltic Sea sediment records: Kotov and Harff (2006) identify periodicities of 900, 500, and 400 years, which they claim reflect climate processes relevant at least to the North Atlantic region. We must therefore consider both the periodic (non-stochastic) and stochastic aspects of our time series when drawing conclusions regarding climate change.

Figure 2.16 presents air temperature in Stockholm, indicating a warmer climate since the end of the nineteenth century, which has been identified as marking the end of the “Little Ice Age” in the Baltic Sea (Omstedt and Chen 2001).

Baltic Sea mean salinity exhibits large variations over long time scales (Winsor et al. 2001, 2003), so systematic increases or decreases may be discerned when limited segments of many years each are considered (see Fig. 2.17). However, the time series extending across the entire twentieth century indicates that thinking in terms of long-term trends makes little sense. Hansson et al. (2010) have reconstructed river runoff to the Baltic Sea, finding no long-term trends over the past 500 years; their study also demonstrated that total river runoff decreased with warmer air temperatures. Omstedt and Hansson (2006a, b) analyzed the Baltic Sea

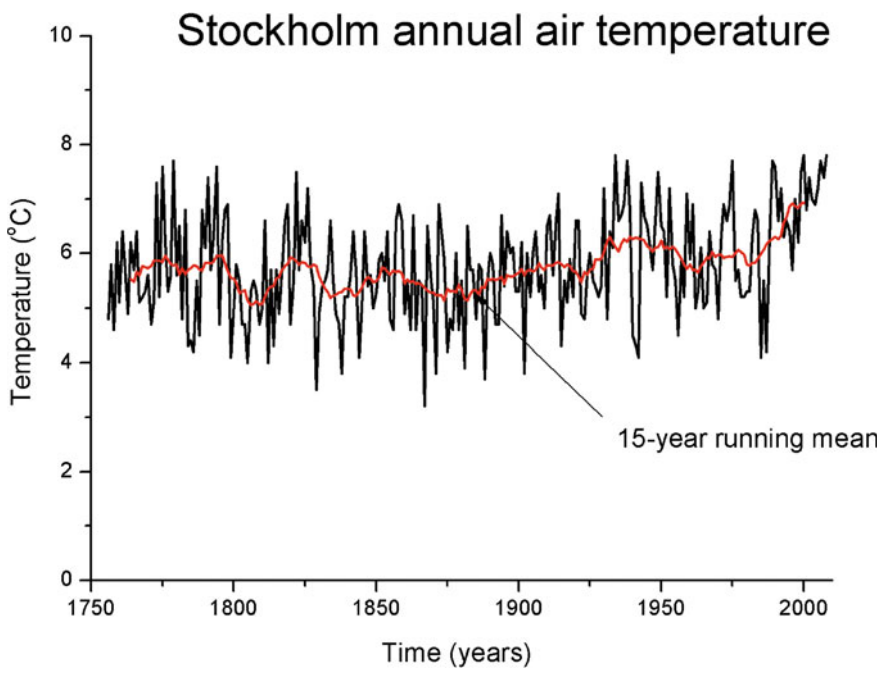

Fig. 2.16 Stockholm annual air temperature; data adjusted for the city effect according to Moberg et al. (2002)

climate system memory and demonstrated that two important time scales should be considered: one is associated with the water balance and has an *e*-folding time of approximately 30 years; the other is associated with the heat balance and has an *e*-folding time of approximately one year. These studies indicate that, on an annual time scale, the Baltic Sea is almost in thermal balance with the atmosphere and that atmospheric changes will rapidly influence the sea ice extent and water temperatures. We therefore expect that the effects of climate warming will first be observed in parameters related to the heat balance, such as water temperature and sea ice extent, and that it will take longer before they can be detected in parameters related to the water balance, such as salinity. This is also in good agreement with BACC assessments (BACC I Author Team 2008; BACC II Author Team 2015), which conclude that the present warming is limited to temperature and directly related variables, such as ice and snow conditions, and that water cycle changes will likely become evident later.

Two very basic climate change questions spring to mind. First, how sensitive is the climate to changes in solar irradiance, atmospheric aerosols, greenhouse gases (including water vapor), and other climate forcing? Second, how large is natural climate variability? Based on proxy data, climate forcing factors have been estimated by several authors (e.g., Crowley 2000). Figure 2.18 depicts the change in radiative forcing over the last 1000 years. The forcing sensitivity between surface

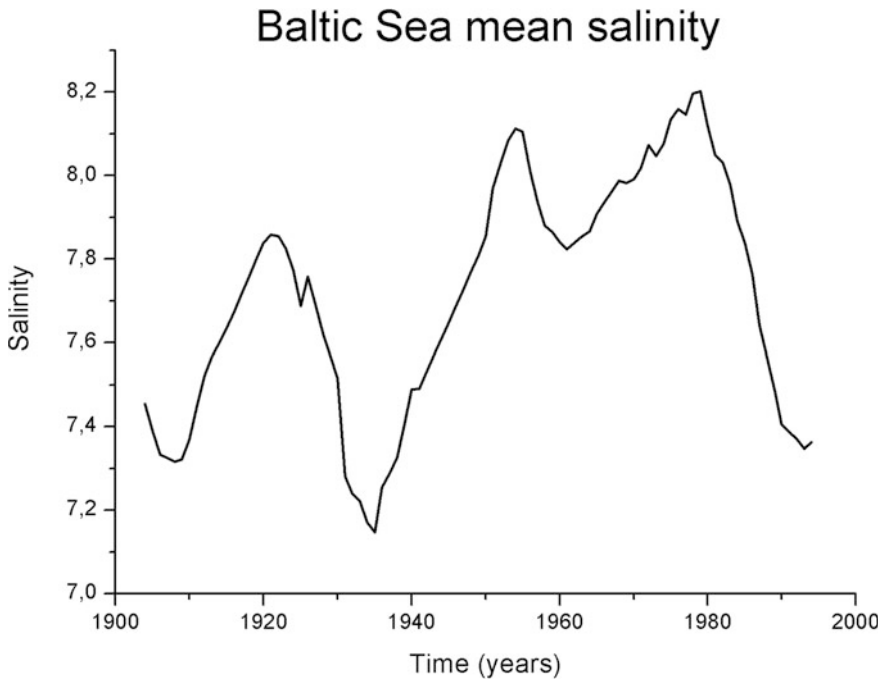

Fig. 2.17 Baltic Sea mean salinity, annually, horizontally, and vertically averaged (from Winsor 2001, 2003)

temperature (ΔT_s) and radiation changes (ΔF) can be studied by considering the net irradiance at the tropopause, which is believed to be a good indicator of global mean temperature (globally and annual averaged), defined as follows (IPCC 2001, p. 354):

$$\Delta T_s / \Delta F = \lambda \tag{2.24}$$

where λ is a constant that, in simplified radiation–convection models, is typically approximately 0.5 K/Wm^{-2}. A change in the radiation balance of 2 Wm^{-2} thus corresponds to a global temperature increase of 1 K.

Currently, the dominant concern is the effects of increased human-produced greenhouse gases and aerosols (IPCC 2013). The increased CO_2 content of the atmosphere is believed to increase the greenhouse effect and therefore warming (the first climate change aspect). How strongly atmospheric CO_2 will increase the atmospheric temperature is under discussion; however, it is generally believed that atmospheric CO_2 first influences the global radiation balance, which may in turn influence the temperature and cloud dynamics. The second aspect of increasing atmospheric CO_2 is its effects on the acid–base (pH) balance in the ocean. Increased atmospheric CO_2 will reduce the ocean pH, which may threaten marine ecosystems.

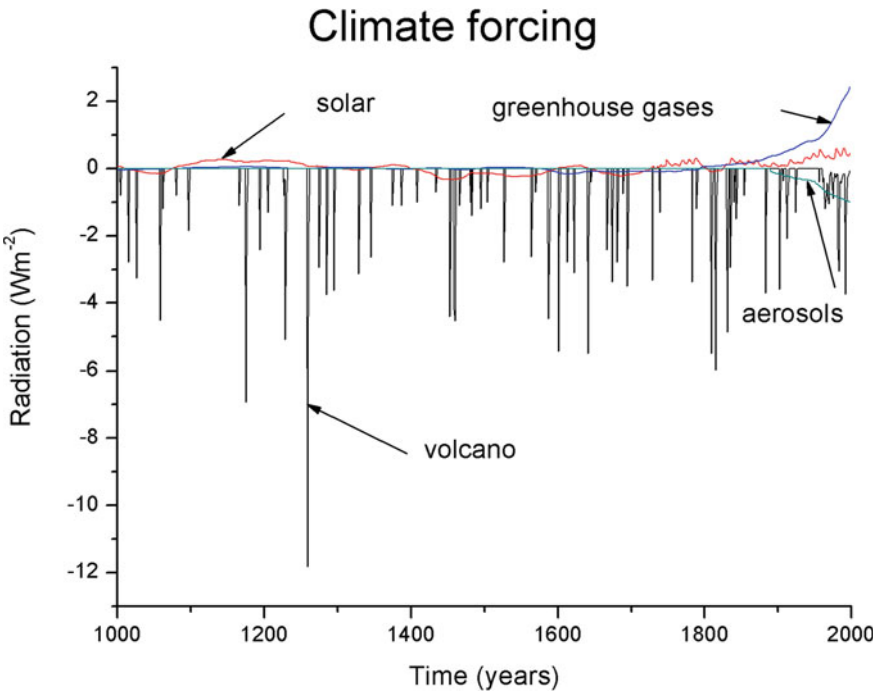

Fig. 2.18 Climate forcing estimates (redrawn from Crowley 2000)

A third aspect of increasing atmospheric CO_2 is its effects on land vegetation and increased biological production on land where water is not a limiting factor. Increased biological production may lead to increasing levels of dissolved organic carbon entering the coastal seas via rivers. Through mineralization processes, this could become an additional source of acid material in the seas.

Few long time series extend to before the eighteenth century, so we should accept that we will probably underestimate variability in both space and time (Storch et al. 2004) by going back only a few hundred years when modeling. Various feedback mechanisms may increase and/or decrease climate change and cause regional differences. Unsurprisingly, it is not easy to attribute present climate change to a single factor, and it is even more difficult to determine the causes of climate change on the regional scale (BACC I Author Team 2008; BACC II Author Team 2015). Determining the various anthropogenic climate effects in combination with natural variability is currently a major research area.

Exercise 2.10
Investigate the climate variability and trend in Stockholm air temperature observations (for the data needed, see Appendix C). What determines the trend? What are the causes of the trend? Can trends tell us anything about the future?

Exercise 2.11
Compare the Stockholm air temperature observations with the long-term variations in sea surface temperatures at Christiansö, near Bornholm Island in the southern Baltic Sea (for the data needed, see Appendix C). Examine the trend of the 15-year running mean data for the period since 1900.

Exercise 2.12
Investigate Stockholm sea level variations relative to climate change (for the data needed, see Appendix C). Assume, as Ekman (2003) does, that the land uplift can be determined from the trend from 1774 to 1864.

Chapter 3
Physical Aspects

3.1 Introduction

The physical processes occurring in water bodies are often of major importance for predicting environmental changes. For example, the water quality in a bay is dependent not only on the load but also on the effectiveness of water exchange with the surrounding sea areas. Typical physical aspects are currents, mixing, water levels, waves, tides, density (which is determined by temperature, salinity, and pressure), sea ice, sea spray, and marine optics and acoustics. In many geophysical applications, a full dataset of relevant parameters is often lacking. Instead, one must combine a number of direct and indirect observations. Knowledge of forcing functions (i.e., meteorological and hydrological conditions), topography, and response functions (e.g., currents, water levels, salinity, temperature, and oxygen) provide a good basis for modeling design. In addition, careful problem analysis and a focused approach will make the modeling work easier.

In this chapter, we will develop our skills at physically modeling lakes and coastal seas. We will use the program for Boundary layers in the Environment (PROBE), a general equation solver for one-dimensional transient or two-dimensional steady-state boundary layers; it was first developed by Svensson (1978). Typical examples of such boundary layers are the Ekman layer and a developing channel flow. The major difficulty with these flows is to characterize the turbulent mixing in mathematical terms. PROBE does this by embodying different kinds of models, including a two-equation turbulence model that calculates mixing coefficients. It is a well-structured program and a suitable teaching tool for studies of lakes, coastal seas, oceans, and the atmosphere—fluid flows in general. A series of equations can be solved using the equation solver and linked runs between coupled sub-basins or boundary layers can be performed. The equation solver lets us build complex but transparent models starting from simple and well-controlled conditions. The main documentation of the program is the *PROBE Manual* (Appendix D). Numerical aspects of solving the equations using the finite volume

A. Omstedt, *Guide to Process Based Modeling of Lakes and Coastal Seas*,
Springer Praxis Books, DOI 10.1007/978-3-319-17990-2_3

method are presented in this manual; they are also available in Versteeg and Malalasekera (1995).

When designing numerical models, several methods should be used to check the results of any application. In initial modeling work, a coarse grid and large time step should be used. To ensure that the numerical solution accurately represents the differential equations, grid and time-step refinements must be carried out. Integral calculations of, for example, volume, salt content, heat content, and nutrient contents are often important check parameters. Conservation checks should therefore always be calculated before the final simulations are performed.

Due to the nonlinearity of the basic equations and the boundary conditions, the numerical prediction of fluid flows is rarely simple. It should be remembered that initial and boundary conditions are often as important as the equations. Analytical solutions or well-controlled laboratory experiments can therefore be very useful for verification studies. Application to geophysical observations is the ultimate test of any model. As Versteeg and Malalasekera (1995) point out: "Throughout, one of the key messages is that CFD (Computer Fluid Dynamics) cannot be professed adequately without reference to experimental validation. The early ideas of the computational laboratory to supersede experimentation have fortunately gone out of fashion."

3.2 Turbulence, Numerical Methods, and Programs

Turbulence is the dominant physical process in transferring momentum, heat, and mass in lakes and coastal seas. In homogeneous fluids, energy is necessarily needed to overcome mechanical friction, while in stratified fluids, energy is also needed to mix heavy fluid or light fluid. In addition, in stratified fluids, energy may be needed to overcome energy loss due to internal wave generation. Internal waves can also break and generate turbulence. Turbulent processes are strongly problem dependent and rely on energy input, geometric conditions, dynamic conditions, and buoyancy. This will be examined in the following sections.

Formal expressions for turbulence can be derived from the time-averaging of the Navier–Stokes equation where the velocity fluctuations give rise to additional stresses on the fluid—so-called Reynolds stresses. Derivations of geophysical fluid dynamics equations are given by Cushman-Roisin and Becker (2011) and for the turbulent equations by Burchard (2002); they can also be found in other standard textbooks, but will not be repeated here. Instead, we will write the general differential equation in a vertically resolved system, which is the main equation modeled in PROBE:

$$\begin{aligned} \frac{\partial \phi}{\partial t} + W\frac{\partial \phi}{\partial z} &= \frac{\partial}{\partial z}\left(\Gamma_\phi \frac{\partial \phi}{\partial z}\right) + S_\phi \\ \Gamma_\phi &= \frac{\mu_{eff}}{\rho \sigma_{\phi eff}} \end{aligned} \tag{3.1}$$

where ϕ is now the mean property (e.g., momentum, temperature, salinity, oxygen, or the concentration of some other chemical compound), W the vertical mean velocity, S_ϕ a source/sink term related to the property considered, Γ_ϕ the effective diffusion coefficient, and μ_{eff} and $\sigma_{\phi eff}$ the effective dynamic viscosity and effective Prandtl–Schmidt number for ϕ, respectively. The coordinates are z in space and t in time. Boundary conditions need to be added to this equation. Equation (3.1) involves processes that act in the vertical dimension and in time; it therefore does not consider changes in the horizontal dimension. However, changes in the horizontal dimension due to, for example, water flows can be modeled by the vertical mean velocity and by integrating the continuity equation (Eq. 2.9), giving:

$$W(z) = \left[Q(z)_{in} - Q(z)_{out}\right]/A(z) \tag{3.2}$$

where the vertical velocity at depth z is calculated from the inflows and outflows at the same level and divided by the water body area at that level.

Equation 3.1 provides the basis for developing our numerical code. The numerics are often structured around a numerical algorithm that can solve the equations. Three numerical solution methods are generally used (i.e., finite difference, finite element, and spectral). The finite volume methods used here were developed from the finite difference formulation and represent a well-established and thoroughly validated approach.

The finite volume method starts by integrating Eq. 3.1 over the (finite) control volumes or grid cells of the solution domain. A grid that resolves the geometry in a finite number of control volumes must be defined (Fig. 3.1). The second step is to derive a general discretization equation from a formal integration of the equation in time and space. The control volume integration distinguishes the finite volume method from other numerical methods and states that the finite-size cells follow the conservation principles. In the present case, the general discretization equation reads:

$$D(i)\theta_d(i) = A(i)\theta_d(i+1) + B(i)\theta_d(i-1) + C(i) \tag{3.3}$$

where θ represents the finite volume form of ϕ, i is the grid cell index going from 1 to N, $A(i)$, $B(i)$, $C(i)$, and $D(i)$ are vectors, and d indicates that the properties are calculated downwards in time. With this choice, the numerical solution technique is fully implicit. The third step is to solve the discretization equation. This can often easily be done using iterative methods. The full derivation of Eq. 3.3 and how it is solved are given in Appendix D.

A brief illustration of the finite volume method is given below in the case of the steady-state diffusion of property ϕ in a one-dimensional domain. The equation reads:

$$\frac{d}{dz}\left(\Gamma\frac{d\phi}{dz}\right) + S = 0 \tag{3.4}$$

The first step is to generate a grid in which each node is surrounded by a control volume using a notation system that can be used in future development (Fig. 3.1).

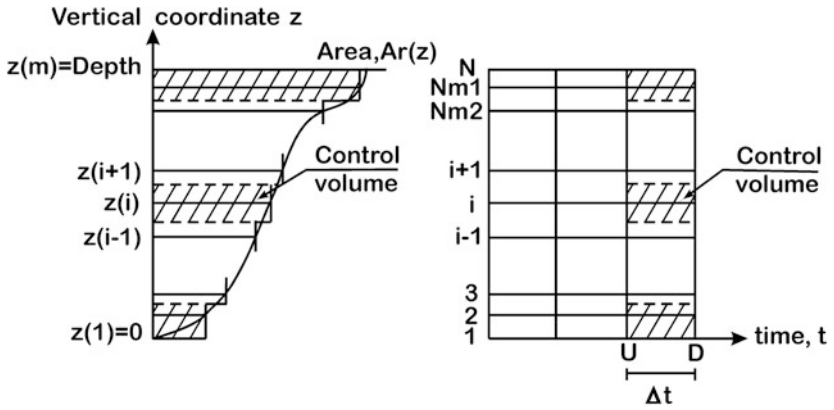

Fig. 3.1 Schematic of a grid that resolves the vertical structure of a sub-basin by changing the area/depth distribution and the corresponding grid in time. This grid is used in the PROBE solver

The next step involves the discretization of the governing equation. This is done by integrating the equation over a control volume, giving:

$$\int_{\Delta V_0} \frac{d}{dz}(\Gamma \frac{d\phi}{dz}) dV_0 + \int_{\Delta V} S dV_0 = (\Gamma A \frac{d\phi}{dz})_{top} - (\Gamma A \frac{d\phi}{dz})_{bot} + \overline{S} \Delta V_0 = 0 \qquad (3.5)$$

where A is the cross-section area and ΔV_0 the control volume. A very attractive feature of the finite volume method is that the discretized equation has a clear physical interpretation. The equation states that the diffusion of ϕ leaving the top face minus the diffusive flux entering the bottom face must balance the source/sink term. We can therefore clearly interpret the conservation properties of the equation.

To derive a useful form of the discretized equation, the interface diffusion coefficient and the gradients at the bottom and top interfaces are required. Using central differencing for the vertical depths, Δz, we write:

$$\begin{aligned}
\Gamma_{top} &= \frac{\Gamma(i+1) + \Gamma(i)}{2} \\
\Gamma_{bot} &= \frac{\Gamma(i) + \Gamma(i-1)}{2} \\
(\Gamma A \frac{d\phi}{dz})_{top} &= \Gamma_{top} A(i) (\frac{\phi(i+1) - \phi(i)}{\Delta z(i)}) \\
(\Gamma A \frac{d\phi}{dz})_{bot} &= \Gamma_{bot} A(i) (\frac{\phi(i) - \phi(i-1}{\Delta z(i)}) \\
\overline{S} \Delta V_0 &= S_u + S_p \phi(i)
\end{aligned}$$

where Δz is the depth interval in the control volume having the area $A(i)$.

By substitution of the equations and some rearrangements, we obtain:

$$d(i)\phi(i) = a(i)\phi(i+1) + b(i)\phi(i-1) + c(i) \tag{3.6}$$

where the coefficients are:

$$a(i) = \frac{\Gamma_{top}}{\Delta z(i)}A(i),\ \mathrm{b}(i) = \frac{\Gamma_{bot}}{\Delta z(i)}A(i),\ \mathrm{c}(i) = S_u,\ \mathrm{d}(i) = a(i) + \mathrm{b}(i) + c(i)$$

Equation 3.6 is in a form that is easily solved using a tri-diagonal matrix algorithm, which is a simplified form of Gaussian elimination that can be used to solve tri-diagonal systems of equations. The interpretation is also easy: The value of ϕ in control volume i depends only on the values above $(i + 1)$ and below $(i-1)$ in the control volume and in the source term.

When working through the chapters of the book, several programs and datasets are needed (see Appendix C); these are organized in one directory for each chapter. Data for the exercises in Chap. 2 are provided in one directory. The directory for Chap. 3 includes several sub-directories needed for modeling the physical aspects. Here, under the file map All files, we find the FORTRAN programs and data needed; the various exercises for Chap. 3 are provided in separate maps. A similar structure is used in the other chapters. Solutions to the various exercises are given in Chap. 6. Appendix A presents a short introduction to FORTRAN, Appendix B defines the nomenclature used in the book, and Appendix C lists all data and programs needed and where to obtain them. The book uses the Intel Visual FORTRAN Compiler (http://software.intel.com/en-us/forums/intel-visual-fortran-compiler-for-windows/); if a different compiler is used, the programs given in All files should be used. The programs are written in FORTRAN 77 and all figures are plotted using ORIGIN (http://www.originlab.com/). Advice on installing PROBE is given in Appendix D. It is recommended that the reader consult the manual (Appendix D) and then reproduce some of the result figures in Chap. 3 to test that the compiler used is being given correct FORTRAN77 commands.

3.3 Modeling the Ekman Ocean Boundary Layer

3.3.1 Introduction

Friction effects at the surface or bottom of the water body act to change the currents and create vertical shear. In geophysical flows, the fluid flow is often turbulent and driven by vertical shear. However, Earth's rotation influences these boundary layers, causing veering. In this section, we learn how to model the structure of both

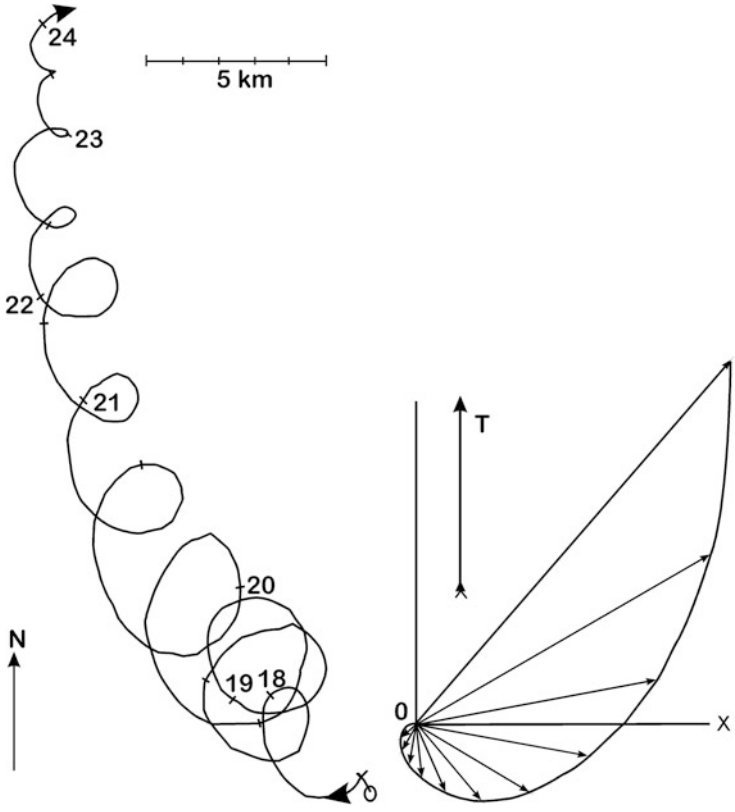

Fig. 3.2 Inertial currents in the surface layer of the Baltic Sea (*left*) and the Ekman spiral in a deep sea (*right*). The figures are redrawn from Gustafsson and Kullenberg (1936) and Ekman (1905), respectively

currents and turbulence in a homogeneous Ekman ocean boundary layer (Fig. 3.2). First, the equations are given, and then the numerical modeling is outlined and discussed. To develop confidence in the modeling, the solution is tested using basic analytical aspects of the boundary layer. We also learn how to test the grid and time-step independence.

3.3.2 Mathematical Formulation

The equations of motion are simplified by assuming that the Rossby number is small, indicating that the nonlinear acceleration terms can be neglected, and that the

Ekman and transient Rossby numbers are close to 1. The transport equations for horizontal momentum then read:

$$\frac{\partial \rho_0 U}{\partial t} = \frac{\partial}{\partial z}\left[\frac{\mu_{eff}}{\rho_0}\frac{\partial \rho U}{\partial z}\right] + f\rho_0 V - C_{decay}\rho_0 U \tag{3.7}$$

$$\frac{\partial \rho_0 V}{\partial t} = \frac{\partial}{\partial z}\left[\frac{\mu_{eff}}{\rho_0}\frac{\partial \rho V}{\partial z}\right] - f\rho_0 U - C_{decay}\rho_0 V \tag{3.8}$$

where U and V are the eastern and northern current components, f the Coriolis parameter, ρ_0 the water density, which in the present equation is treated as constant and equal to 1000 ($m^3\ s^{-1}$), C_{decay} a constant associated with damping, and μ_{eff} the effective dynamic viscosity. Note that we have added a sink term (the last term on the right in Eqs. 3.7 and 3.8) due to inertial wave drag. With $C_{decay} = 0$, the equation represents the transient Ekman flow. The nomenclature is given in Appendix B.

The effective dynamic viscosity, μ_{eff}, is now written as:

$$\frac{\mu_{eff}}{\sigma_{eff}} = \frac{\mu}{\sigma} + \frac{\mu_T}{\sigma_T} \tag{3.9}$$

where μ and μ_T are the dynamic and turbulent viscosities, and σ, σ_T, and σ_{eff} are the Prandtl, turbulent Prandtl, and effective Prandtl numbers, respectively.

Vertical turbulent transport in the surface boundary layer is calculated using the so-called k-ε model, a two-equation model of turbulence in which transport equations for turbulent kinetic energy, k, and its dissipation rate, ε, are calculated. The transport equation for k is:

$$\frac{\partial k}{\partial t} = \frac{\partial}{\partial z}\left[\frac{\mu_{eff}}{\rho_0 \sigma_k}\frac{\partial k}{\partial z}\right] + \frac{\mu_{eff}}{\rho_0}\left[\left(\frac{\partial U}{\partial z}\right)^2 + \left(\frac{\partial V}{\partial z}\right)^2\right] - \varepsilon \tag{3.10}$$

where σ_k is the Schmidt number for k. The corresponding equation for ε reads:

$$\frac{\partial \varepsilon}{\partial t} = \frac{\partial}{\partial z}\left[\frac{\mu_{eff}}{\rho_0 \sigma_\varepsilon}\frac{\partial \varepsilon}{\partial z}\right] + C_{1\varepsilon}\frac{\mu_{eff}}{\rho_0}\frac{\varepsilon}{k}\left[\left(\frac{\partial U}{\partial z}\right)^2 + \left(\frac{\partial V}{\partial z}\right)^2\right] - C_{2\varepsilon}\frac{\varepsilon^2}{k} \tag{3.11}$$

where σ_ε is the Schmidt number for ε, and $C_{1\varepsilon}$ and $C_{2\varepsilon}$ are constants. In the Ekman boundary layer, we assume that the fluid flow is turbulent; the effective dynamic viscosity can then be calculated from:

$$\mu_{eff} = C_\mu \rho \frac{k^2}{\varepsilon} \tag{3.12}$$

where C_μ is a constant.

Wind stresses τ_x^a and τ_y^a are calculated using a standard bulk formulation; the boundary conditions for the momentum equations are:

$$\frac{\mu_{eff}}{\rho_0}\frac{\partial \rho_0 U}{\partial z} = \tau_x^a \tag{3.13}$$

$$\frac{\mu_{eff}}{\rho_0}\frac{\partial \rho_0 V}{\partial z} = \tau_y^a \tag{3.14}$$

where the wind stress components in both the x and y directions can be calculated from:

$$\tau_x^a = \rho^a C_d^a U^a W^a \tag{3.15}$$

$$\tau_y^a = \rho^a C_d^a V^a W^a \tag{3.16}$$

where index a represents air, ρ^a the air density, which equals 1.3 ($m^3\ s^{-1}$), U^a and V^a the wind components in the x and y directions, respectively, $W^a = \sqrt{U^{a2} + V^{a2}}$ the wind speed, and C_d^a the wind stress coefficient with a typical value of 1.3×10^{-3}, increasing with increasing wind speeds. Zero velocities are used for the lower boundary condition.

From the steady-state momentum equation, it can be demonstrated that the mass transport in the Ekman ocean boundary layer is to the right of the wind (in the Northern Hemisphere) and of magnitude:

$$\overrightarrow{M}_E = \frac{\overrightarrow{\tau^a} \times \overrightarrow{k}}{\rho f} \tag{3.17}$$

where the arrows indicate that we are dealing with vectors and $\overrightarrow{k}$ represents the unit vector in the vertical direction and is positive upwards. Ekman mass transport can be calculated from the numerical model according to:

$$M_E = \sqrt{\left(\int_0^D U dz\right)^2 + \left(\int_0^D V dz\right)^2} \tag{3.18}$$

The analytical expression in Eq. 3.17 will be used to test numerical calculations from Eq. 3.18.

3.3.3 Details of Calculations

Equations are solved for a steady wind of 10 m s^{-1} blowing over a 200-m-deep sea. The Coriolis parameter corresponds to the latitude of 60° north. The FORTRAN settings of the case are presented in the subroutine `case_ex1.f` (for the programs needed, see Appendix C) and the main program is `probe2002.f`. The numerical solution has not yet been tested for grid and time-step independence; this will be part of Exercise 3.1. In `subroutine case_ex1.f`, all input and output files are defined.

3.3.4 Results

The results of the calculations, shown in Fig. 3.3a, indicate that the numerical simulation displays strong inertial oscillation. After several inertial periods, the numerical solution slowly approaches the steady state. The number of oscillations needed before the steady-state solution is reached depends on friction effects that can damp the oscillation. Friction effects could be due to either physical (i.e., surface or bottom friction or internal wave drag) or numerical factors. Liljebladh and Stigebrandt (2000) estimated that the inertial oscillation in the Baltic Sea is damped by inertial wave interaction with a typical decay coefficient of $C_{\text{decay}} = 1/(32 \times 3600)$ (s^{-1}). The results of the calculation using internal wave interaction are depicted in Fig. 3.3b and indicate much more realistic damping compared with the observations on the left-hand side of Fig. 3.2.

Exercise 3.1
Run the Ekman boundary layer model until steady state is reached using the decay coefficient of Liljebladh and Stigebrandt (2000). Investigate grid and time-step independence: How many grid cells are needed? How large should the time step be? *Hint*: Link the main program `probe2002.f` with the `case_ex1.f` subroutine that defines the present application. Consult the *PROBE Manual* in Appendix D on how to use PROBE.

3.3.5 Discussion

We have formulated and coded our first model of the upper layers of large lakes or coastal seas. Though we have not dealt with breaking surface waves or Langmuir

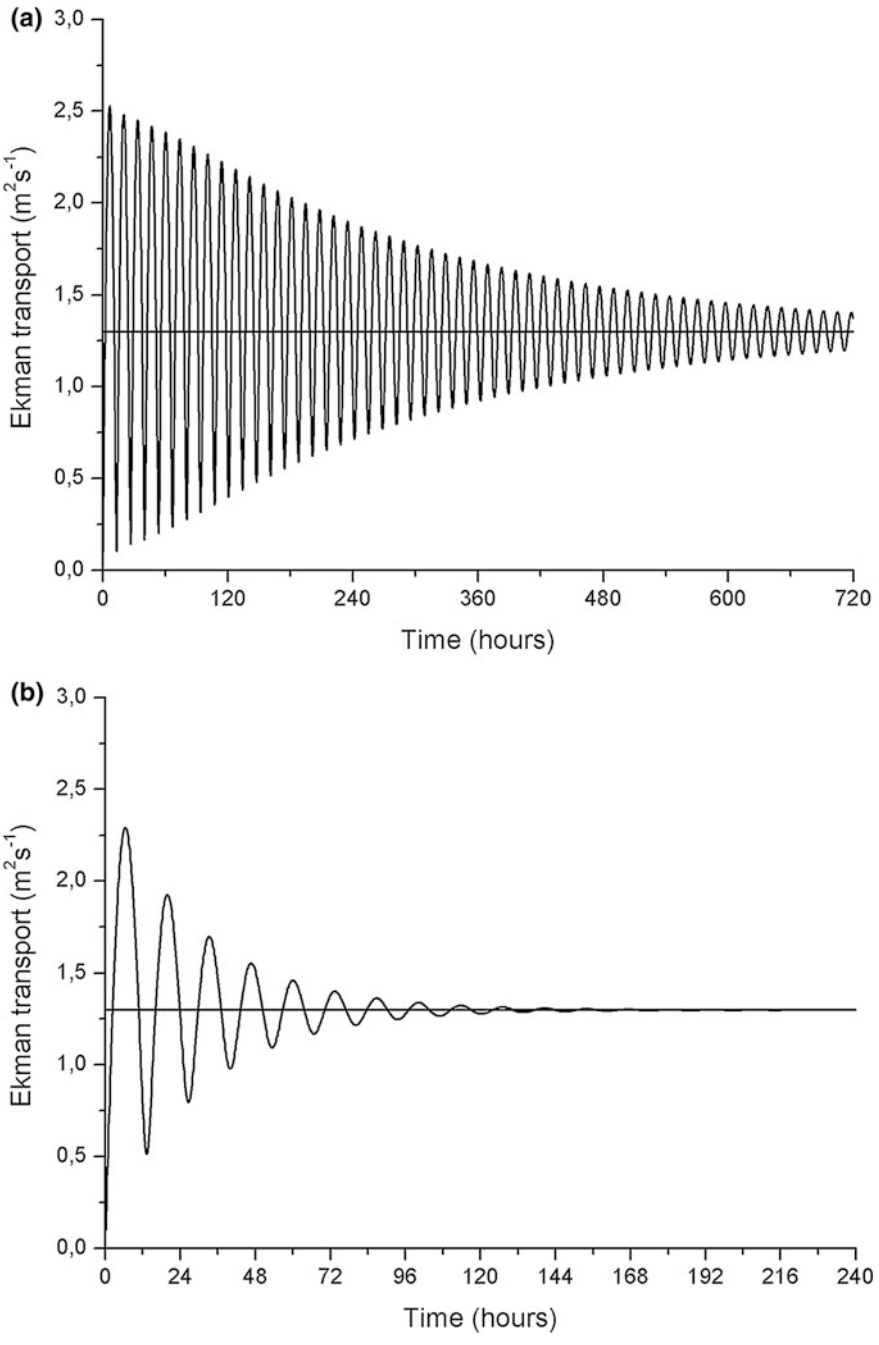

Fig. 3.3 Transient and steady-state Ekman transport based on the numerical (time-dependent curve) and analytical (constant curve) models, respectively. In **a** $C_{decay} = 0$ and in **b** $C_{decay} = 1/(32 \times 3600)$. Note the different scales on the time axes

circulation in the model, it nevertheless provides useful information about effects associated with, for example, changes in water depth, wind speed, and wind direction. Analytical solutions for the surface and bottom Ekman boundary layers can be found in Cushman-Roisin and Becker (2011).

3.4 Modeling Shallow and Deep Lakes

3.4.1 Introduction

This section demonstrates how to model lakes (Fig. 3.4). For shallow lakes, we derive an analytical slab model. By comparing the slab model with a vertically resolved numerical model, we can investigate the importance of depth in lake modeling. In many situations, slab models can be applied, at least in the case of shallow lakes. In the case of deeper lakes, the formation and break-up of the thermocline must be considered. In very deep lakes, we must also keep in mind that the temperature of maximum density is pressure dependent. In making simulations, we read weather data from meteorological observations and calculate the corresponding heat and momentum fluxes. For the deeper lakes, we learn how to increase the number of grid cells used and also how to modify the equation of state.

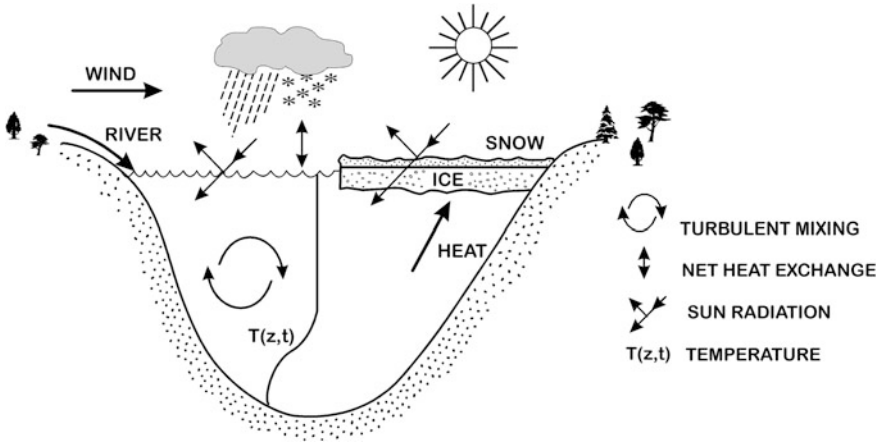

Fig. 3.4 Schematic of physical processes in a lake

3.4.2 Mathematical Formulation

Momentum equations and corresponding boundary conditions have already been given in Sect. 3.3, so they will not be repeated here. Instead, we add some new equations for lake modeling. The conservation equation for heat reads:

$$\frac{\partial \rho c_\rho T}{\partial t} = \frac{\partial}{\partial z}\left[\frac{\mu_{eff}}{\rho \sigma_{eff}} \frac{\partial \rho c_\rho T}{\partial z}\right] + \Gamma_{sun} \tag{3.19}$$

where c_p and T are the heat capacity and temperature of water, and Γ_{sun} the source term for short-wave radiation. The source term is given by:

$$\Gamma_{sun} = F_s^w (1-\eta) e^{-\beta(D-z)} \tag{3.20}$$

where F_s^w is the short-wave radiation through the water surface, η the infrared fraction of short-wave radiation trapped in the surface layer, β the bulk absorption coefficient of the water, and D the water depth.

To relate density and temperature we need to introduce the equation of state, which is approximated according to:

$$\rho = \rho_0 \left(1 - \alpha_1 \left(T - T_{\rho m}\right)^2\right) \tag{3.21}$$

where ρ_0 is a reference density, α_1 a coefficient, and $T_{\rho m}$ the temperature of maximum density. In deeper lakes, pressure effects become important (Carmack and Weiss 1991) and could be added to $T_{\rho m}$. The pressure effect is related to depth, and the temperature of maximum density is:

$$T_{\rho m} = 3.98 - 0.0021(D - z) \tag{3.22}$$

where D is the water depth.

For turbulence, we use the k-ε model but now add the effect of temperature stratification. The transport equations for k and ε then read:

$$\frac{\partial k}{\partial t} = \frac{\partial}{\partial z}\left[\frac{\mu_{eff}}{\rho \sigma_k} \frac{\partial k}{\partial z}\right] + \frac{\mu_{eff}}{\rho}\left[\left(\frac{\partial U}{\partial z}\right)^2 + \left(\frac{\partial V}{\partial z}\right)^2\right] + P_b - \varepsilon \tag{3.23}$$

$$\frac{\partial \varepsilon}{\partial t} = \frac{\partial}{\partial z}\left[\frac{\mu_{eff}}{\rho \sigma_\varepsilon} \frac{\partial \varepsilon}{\partial z}\right] + C_{1\varepsilon} \frac{\mu_{eff}}{\rho} \frac{\varepsilon}{k}\left[\left(\frac{\partial U}{\partial z}\right)^2 + \left(\frac{\partial V}{\partial z}\right)^2\right] + C_{3\varepsilon} \frac{\varepsilon}{k} P_b - C_{2\varepsilon} \frac{\varepsilon^2}{k} \tag{3.24}$$

$$\mu_{eff} = C_\mu \rho \frac{k^2}{\varepsilon} \tag{3.25}$$

where $C_{3\varepsilon}$ is a new coefficient needed in the turbulence model; P_b is the production/destruction due to stratification and can be related to temperature according to:

$$P_b = \frac{\mu_T}{\rho}\left(-\frac{g2\alpha_1\left(T - T_{\rho m}\right)}{\sigma_T}\frac{\partial T}{\partial z}\right) \tag{3.26}$$

Now that we have added a new equation for heat we must also consider its surface boundary condition:

$$\frac{\mu_{eff}}{\rho\sigma_{eff}}\frac{\partial \rho c_p T}{\partial z} = F_n \tag{3.27}$$

$$F_n = F_h + F_e + F_{lu} + F_{ld} + \eta F_s^w \tag{3.28}$$

where the full heat balance at the air–water interface needs to be considered. The various terms are as follows: F_n is the net heat flux, F_h the sensible heat flux, F_e the latent heat flux, $F_{l\mathrm{u}}$ the long-wave radiation from water to atmosphere, F_{ld} the long-wave radiation from atmosphere to water, and F_s^w the sun radiation to the open water surface. The lower boundary condition assumes a zero flux condition (i.e., no sediment heat flux).

For a well-mixed lake, we do not need to consider vertical variation; instead, Eq. 3.19 can be vertically integrated and boundary conditions could be introduced. The lake model (slab) then is as follows:

$$\frac{d\rho c_p T}{dt} = -\frac{1}{D}\left(F_h + F_e + F_{lu} + F_{ld} + F_s^w\right) \tag{3.29}$$

Note that all fluxes are defined as positive in the positive z direction, meaning, for example, that sun radiation is always negative. We should remember that heat may be stored in the sediments and become an important heat flux that must be added to the model. For parameterization of the various fluxes as well as the drag coefficient, see the appendix in Omstedt and Axell (2003).

3.4.3 Details of Calculations

Equations are solved for a 50-m-deep lake using meteorological observations from one station, Gotska Sandön in the central Baltic Sea, over a one-year period. The numerical solution has not been tested for grid and time-step independence. The FORTRAN settings of the case are presented in the subroutine `case_ex2.f` (for the programs needed, see Appendix C). All flux calculations are made in the

subroutine `probeflx_ice.f`. They are also compared with both slab model results and results from a model for a very deep lake, for which we need to consider pressure effects in the temperature of maximum density. In the case of the very deep lake, we need to increase the number of grid cells and change the equation of state; see `case_ex2b.f` and Sect. 5.5 in the *PROBE Manual* (Appendix D).

3.4.4 Results

The results of the calculations are given in Fig. 3.5a. A strong seasonal cycle of surface temperatures is depicted as are variations in the bottom layer. Differences between surface and bottom temperatures clearly indicate that a 50-m-deep lake needs a vertically resolved model. The slab model does a good job, but cannot be used in summer. In Fig. 3.5b, we compare the output of a resolved model with that of the slab model in the case of a 10-m-deep lake. Meteorological forcing mixes the lake completely, and both the slab and the vertically resolved models produce very similar results. Figure 3.6 shows the results for a 500-m-deep lake. The figures indicate that we need to consider pressure effects in very deep lakes, particularly when analyzing effects near the temperature of maximum density.

Exercise 3.2
Compare the slab model with the vertically resolved model, and determine the typical lake depth at which the slab model can be used. Check heat conservation in the vertically resolved model.

3.4.5 Discussion

In Sweden, there are approximately 92,000 lakes larger than 100 × 100 m^2, corresponding to approximately 9 % of the land area. To model the lake effects in high-resolution atmospheric models (HIRLAM), Ljungemyr et al. (1996) introduced lake models that are coupled with the atmospheric model. In this application, slab models were used for all lakes under 10 m deep. Vertically resolved models were used for deeper lakes, though pressure effects were ignored. For Lake Baikal, Carmack and Weiss (1991) demonstrated the importance of also including pressure effects in the equation of state.

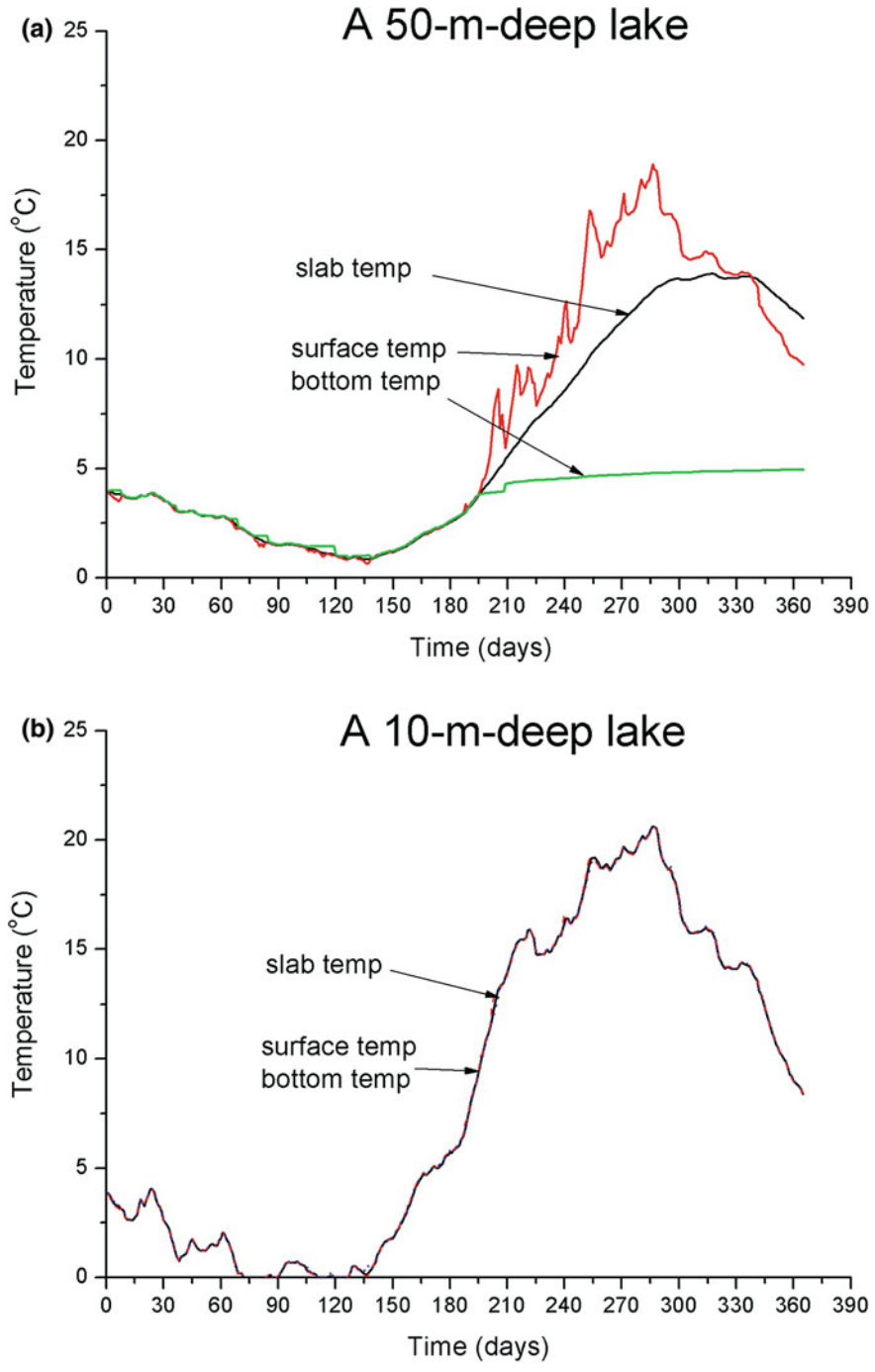

Fig. 3.5 Seasonal cycle of surface and deep water temperatures for **a** a 50-m-deep vertically resolved and not-resolved lake and **b** for a 10-m-deep lake

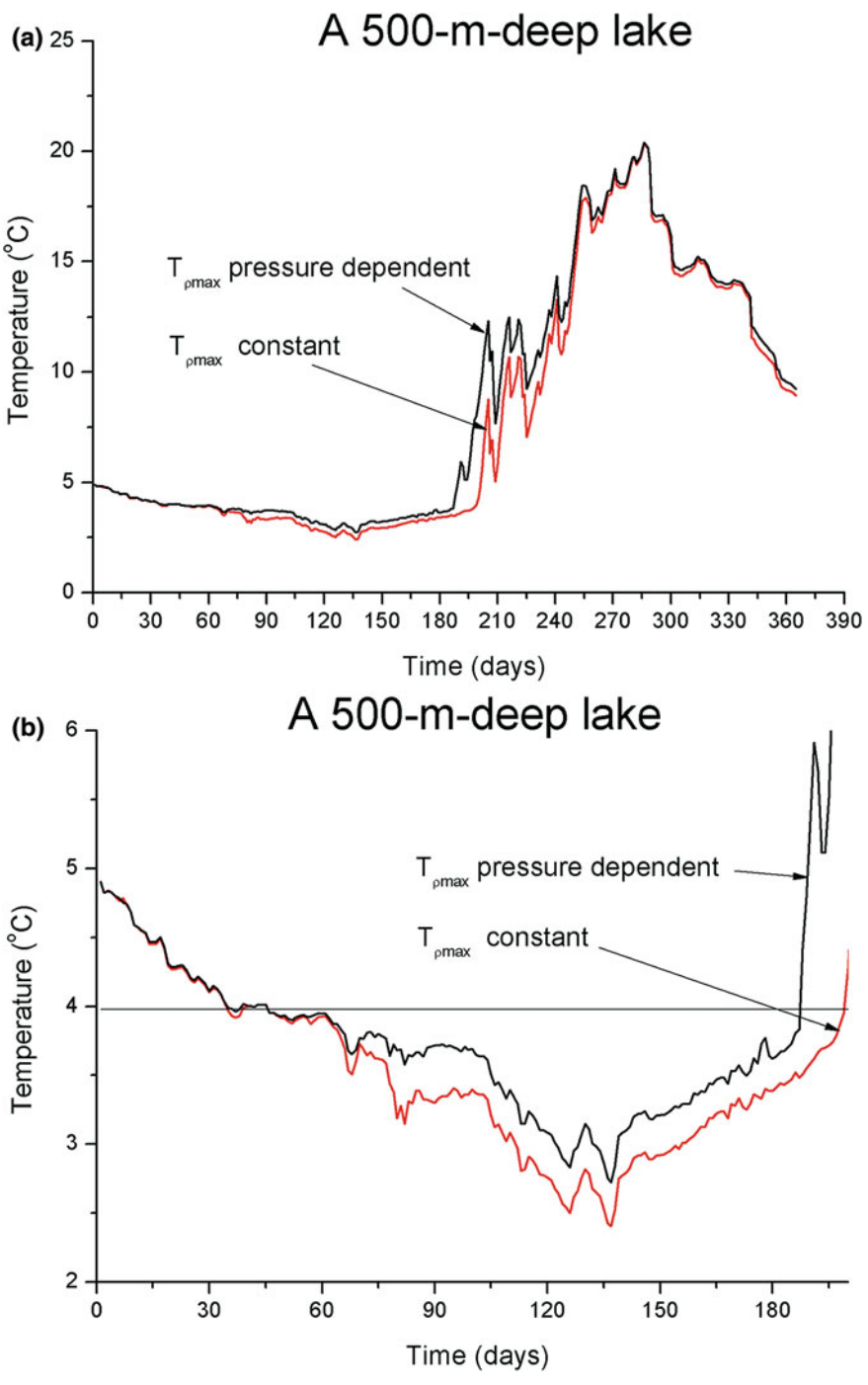

Fig. 3.6 Seasonal cycle of surface water temperatures for a 500-m-deep vertically resolved lake model with (*black lines*) and without (*red lines*) pressure effects on the temperature of maximum density

3.5 Modeling the Ekman Ocean Boundary Layer Influenced by Temperature and Salinity

3.5.1 Introduction

In coastal seas (Fig. 3.7), the turbulence is strongly influenced by temperature and salinity variations. In this section, we learn how to add one more equation, the salinity equation, to the vertically resolved lake model. We also add basin geometry, river runoff, inflows, and outflows to the model. We examine the conservation properties of both heat and salinity and find that salinity conservation is quite easily achieved. Heat conservation requires that sea ice be introduced into the model; this matter will be treated in Sect. 3.6.

3.5.2 Mathematical Formulation

Just as in Sect. 3.3, we start with the Ekman boundary layer equation and the heat equation together with its boundary conditions. We will not repeat them here; instead, we will add an equation needed when modeling marine water bodies. We will also consider the estuarine circulation by adding inflows and outflows to the model. The heat conservation equation then reads:

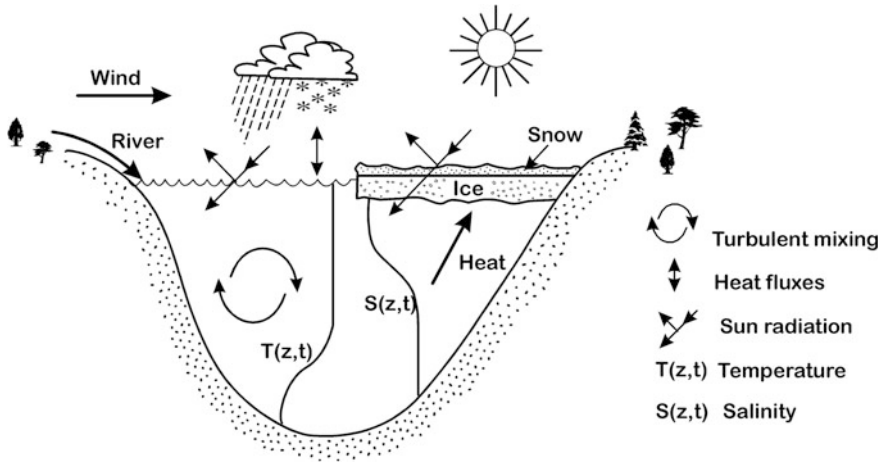

Fig. 3.7 Schematic of physical processes in a coastal sea

$$\frac{\partial \rho c_p T}{\partial t} + W\frac{\partial \rho c_p T}{\partial z} = \frac{\partial}{\partial z}\left[\frac{\mu_{eff}}{\rho \sigma_{eff}}\frac{\partial \rho c_p T}{\partial z}\right] + \Gamma_{sun} \tag{3.30}$$

and

$$W = [Q_{in} - Q_{out}]/A \tag{3.31}$$

where the difference between inflows and outflows divided by the area gives the vertical velocity. We now add a new equation for salt conservation to the lake model presented in Sect. 3.4:

$$\frac{\partial S}{\partial t} + W\frac{\partial S}{\partial z} = \frac{\partial}{\partial z}\left[\frac{\mu_{eff}}{\rho \sigma_{eff}}\frac{\partial S}{\partial z}\right] \tag{3.32}$$

where S is salinity.

The turbulence model is the same as that presented in Sect. 3.4, but the vertical salinity gradient now enters the source/sink term (P_b):

$$P_b = \frac{\mu_T}{\rho}\left(-\frac{g 2\alpha_1 (T - T_{\rho m})}{\sigma_T}\frac{\partial T}{\partial z} + \frac{g\alpha_2}{\sigma_S}\frac{\partial S}{\partial z}\right) \tag{3.33}$$

where σ_T and σ_S are now the turbulent Prandtl/Schmidt numbers. Vertical dynamic eddy viscosity is calculated from the k-ε model, adding a parameterization of the deep-water mixing according to Stigebrandt (1987) to allow for the effects of breaking internal waves:

$$\mu_{eff} = C_\mu \rho \frac{k^2}{\varepsilon} + \rho \sigma_T \nu_T^d \tag{3.34}$$

$$\nu_T^d = \alpha_{deep} N^{-1} \tag{3.35}$$

N is the Brunt–Väisälä frequency ($N^2 = -\frac{g}{\rho_0}\frac{d\rho}{dz}$) and α_{deep} is a constant that can be estimated based on temperature, salinity, and oxygen data (e.g., Axell, 1998).

The boundary condition for the salt equation reads:

$$\frac{\mu_{eff}}{\rho \sigma_{eff}}\frac{\partial S}{\partial z} = S_{sur}(P - E) \tag{3.36}$$

where (P−E) is the net precipitation rate and S_{sur} the surface salinity. Note that there is a clear coupling between the heat cycle (i.e., the latent heat flux, F_e) and the water cycle (i.e., evaporation $E = \frac{F_e}{L_e \rho}$, where L_e is latent heat of evaporation). Precipitation (P) and evaporation (E) rates are always treated as positive quantities. For the lower boundary condition, a zero flux condition is assumed.

Salinity effects also enter into the equation of state and can be approximated as:

$$\rho = \rho_0\left(1 - \alpha_1\left(T - T_{\rho m}\right)^2 + \alpha_2 S\right) \tag{3.37}$$

where α_1 and α_2 are constants and $T_{\rho m}$ is the temperature of maximum density (a function of salinity) and can be approximated for surface waters as:

$$T_{\rho m} = 3.98 - 0.22S \tag{3.38}$$

Salinity also influences heat capability, and for surface water it can be approximated as:

$$c_p = 4217.4 - 3.7T - 7.6S \tag{3.39}$$

More precise formulas can be found in Millero (1978) and Millero et al. (1973).

3.5.3 Details of Calculations

Equations are solved for a 100-m-deep basin with the geometry of Bothnian Bay, a sub-basin of the Baltic Sea. The weather data file comprises data from the same basin. A two-year run is performed and surface temperatures drop to the freezing point. The present treatment of the turbulence was first introduced by Omstedt (1990a) and has since been used in several Baltic Sea applications. A simple assumption is introduced in this section, namely, that the surface temperature never drops below freezing. Conservation checks are calculated and constant river runoff into the basin is assumed. The FORTRAN settings of the case are presented in the subroutine `case_ex3.f` (for the programs needed, see Appendix C), which is linked to the main program and to subroutines for heat fluxes and turbulent mixing.

3.5.4 Results

The results of the calculations appear in Fig. 3.8. The cooling of the surface layer, depicted in Fig. 3.8a, is strongly influenced by the halocline depth, shown in Fig. 3.8b. Salinity becomes homogeneous after a one-year run, after which stratification is due solely to temperature, because estuarine circulation is not included in this run. Estuarine circulation can be studied by adding river runoff (Q_r = 3000 m^3 s^{-1}) and a 3.5-times-greater inflow of more saline deep water to the model (Fig. 3.9). The model is now run for a five-year period; the temperature structure indicates that the winter temperatures extend to a depth of approximately 60 m.

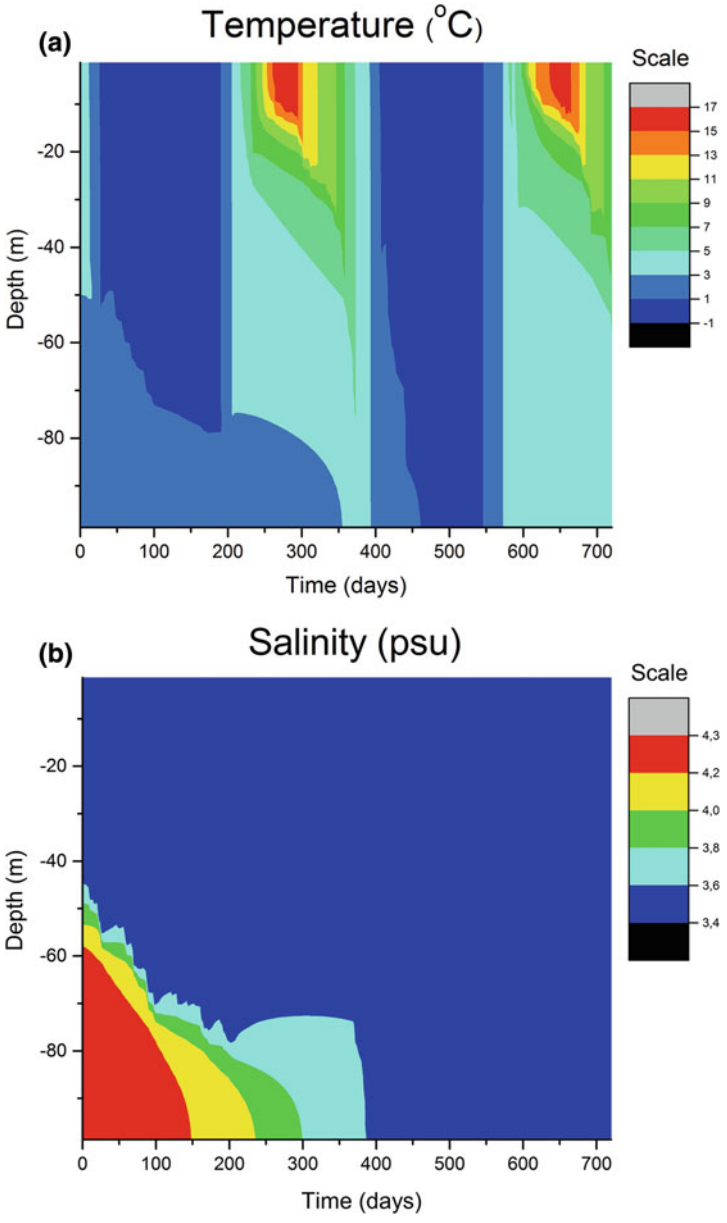

Fig. 3.8 Calculated **a** temperatures and **b** salinities based on typical autumn conditions in Bothnian Bay; estuarine circulation is excluded from the calculations

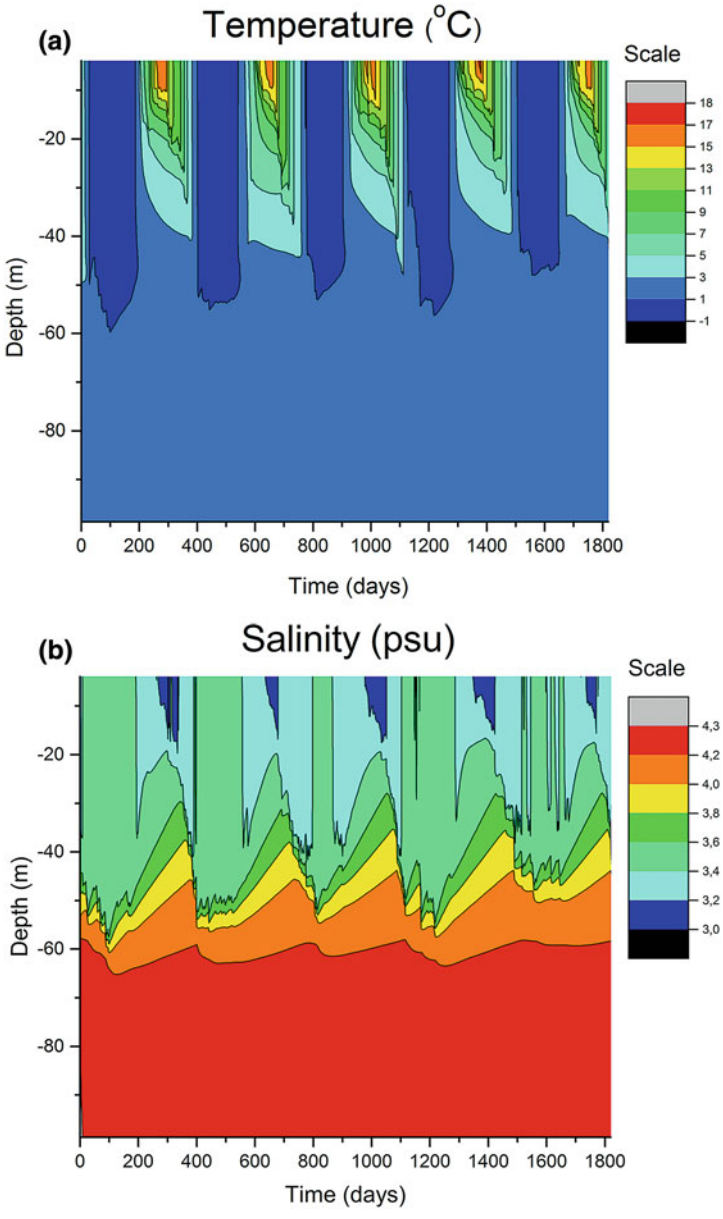

Fig. 3.9 Calculated **a** temperatures and **b** salinities based on typical autumn conditions in Bothnian Bay; estuarine circulation is included in the calculations

Salinity stratification is kept at realistic levels and surface salinity drops in summer due to the reduced mixed layer associated with the thermocline.

Heat and salt conservation are depicted in Fig. 3.10. As can be seen, salt conservation is well controlled, but this is not the case for heat conservation. Heat conservation changes when the sea surface temperature is near freezing, so the assumption with regard to conservation principles fails in the winter.

Exercise 3.3
Model estuarine circulation by adding river runoff (Q_r = 3000 m^3 s^{-1}) and a 3.5-times-greater inflow of more saline deep water to the model. Assume that inflows and outflows balance. What is the typical stratification spin-up time for the basin? For how long will the initial conditions influence the results? *Hint:* Use the *e*-folding time (i.e., the time needed for the salinity or temperature to increase or decrease by a factor of *e*) as an indication of the spin-up time.

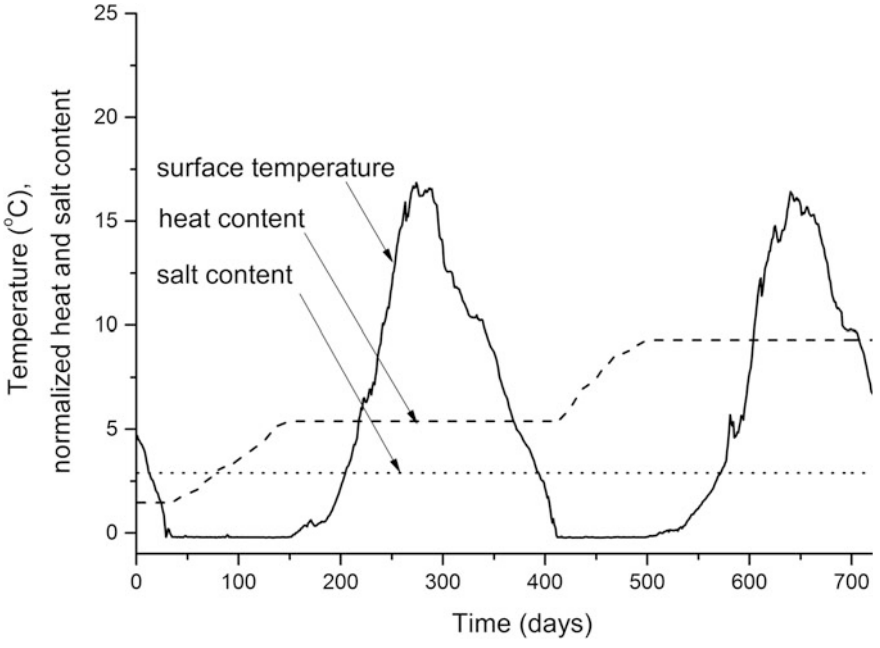

Fig. 3.10 Calculated sea surface temperature (*solid line*), heat content (*dashed line*), and salt content (*dotted line*) over a two-year simulation

3.5.5 Discussion

Stratification strongly affects turbulent mixing, particularly in estuaries. An analytical solution for the mixed layer depth associated with brackish outflowing water was developed by Rodhe (1991) and compared with the results of the PROBE model by Broström and Rodhe (1996). As salinity in estuaries is often not well mixed in the vertical, this can strongly influence the temperatures. The importance of both temperature and salinity gradients in mixed-layer dynamics was demonstrated by Omstedt et al. (1983) when they studied surface water cooling. Eilola (1997) examined the formation of the spring thermocline and the importance of river runoff in mixed-layer dynamics.

Omstedt and Hansson (2006a, b) have examined the stratification spin-up time for the Baltic Sea, demonstrating that two time scales need to be considered: one of approximately 30 years associated with the water balance (salinity) and another of approximately one year associated with the heat balance (temperature). The model equations are strongly influenced by initial conditions until the spin-up time has been reached. Afterwards, the equations are mainly influenced by boundary conditions, such as air–sea interaction, and basin inflows and outflows.

3.6 Modeling an Ice-Covered Ocean Boundary Layer

3.6.1 Introduction

Ice plays an important role in the heat and water exchange in cold regions (Fig. 3.11). The role of sea ice is particularly related to changes in heat and salt fluxes and in momentum exchange. In addition, river runoff and flow through channels and straits are influenced by sea ice. In this section, we will learn how to add sea ice to our model from Sect. 3.5 and demonstrate that the model is now in accordance with the heat and salt conservation principles. We will then investigate the annual mean heat budget and the role of sea ice with respect to the total heat budget.

3.6.2 Mathematical Formulation

The equations for momentum, heat, salinity, and turbulence and the equation of state are much the same as those presented earlier and will not be repeated here. However, boundary conditions do change under ice-covered conditions, so they are

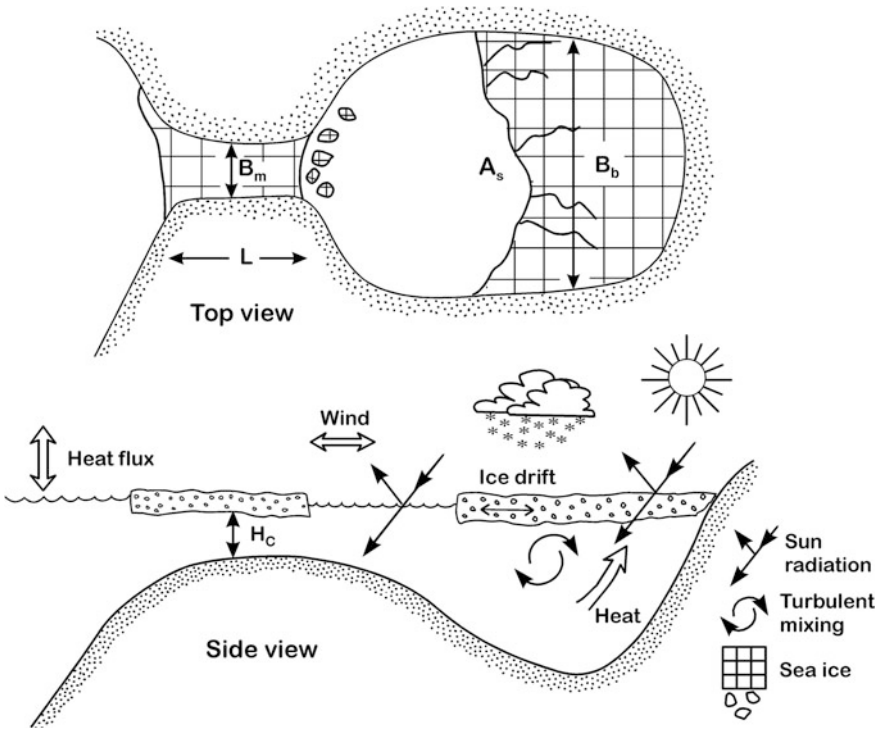

Fig. 3.11 Schematic of the upper layers of the ocean as influenced by sea ice

presented here. The boundary conditions for the momentum equations during ice cover are:

$$\frac{\mu_{eff}}{\rho_0}\frac{\partial \rho_0 U}{\partial z} = \tau_x^i \tag{3.40}$$

$$\frac{\mu_{eff}}{\rho_0}\frac{\partial \rho_0 V}{\partial z} = \tau_y^i \tag{3.41}$$

The stress terms between ice and water, i.e., τ_y^i and τ_y^i, are:

$$\tau_x^i = \rho_0 C_d^i \left(U^i - U\right)\left|W^i - W\right. \tag{3.42}$$

$$\tau_y^i = \rho_0 C_d^i \left(V^i - V\right)\left|W^i - W\right. \tag{3.43}$$

where U^i and V^i are the ice drift components in the x and y directions, respectively, $W^i = \sqrt{U^{i2} + V^{i2}}$ the ice drift, and C_d^i the ice–water drag coefficient. The last

variable depends on ice types, and has a value of approximately 1–20 × 10^{-3} (Omstedt 1998). For the lower boundary, zero velocities are used.

The boundary conditions for the heat equation during ice season are:

$$T(z=0) = T_f(S_o) \tag{3.44}$$

$$\frac{\mu_{eff}}{\rho_0 \sigma_{eff}} \frac{\partial \rho_0 c_p T}{\partial z} = F_w \tag{3.45}$$

where T_f is the freezing point at the interfacial salinity, S_0, and F_w is the heat flux from water to ice. For the lower boundary condition, a zero-flux condition (no sediment heat flux) is used.

Boundary conditions for the salinity equation during the period of ice cover are:

$$\frac{\mu_{eff}}{\rho_0 \sigma_{eff}} \frac{\partial S}{\partial z} = \frac{\rho_i}{\rho_0} \frac{dh_i}{dt} (S_i - S_0) \tag{3.46}$$

where h_i is the ice thickness, ρ_i the ice density, and S_i the ice salinity. The ice growth/melting play similar roles in ice-covered seas as does net precipitation ($P-E$) in open waters (Eq. 3.36). For the lower boundary condition, a zero-flux condition is used.

To bridge the fully turbulent ocean layer beneath the drifting ice and the viscous sublayer adjacent to it, we introduce wall functions. McPhee, Maykut, and Morrison (1987) tested several wall functions, finding that fully turbulent models predicted unrealistically high melting rates and that viscous sub-layer models underestimated the melting. Quite realistic values, however, were obtained using wall function formulations according to Yaglom and Kader (1974); these formulations were also applied in Baltic Sea modeling by Omstedt (1990c). Wall functions can be expressed as follows:

$$\begin{aligned} St_T^{-1} &= b\left(\frac{u_* z_0}{\nu}\right)^{0.5} \mathrm{Pr}_L^{0.67} \\ St_S^{-1} &= b\left(\frac{u_* z_0}{\nu}\right)^{0.5} Sc_L^{0.67} \end{aligned} \tag{3.47}$$

where St_T and St_S are the Stanton numbers for temperature and salinity, respectively, u_* and z_0 the parameters for friction velocity and roughness, respectively, b a constant equal to 1.57, Pr_L (= 13.8) the laminar Prandtl number, and Sc_L (= 2432) the laminar Schmidt number.

When modeling ice growth and decay, we consider only a few of the basic processes. Columnar ice (h_i^c) grows proportionally to the square root of heat loss. In open water, however, ice grows faster due to the formation of frazil ice (h_i^f), which

grows linearly with heat loss. The rates of columnar and frazil ice growths are formulated as:

$$\rho_i L_i \frac{dh_i^c}{dt} = \frac{k_i k_s}{k_i h_s + k_s h_i^c}\left(T_f - T_{sur}\right) - F_w \tag{3.48}$$

$$\frac{dh_i^f}{dt} = \frac{F_n}{L_i \rho_i} \tag{3.49}$$

where ρ_i is ice density, L_i latent heat of ice, T_{sur} upper ice surface temperature, h_s snow thickness, and k_i and k_s the thermal conductivity of ice and snow, respectively.

For polar and subpolar seas, it is important to model the extent of open and ice-covered areas. Change in the horizontal extent of ice is due partly to ice drift and waves and partly to thermodynamic processes. Change in the position of the ice edge, X_f, can be expressed as a balance between ice drift and horizontal ice growth, as follows:

$$\frac{dX_f}{dt} = U^i - \frac{X_f}{h_i}\frac{F_n}{\rho_i L_i} \tag{3.50}$$

Horizontal ice edge growth or decay depends on a balance between ice drift and ice formation/melting. The ice drift equation reads:

$$U^i = \begin{cases} U_{free}^i - \dfrac{\alpha_{ip} P_i}{X_d - X_f} & U^i \geq 0 \\ U_{free}^i & U^i \leq 0 \end{cases} \tag{3.51}$$

where U_{free}^i is assumed to be 2 % of the wind speed, P_i is ice strength (Nm^{-2}), and α_{ip} is a coefficient with the unit ($\mathrm{m}^2\ \mathrm{skg}^{-1}$). It is assumed that ice drift in a positive x direction represents onshore ice drift, while ice drift in a negative x direction represents offshore ice drift. When calculating the ice strength, we follow Hibler (1979) and write:

$$P_i = P_* h_i e^{-c_i(1-A_i)} \tag{3.52}$$

where P_* and c_i are often treated as constants and A_i is the ice concentration. In coastal seas, the parameterization of ice strength has been shown to be proportional to the square of the ice thickness (Overland and Pease 1988; see also, or Omstedt 1990c).

3.6.3 Details of Calculations

We start with the model developed in Sect. 3.5. Meteorological forcing data are replaced with data from Bothnian Bay, a northern Baltic Sea sub-basin that is ice covered every year. Wall functions (i.e., Stanton numbers) are introduced for the ice-covered case, but we do not introduce the ice front model yet; instead, we calculate only the ice growth and decay. The FORTRAN settings of the case are presented in the subroutine `case_ex4.f` (for the programs needed, see Appendix C).

3.6.4 Results

The results of a five-year run are depicted in Fig. 3.12. From the figure, we can see that the heat conservation law is well modeled. Interannual variability can be examined by looking at the annual maximum ice thickness and temperature. Sea surface salinity and salt content are depicted in Fig. 3.13. As can be seen, the model also conserves salinity.

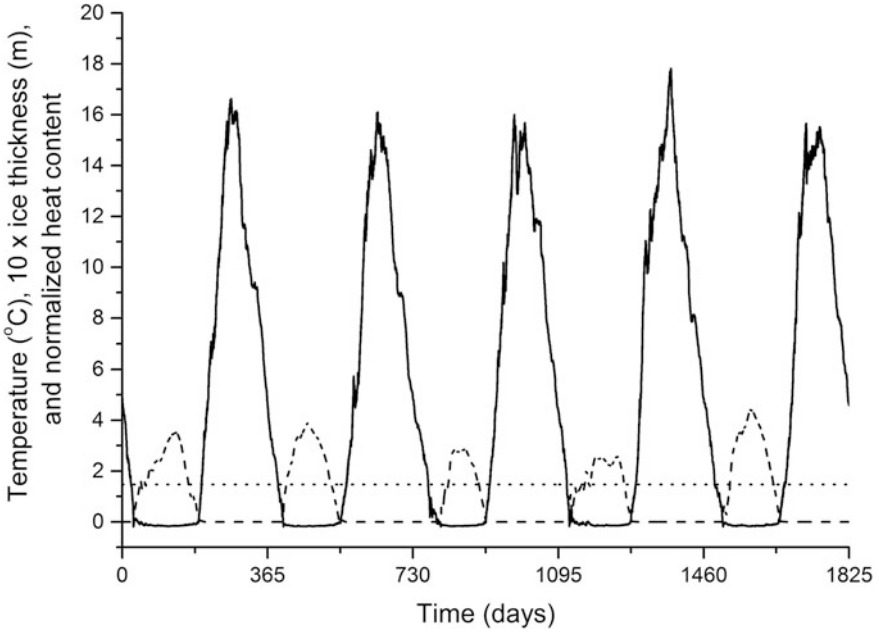

Fig. 3.12 Five-year simulation indicating that the model now conserves heat. The figure shows sea surface temperature (*solid line*), ice thickness multiplied by 10 (*dashed line*), and normalized heat content (*dotted line*)

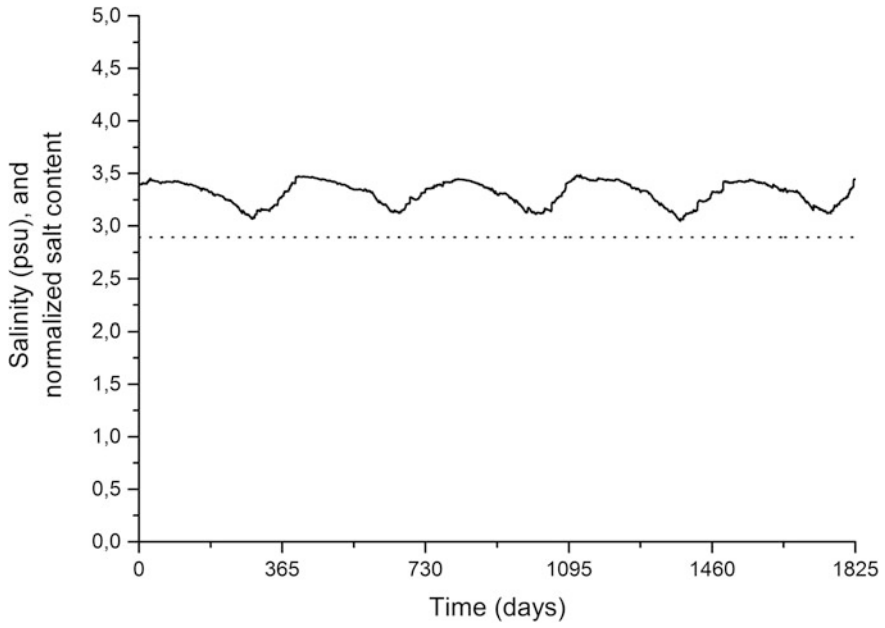

Fig. 3.13 Five-year simulation indicating that the model conserves salt. The figure shows sea surface salinity (*solid line*) and normalized salt content (*dotted line*)

Exercise 3.4
Examine the heat balance of an ice-covered water body. Run the model for a period of five years, and plot both the sensible and latent heat fluxes, net long-wave radiation, solar radiation, and the heat flow from water to ice. How does adding sea ice to the model alter the radiation balance?

3.6.5 Discussion

In the present model, we have only dealt with some basic aspects of the ice. Snow ice and ice ridging may considerably change the ice growth and decay (e.g., Launiainen et al. 2001; Saloranta 1998). Changes in ice concentration have been dealt with in a simplified way by only considering onshore and offshore winds and are available in the PROBE-Baltic model system presented in Chap. 5. Further studies of sea ice drift and turbulent mixing beneath sea ice can be found in, for example, Leppäranta (2011) and McPhee (2008).

3.7 Modeling Turbulence in the Upper Layers of the Ocean

3.7.1 Introduction

Turbulence is a key factor in the functioning of many marine systems (Fig. 3.14) and several models of turbulence have been developed (Burchard 2002). There are various schemes for classifying turbulence models; in this section we will follow that of Rodi (1987). We start with simple, zero-equation models, which do not involve transport equations for the turbulence quantities. We then consider one-equation models that solve the turbulent kinetic energy equation. Finally, we compare the results of one-equation models with those of a two-equation model of turbulence, the k-ε model. As turbulent flows contain length and time scales that change dramatically from one flow to another, one may argue that two-equation models constitute the minimum physically acceptable level of closure (Speziale 1996). This is the main reason a general equation solver such as PROBE includes two-equation models as standard tools for boundary layer applications.

3.7.2 Mathematical Formulation

3.7.2.1 Zero-Equation Models

We now offer three examples of zero-equation models. Svensson (1979) analyzes the turbulent Ekman boundary layer using the k-ε model and finds that eddy viscosity in the homogeneous case can be calculated according to:

$$v_T = 0.026\frac{u_*^2}{f} \tag{3.53}$$

The friction velocity, u_*, is defined as equal to $\sqrt{\frac{\tau}{\rho}}$, where τ is assumed to equal the air stress, i.e., $\tau = \rho^a C_d^a W^a$.

The formulation indicates that wind and the Earth's rotation are the parameters that may influence eddy viscosity.

Pacanowski and Philander (1981) examined the vertical mixing in tropical oceans, suggesting a Richardson number-dependent eddy viscosity parameterization:

$$v_T = \frac{v_0}{(1+5R_i)^2} + v_b \text{ where } R_i = \frac{-\frac{g}{\rho_0}\frac{\partial \rho}{\partial z}}{\left[\left(\frac{\partial U}{\partial z}\right)^2 + \left(\frac{\partial V}{\partial z}\right)^2\right]} \tag{3.54}$$

where v_0 and v_b are constants that in their study are set to 10^{-2} ($m^2\ s^{-1}$) and 10^{-4} ($m^2\ s^{-1}$), respectively, and R_i is the Richardson number. This formulation was developed for the tropical oceans and mainly considered the importance of

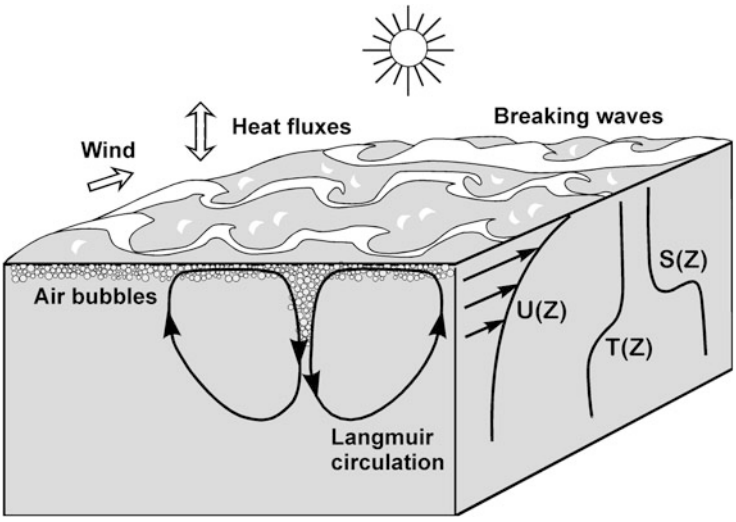

Fig. 3.14 Schematic of the problem

stratification in eddy viscosity formulation, but did not take into account wind dependence.

In a data assimilation system for the Baltic Sea, Sokolov et al. (1997) introduced an eddy viscosity parameter which, according to Marchuk, is formulated as:

$$v_T = (0.05h)^2 \sqrt{\left(\frac{\partial u}{\partial z}\right)^2 + \left(\frac{\partial v}{\partial z}\right)^2 - \frac{g}{\rho_0}\frac{\partial \rho}{\partial z}} \tag{3.55}$$

The constant h in the equation was set equal to 2 (m). The formulation considers both stratification effects and winds through the velocity shear.

3.7.2.2 One-Equation Models

Several one-dimensional models have been used, particularly in meteorology. We now use a one-dimensional model from Rodi (1987) based on the turbulent kinetic energy equation:

$$\frac{\partial k}{\partial t} = \frac{\partial}{\partial z}\left[\frac{\mu_{eff}}{\rho\sigma_k}\frac{\partial k}{\partial z}\right] + \frac{\mu_{eff}}{\rho}\left[\left(\frac{\partial U}{\partial z}\right)^2 + \left(\frac{\partial V}{\partial z}\right)^2\right] + P_b - \varepsilon \tag{3.56}$$

To resolve this equation, we must make an assumption about the dissipation of the turbulent kinetic energy, ε. From dimensional analysis, ε can be related to the turbulent kinetic energy, k, as follows:

$$\varepsilon = c_D \frac{k^{1.5}}{L} \tag{3.57}$$

where L is the length scale for large-scale motion. The key problem with one-equation models is specifying this length scale, and there are various suggestions for doing this. Here we assume that L can be written:

$$L = 0.4(D - z) \tag{3.58}$$

Furthermore, from dimensional analysis, we can write eddy viscosity as:

$$\nu_T = C_\mu \frac{k^2}{\varepsilon} \tag{3.59}$$

The length scale parameterization in Eq. 3.58 ignores stratification and rotation effects, but should be reasonable, for example, for channel flows. A one-equation model for geophysical applications developed by Axell and Liungman (2001) is also an option in the PROBE program.

3.7.2.3 Two-Equation Models

For two-equation models, we apply the k-ε model presented earlier.

3.7.3 Details of Calculations

We consider an Ekman boundary layer influenced by temperature and salinity, with estuarine circulation and sea ice as described in Sect. 3.6. Equations are solved for a 100-m-deep basin, and the turbulence models presented above are used. The FORTRAN settings of the cases are presented in the following subroutine cases (for the programs needed, see Appendix C): `case_ex5a.f`, `case_ex5b.f`, `case_ex5c.f`, `case_ex5d.f`, `case_ex5e.f`, `case_ex5f`, `case_ex5 g.f`, and `case_ex5 h.f`. These examples demonstrate that it is simple to investigate the various turbulence models available in the literature, but the results indicate that few are suitable for marine applications.

3.7.4 Results

The results of the calculations using the turbulence models of Omstedt (1990a) and Pacanowski and Philander (1981) are illustrated in Figs. 3.15 and 3.16. Results

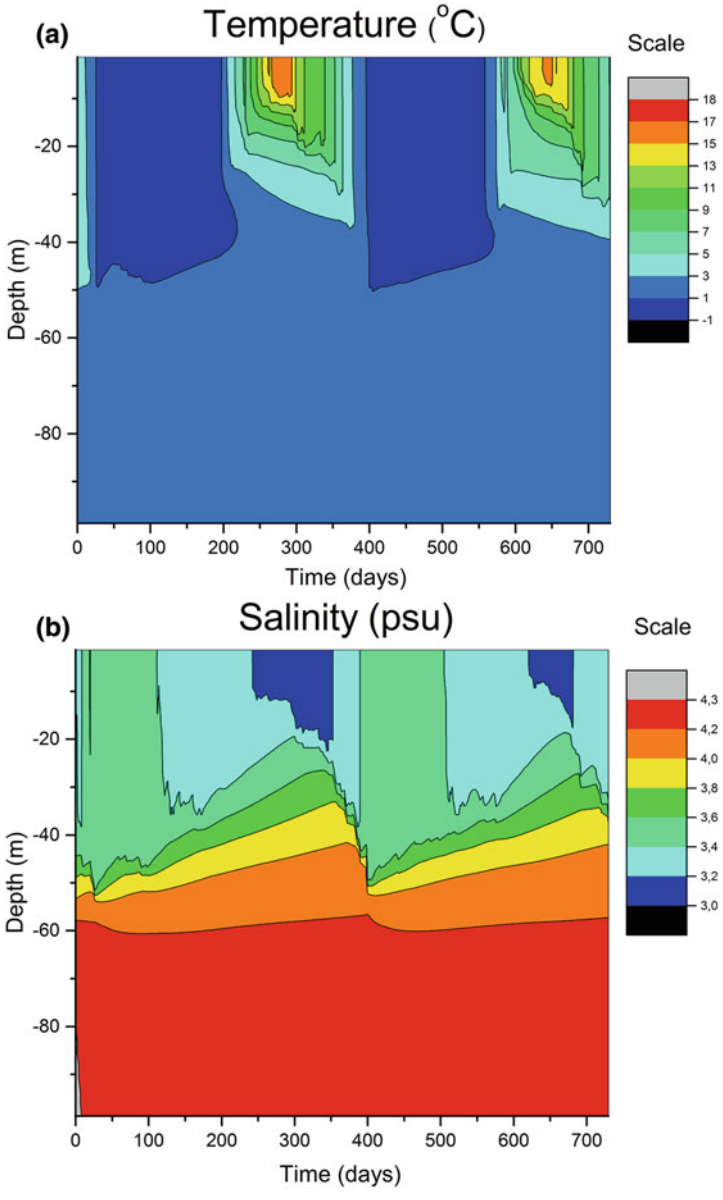

Fig. 3.15 Simulations of the **a** temperature and **b** salinity structure using the turbulence model of Omstedt (1990a)

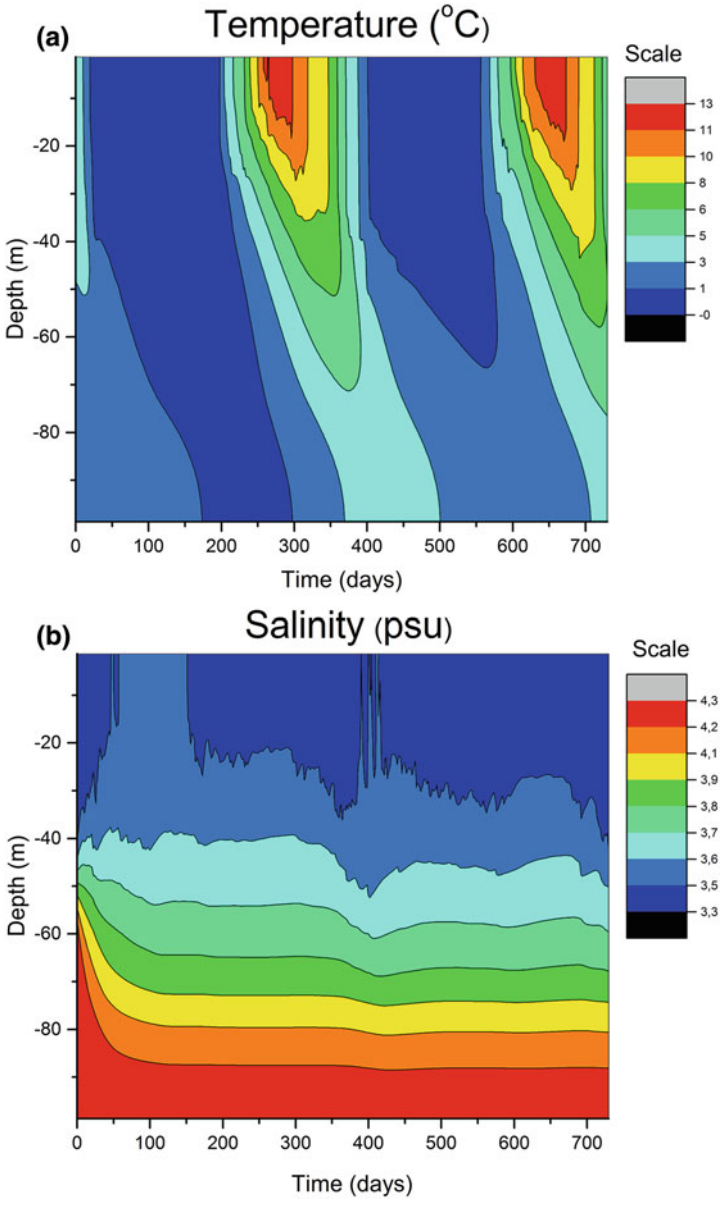

Fig. 3.16 Simulations of the **a** temperature and **b** salinity structure using the turbulence model of Pacanowski and Philander (1981)

obtained from the former parameterization agree well with observations, but the latter results over mix the system. It is clear that the mathematical formulation of turbulent mixing is an important aspect of marine modeling.

Exercise 3.5
Test some of the turbulence models presented in this section and offered as options in the main PROBE program. Present the results produced by three of the turbulence formulations and state whether or not they could be used and, if so, when?

3.7.5 Discussion

In the present section, we have dealt with only high-Reynolds-number turbulence models. For situations with highly reduced turbulence, low-Reynolds-number models are needed. This is the case, for example, at the melting ice–water interface (Svensson and Omstedt 1990) and at the water–bottom sediment interface (Svensson and Rahm 1988). A one-dimensional water column model for marine applications is being actively developed in the General Ocean Turbulence Model (GOTM) community (see http://www.gotm.net/).

3.8 Modeling Tidal Dynamics in the Ocean

3.8.1 Introduction

Large parts of the world's oceans are dominated by tides driven by the positions of celestial bodies, such as the Moon and Sun, and by the local gravitational attraction on Earth (Fig. 3.17). The tidal force is a body force acting throughout the water column and not, like wind stress, acting only at the water–air interface. Tidal motion is therefore more important in the deeper parts of the ocean (Cushman-Roisin and Becker 2011). Through tidal currents, shear increases turbulence in the bottom boundary layer. In addition, through interaction with local topography, tides can generate internal waves that can radiate away and dissipate elsewhere.

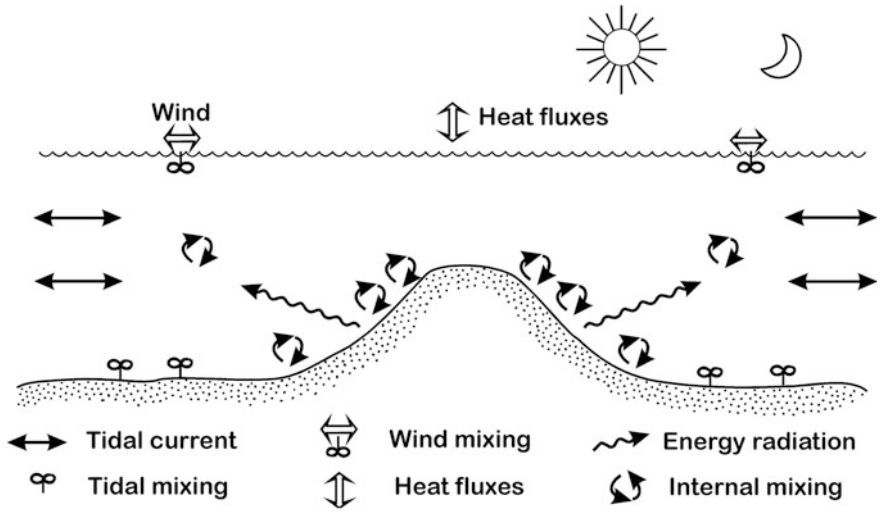

Fig. 3.17 Schematic of mixing processes in a sea with wind and tide

3.8.2 Mathematical Formulation

Tidal motion (momentum) can be formulated as:

$$\frac{\partial \rho U}{\partial t} = \frac{\partial}{\partial z}\left[\frac{\mu_{eff}}{\rho}\frac{\partial \rho U}{\partial z}\right] + f\rho V - \frac{\partial P_w}{\partial x} \tag{3.60}$$

$$\frac{\partial \rho V}{\partial t} = \frac{\partial}{\partial z}\left[\frac{\mu_{eff}}{\rho}\frac{\partial \rho V}{\partial z}\right] - f\rho U - \frac{\partial P_w}{\partial y} \tag{3.61}$$

$$P_w = \rho_0 g\eta + P_a \tag{3.62}$$

where P_w is the water pressure, P_a the atmospheric pressure, and η the sea level; the sea level can be formulated as:

$$\eta = \eta_0 \sin\left(\frac{2\pi}{T_{tide}}t - \phi_{tide}\right) \tag{3.63}$$

where T_{tide} is the tide period and ϕ_{tide} the phase difference. Some principal tidal components are the lunar tide, M_2, with a period of 12.42 h, and the solar tide, S_2, with a period of 24 h.

For the turbulence model and boundary conditions, we follow earlier sections and apply the k-ε model.

3.8.3 Details of Calculations

The modeling of tidal motion adds horizontal pressure gradients from sea level variations to source terms in the Ekman boundary layer model presented in Sect. 3.3. Equations are solved for a 100-m-deep basin, a wind speed of 10 m s^{-1}, and a bottom roughness of 0.01 m. Here, sea level variations are assumed to be due to the M_2 tide, while the horizontal scale over which the sea level varies is set to 1000 km. The FORTRAN settings of the cases are presented in the subroutine `case_ex6.f` (for the programs needed, see Appendix C).

3.8.4 Results

Figure 3.18 depicts the results of analyzing dynamic turbulent viscosity in two cases, one with and the other without tidal forcing. When tides are excluded, only the wind stress is capable of setting up vertical current shear that generates turbulence. In the other case, we also add tidal currents that act throughout the whole water column and generate strong bottom shear and increased turbulence.

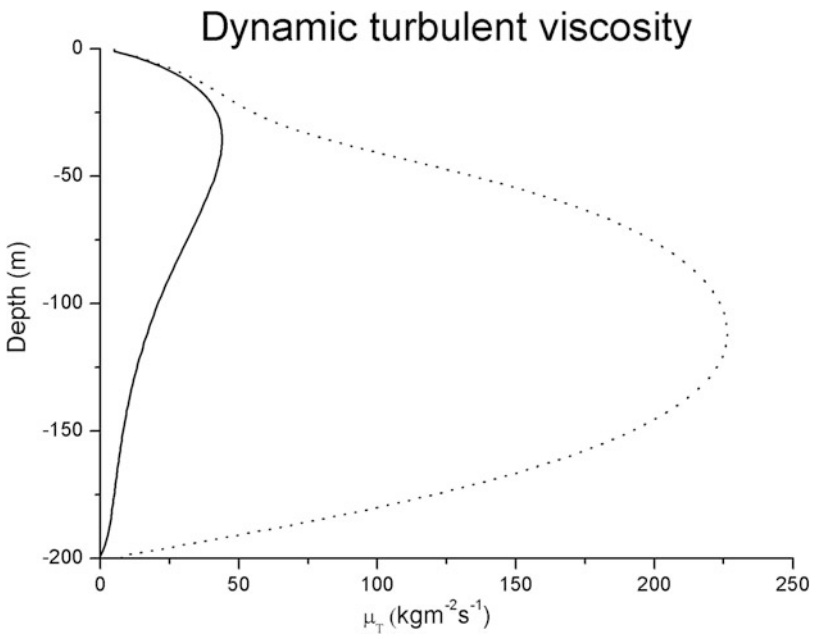

Fig. 3.18 Modeling turbulence in a water column generated by winds (*solid line*) and winds and tides (*dotted line*)

Exercise 3.6
Introduce tides into the model and estimate the tidal amplitude needed to destroy the density stratification caused by the estuarine circulation in Bothnian Bay in the northern Baltic Sea.

Hint: Tidal motions in Bothnian Bay are very small but we use this model setup to illustrate the importance of tidal mixing.

3.8.5 Discussion

Tides interact strongly with topography, which can both damp and amplify the sea level variations; therefore, for specific coastal seas, we need to consult sea level data and, for Polar Regions, we could consult the tidal modeling community (e.g., Earth and Space Research, http://www.esr.org/ptm_index.html). It is obvious that tidal motions can strongly influence vertical mixing. This is the case, for example, in the North Sea, and is a reason why large parts of the North Sea are well mixed. In Polar Regions, the interaction between tides and sea ice also needs to be considered.

Chapter 4
Biogeochemical Aspects

4.1 Introduction

Biogeochemical modeling of the sea calls for the consideration of many important processes (Fig. 4.1). The description of a marine system is often divided into physical, chemical, and biological components. The *physical component* includes all aspects of currents, waves, mixing, light penetration, stratification, and ice; in connection with this, we often speak of the physical pump bringing denser surface water down to deeper layers and advecting bottom water up to the surface layers. The *chemical component* includes various aspects of chemical reactions and involves equations based on chemical reactions and stoichiometrics. For example, the carbon cycle involves both CO_2 solubility and chemical reactions. We can speak of a solubility pump, for example, as CO_2 dissolves more easily in cold water. The *biological component* or biological pump results from phytoplankton (i.e., microscopic plants) taking up CO_2 from the surface layer of the sea, where photosynthesis takes place, and converting it into organic carbon. By means of sinking and mineralization, the organic carbon is transformed back into CO_2 and thus inorganic carbon. These physical, chemical, and biological processes actively interact and involve many interesting modeling aspects; basic understanding of these aspects is needed together with reliable datasets that include marine and atmospheric information, atmospheric deposition information, and river load information. The nomenclature is defined in Appendix B, which includes parameters symbolizing chemical and biological properties. To avoid potential confusion regarding, for example, the letters "C" (which could denote either concentration or carbon) and "S" (which could symbolize either salinity or sulfur), all ions and molecules are written in Roman type (e.g., $CO_{2g} \leftrightarrow CO_{2aq} + H_2O$). All other parameters are written in *italics* (e.g., $v_T \frac{\partial \rho U}{\partial z} = \rho_a c_d^a U^a W^a$). We use two ways to refer to concentrations of plankton and chemical substances: in the form ${}^{\phi}C$, where ϕ symbolizes the parameter in question, or written as chemical symbols within brackets, for example, $[CO_2]$.

A. Omstedt, *Guide to Process Based Modeling of Lakes and Coastal Seas*,
Springer Praxis Books, DOI 10.1007/978-3-319-17990-2_4

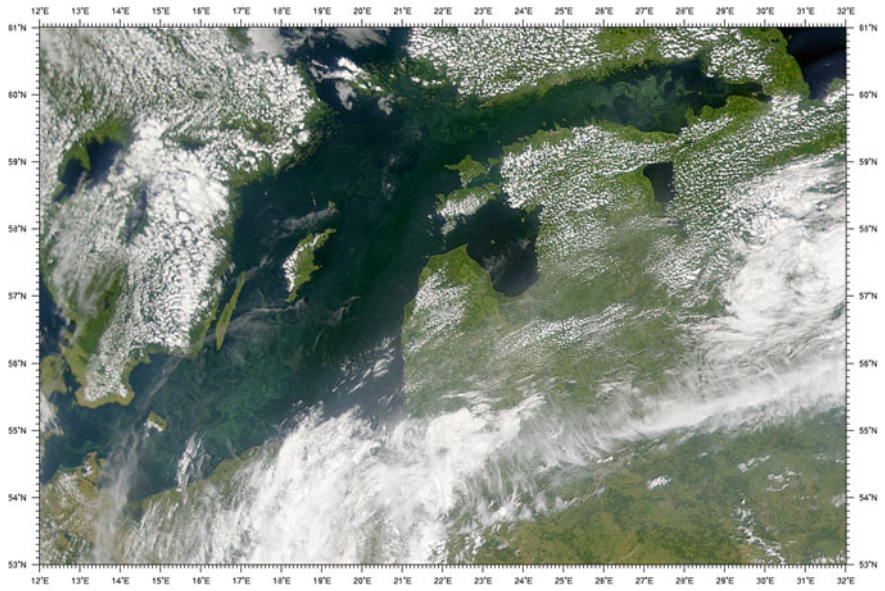

Fig. 4.1 Satellite image of phytoplankton bloom in the Baltic Sea, 27 July 2001. The image indicates a strong coupling between sea, atmosphere, and land (SeaWiFS satellite, NASA/Goddard Space Flight Centre, http://visibleearth.nasa.gov/)

As regards physical modeling, we must learn how to evaluate our results from numerical, physical, and biochemical points of view. One main advantage of using a general equation solver is that it lets us work with a numerical code that can handle coupled model systems in an effective manner. This means that all equations are solved in the same grid and using the same numerical methods, so that we are dealing with fully coupled physical and biochemical models.

4.2 Basic Equations, Stoichiometrics, and Unit Transformations

In this section, we introduce conservation equations for variables, ϕ, such as oxygen, nutrients, carbon, and plankton. The underlying rationale of this is to treat the water as a mixture of species high enough in concentration that we can treat each control volume as well mixed. At high concentrations, however, the species in the mixture may start to interact with the physical properties (i.e., viscosity, density, and light penetration), which then may invalidate our approach. The mixture is also treated as a continuum. This implies that the temporal and spatial scales used in the numerical models must be much larger than the molecular or species size. As the average distance between two water molecules is approximately 10^{-10} m, this is

generally no problem. However, we may need to withdraw the continuum assumption for various ecosystems. As an extreme example, we cannot introduce a concentration model for fish without considering the spatial and temporal resolution of our model. An interesting analogue is sea ice, which can be treated as a continuum only if enough ice floes are present in each grid cell.

All conservation equations can formally be written as:

$$\frac{\partial \phi}{\partial t} + \frac{\partial}{\partial x_i} U_i \phi = \frac{\partial}{\partial z}\left(\Gamma_\phi \frac{\partial \phi}{\partial z}\right) + S_\phi \quad i = x, y, z \tag{4.1}$$

The various terms can be understood as change of property ϕ due to time variation, advection, diffusion, and source/sink, respectively.

For a time-dependent and vertically resolved boundary layer, all conservation equations can be calculated from Eq. 4.1. For example, if we are interested in the concentration of a chemical variable, ${}^{a}C$, we can write the equation as:

$$\frac{\partial {}^{a}C}{\partial t} + W \frac{\partial {}^{a}C}{\partial z} = \frac{\partial}{\partial z}\left(\Gamma_{{}^{a}C} \frac{\partial {}^{a}C}{\partial z}\right) + S_{{}^{a}C} \tag{4.2}$$

The boundary condition at surface and bottom can be calculated from:

$$\Gamma_{{}^{a}C} \frac{\partial {}^{a}C}{\partial z} = F_{{}^{a}C} \tag{4.3}$$

where $F_{{}^{a}C}$ is the flux of the concentration ${}^{a}C$ at the surface or at the bottom. The boundary condition at the surface associated with a gas exchange is often written as:

$$F_{{}^{a}C} = k_C \left({}^{a}C - \alpha_s^a C_{air}\right) \tag{4.4}$$

where k_C is the transfer velocity (m s^{-1}) of ${}^{a}C$, α_s the dimensionless Ostwald solubility coefficient defined as the volume of gas dissolved per unit volume of solvent, and ${}^{a}C_{air}$ the concentration of ${}^{a}C$ in the air. In the transfer function, molecular diffusion coefficients, written in Schmidt number form (defined as the ratio between the kinematic viscosity and diffusivity of the studied gas), and wind speed enter the parameterization. These values are functions of temperature and salinity.

Flux parameterization may also be written in terms of partial pressure. This is the case with carbon dioxide, as its partial pressure is easier to measure than its concentration. We then write the flux as:

$$F_{\mathrm{CO}_2} = k_C K_0 \left(p\mathrm{CO}_2^w - p\mathrm{CO}_2^a\right) \tag{4.5}$$

where K_0 is the solubility coefficient (mol kg^{-1} atm^{-1}) of carbon dioxide (e.g., Donelan and Wanninkhof 2002). The unit used for F_{CO_2} is often mol m^{-2} s^{-1}; to obtain this unit, F_{CO_2} should be multiplied by water density, as the solubility

coefficient refers to water. In the literature, various concentration units are used for the state variables. A good introduction to ocean biogeochemical dynamics and to typical concentration ranges for elements in ocean waters is presented by Sarmiento and Gruber (2006).

For all concentration equations, we will use the unit mol kg^{-1} of seawater, as recommended by Dyrssen and Sillén (1976), to produce a pressure- and temperature-independent scale. Oxygen concentrations, however, are often presented in mL O_2 L^{-1} in light of oceanographic tradition.

Chemical stoichiometrics is the area that considers the quantities of material consumed and produced in chemical reactions based on conservation of mass. Chemical stoichiometric relationships and chemical reaction formulas are used to describe the proportions of compounds involved in chemical reactions. The expression to the left of the arrow represents the elements before the reaction, while the expression to the right of the arrow represents the end products of the reaction. To solve a stoichiometric problem, we should write the balance equation for the chemical reaction and convert the known masses into moles.

Table 4.1 shows the relationship between one mole and the weight of some common elements.

Oxygen unit transformations then give the weight of 1 mol of O_2 as equal to 31.988 g. The molar volume of an ideal gas at one atmospheric pressure and zero degrees Celsius is 22.414 L mol^{-1}. If oxygen is regarded as an ideal gas at standard pressure and temperature, the volume of 1 mol of O_2 thus equals 22.414 L. One L of O_2 contains 1/22.414 mol, so the weight of 1 L of O_2 equals 31.988/22.414 g.

For modeling purposes, we often need to transform given loads to correct units. For example, if the nutrient data are presented in the form ton $month^{-1}$, they must be transformed into mol kg^{-1} to be compatible with our biochemical equations. This can be done using the following transformation. With $Q_f\,{}^N C = a_1$ (ton month^{-1}) and the river runoff expressed in SI units, $Q_f = a_2$ $(m^3\ s^{-1})$, and given that 1 L of freshwater weighs approximately 1 kg, river runoff is transformed to $Q_f \approx a_2 \times 2.6 \times 10^9$ kg $month^{-1}$. The concentration then has the value: ${}^N C \approx \frac{a_1}{a_2 * 2.6 \times 10^3}$ (g kg^{-1}) or ${}^N C \approx \frac{a_1}{a_2 * 2.6 \times 10^3} \frac{1}{m}$ (mol kg^{-1}).

Here, m (g mol^{-1}) is the molecular weight of, for example, nitrogen (m = 14.0067) or phosphorus (m = 30.9738).

Table 4.1 Some chemical elements, symbols, and weights

Element	Symbol	Weight of 1 mol of substance ($gmol^{-1}$)
Carbon	C	12.011
Phosphorus	P	30.9738
Nitrogen	N	14.0067
Silicon	Si	28.0855
Oxygen	O	15.9994
Sulfur	S	32.06

4.3 Modeling the Dynamics of Oxygen

4.3.1 Introduction

In this section, we learn how to model oxygen. We add one equation for oxygen to the physical model we developed in the previous chapter. In the oxygen dynamics, we first consider just the oxygen flux between atmosphere and water and the consumption of oxygen due to the mineralization of organic matter (Fig. 4.2). We find a strong link between the physical modeling and the oxygen modeling, in which temperature, salinity, ice, and mixing all strongly influence the oxygen concentration calculated.

4.3.2 Mathematical Formulation

For the equations of the physical model, the reader is referred to Chap. 3. In the following, we consider only changes associated with the oxygen dynamics. The oxygen equation reads:

$$\frac{\partial^{O_2} C}{\partial t} + W\frac{\partial^{O_2} C}{\partial z} = \frac{\partial}{\partial z}\left[\frac{\mu_{eff}}{\rho\sigma_{O_2}}\frac{\partial^{O_2} C}{\partial z}\right] + S_{O_2} \tag{4.6}$$

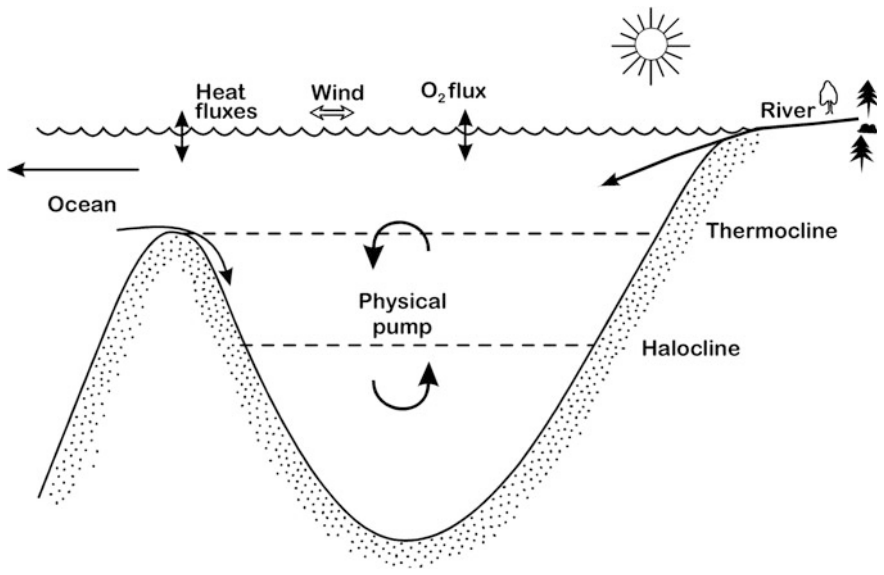

Fig. 4.2 Schematic of the problem, adding oxygen dynamics to our physical model

$$S_{O_2} = -M_{O_2} \tag{4.7}$$

where ${}^{O_2}C$ is the oxygen concentration and S_{O_2} is a sink term associated with oxygen consumption by biochemical oxygen demand (i.e., mineralization). We calculate the oxygen concentration in mol kg^{-1} but transform it in the outputs to mL L^{-1}; this is done by multiplying mol kg^{-1} by the conversion factor of $1/(44.6 \times 10^{-6})$. In the present chapter, we neglect photosynthesis and respiration processes; we only assume constant oxygen consumption due to mineralization, using typical values observed below the halocline in the Baltic Sea during periods of stagnation (Stigebrandt and Wulff 1987). Schneider et al. (2010) found that the mineralization occurred mainly at the sediment surface and that the rates did not depend on redox conditions. If the source term is given as a constant value, it represents a zero-order reaction. Rasmussen et al. (2003) have investigated the oxygen dynamics at the entrance of the Baltic Sea using both zero- and first-order dynamics. A similar approach was used by Gustafsson and Omstedt (2009) when modeling the oxygen dynamics of the Baltic Sea.

The air–water surface boundary condition is expressed as follows:

$$F_{O_2} = k_C\left({}^{O_2}C - {}^{O_2}C_{sat}\right) \tag{4.8}$$

where k_C is the transfer velocity, which is wind speed dependent (Wanninkhof et al. 2009), and ${}^{O_2}C_{sat}$ is the saturation oxygen concentration at the surface. The oxygen flux is expressed in mol kg^{-1} m s^{-1}. The saturation oxygen concentration can be calculated from the salinity and temperature using the formula of Weiss (1970).

The sediment–water surface boundary condition is treated as a flux boundary condition, but excludes water–sediment dynamics.

4.3.3 Details of Calculations

Six physical equations and one equation for oxygen are solved to model a 250-m-deep basin with a geometry roughly similar to that of the Baltic Sea. Five-year runs are performed, and we start running the model on 1 November 1990. The conservation budgets are calculated for oxygen as well. It should be noted that, for the purpose of conservation checks, we need to consider the internal sink due to oxygen consumption in biological mineralization. We assume that the oxygen air–water flux is zero during ice-covered periods. Mineralization is assumed to be active only under the halocline and at a constant rate. The FORTRAN settings of the case are presented in subroutine `case_ex7.f` (for the programs needed, see Appendix C).

4.3.4 Results

The results of the calculations are presented in Fig. 4.3. Sea surface temperature and oxygen concentration manifest clear seasonal cycles, with higher oxygen levels at low temperatures and lower levels at high summer temperatures. Deep water oxygen concentrations are reduced due to biological mineralization at a rate of 1 mL L^{-1} $year^{-1}$. The conservation check indicates that oxygen is conserved in the model. Figure 4.4 presents more details concerning the dynamics of oxygen. For example, both the thermocline (seasonal variations) and the halocline (permanent features) strongly influence the oxygen dynamics. The thermohaline circulation, however, is quite unrealistic, as no estuarine circulation has been added to the model.

Exercise 4.1
Introduce estuarine circulation into the model by assuming that river inflow and deep water inflow both equal 15,000 m^3 s^{-1} and that the oxygen concentration in the inflowing deep water is of surface origin. Calculate oxygen variation over a five-year period. Introduce one extra equation for water age, assuming that it is zero at the surface. What is the typical age of the deep water? *Hint*: Set the source term in the equation for water age to equal 1/year = 3.17×10^{-8} s^{-1}.

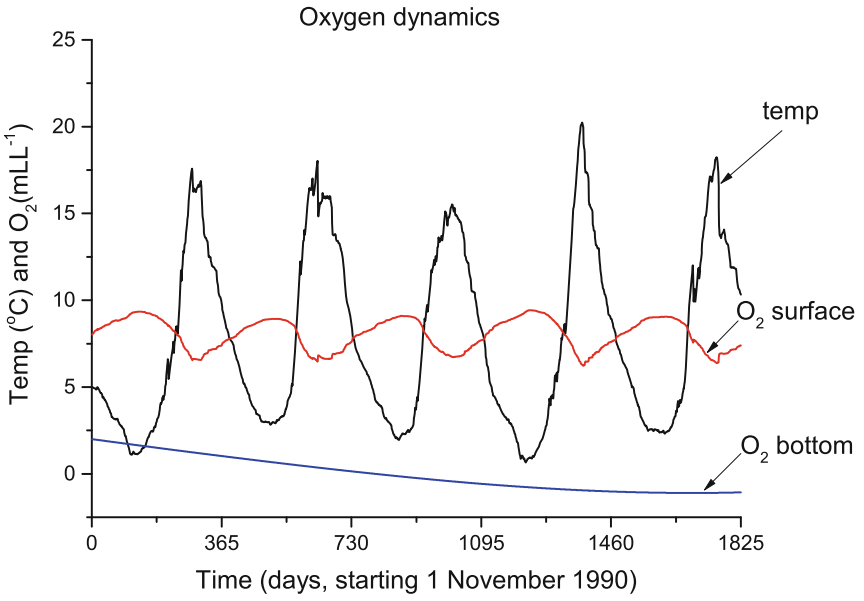

Fig. 4.3 Calculated time series of surface temperature and of surface and bottom water oxygen concentrations

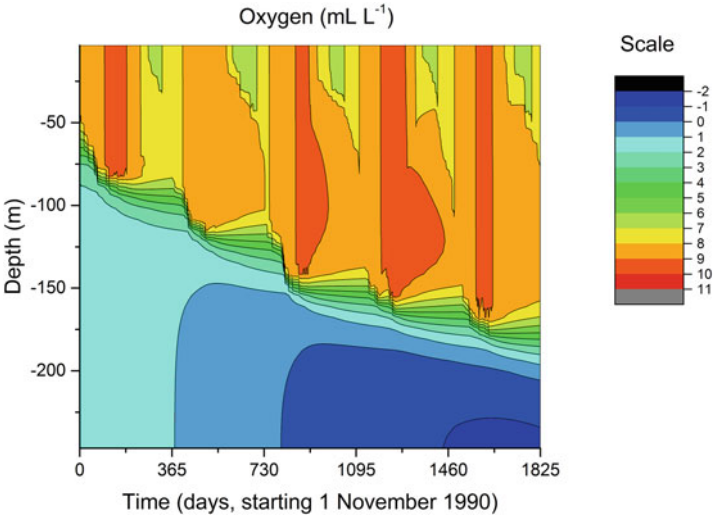

Fig. 4.4 Calculated oxygen concentrations

4.3.5 Discussion

The present model assumes an oxygen flux from atmosphere to water and a constant rate of oxygen consumption below the halocline. Photosynthesis and respiration processes are not dealt with. These processes require a plankton model, which is the subject of the next section.

4.4 Modeling Plankton Growth/Decay

4.4.1 Introduction

In this section, we will learn how to model plankton growth/decay and add this to the oxygen model. Plankton growth/decay is associated with photosynthesis/respiration (Fig. 4.5). The chemical reaction for photosynthesis can be written as:

$$\begin{aligned} &106CO_2 + 16NH_3^- + H_3PO_4 + 16H^+ + 122H_2O \\ &\leftrightarrow (CH_2)_{106}(NH_3)_{16}(H_3PO_4)_1 + 138O_2 \end{aligned} \tag{4.9}$$

using the standard Redfield values. Note that when the plankton are forming $(CH_2O)_{106}(NH_3)_{16}(H_3PO_4)_1$, we must also add oxygen to the water column (from photosynthesis). On the other hand, oxygen is consumed during mineralization. Many models are available for plankton modeling (e.g., Erlandsson 2008; Fennel and Neumann 2004); however, we will follow Erlandsson (2008).

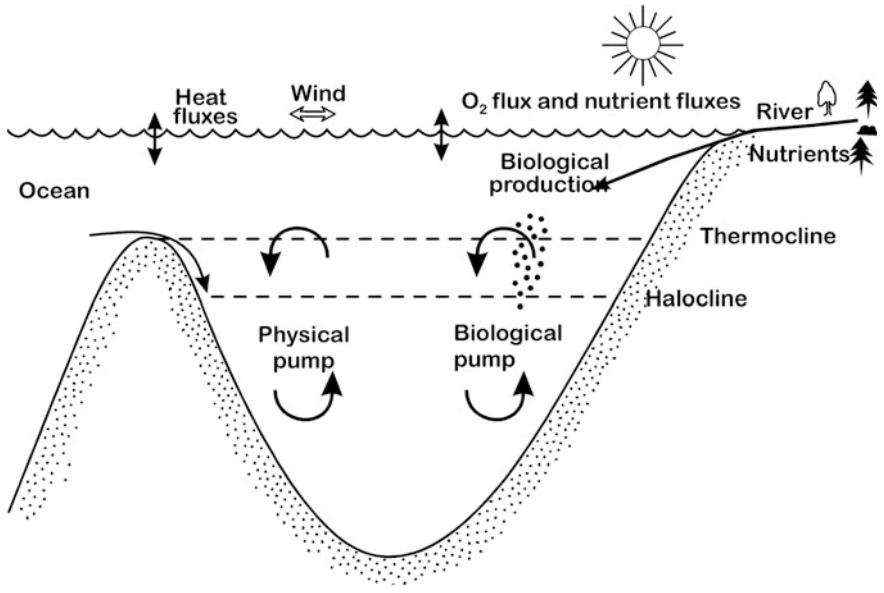

Fig. 4.5 Schematic of the problem, adding oxygen and plankton dynamics to our physical model

4.4.2 Mathematical Formulation

The oxygen and primary production equations read:

$$\begin{cases} \frac{\partial^{O_2}C}{\partial t} + W\frac{\partial^{O_2}C}{\partial z} = \frac{\partial}{\partial z}\left[\frac{\mu_{eff}}{\rho\sigma_{O_2}}\frac{\partial^{O_2}C}{\partial z}\right] + S_{O_2} \\ \frac{\partial^{pp}C}{\partial t} + W\frac{\partial^{pp}C}{\partial z} = \frac{\partial}{\partial z}\left[\frac{\mu_{eff}}{\rho\sigma_{^{pp}C}}\frac{\partial^{pp}C}{\partial z}\right] + S_{^{pp}C} \end{cases} \tag{4.10}$$

where ${}^{pp}C$ is the plankton concentration in mol kg^{-1}. To the oxygen source/sink term, we add the oxygen produced by photosynthesis. The source terms are:

$$\begin{cases} S_{O_2} = s_{O_2} G_p\, {}^{pp}C - \alpha_{1\min} e^{\alpha_{2\min} T}\, {}^{pp}C \\ S_{^{pp}C} = G_p\, {}^{pp}C + w_p \frac{\partial^{pp}C}{\partial z} - \alpha_{1\min} e^{\alpha_{2\min} T}\, {}^{pp}C / s_{O_2} \end{cases} \tag{4.11}$$

where the sink/source term in the oxygen equation, S_{O_2}, now includes both plankton growth and mineralization; the source terms in the plankton equation, $S_{^{pp}C}$, include plankton growth, $G_p\, {}^{pp}C$, sedimentation, $w_p \frac{\partial^{pp}C}{\partial z}$, and mineralization, $\alpha_{1\min} e^{\alpha_{2\min} T}\, {}^{pp}C$. The constant s_{O_2} is the Redfield value for oxygen, which equals 138. The mineralization rate follows Edman and Omstedt (2013), where $\alpha_{1\,\min}$ and $\alpha_{2\,\min}$ are constants equal to 0.034 (day^{-1}) and 0.05, respectively. Plankton growth is limited by available light, I_{lim}, and nutrients, N_{lim}, which are described in a simple way here, as nutrient dynamics are not yet included. Maximum growth, G_{max}, is assumed to be temperature dependent and reduced by plankton respiration, Br:

$$\begin{cases} G_p = I_{lim} N_{lim} G_{max}(1 - Br) \\ I_{lim} = \frac{\Gamma_{sun}/\Gamma_0}{\sqrt{1+(\Gamma_{sun}/\Gamma_0)^2}} \\ N_{lim} = \begin{cases} 1 & \text{for November}-\text{April} \\ 0 & \textit{for} \text{ May}-\text{October} \end{cases} \\ G_{\max} = G_0 \mathrm{e}^{(c_g T)} \end{cases} \tag{4.12}$$

where Γ_{sun} is the source term in the heat conservation equation (Eq. 3.20), Γ_0 a constant equal to 30 Wm^{-2}, and c_g a constant in the plankton growth expression.

The boundary conditions follow those outlined in earlier chapters; in the plankton equation we assume zero flux conditions at both the surface and bottom of the coastal sea.

4.4.3 Details of Calculations

Six physical equations together with one equation for oxygen and one equation for the plankton concentration are now solved for a 250-m-deep basin. The FORTRAN settings of the case are presented in subroutine `case_ex8.f` (for the programs needed, see Appendix C). In the present chapter, we simplify the nutrient dynamics and neglect the estuarine circulation by assuming no freshwater inflow. We assume that nutrients do not limit the plankton growth from November to April, but that they do so completely from May to October. The plankton are also assumed to respire at a constant rate (i.e., `Br = 0.1`).

4.4.4 Results

The results of calculations are presented in Figs. 4.6, 4.7 and 4.8. The sea surface oxygen concentration now displays an increase associated with plankton growth and becomes oversaturated with oxygen. Plankton grows and mixes in the surface layer, while in deeper layers it decays due to mineralization. During periods of increased plankton bloom, the plankton may sink to the bottom and add biological material to the bottom boundary layer. The interaction with the benthic bottom layer, however, is not introduced into the modeling.

Exercise 4.2
Examine the sensitivity of plankton growth by studying the importance of light penetration and Secchi depth. *Hint*: Assume that the extinction coefficient of short-wave radiation can be calculated from $\beta_w = \beta_{w1} + 0.4 \times 10^6 \, {}^{pp}C$ and Secchi depth from $Z_s = \frac{1.7}{\beta_w}$.

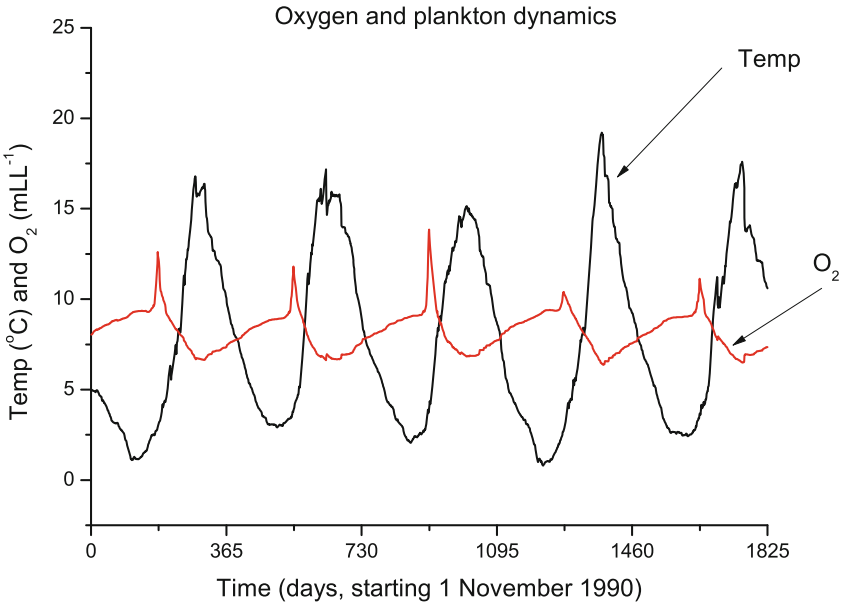

Fig. 4.6 Calculated oxygen concentrations (surface and bottom values denoted by *red* and *blue curves*) and sea surface temperatures (*black line*) over a five-year period

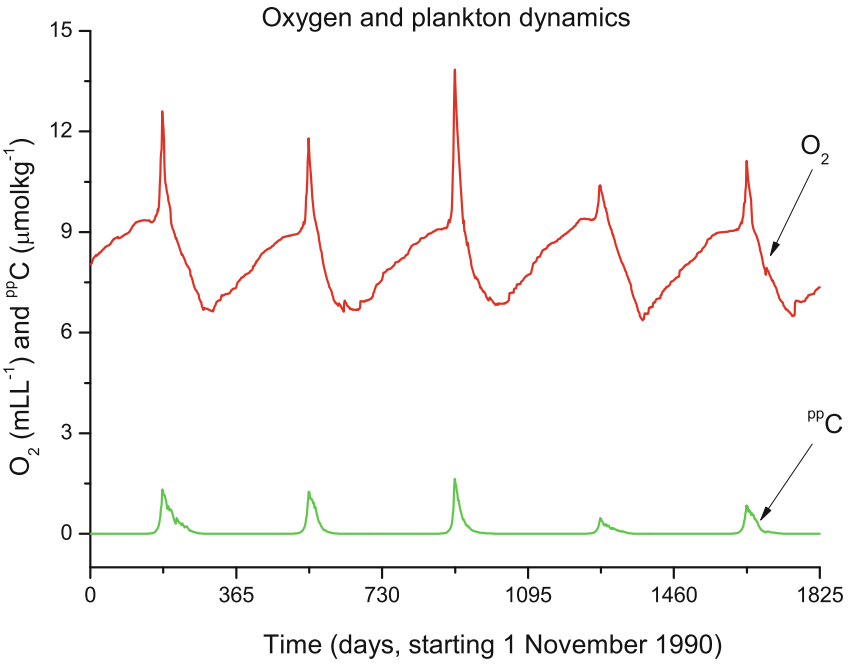

Fig. 4.7 Calculated sea surface oxygen (*black line*) and plankton concentrations (*green line*) over a five-year period

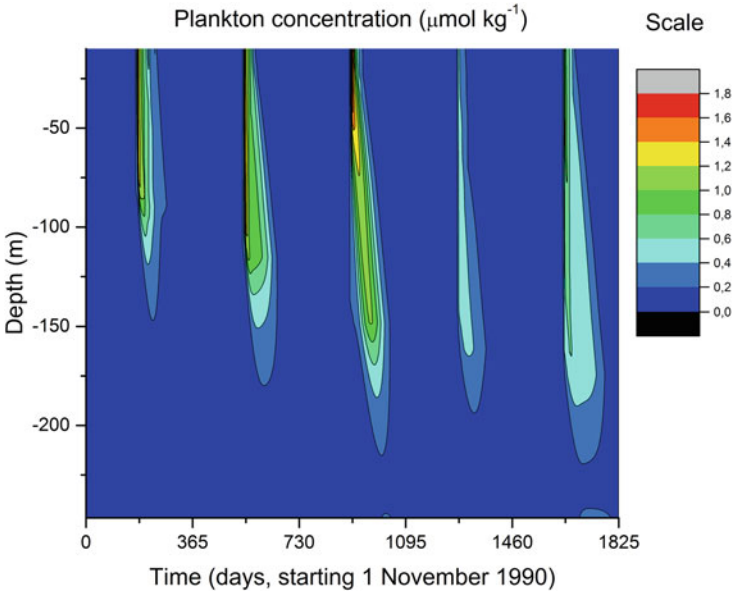

Fig. 4.8 Calculated plankton concentrations over a five-year period

4.4.5 Discussion

The present model assumes simple dynamics and source/sink terms related to plankton growth, mineralization, and sinking. We consider only one species of plankton and exclude grazing by zooplankton. Before further considering the plankton species, we need a method for evaluating biological production. In general, most models rely on nutrient concentrations. Therefore, in the next section we will examine nutrient and plankton dynamics.

4.5 Modeling the Dynamics of Nutrients

4.5.1 Introduction

In the plankton model presented in Sect. 4.4, we prescribed only the limiting nutrients; this section will add nutrient dynamics to the plankton model. In the Baltic Sea, the spring bloom often starts in early April (Fig. 4.9), accompanied by a strong reduction in both nitrate (NO_3) and phosphate (PO_4) levels. The spring bloom is often *nitrate* limited, leaving phosphate available to other species. When the temperature increases, blue-green algae may grow, using up all available *phosphate* in the surface layer. Bulk plankton growth is therefore controlled by the available

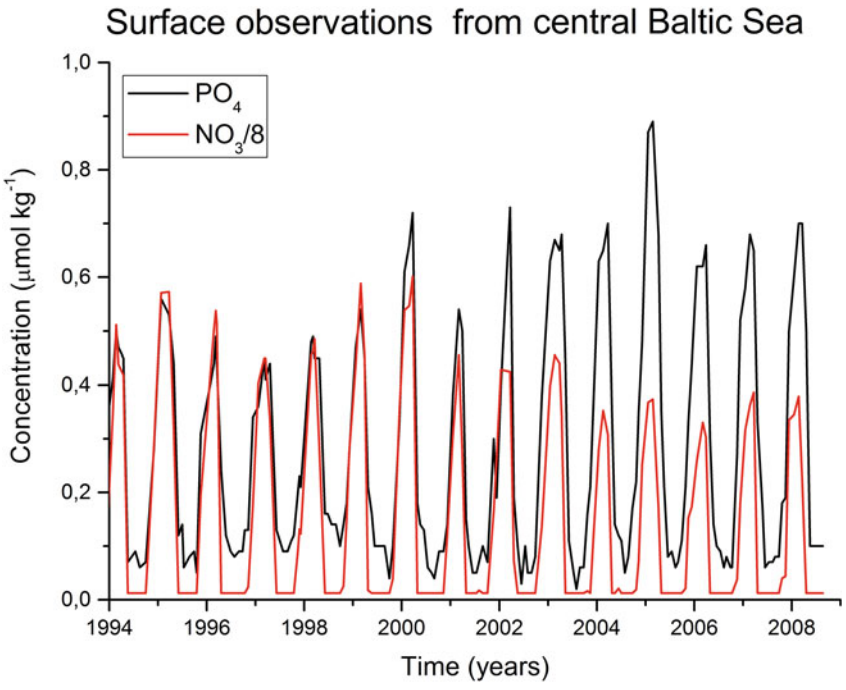

Fig. 4.9 Observed nutrient concentrations in the upper surface layer of the Baltic Sea

amount of *phosphate*, while the *nitrate* dynamics retard the consumption of *phosphate*. In the following, we will first consider only plankton that is *phosphate* limited. Regarding the phosphate dynamics, we also need to consider the transition from oxic to anoxic conditions, when phosphate is suddenly liberated at the sediment–water interface, resulting in an increased concentration of phosphate (e.g., Emeis et al. 2000).

4.5.2 Mathematical Formulation

We now add a nutrient equation to our plankton model (we will only resolve the phosphate dynamics and parameterize all other effects) as follows:

$$\frac{\partial^n C}{\partial t} + W\frac{\partial^n C}{\partial z} = \frac{\partial}{\partial z}\left[\frac{\mu_{eff}}{\rho\sigma_{^nC}}\frac{\partial^n C}{\partial z}\right] + S_{^nC} \tag{4.13}$$

where ${}^nC$ represents the nutrient concentration that limits the bulk plankton growth.

In line with the modeling presented in Sect. 4.4, we write:

$$\begin{cases} S_{n_C} = -s_p G_p{}^{pp}C + s_p \alpha_{1\min} e^{\alpha_{2\min} T}{}^{pp}C / s_{o_2} + \alpha_{2s} A_{sed} w_{psed} \\ \alpha_{2s} = \begin{cases} 0 & \text{if} \quad O_2 \succ 0 \text{ ml/l} \\ 1 & \text{if} \quad O_2 \leq 0 \text{ ml/l} \end{cases} \end{cases} \tag{4.14}$$

where the constant s_p is the stoichiometric relationship between plankton and phosphorus and equals 1, and α_{2s} is a constant that switches between oxic and anoxic conditions. The plankton growth term is limited by available light and nutrient conditions; as we now introduce nutrient dynamics, we can also improve our parameterization of nutrient limitation by writing:

$$N_{lim} = \frac{{}^{n}C}{\left(k_{1/2} + {}^{n}C\right)} \tag{4.15}$$

where $k_{1/2}$ gives the ${}^{n}C$ concentration when $N_{lim} = 0.5$, which for phosphate typically equals 0.05×10^{-6} mol P kg^{-1}. The nutrient limitation formulation is known as the Michaelis and Menten equation (see, e.g., Fennel and Neumann 2004). Phosphate flows from anoxic sediments are modeled by adding an extra process to the source term (Eq. 4.14). The release of phosphate from the sediment area, A_{sed}, is set to $w_{psed} = 0.44$ mmol P m^{-2} s^{-1}, following the results of Conley et al. (2002). Nutrients are also added through river runoff.

4.5.3 Details of Calculations

We now have added an equation for nutrients to the plankton model presented in Sect. 4.4. The FORTRAN settings of the case are presented in subroutine `case_ex9a.f` (for the programs needed, see Appendix C). Estuarine circulation is not included and the density stratification becomes increasingly unrealistic. A phosphate flux associated with phosphate release from sediments under anoxic conditions is added to the model.

4.5.4 Results

The results of the calculations are presented in Figs. 4.10 and 4.11. Spring bloom reduces the surface layer nutrient concentration in spring and summer (Fig. 4.10). Due to autumn and winter mixing, the nutrient concentration in the surface layer is re-established. Increasing phosphate concentrations associated with leakage from anoxic sediments are illustrated in Fig. 4.11. Under anoxic conditions, phosphorus-rich sediment may strongly increase eutrophication.

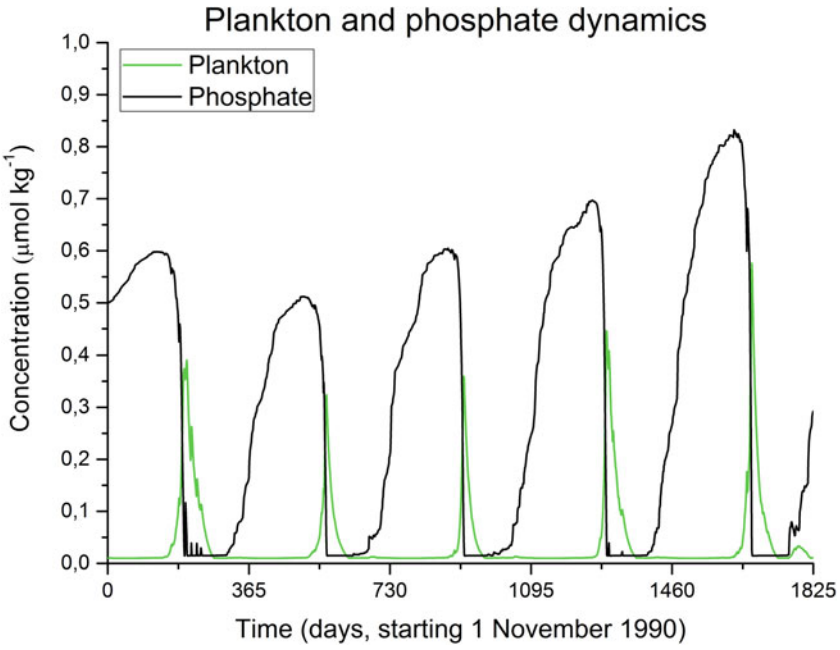

Fig. 4.10 Calculated phosphorus and plankton surface concentrations over a five-year period

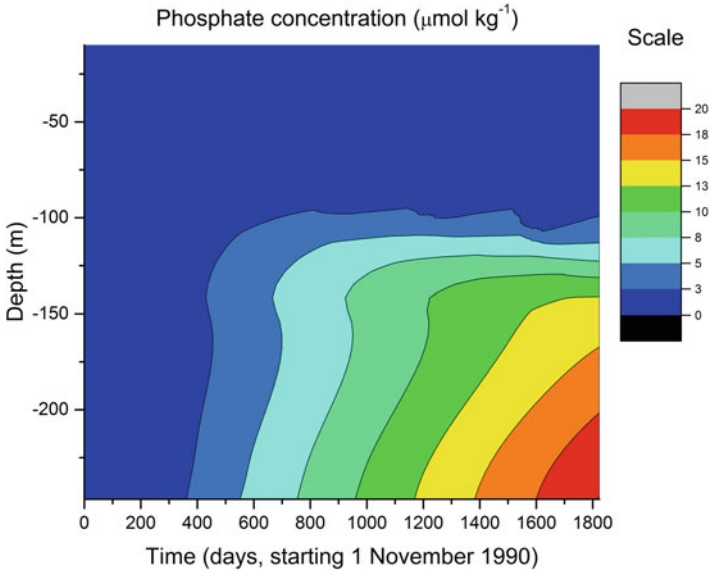

Fig. 4.11 Calculated phosphorus concentration over a five-year period

Exercise 4.3
So far in our biogeochemical modeling of the sea, we have considered only one group of `P`-limited algae. In this exercise add another equation for nitrate. Model plankton dynamics using two plankton types, one for a group of `P`-limited and `N`-limited algae, and another for a group of blue–green algae limited only by *phosphorus*. The latter plankton group should also be assumed to be temperature and salinity limited. *Hint:* Look into subroutine `case_ex9b.f`.

4.5.5 Discussion

Nutrients could easily be adjusted to winter conditions through data assimilation. A better method, however, is to model the vertical circulation and mineralization of biological material in a realistic fashion. Multiyear runs will then teach us whether our numerical model can reproduce conservation, mixing, and vertical circulation.

4.6 Modeling Dissolved Inorganic Carbon

4.6.1 Introduction

In this section, we will learn how to model the dissolved inorganic carbon cycle, partial pressure of CO_2, and pH in seawater. Dissolved inorganic carbon is the major chemical component needed in modeling the ocean carbon cycle. The deep ocean contains by far most of the carbon on Earth (Fig. 4.12). The biological component of the ocean carbon cycle also plays a role, as CO_2 is used in photosynthesis, particularly in nutrient-rich regions such as coastal seas. However, we will first ignore the coupling with biological processes and consider only how the physical and chemical systems interact. The focus is on the transport and storage of CO_2 in the sea; only inorganic carbon is considered in this section. Modeling the marine carbonate system is presented in greater detail, for example, by Zeebe and Wolf-Gladrow (2001) and Edman and Omstedt (2013).

Carbon dioxide from the atmosphere dissolves in the surface water and undergoes rapid chemical reactions, only a small fraction remaining as carbon dioxide. The reactions that occur when carbon dioxide dissolves in seawater are as follows:

$$\begin{cases} CO_{2g} \leftrightarrow CO_{2aq} \\ CO_{2aq} + H_2O \leftrightarrow H_2CO_{3aq} \\ H_2CO_{3aq} \leftrightarrow H^+_{aq} + HCO^-_{3aq} \\ H^+_{aq} + HCO^-_{3aq} \leftrightarrow 2H^+_{aq} + CO^{2-}_{3aq} \end{cases} \tag{4.16}$$

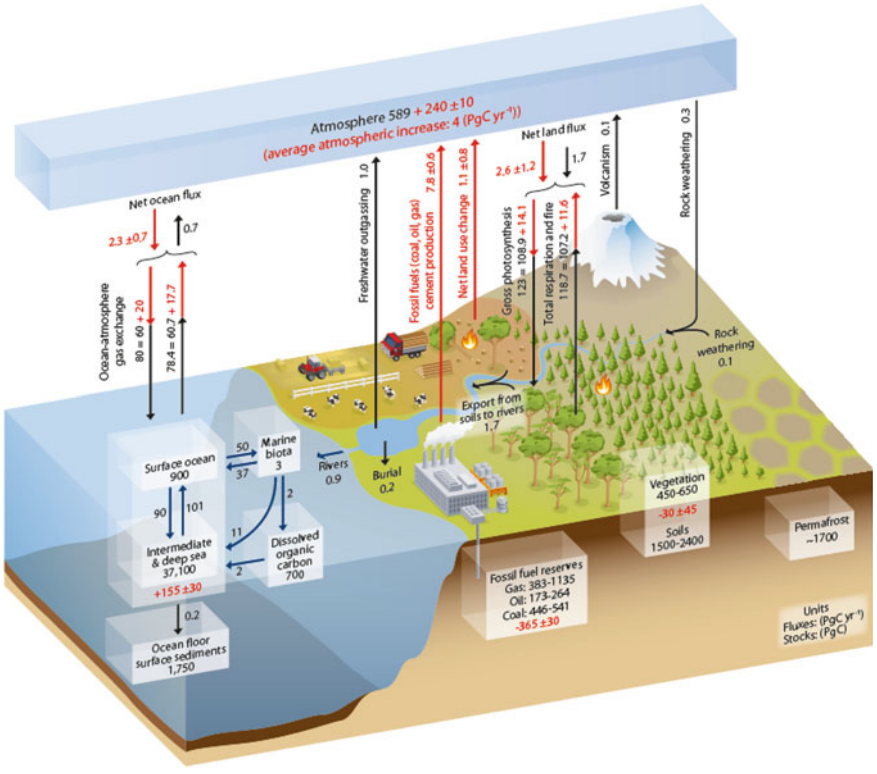

Fig. 4.12 The global carbon cycle (IPCC 2013, Fig. 6.1). The preindustrial fluxes are shown in black and the cumulative anthropogenic fluxes (1750–2011) in *red*

Limestone, however, may also go into solution, generating carbonate ions:

$$\begin{cases} CaCO_{3s} \leftrightarrow Ca^{2+}_{aq} + CO^{2-}_{3aq} \\ CO_{2aq} + CO^{2-}_{3aq} + H_2O \leftrightarrow 2HCO^{-}_{3aq} \end{cases} \tag{4.17}$$

In addition, the contribution of boron in connecting a proton needs to be considered:

$$B(OH)_3 + H_2O \leftrightarrow B(OH)^{-}_4 + H^+ \tag{4.18}$$

The chemical reactions in Eqs. 4.16 and 4.17 include the following components of the inorganic carbon cycle: carbon dioxide, CO_2, carbonic acid, H_2CO_{3aq}, bicarbonate, HCO^{-}_{3aq}, and carbonate, CO^{2-}_{3aq}; the sum of these components is referred to as the total dissolved inorganic carbon, C_T. The solubility and dissociation constants of carbonic acid are as follows:

$$\begin{cases} K_o = \dfrac{[CO_2]}{fCO_{2aq}} \\ K_1 = \dfrac{[H^+][HCO_3^-]}{[CO_{2aq}]} \\ K_2 = \dfrac{[H^+][CO_3^{2-}]}{[HCO_3^-]} \\ K_B = \dfrac{[H^+][BO_4^-]}{[B(OH)_3]} \\ K_W = [H^+][OH^-] \end{cases} \tag{4.19}$$

where fCO_{2aq} is the fugacity of carbon dioxide, which almost equals the partial pressure of carbon dioxide, and K_0, K_1, K_2, K_B, and K_W are dependent on temperature, salinity, and pressure (Dickson et al. 2007; Omstedt et al. 2010). The marine chemical system (Zeebe and Wolf-Gladrow 2001) is defined by:

$$\begin{cases} C_T = [CO_2^*] + [HCO_3^-] + [CO_3^{2-}] \\ A_T \approx [HCO_3^-] + 2[CO_3^{2-}] + [B(OH)_4^-] + [OH^-] - [H^+]\,b \\ B_T = [B(OH)_3] + [B(OH)_4^-] \end{cases} \tag{4.20}$$

where $[CO_2^*] = [CO_{2aq}] + [H_2CO_3]$ is the notation that will be used here, as these ions are not chemically separable, and A_T and B_T are total alkalinity and total boron, respectively. Note that minor components are neglected in the definition of total alkalinity, some needing to be reconsidered, for example, under anoxic conditions. The concentration unit is mol kg^{-1} seawater.

The system defined by Equation systems 4.19 and 4.20 includes four unknowns: A_T, C_T, fCO_2, and $[H^+]$ (or $[H^+] = 10^{-pH}$). With two of these known we can calculate the other two. The state variables are A_T and C_T, and they will be modeled and treated as the known quantities.

If the ocean concentrations of total inorganic carbon and total alkalinity are known, we can derive a simplified relationship for the partial pressure (e.g., by ignoring the presence of boric acid; Sarmiento and Gruber 2006). The simplified analytical relationship reads:

$$pCO_{2aq} \approx \frac{K_2}{K_0 K_1}\left[\frac{(2C_T - A_T)^2}{A_T - C_T}\right] \tag{4.21}$$

The important aspect of this simplified equation is that the partial pressure of carbon dioxide in the water is dependent on the difference between total alkalinity and total inorganic carbon, which largely depends on the carbonate ion concentration.

With A_T and C_T known, there is no analytical solution for calculating the partial pressure of carbon dioxide more fully; instead, we use iterative methods (i.e., the Newton–Raphson method) and solve the carbon dioxide according to Anderson, Turner, Wedborg et al. (1999), as follows:

$$\begin{cases} p\mathrm{CO}_2 = \dfrac{C_T\left[\mathrm{H}^+\right]^2}{K_0\left(\left[\mathrm{H}^+\right]^2 + K_1\left[\mathrm{H}^+\right] + K_1K_2\right)} \\ A_T = \dfrac{C_TK_1\left(\left[\mathrm{H}^+\right] + 2K_2\right)}{\left(\left[\mathrm{H}^+\right]^2 + K_1\left[\mathrm{H}^+\right] + K_1K_2\right)} + \dfrac{B_T}{\left(1 + \left[\mathrm{H}^+\right]/K_B\right)} + K_W/\left[\mathrm{H}^+\right] - \left[\mathrm{H}^+\right] \end{cases} \tag{4.22}$$

where the total boron concentration can be calculated as $B_T = 0.00042 \times S/35$.

4.6.2 Mathematical Formulation

For the physical model equations, the reader is referred to Chap. 3. In the following, we consider only the changes we need to make when modeling the dynamics of inorganic carbon. Two equations must be considered, but we also add the oxygen equation, as carbon and oxygen are closely linked. The state variables are total dissolved inorganic carbon, C_T, and total alkalinity, A_T:

$$\begin{cases} \frac{\partial^{O_2}C}{\partial t} + W\frac{\partial^{O_2}C}{\partial z} = \frac{\partial}{\partial z}\left[\frac{\mu_{eff}}{\rho\sigma_{O_2}}\frac{\partial^{O_2}C}{\partial z}\right] + S_{O_2} \\ \frac{\partial C_T}{\partial t} + W\frac{\partial C_T}{\partial z} = \frac{\partial}{\partial z}\left[\frac{\mu_{eff}}{\rho\sigma_{C_TC}}\frac{\partial C_T}{\partial z}\right] + S_{C_T} \\ \frac{\partial A_T}{\partial t} + W\frac{\partial A_T}{\partial z} = \frac{\partial}{\partial z}\left[\frac{\mu_{eff}}{\rho\sigma_{A_TC}}\frac{\partial A_T}{\partial z}\right] + S_{A_T} \end{cases} \tag{4.23}$$

where S_{C_T} denotes sources/sinks of C_T. Carbon dioxide enters the C_T equation through the atmosphere–ocean boundary layer as a flux and enters the source term through biological production (i.e., photosynthesis/mineralization). In the A_T equation, we have sources/sinks due to total alkalinity changes, for example, due to limestone or shell-forming organisms. In the present case, we consider only the inorganic carbon dynamics and assume no primary production or mineralization of biological material, so these terms are expressed as follows:

$$\begin{cases} S_{\mathrm{O}_2} = 0 \\ S_{C_T} = 0 \\ S_{A_T} = 0 \end{cases} \tag{4.24}$$

The air–water surface boundary conditions are as follows:

$$\begin{cases} \frac{\mu_{eff}}{\rho\sigma_{\mathrm{O}_2}}\frac{\partial^{O_2}C}{\partial z} = F_{\mathrm{O}_2} \\ \frac{\mu_{eff}}{\rho\sigma_{C_T}}\frac{\partial C_T}{\partial z} = F_{\mathrm{CO}_2} \\ \frac{\mu_{eff}}{\rho\sigma_{A_T}}\frac{\partial A_T}{\partial z} = 0 \end{cases} \tag{4.25}$$

while the CO_2 flux, F_{CO_2}, is controlled by the difference in partial pressure:

$$F_{CO_2} = k_{wCO_2} K_0 \left(pCO_2^w - pCO_2^a \right) \tag{4.26}$$

where k_{wCO_2} (m s^{-1}) is the transfer velocity, K_0 (mol kg^{-1} atm^{-1}) the gas solubility of CO_2, and $pCO_2{}^w$ and $pCO_2{}^a$ the partial pressure of CO_2 in the water and atmosphere, respectively. Note that the unit for the CO_2 flux is m s^{-1} mol kg^{-1} atm^{-1} and, if we multiply the flux by density, we have the unit mol m^{-2} s^{-1}.

Calculating the partial pressure of CO_2 in water involves eight equations and ten unknowns. To close this equation system, we must know two variables; accordingly, we will calculate the total inorganic carbon, C_T, and total alkalinity, A_T, the variables we must know to calculate pH and the partial pressure of CO_2 in seawater.

Transfer velocity is described in terms of the Schmidt number, defined as the ratio between the kinematic viscosity of water and the diffusivity of gas in water. These parameters are often assumed to be temperature dependent (see also the parameterization of oxygen flux). A common approach is to formulate k_{wCO_2} as a quadratic or cubic function of wind. We will follow Wanninkhof et al. (2009) and write:

$$k_{wCO_2} = 0.31 \sqrt{\frac{660}{S_c}} W_a^2 \frac{0.01}{3600} \tag{4.27}$$

where we have transformed the formula into SI units. For the Schmidt number, we use the following relationship:

$$S_c = 2073.1 - 125.62T + 3.6276T^2 - 0.043219T^3 \tag{4.28}$$

where T is the temperature in °C.

Solubility, K_0, is a function of temperature and can be calculated according to Dickson et al. (2007). The sediment–water surface boundary condition is treated as a flux boundary condition without any water–sediment dynamics involved.

In the boundary conditions for river runoff, we can use experimental knowledge of how salinity and total alkalinity are related (Hjalmarsson et al. 2008). We may assume that the total inorganic carbon content of river water is in equilibrium with the atmospheric partial pressure of CO_2. However, many rivers are oversaturated (e.g., Humborg et al. 2009), and this needs to be included in the lateral boundary condition associated with river inflow. For the inflowing deep ocean water, we assume a constant total alkalinity and a constant total inorganic carbon concentration.

4.6.3 Details of Calculations

Equations are solved for a 250-m-deep estuary with a geometry similar to that of the Baltic Sea. The two new equations are modeled as equation numbers 11 and 12 in

subroutine `case_ex10a.f`. In the example, we do not solve for nutrient and plankton concentrations. The atmospheric partial pressure of CO_2 is assumed to be constant. We use an autumn convection value similar to that used before, by prescribing the winter values of C_T and A_T. Note that all concentrations are now expressed in mol kg^{-1}. The FORTRAN settings of the case are presented in subroutine `case_ex10a.f` (for the programs needed, see Appendix C), where the equations for nutrient and plankton concentrations need to be inactive.

4.6.4 Results

Figure 4.13 presents the calculated partial pressure of CO_2. As no primary production is taking place, the carbon dioxide partial pressure in water becomes mostly oversaturated and is influenced strongly by temperature. The pCO_2^w increases in summer and decreases in winter. The flux calculations presented in Fig. 4.14 therefore indicate outgassing from the sea, particularly in summer. In coastal seas, pCO_2^w is instead often controlled by primary production, which will be treated in the next section.

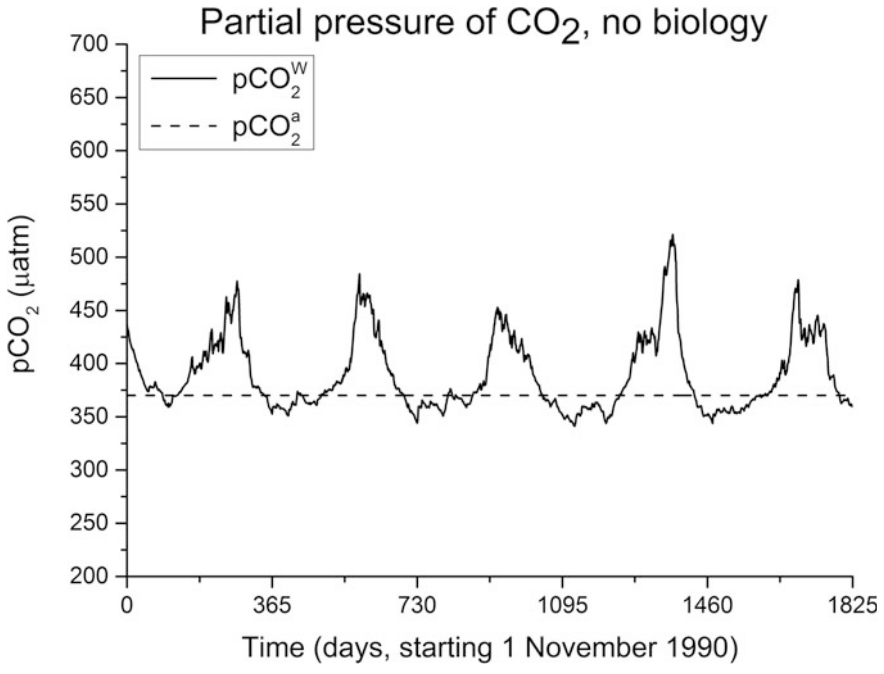

Fig. 4.13 Calculated partial pressure of CO_2 flux without primary production

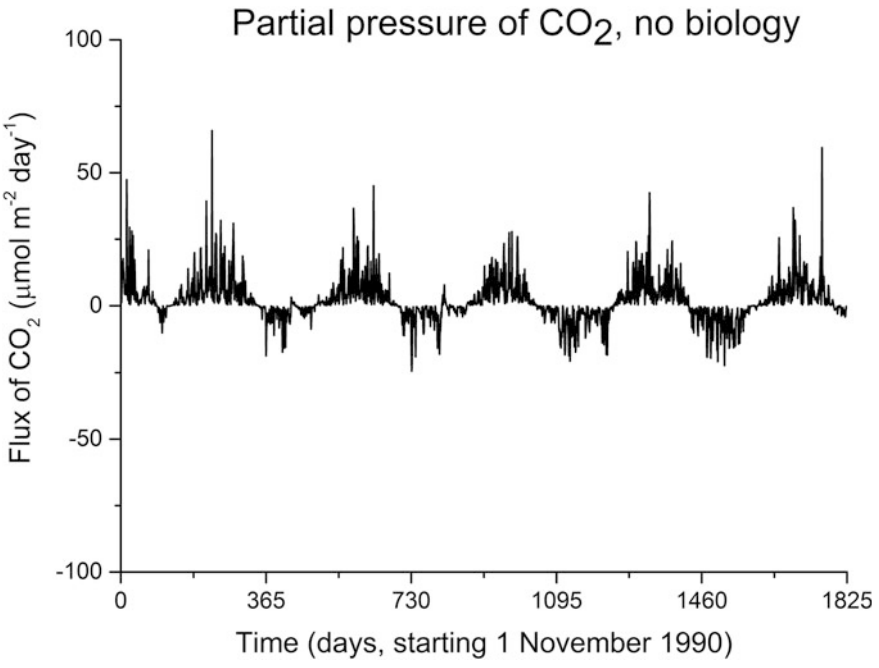

Fig. 4.14 Calculated CO_2 flux in a coastal sea without primary production. Note that positive fluxes imply that the flow is out of the sea

Exercise 4.4
The rivers entering the Baltic Sea are generally oversaturated with CO_2, typical concentrations being 1350 µatm (Humborg et al. 2009), and total alkalinity averages 1200 µmol kg^{-1}. Calculate the typical C_T and A_T concentrations in the Baltic Sea, assuming river runoff of 15,000 m^3 s^{-1} and an equally large inflow of saline water of 17 salinity units. The typical total alkalinity and total inorganic carbon concentrations in the inflowing water equal 2000 and 1800 µmol kg^{-1}, respectively. *Hint:* Assume steady state and apply conservation arguments.

4.6.5 Discussion

The effects of primary production and mineralization will be analyzed in the next section. So far in the modeling, we have not considered ice versus open water; the effects of ice growth/decay and CO_2 dynamics therefore need further consideration. The CO2SYS program (http://cdiac.ornl.gov/ftp/co2sys/) for CO_2 calculations is a useful tool for conducting various numerical tests of carbon chemistry.

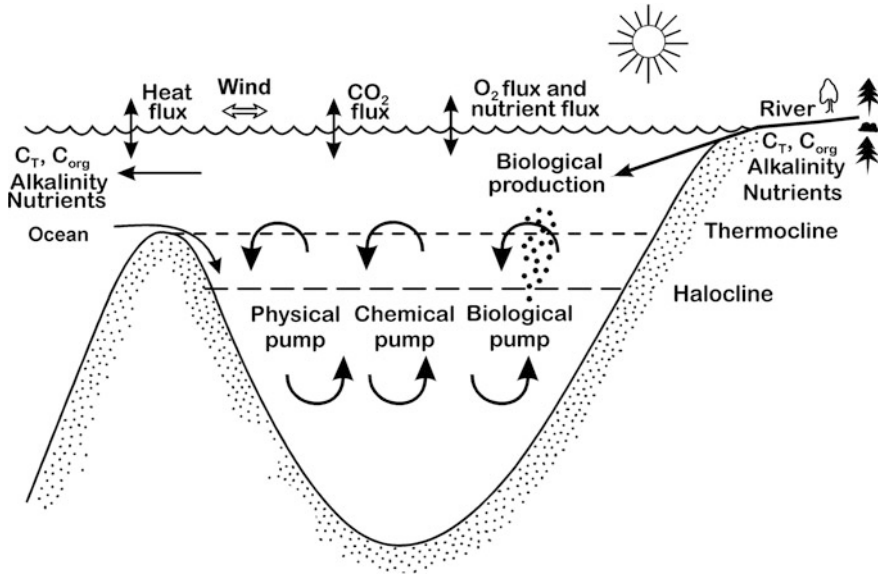

Fig. 4.15 The carbon cycle in a coastal sea including biological factors

4.7 Modeling the Dynamics of Plankton, Oxygen, and Carbon

4.7.1 Introduction

In this section, we will learn how to analyze the coupling between biological production and the dynamics of carbon/oxygen (Fig. 4.15). The plankton model presented in Sect. 4.5 will now be used, together with the inorganic carbon model presented in Sect. 4.6. We will find a strong interaction between their dynamics.

4.7.2 Mathematical Formulation

For the equations of the physical model, the reader is referred to Chap. 3. In the following, we consider only the changes needed to model carbon dynamics. The state variables are total inorganic carbon, C_T, and total alkalinity, A_T. We must also consider the dynamics of primary production, nutrients, and oxygen. We now summarize what we have learned from the previous chapters.

The conservation equations read:

$$\begin{cases} \frac{\partial {}^{O_2}C}{\partial t} + W\frac{\partial {}^{O_2}C}{\partial z} = \frac{\partial}{\partial z}\left[\frac{\mu_{eff}}{\rho\sigma_{O_2}}\frac{\partial {}^{O_2}C}{\partial z}\right] + S_{{}^{O_2}C} \\ \frac{\partial {}^{pp}C}{\partial t} + W\frac{\partial {}^{pp}C}{\partial z} = \frac{\partial}{\partial z}\left[\frac{\mu_{eff}}{\rho\sigma_{{}^{pp}C}}\frac{\partial {}^{pp}C}{\partial z}\right] + S_{{}^{pp}C} \\ \frac{\partial {}^{n}C}{\partial t} + W\frac{\partial {}^{n}C}{\partial z} = \frac{\partial}{\partial z}\left[\frac{\mu_{eff}}{\rho\sigma_{{}^{n}C}}\frac{\partial {}^{n}C}{\partial z}\right] + S_{{}^{n}C} \\ \frac{\partial C_T}{\partial t} + W\frac{\partial C_T}{\partial z} = \frac{\partial}{\partial z}\left[\frac{\mu_{eff}}{\rho\sigma_{C_T C}}\frac{\partial C_T}{\partial z}\right] + S_{C_T} \\ \frac{\partial A_T}{\partial t} + W\frac{\partial A_T}{\partial z} = \frac{\partial}{\partial z}\left[\frac{\mu_{eff}}{\rho\sigma_{A_T C}}\frac{\partial A_T}{\partial z}\right] + S_{A_T} \end{cases} \tag{4.29}$$

where S_{C_T} denotes sources/sinks of CO_2 connected with biological production (i.e., photosynthesis/mineralization). The symbols are as follows: ${}^{pp}C$ is the phytoplankton concentration, ${}^{n}C$ the concentration of the limiting nutrient modeled as dissolved inorganic phosphate, PO_4, and O_2 the oxygen concentration.

We will only consider plankton growth, sedimentation, and mineralization. The source/sink terms read:

$$\begin{cases} S_{O_2} = s_{O_2} G_p {}^{pp}C - \alpha_{1\min} e^{\alpha_{2\min} T} {}^{pp}C \\ S_{{}^{pp}C} = G_p {}^{pp}C + w_p \frac{\partial {}^{pp}C}{\partial z} - \alpha_{1\min} e^{\alpha_{2\min} T} {}^{pp}C / s_{O_2} \\ S_{{}^{n}C} = -s_P G_p {}^{pp}C + s_P / s_{O_2} \alpha_{1\min} e^{\alpha_{2\min} T} {}^{pp}C + \alpha_{2s} A_{sed} w_{psed} \\ S_{C_T} = -G_p {}^{pp}C s_{CO_2} + s_{CO_2} / s_{O_2} \alpha_{1\min} e^{\alpha_{2\min} T} {}^{pp}C \\ S_{A_T} = 0 \end{cases} \tag{4.30}$$

where G_p is the net growth of bulk phytoplankton, w_p the sinking velocity of the bulk phytoplankton, and s_{O_2}, s_P, and s_{CO_2} the stoichiometric relationships that transform plankton concentrations to oxygen, phosphorus, and carbon with constants of 138, 1, and 106, respectively. Note that we assume that the phytoplankton do not produce shells; if the plankton are assumed to produce or dissolve shells, this should be entered as a sink/source term in the A_T equation.

The air–water surface boundary conditions are described by the following:

$$\begin{cases} \frac{\mu_{eff}}{\rho\sigma_{O_2}}\frac{\partial {}^{O_2}C}{\partial z} = F_{O_2} \\ \frac{\mu_{eff}}{\rho\sigma_{{}^{pp}C}}\frac{\partial {}^{pp}C}{\partial z} = 0 \\ \frac{\mu_{eff}}{\rho\sigma_{{}^{n}C}}\frac{\partial {}^{n}C}{\partial z} = 0 \\ \frac{\mu_{eff}}{\rho\sigma_{C_T}}\frac{\partial C_T}{\partial z} = F_{CO_2} \\ \frac{\mu_{eff}}{\rho\sigma_{A_T}}\frac{\partial A_T}{\partial z} = 0 \end{cases} \tag{4.31}$$

where the fluxes read:

$$\begin{cases} F_{O_2} = k_C({}^{O_2}C - {}^{O_2}C_{sat}) \\ F_{CO_2} = k_{wCO_2}\alpha_{CO_2}\left(pCO_2^w - pCO_2^a\right) \end{cases} \tag{4.32}$$

River water adds both carbon and nutrients to the water; for nomenclature, see Appendix B.

4.7.3 Details of Calculations

Equations are solved for a 250-m-deep estuary with a geometry similar to that of the Baltic Sea. The FORTRAN settings of the case are presented in `case_ex10b.f` (for the programs needed, see Appendix C), in which the equations for nutrient and plankton concentrations need to be active (see Chap. 1 in the subroutine).

4.7.4 Results

Figure 4.16 presents carbon dioxide partial pressure calculated by modeling. The partial pressure of CO_2 is now reduced in summer, and displays decreasing values associated with increased primary production. While flux has both positive and negative signs (Fig. 4.17), flux into the sea is increasing. During primary production, the partial pressure in water decreases and becomes less than in the atmosphere, so CO_2 flux is *into* the sea. Primary production thus overcomes the temperature effect in summer. In winter, the partial pressure in water is greater than

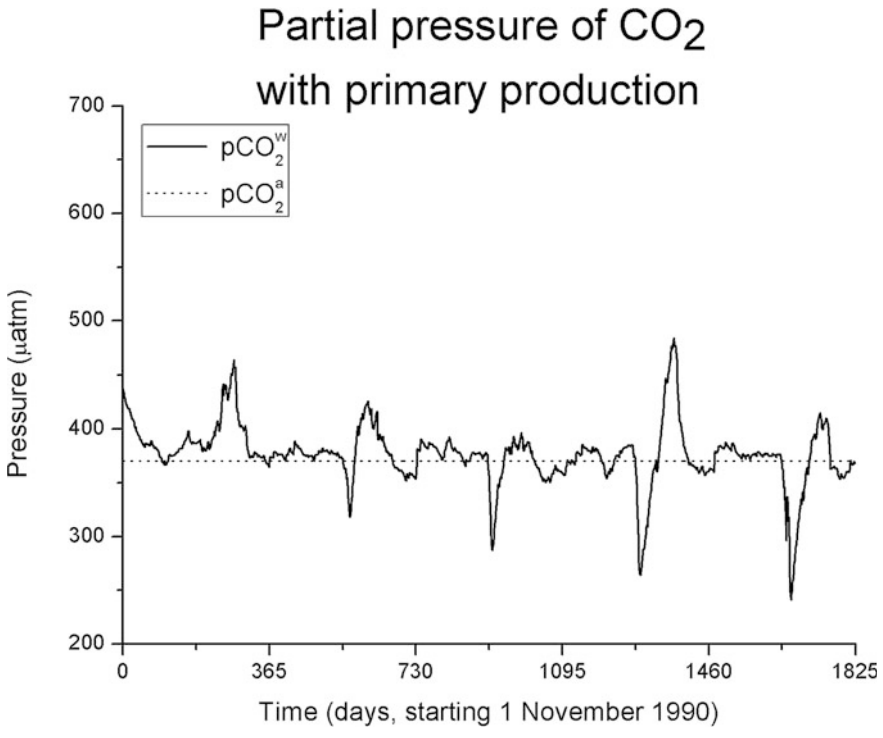

Fig. 4.16 Calculated partial pressure of CO_2 with primary production

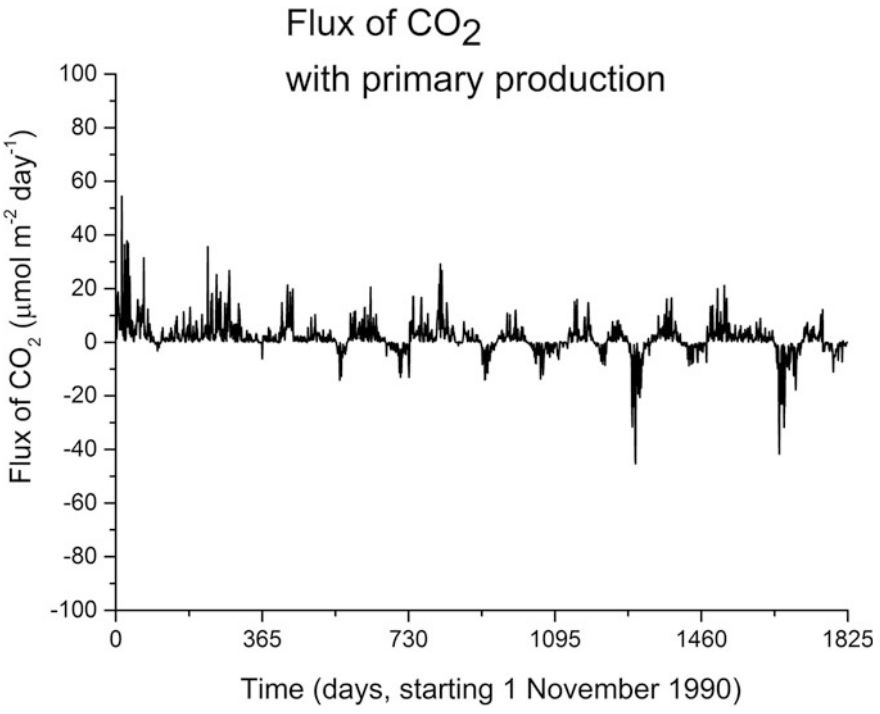

Fig. 4.17 Calculated CO_2 flux with primary production

in the atmosphere and the flux goes *out of* the sea. Observations of the partial pressure of CO_2 in coastal seas yield important information about biological production and could be used when developing and testing ecosystem models (Schneider et al. 2006).

Exercise 4.5
Observations from the central Baltic Sea indicate that the partial pressure of CO_2 in the water declines to nearly 150 μatm in summer. Several mechanisms may explain this, including the fact that nutrients are recycled more actively in the photic zone than is carbon. Explore this by letting the phosphorus recycle during primary production. *Hint:* Use PFRAC in `case_ex10b.f`. Include estuarine circulation, which generates oxygen-rich bottom water and inhibits phosphorus leakage from bottom sediments. Assume inflow values according to Exercise 4.4.

4.7.5 Discussion

Changes due to eutrophication, climate change, and marine acidification may severely affect the carbon and nutrient cycles and therefore marine ecosystems. The CO_2 and O_2 dynamics are central to these changes in marine biogeochemical cycles and to ecosystem health. In our modeling, organic carbon and the effects of various algae species need further consideration. We have also not yet considered the carbon system in anoxic waters. This will be the topic for the next section.

4.8 Modeling the Dynamics of CO_2 in a Redox Environment

4.8.1 Introduction

In this section, we will learn how to model the carbon system under oxic and anoxic conditions. Coastal seas face severe threats, and dead zones caused by insufficient oxygen concentrations have spread exponentially since 1960 (Diaz and Roseberg 2008). The largest anthropogenic hypoxic area in the world is believed to be in the Baltic Sea (Carstensen et al. 2014), where the hypoxic area has increased ten-fold over the past 115 years; Fig. 4.18 shows such an area from autumn 2010. Many biogeochemical processes are sensitive to shifts between oxic and anoxic water

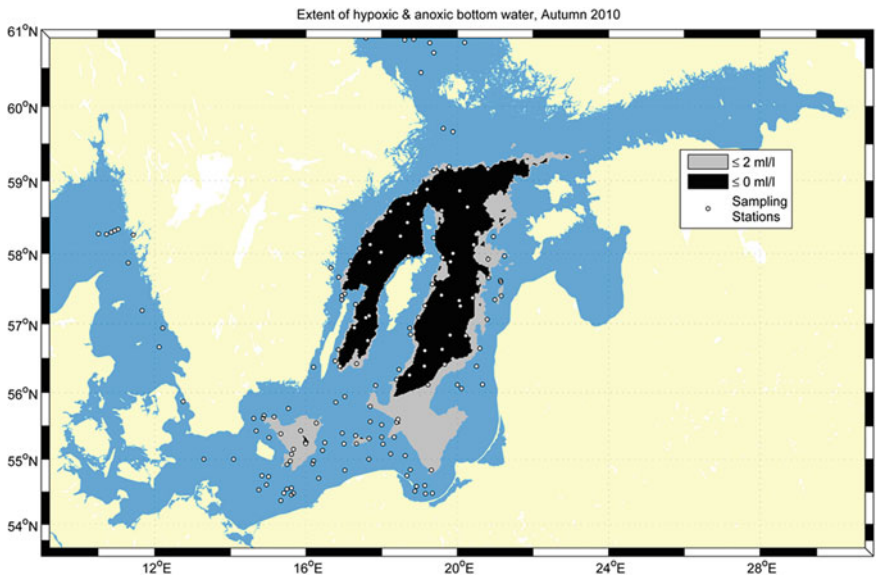

Fig. 4.18 Extent of hypoxic and anoxic bottom water during autumn 2010 (figure courtesy of SMHI)

conditions and they need to be considered in the modeling. For example, we have already learned that phosphorus starts to leak from the sediment under anoxic conditions, becoming an important source of nutrients in the water column. At the same time, total alkalinity increases, thereby increasing the water buffer capacity. The biogeochemical model presented in Sect. 4.7 will be extended by adding chemical reactions in redox environments according to the model of Edman and Omstedt (2013).

4.8.2 Mathematical Formulation

Organic matter mineralizes through oxygen reduction and when the water becomes anoxic through nitrate and sulfur reduction. The total mineralization is the sum of the various mineralization processes according to:

$$M_T = M_{\mathrm{O}_2} + M_{\mathrm{NO}_3} + M_{\mathrm{SO}_4} \tag{4.33}$$

where the terms denote total mineralization and mineralization due to oxygen, nitrate, and sulfur reduction, respectively.

In the marine dissolved-CO_2 system, we need to reconsider the definition of total alkalinity and include ammonium, phosphorous, and sulfur as well:

$$\begin{aligned} A_T \approx\ & \left[\mathrm{HCO_3^-}\right] + 2\left[\mathrm{CO_3^{2-}}\right] + \left[\mathrm{B(OH)_4^-}\right] + \left[\mathrm{HPO_4^{2-}}\right] + 2\left[\mathrm{PO_4^{3-}}\right] \\ & + \left[\mathrm{NH_3}\right] + \left[\mathrm{HS^-}\right] + \left[\mathrm{OH^-}\right] - \left[\mathrm{H^+}\right] \end{aligned} \tag{4.34}$$

where protons are added due to two phosphorus components, i.e., HPO_4^{2-} and PO_4^{3-}, as well as ammonia, NH_3, and hydrosulfide, HS^{-1}. The total alkalinity definition is an approximation, but the additional species make a small contribution to the total alkalinity. In the following section, we will simplify the Edman and Omstedt (2013) model by considering only changes in alkalinity due to sulfur reduction.

The conservation equations follow Eq. 4.29, but the source and sink terms now read:

$$\begin{cases} S_{\mathrm{O}_2} = s_{\mathrm{O}_2} G_p{}^{pp} C - M_T \\ S_{pp C} = G_p{}^{pp} C + w_p \frac{\partial^{pp} C}{\partial z} - M_T s_{\mathrm{O}_2} \\ S_{n C} = -s_{\mathrm{p}} G_p{}^{pp} C + s_P / s_{\mathrm{O}_2} M_T + \alpha_{2s} A_{sed} w_{psed} \\ S_{C_T} = -G_p{}^{pp} C s_{\mathrm{CO}_2} + s_{\mathrm{CO}_2} / s_{\mathrm{O}_2} M_T \\ S_{A_T} = M_{\mathrm{SO}_4} \end{cases} \tag{4.35}$$

The oxic mineralization rate depends on the total mineralization rate of organic matter, where we now consider only oxygen and sulfur reduction. The reduction of 1 mol of sulfate is equivalent to the production of 2 mol of negative oxygen (i.e., –2

CO_2 = HS^-). This needs to be considered, as we are modeling sulfate as negative oxygen. Sulfate is reduced during anoxic mineralization as follows:

$$M_{SO_4} = M_T(1 - \gamma_{O_2}) \text{ where } \gamma_{O_2} = 1 \text{ if } O_2 > 0 \text{ or } 0 \text{ if } O_2 \leq 0 \tag{4.36}$$

4.8.3 Details of Calculations

Equations are solved for a 250-m-deep sea with inflowing dense water that generates strong stratification. The oxygen ventilation of the bottom water is weak, so we instead assume that the inflowing water does not add oxygen. We set `PFRAC = 0.5` to increase the mineralization, and during anoxic bottom water conditions, the alkalinity-generating source terms create alkalinity due to sulfate reduction. The FORTRAN settings of the case are presented in `case_ex10c.f`, where the alkalinity generation during anoxic conditions is modeled according to $M_{SO_4} = M_T$.

4.8.4 Results

Figure 4.19a and b presents the modeled oxygen and salinity structure, with strong salinity stratification and mineralization in deeper layers causing hypoxia and anoxic deep water. The modeled total alkalinities are illustrated in Fig. 4.19c. The total alkalinity is increasing in deep water due to sulfate reduction. The difference between a model run with and without alkalinity generation is illustrated in Fig. 4.19d, where the alkalinity increase occurs at a depth of approximately 120 m with no increase in bottom layers due to dilution from inflowing less alkaline water.

Exercise 4.6
When introducing the dynamics of CO_2 in a redox environment, models are developed that can be used for analyzing multiple factors stressing the marine ecosystem, for example, climate change, eutrophication, and marine acidification. Examine the surface pH change in a warmer atmosphere containing increased CO_2. Examine a 4 °C temperature increase with an atmospheric carbon dioxide partial pressure of 1000 μatm. Which is more important for the pH change, temperature increase or atmospheric CO_2 increase? *Hint:* Start from subroutine `case_ex10c.f` and change the air temperature and atmospheric carbon dioxide partial pressure one by one according to the exercise.

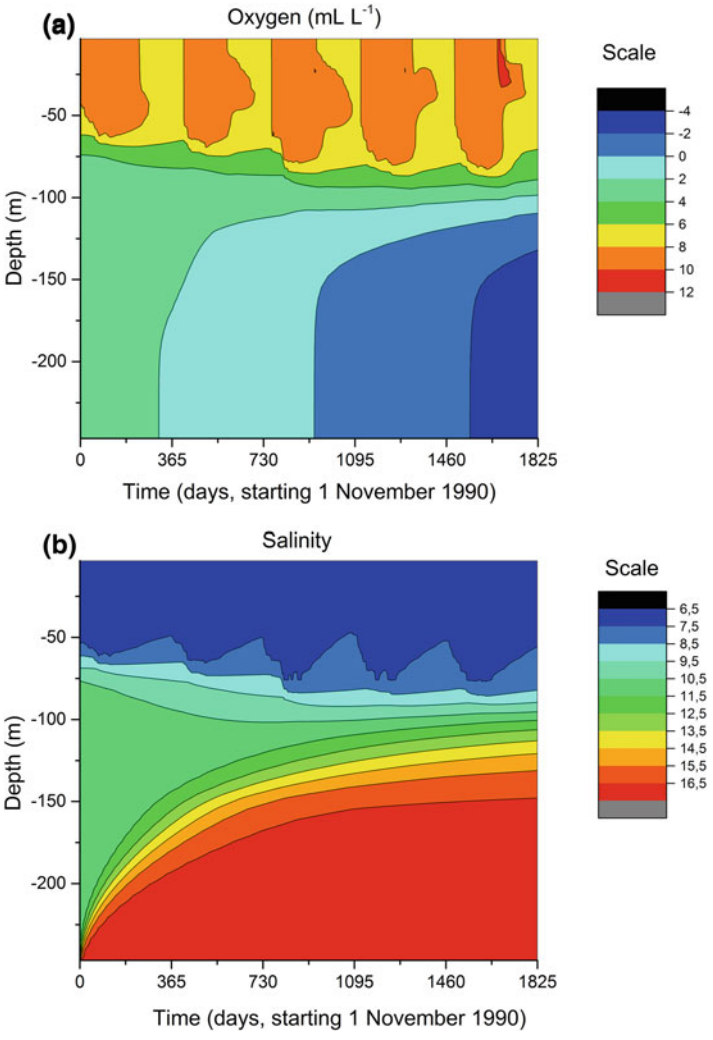

Fig. 4.19 Calculated. **a** oxygen concentration, **b** salinity, **c** total alkalinity with sulfate reduction, and **d** difference between total alkalinity with and without sulfate reduction

4.8.5 Discussion

The acid–base balance in coastal seas also needs to take account of the inflow from rivers, which add organic and inorganic carbon components. The influence of dissolved organic matter in the Baltic Sea was recently analyzed by Kuli´nski et al.

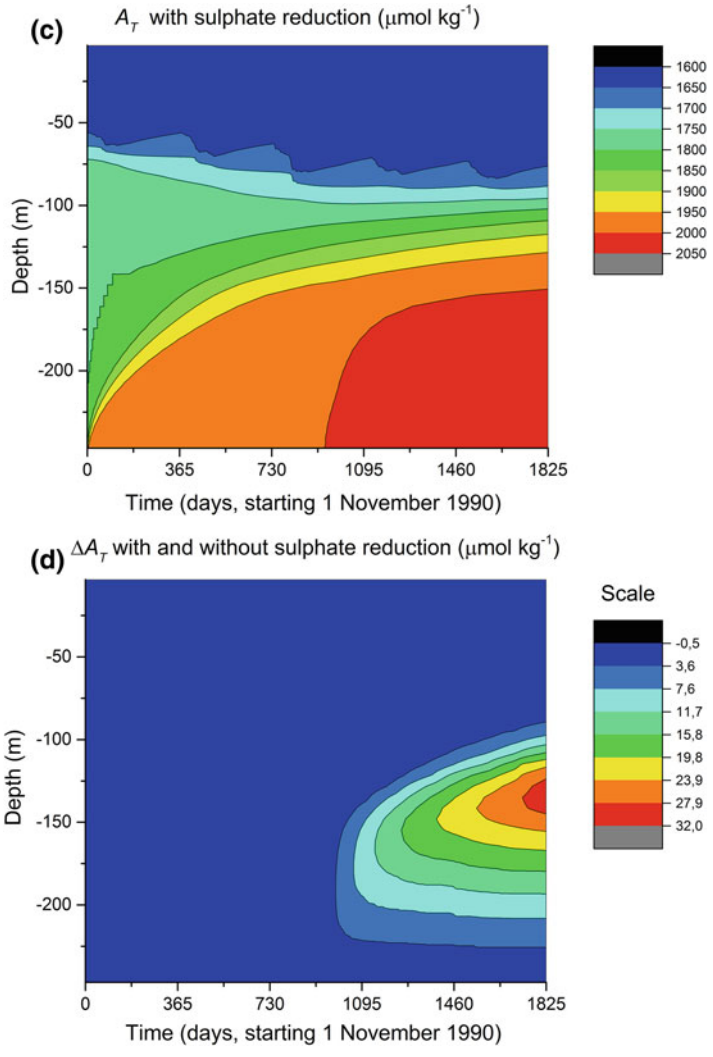

Fig. 4.19 (continued)

(2014). In their study, the organic alkalinity was shown to account for some percentage of the total alkalinity; still, the effects of organic matter from river water need further consideration. Also the total alkalinity loads versus internal generation need further considerations (Gustafsson et al. 2014).

Chapter 5
Construction of Nets of Sub-basins

5.1 Modeling Two Coupled Sub-basins

5.1.1 Introduction

In many aquatic applications, geometry and dynamics split a water body into regions controlled by different physical processes (Fig. 5.1). A useful approach is to model the system as a net of sub-basins and separately examine the effects of local factors and the interactions between surrounding basins. This approach is an obvious choice for water bodies with complex geometries due to straits, bays, islands, estuaries, and semi-enclosed seas, but it could also be used in mass balance studies of large water bodies such as oceans; for example, we could examine the water balance by looking at the exchange of water between the Arctic and Atlantic oceans. In this chapter, we will first learn how to couple two coastal basins and how to include a moving grid for calculating changes in water levels. From the exercise, we will learn how to expand the two-basin model to a three-basin model. Then we will examine a fully coupled sub-basin system that divides the Baltic Sea into 13 sub-basins. Coupling between the sub-basins is through the exchange of water and properties between the sub-basins. The same method has already been used for complex lakes such as lakes Mälaren and Vänern in Sweden, archipelago seas (e.g., Engqvist and Omstedt 1992; Engqvist and Stenström 2004; Sahlberg 2009), coastal zones (e.g., Sahlberg 2009, http://vattenwebb.smhi.se/kustzondiff/), the Baltic Sea (e.g., Gustafsson 2000a, b; Omstedt 1987a, 1990a, Omstedt and Axell 2003; Stigebrandt 1983, 1987), the Mediterranean Sea (e.g., Shaltout and Omstedt 2012, 2014), the Mackenzie shelf/estuary and the Laptev Sea (e.g., Omstedt Carmack and Macdonald 1994; Wåhlström et al. 2012, 2013).

A. Omstedt, *Guide to Process Based Modeling of Lakes and Coastal Seas*,
Springer Praxis Books, DOI 10.1007/978-3-319-17990-2_5

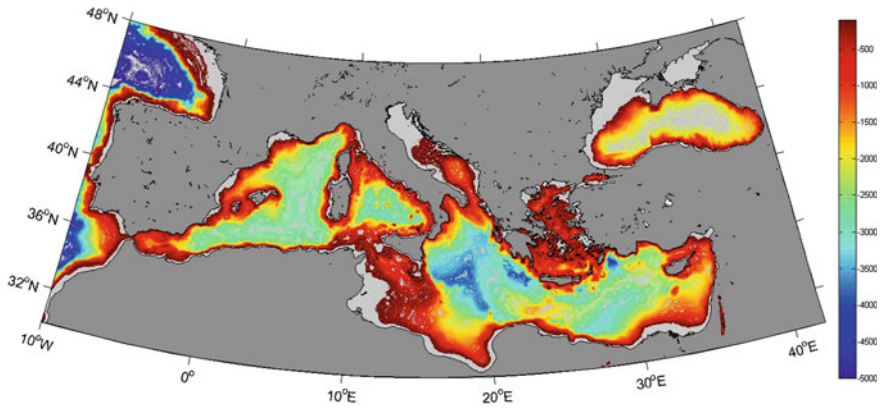

Fig. 5.1 The bathymetry of the Mediterranean–Black Sea system depicting narrow straits, deep sub-basins, and archipelago seas

5.1.2 Mathematical Formulation

In this section, we will first model a two-basin coupled system. Modeling starts from the mathematical model developed in Chap. 3 and adds the effects of horizontal exchange between the two sub-basins. For both basins, the following equations are used.

The transport equations for horizontal momentum read:

$$\frac{\partial \rho U}{\partial t} + W\frac{\partial \rho U}{\partial z} = \frac{\partial}{\partial z}\left[\frac{\mu_{eff}}{\rho}\frac{\partial \rho U}{\partial z}\right] + f\rho V \tag{5.1}$$

$$\frac{\partial \rho V}{\partial t} + W\frac{\partial \rho V}{\partial z} = \frac{\partial}{\partial z}\left[\frac{\mu_{eff}}{\rho}\frac{\partial \rho V}{\partial z}\right] - f\rho U \tag{5.2}$$

$$W(z) = \left[Q(z)_{in} - Q(z)_{out}\right]/A(z) \tag{5.3}$$

where U and V represent currents to the east and north, respectively, W vertical velocity calculated from the differences between inflows and outflows, A area, f the Coriolis parameter, ρ water density, and μ_{eff} effective dynamic viscosity.

Vertical velocity is derived by integrating the continuity (Eq. 2.9), while the different sub-basins are coupled by adding the properties transported by the inflows. Outflow properties are calculated from the sub-basin itself.

The conservation equation for heat reads:

$$\frac{\partial \rho_0 c_p T}{\partial t} + W\frac{\partial \rho_0 c_p T}{\partial z} = \frac{\partial}{\partial z}\left[\frac{\mu_{eff}}{\rho_0 \sigma_{eff}}\frac{\partial \rho_0 c_p T}{\partial z}\right] + \Gamma_{sun} + \Gamma_h \tag{5.4}$$

$$\Gamma_{sun} = F_s^w (1-\eta) \mathrm{e}^{-\beta(D-z)} \tag{5.5}$$

$$\Gamma_h = \rho c_p \left(\frac{Q_{in} T_{in}}{\Delta V_{in}} - \frac{Q_{out} T}{\Delta V_{out}} \right) \tag{5.6}$$

where Γ_{sun} and Γ_h are source terms associated with solar radiation and heat associated with the inflow and outflow; T_{in} is the inflow temperature, and ΔV_{in} and ΔV_{out} volumes at the depth where inflow and outflow occur. When inflowing heat is greater/less than the outflowing heat, Eq. 5.6 tells us that the source term adds/subtracts heat to the basin.

The conservation equation for salinity reads:

$$\frac{\partial S}{\partial t} + W \frac{\partial S}{\partial z} = \frac{\partial}{\partial z} \left[\frac{\mu_{eff}}{\rho_0 \sigma_{eff}} \frac{\partial S}{\partial z} \right] + \Gamma_s \tag{5.7}$$

$$\Gamma_s = \frac{Q_{in} S_{in}}{\Delta V_{in}} - \frac{Q_{out} S}{\Delta V_{out}} - \frac{Q_f S_{sur}}{\Delta V_{sur}} \tag{5.8}$$

where Γ_s is the source term for salt transports associated with the inflows and outflows, and S_{sur} is surface salinity. From Eq. 5.8 we can learn that the river runoff always reduces the salinity.

5.1.3 Details of Calculations

Equations are solved for a 250-m-deep inner basin coupled to a 100-m-deep outer basin. Initial conditions assume constant salinity and temperature profiles in the outer basin, while the salinity and temperature profiles are stratified in the inner basin. River runoff is assumed to be 15,000 $m^3\ s^{-1}$ into the inner basin and zero into the outer basin. Coupling between the sub-basins occurs through baroclinic exchanges, with inflow to the inner basin equaling river runoff and outflow from the inner basin equaling twice the river inflow. We use two datasets for the meteorological forcing. The FORTRAN settings of the case are presented in the subroutines `basin1.f` and `basin2.f`. Note that a moving grid can be specified in the subroutines by setting `MOVE=.TRUE.`, and that the variable names of the properties that change between the two basins need to be available in both basins (see `Comp2.inc`).

5.1.4 Results

The results of a coupled simulation are presented in Figs. 5.2 and 5.3. The salinity response of the outer basin is presented in Fig. 5.2. The calculation shows the

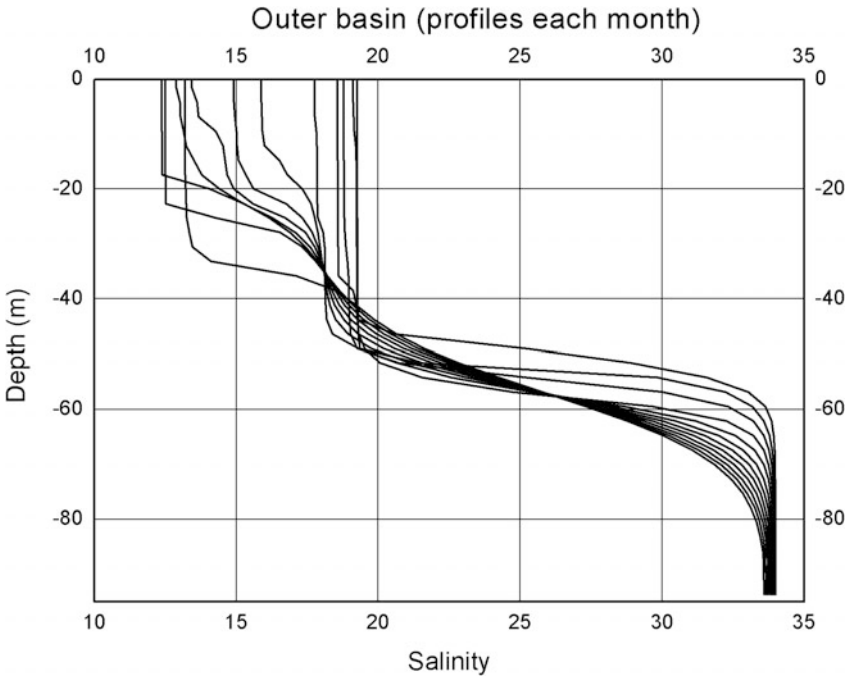

Fig. 5.2 The salinity response in the outer basin over a one-year run

development of a brackish surface layer in the upper 20 m of the basin. Figure 5.3 presents the corresponding result for the inner basin, where the inflowing water forms a dense bottom layer.

Exercise 5.1
Add a third basin and present the salinity variations for the new coupled system. *Hint*: Add a new inner basin to the two-basin model and assume river runoff of 5000 $m^3\ s^{-1}$ into the new basin. Assume a sill depth of 20 m between the outer and middle basins and of 30 m between the middle and inner basins.

5.1.5 Discussion

In this section we do not deal with horizontal mixing processes such as front mixing and dense bottom current mixing. These processes are often crucial; suggestions for how to model them are available in the literature. For example, Stigebrandt (1987) introduced a model incorporating dense bottom currents and a buffer volume in the

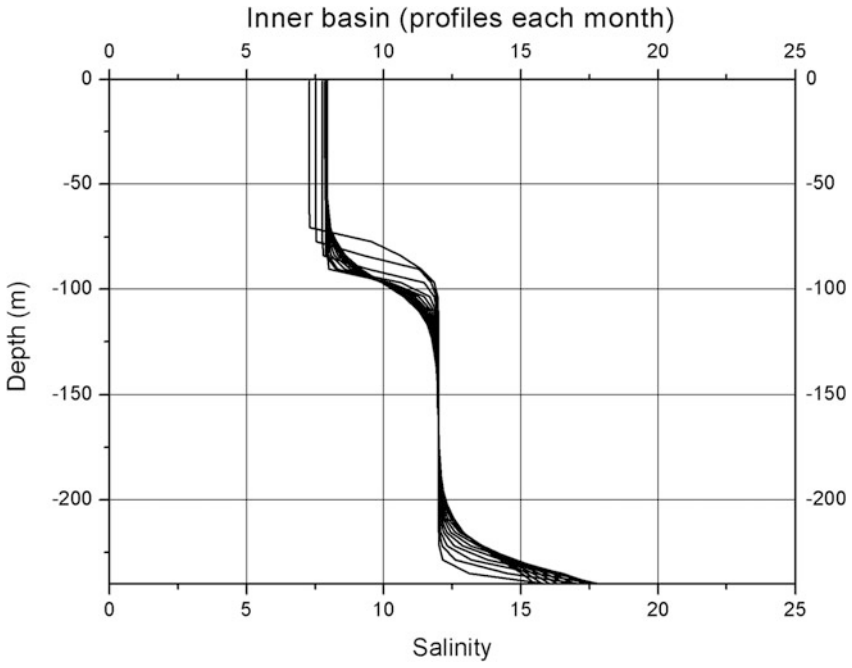

Fig. 5.3 The salinity response in the inner basin over a one-year run

Baltic Sea entrance area. Mattsson (1996) introduced a buffer volume, as well as selected withdrawal, in the Öresund. Several aspects of plume mixing and dense bottom currents can easily be tested and evaluated in the coupled-basin modeling.

5.2 The PROBE-Baltic Model System: Physical Aspects

5.2.1 Introduction

The PROBE-Baltic model (Fig. 5.4) is a process-based model applied to the Baltic Sea; its development started in the early 1980s. The first problems considered were the cooling of the sea surface layer around the temperature of maximum density (Omstedt 1983; Omstedt et al. 1983) and the forecasting of sea surface cooling (Omstedt 1984).

A four-basin coupled model of the Baltic Sea entrance area was then formulated to analyze the effects of advection on surface heat balance (Omstedt 1987a, b). In 1990, the first version of PROBE-Baltic was published (Omstedt 1990a); it divided the Baltic Sea into 13 sub-basins (Fig. 5.5) and began to be used as a forecasting model (Omstedt 1990b). Sea ice was not included at this stage, but a new ice model of coastal seas was developed (Omstedt 1990c). Sea ice processes were later

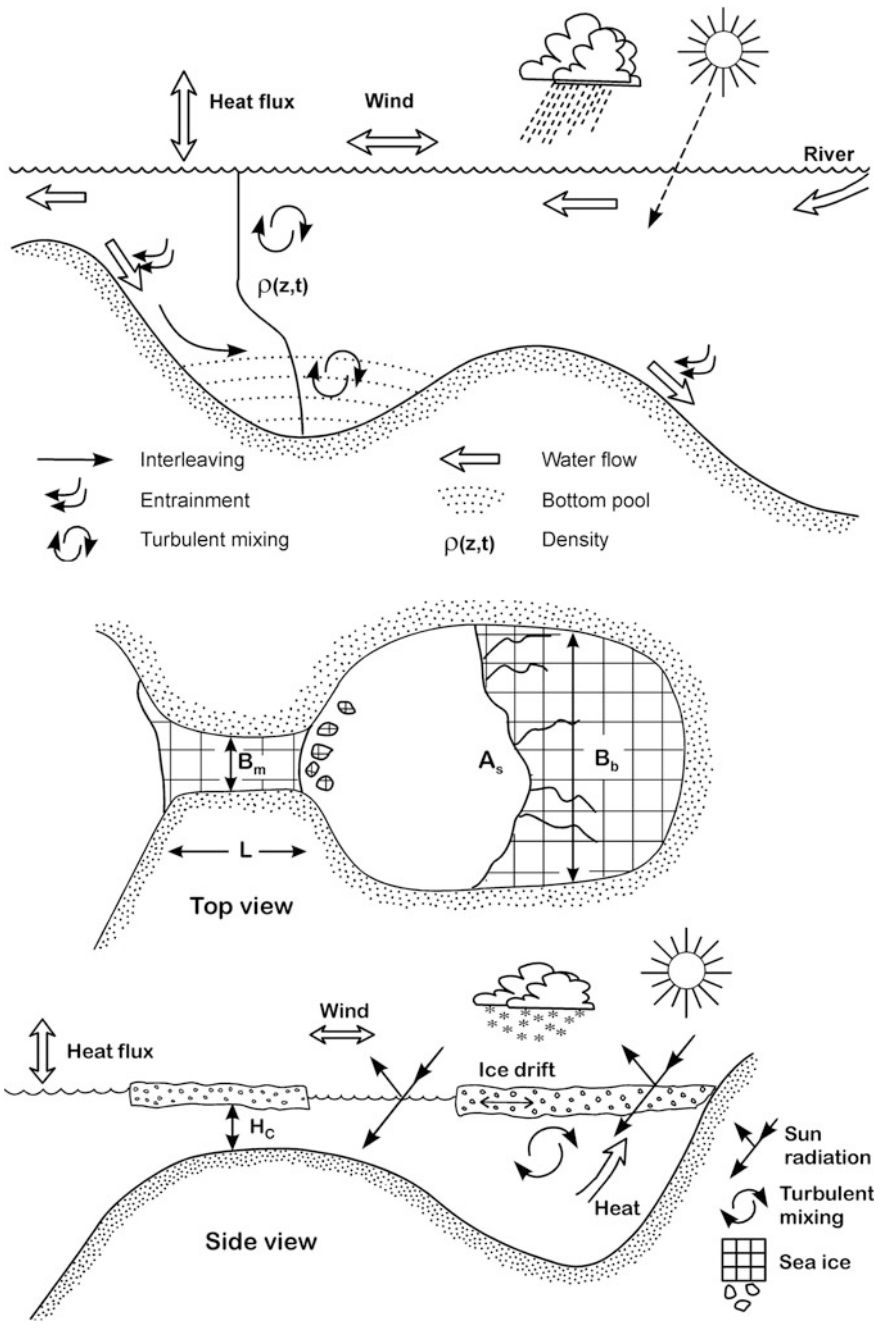

Fig. 5.4 Some of the major physical processes modeled in PROBE-Baltic

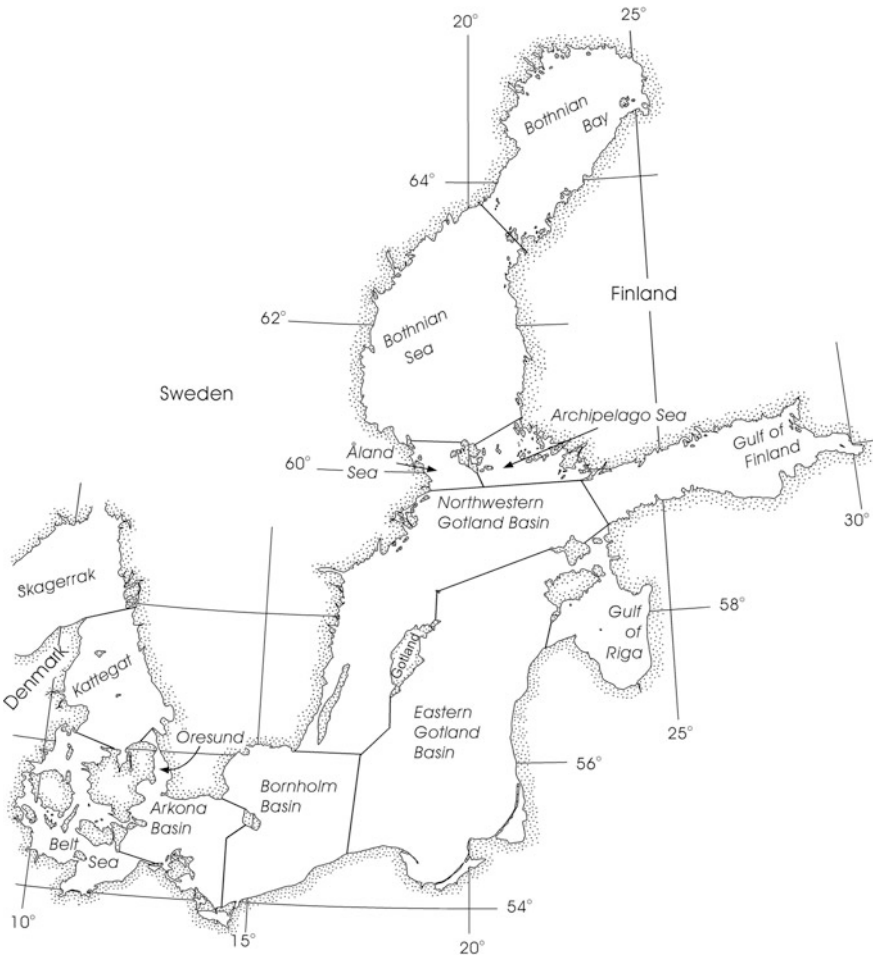

Fig. 5.5 The division of the Baltic Sea–Skagerrak system into thirteen natural sub-basins defining the sub-basins of the PROBE-Baltic model

included in PROBE-Baltic, and a coupled ice–ocean version was published in 1996, in which the climate sensitivity of the Baltic Sea was examined (Omstedt and Nyberg 1996). Deep-water circulation, salinity, and temperature variations were later examined using this coupled version (Omstedt and Axell 1998, 2003). The 2003 paper fully describes the physical modeling, so this material will not be repeated here. The PROBE-Baltic model has also been used in a number of other studies related to climate, water, and heat balances (e.g., Hansson and Omstedt 2008; Norman et al. 2013; Omstedt et al. 2000; Omstedt and Hansson 2006a, b; Omstedt et al. 1997; Omstedt and Nohr 2004; Omstedt and Rutgersson 2000; Rutgersson et al. 2001; Rutgersson et al. 2002).

The biogeochemical modeling undertaken by the PROBE-Baltic model currently includes oxygen dynamics (Gustafsson and Omstedt 2009) and the dynamics of plankton, nutrients, and carbon in the Baltic Sea (Edman and Omstedt 2013; Omstedt et al. 2010, 2012, 2009). The work was inspired by new measurements of the CO_2 system made by Bernd Schneider's group at the Leibniz Institute for Baltic Sea Research, Warnemuende, Germany (Schneider et al. 2006) and by the modeling of the nutrient balances and eutrophication of the Baltic Sea by several researchers (e.g., Marmefelt et al. 1999; Savchuk and Wulff 2007; Stigebrandt and Wulff 1987).

The main aim of this and the following sections is to introduce the reader to the PROBE-Baltic model, which incorporates fully coupled physical and biogeochemical modeling systems. Any model system should include numerical code and initial, forcing, and validation data. Great efforts have been made to develop these modeling aspects in the PROBE-Baltic system, and forcing files extending back to year 1500 are now available. The present educational version of PROBE-Baltic, however, will deal only with simulations from 1958 to 2012; supplementary material for longer runs is available and described in Appendix C.

5.2.2 Mathematical Formulation

The modeling of transport equations for horizontal momentum, conservation of heat and salt, and turbulence follow the mathematical formulations discussed in Sect. 5.1.2; therefore, they will not be repeated here. In the following, we will discuss some basic aspects of modeling. Vertical mixing is associated with a transient turbulent Ekman layer. However, for the Danish Straits, a transient turbulent channel model is introduced instead, with one channel model for the Great Belts and another for the Öresund. The transport equation reads:

$$\frac{\partial \rho_0 U}{\partial t} + W\frac{\partial \rho_0 U}{\partial z} = \frac{\partial}{\partial z}\left[\frac{\mu_{eff}}{\rho_0}\frac{\partial \rho_0 U}{\partial z}\right] - g\rho_0\frac{\partial \zeta}{\partial x} \tag{5.9}$$

where U represents the current component in the channel direction, W the vertical velocity calculated from the differences between the inflow and outflow, g a gravity constant, ρ_0 water density, ζ sea level, and μ_{eff} effective dynamic viscosity. In the following, we consider only variations in the x dimension and sea level variations calculated from differences from surrounding sub-basins.

The various sub-basins are horizontally coupled to each other through the inflows and outflows and their upstream properties. For the Baltic Sea, we use three types of models according to Stigebrandt (2001). Barotropic exchange driven by sea level variations across the Danish straits is calculated from:

$$Q_b^2 = \frac{1}{c_s}\Delta z \tag{5.10}$$

where Δz is the sea level difference between the surrounding basins, Q_b barotropic inflow and outflow through the Baltic Sea entrance area, and c_s a strait-specific constant.

Baroclinic exchange associated with stratified fluids often has a large impact. In straits wider than the Rossby radius of deformation, we assume a geostrophic baroclinic formulation for surface water outflows as follows:

$$Q_g = \frac{g\left(\frac{\rho_2-\rho_1}{\rho_0}\right)H_{sur}^2}{2f} \tag{5.11}$$

where H_{sur} represents the mixed surface layer thickness of density ρ_1 overlying a deeper layer of density ρ_2. For deep water inflows, the corresponding formulation reads:

$$Q_g = \frac{g\left(\frac{\rho_2-\rho_1}{\rho_0}\right)\left(H_{sill} - H_{sur}\right)^2}{2f} \tag{5.12}$$

where H_{sill} is the sill depth.

For straits narrower than the internal Rossby radius of deformation, geostrophic flow will not constrain the flow, so we consider geometrical constriction instead and the concept of baroclinic controls can then be applied. Basic assumptions in the derivation are that the strait flow can be simplified as a two-layer flow and that the flow is in steady state (i.e., no time variations), then:

$$Q_{bc}^{\max} \approx Q_f\left(\frac{1}{16F_e^2}\right)^{\frac{1}{3}} \tag{5.13}$$

where the estuarine Froude number, F_e, is defined by:

$$F_e^2 = \frac{Q_f^2}{g\alpha_2 S_b H_c^3 B_s^2} \tag{5.14}$$

where S_b is the salinity in the lower layer, H_c the channel depth, B_c the channel width, and α_2 the salinity coefficient in the equation of state and equal to 8×10^{-4}.

Overflows may generate dense bottom currents starting at the sill depth and penetrating deeper layers. Stigebrandt (1987) developed a model for inflowing dense bottom water assuming non-rotating gravity currents and applied it to the Baltic Sea. The model includes water sinking along a sloping bottom (x direction); the specific flow, defined as the ratio of the flow volume and current width (q m^2 s^{-1}), will then increase downstream due to entrainment as follows:

$$\frac{dq}{dx} = w_e \tag{5.15}$$

where w_e is the entrainment velocity, which in this case reads:

$$w_e = 2m_0\sqrt{c_d^b}sU_d \tag{5.16}$$

where s is the inclination of the boundary between the bottom current and surrounding water, U_d downstream velocity, c_d^b the drag coefficient associated with bottom friction (assumed to be 3×10^{-3}), and m_0 an empirical constant ($m_0 \approx 0.6$).

As water is entrained into the bottom current, the properties change. Downstream changes in the salinity and temperature of the dense bottom current are described by:

$$dS_d = \frac{dq(S_e - S_d)}{q + dq} \tag{5.17}$$

$$dT_d = \frac{dq(T_e - T_d)}{q + dq} \tag{5.18}$$

where dS_d, dT_d, and dq represent the change in inflowing salinity, temperature, and specific flow volume, respectively; index d corresponds to the dense current and index e to the surrounding water. The dense bottom current changes its density and will end up in the downstream basin at a level at which inflowing water and the surrounding water are equal in density.

5.2.3 Details of Calculations

The model system is organized into a number of directories. The full model, including the Intel Visual FORTRAN platform under the directory `probe_baltic`, should be copied to the D: drive from which it can be run. If other drives are used, all addresses in the programs need to be changed. The structure of the directories is outlined below:

```
probe_baltic
   interpolating
   p13_70
      data
      in
      ori_graph
      ori_surf
      Out
      Phy
```

where p13_70 includes the full system, with forcing data in **data**, initialization routines in in, output files in Out, and all FORTRAN files in Phy. As PROBE-Baltic uses moving grid cells associated with sea level variation, the output files often need to be interpolated to a regular grid before being plotted using standard plotting programs. This is done in the **interpolating** directory, and the interpolated files are written to ori_graph for time series plots and to ori_surf for surface plots. To run the model system, we must consider the following:

1. Changes in initial data: The In directory includes initialization tables from which both time and starting profile can be changed. The physical parameters are given in INIT_TABF58.DAT and the biogeochemical parameters in INIT_TABB58.DAT. After correcting the date and initial profiles, one must run the Finit.vfproj and copin_xx.bat files.
2. Changes in simulation time: In p13_70, the DATE.DAT file must be specified with regard to the starting time (must be the same as in INIT_TABF58.DAT and TABB58.DAT) and running time must be specified in hours.
3. Change in model setup: This includes the kind of model we would like to use. In basin1.f, three models are currently available:

   IBIO=1 The PROBE-Baltic and the CO_2–O_2 model system
   IBIO=2 The PROBE-Baltic physical model system
   IBIO=3 The PROBE-Baltic physical part with simplified O_2 dynamics

4. Changes in model setup: After opening the Visual Fortran project Fversion1.vfproj under the probe_baltic directory and making the necessary changes in the FORTRAN files, the project can be built and the system is ready to run.

When the run is ready, interpolation can be done under the interpolating directory. In this directory, one needs to run Finterpolering.vfproj. First, however, the IBIO model must be defined in the to_surf_graph.for subroutine. The starting time, stop time, and number of profiles (npr) should be defined.

In this chapter, we will first investigate the physical properties and, therefore, use the IBIO=2 model version.

5.2.4 Results

Figures 5.6, 5.7 and 5.8 present time series of temperature, salinity, ice thickness, and ice concentration in Bothnian Bay, the most northerly sub-basin in the Baltic Sea. The simulation indicates large seasonal and interannual variation. When analyzing interannual variation, it is often useful to consider maximum summer temperature, which varies in the present simulation between approximately 13 and 19 °C. Note also that the model calculation indicates an increasing bottom temperature.

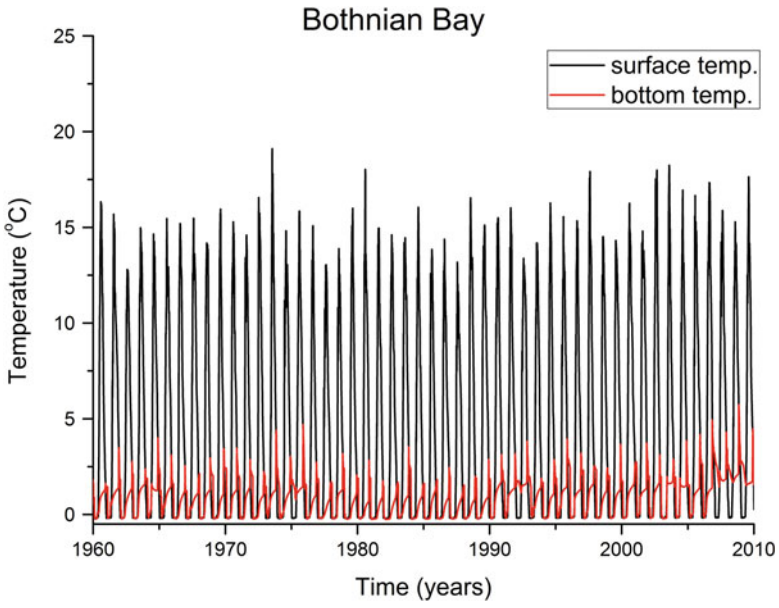

Fig. 5.6 Calculated surface and bottom temperatures in Bothnian Bay

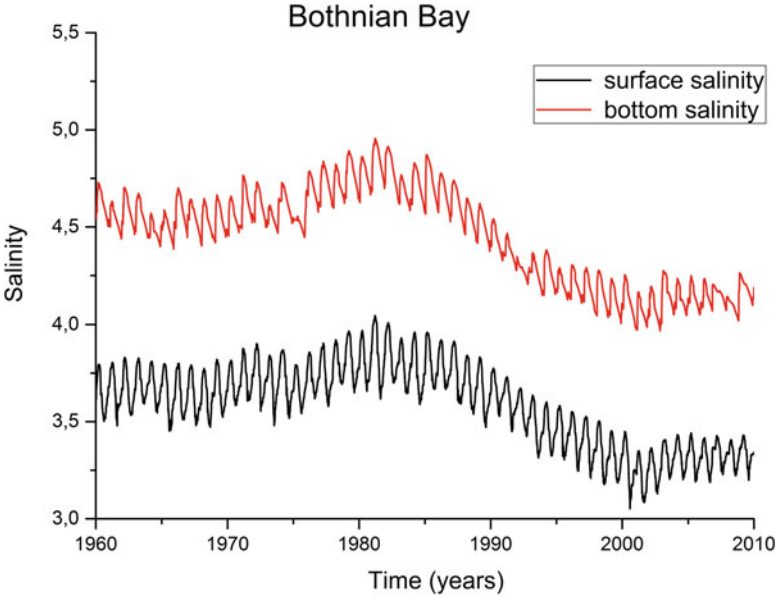

Fig. 5.7 Calculated surface and bottom salinities in Bothnian Bay

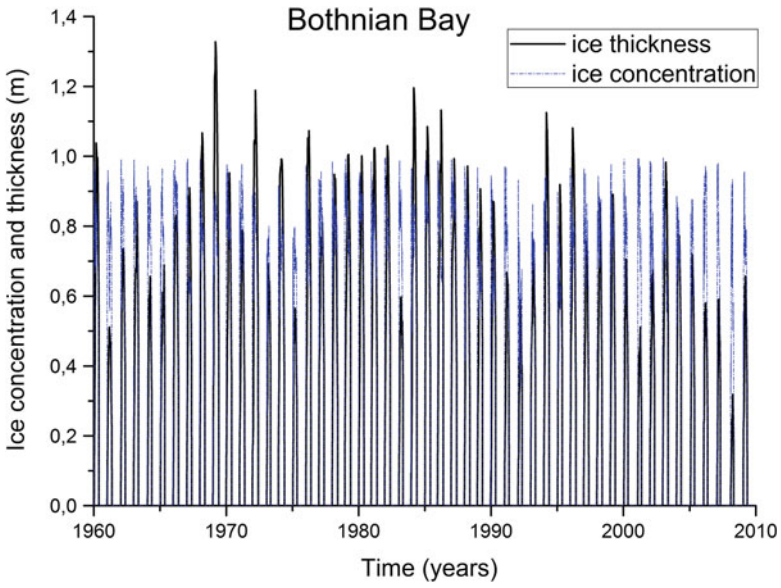

Fig. 5.8 Calculated sea ice concentration and thickness in Bothnian Bay

Seasonal variation in surface salinity is due to the summer thermocline, which reduces the mixing depth. This implies that the river water spreads out into a thinner layer and reduces the surface salinity. Deep water temperature and salinity data indicate inflows to Bothnian Bay every year. In Fig. 5.7, we can also see variations over longer time scales, with a decrease in salinity from approximately 1982 to 2001, after which it increases. This variation is also noticeable in observed mean Baltic Sea salinity (Winsor et al. 2001, 2003).

The ice thickness and concentration indicate that the ice concentration rapidly increases early in winter; later, however, the ice cover may shrink and deform due to changing wind patterns and ice ridging. The calculations indicate that every year the sea is covered with ice. Interannual variation during the simulation is quite large, and the ice thickness ranges from 0.3 to 1.3 m during the studied period.

A useful test of any marine numerical model is to plot a temperature–salinity (T–S) diagram (Fig. 5.9). Calculations in this figure are from the central Baltic Sea for a ten-year period. The T–S structure indicates three typical water masses. The first is the surface layer, characterized by large temperature and small salinity variations. The second is the halocline depth, characterized by rather small variations in both salinity and temperature. The third water mass is the deep water, characterized by large salinity but small temperature variations.

From the T–S diagram and by comparing calculated and observed data, we can learn much about many important aspects of the model. The calculated T–S structure may indicate whether the model has strong numerical diffusion, whether

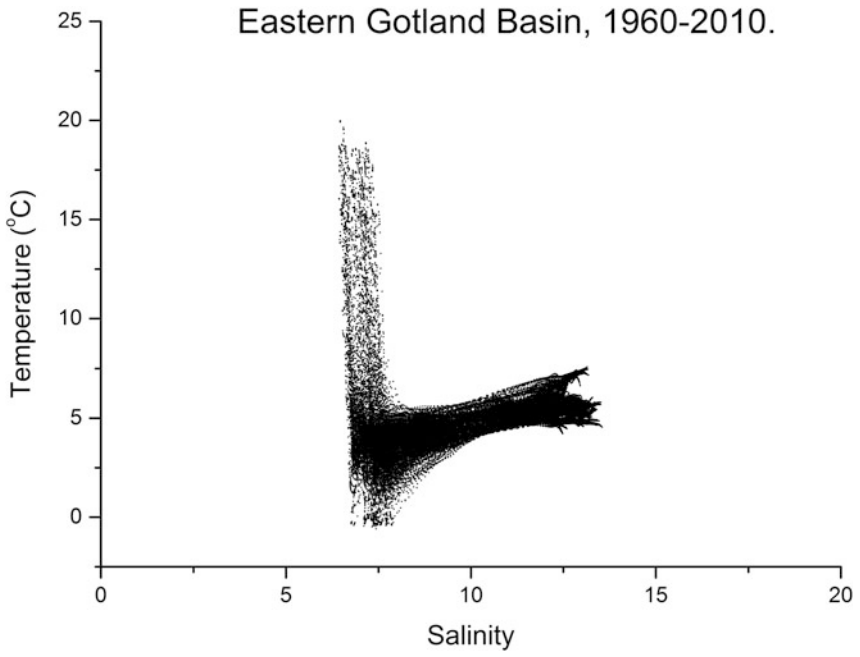

Fig. 5.9 Calculated salinity–temperature (T–S) diagram for the Eastern Gotland Basin

the deep-water mixing is reasonably parameterized, and whether the modeling of inflowing water masses is correct.

Exercise 5.2
Run the PROBE-Baltic model system for the 1958–2012 period, but only take physical aspects into consideration. Examine the calculated ice thickness in the Gulf of Riga over the 1960–2012 period. What is the typical calculated ice thickness in the Gulf?

5.2.5 Discussion

The model system can now be used in various studies, and new understanding of the processes involved in heat fluxes, sea ice, turbulent mixing, strait flows, and dense bottom currents can be tested. In addition, new knowledge of climate and environmental change can be evaluated, as can new ideas for managing the sea using different engineering suggestions.

5.3 The PROBE-Baltic Model System: Oxygen Aspects

5.3.1 Introduction

The oxygen dynamics are influenced by air–sea interaction, biological production, and the mineralization of biological material. The inflowing of dense surface water to deeper layers may increase the oxygen concentration, while stagnation periods without inflows may reduce the oxygen concentration through mineralization (Fig. 5.10). Organic matter mineralizes through oxygen reduction and when the water become anoxic through nitrate and sulfur reduction (Edman and Omstedt 2013). From studies of mineralization during stagnation periods, bulk mineralization rates can be estimated and will be applied in this chapter. Oxygen modeling is examined in the next section.

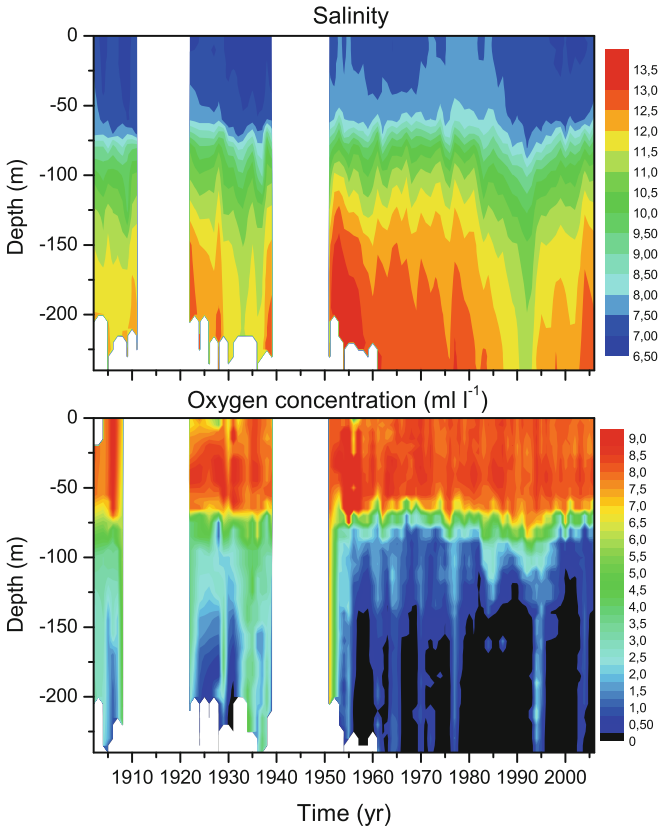

Fig. 5.10 Observed salinity and oxygen concentration (mL L^{-1}) at station BY15 in the central Baltic Sea (from Gustafsson and Omstedt 2009)

5.3.2 Mathematical Formulation

All equations are written in their conservative form. The physical mathematical formulation is outlined in Sect. 5.2 and the oxygen equation is written as follows:

$$\frac{\partial {}^{O_2}C}{\partial t} + W\frac{\partial {}^{O_2}C}{\partial z} = \frac{\partial}{\partial z}\left[\frac{\mu_{eff}}{\rho_0 \sigma_{O_2}}\frac{\partial {}^{O_2}C}{\partial z}\right] + S_{O_2} \tag{5.19}$$

where ${}^{O_2}C$ is the concentration of oxygen, μ_{eff} the effective dynamic turbulent viscosity, σ_{O_2} the Schmidt number, and ρ density; S_{O_2} is a source/sink term associated with plankton growth and mineralization.

The boundary condition for the air–water interface is given by:

$$F_{O_2} = k_C({}^{O_2}C - {}^{O_2}C_{sat}) \tag{5.20}$$

where $O_{2\text{sur}}$ is the saturation oxygen concentration at the surface, which depends on temperature and salinity (Weiss 1970).

The source/sink term can be formulated as follows:

$$S_{O_2} = s_{O_2} G_p {}^{pp}C - M_T \tag{5.21}$$

where M_T is the total mineralization rate attributable to various mineralization processes. Here we simplify the source/sink term and assume that it can be written:

$$S_{O_2} = -\alpha_{1\text{min}} w_{\text{min}} \tag{5.22}$$

where w_{min} is the mineralization rate below the thermocline and $\alpha_{1\text{min}}$ is a constant that we can determine from observations during stagnation periods.

Downstream change in the amount of oxygen in the dense bottom current also needs to be considered and, following an approach similar to that used in Sect. 5.2.2 of this chapter, this change reads:

$$d^{O_{2d}}C = \frac{dq({}^{O_{2e}}C - {}^{O_{2d}}C)}{q + dq} \tag{5.23}$$

where $d^{O_{2d}}C$ denotes the oxygen change in the dense bottom current; index d corresponds to the dense current and index e to the surrounding water.

5.3.3 Details of Calculations

For oxygen calculations, the PROBE-Baltic system can be run using `IBIO = 3`, which should be specified in `basin1.f`. Note also that `IBIO` needs to be changed in the interpolation program `to_surf_graph.for` as well as the interpolation

Table 5.1 Mineralization rates for some Baltic Sea sub-basins determined from observations (from Gustafsson and Omstedt 2009)

Sub-basin	Mineralization rate (mL O_2 L^{-1} $year^{-1}$)
Öresund	10
Belt sea	10
Arkona basin	10
Bornholm basin	4.5
Eastern Gotland basin	2

program. From oxygen observations, Gustafsson and Omstedt (2009) determined the mineralization rates as presented in Table 5.1.

The mineralization rates in mL O_2 L^{-1} $year^{-1}$ can be transformed to μmol kg^{-1} by multiplying them by $44.6 \times 10^{-6}/(365 \times 24 \times 3600)$. Mineralization rates according to Table 5.1 are used in the PROBE-Baltic system but only in the `IBIO = 3` version.

5.3.4 Results

The results of a 50-year model simulation are discussed below. Figs. 5.11 and 5.12 present some results for the central Baltic Sea. The concentration of surface oxygen displays a clear seasonal cycle, with increased oxygen concentration in winter due

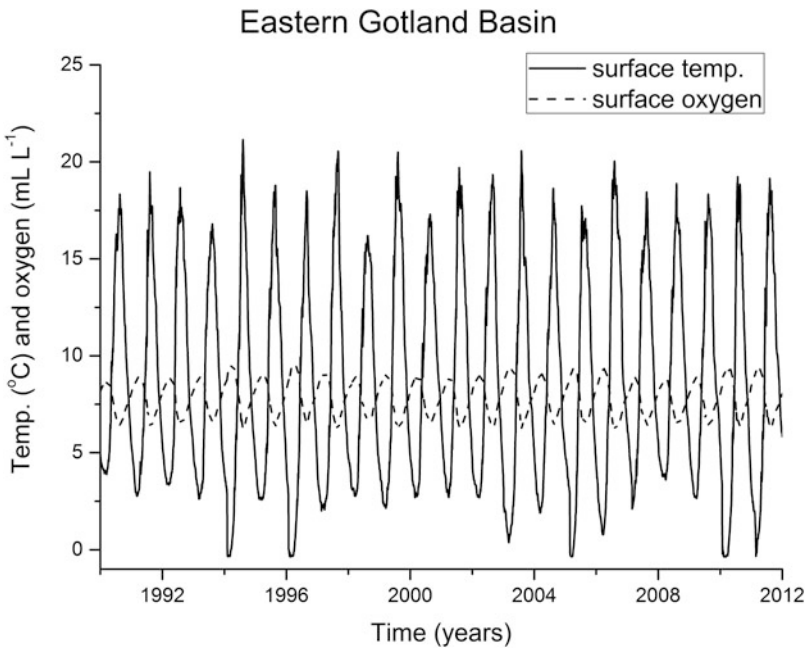

Fig. 5.11 Calculated surface temperature and oxygen concentration in the central Baltic Sea

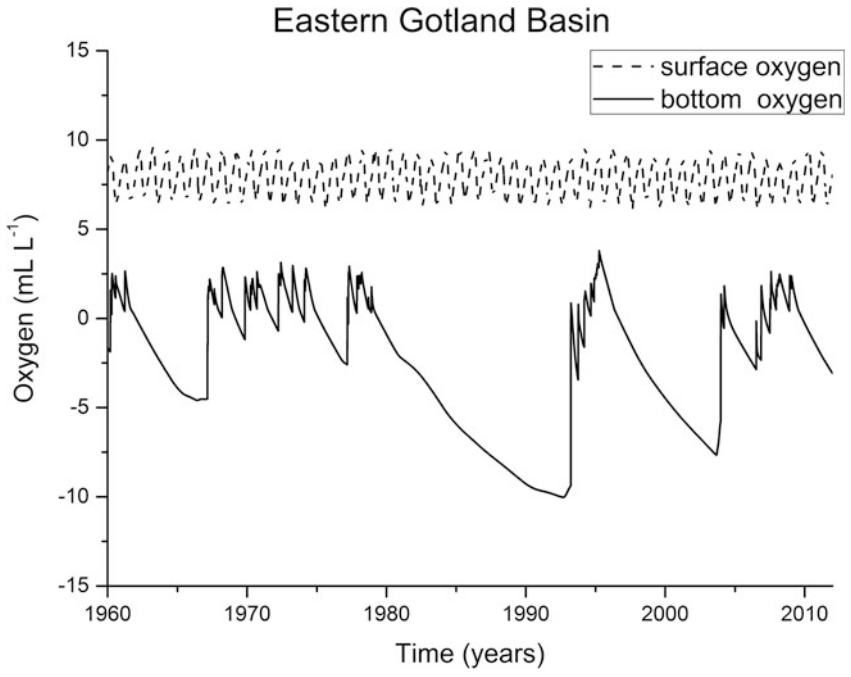

Fig. 5.12 Calculated oxygen concentration in the central Baltic Sea

to higher oxygen solubility in cold water. Biological production is not included in the present oxygen model, which is why oversaturation during primary production is not modeled using `IBIO=3`. Biological production can easily be included by running the `IBIO=1` model.

Calculated concentrations of surface oxygen are determined mainly by the interaction between the sea and air and by the solubility of oxygen in the surface water. In the deeper layer (Fig. 5.12), the alternation between stagnation and inflow periods strongly influences the concentration of oxygen.

Exercise 5.3
Run the PROBE-Baltic oxygen model and investigate the dynamics of salinity and oxygen over the 1960–2012 period. *Hint*: Compare the model results with the observed results presented in Fig. 5.10.

5.3.5 Discussion

Though the oxygen dynamics have been treated in a simplified way, it is interesting to note that the results are fairly realistic. This implies that physical transport is important for biogeochemical systems and that much can be learned from a good description of the physical transport. Modeling the mineralization of biological material, however, is a major scientific issue that needs further consideration.

5.4 The PROBE-Baltic System: Biogeochemical Aspects

5.4.1 Introduction

The present version of the model simulates the CO_2–O_2 dynamics. This requires consideration of several processes related to the physical, chemical, and biological aspects of the coastal seas. CO_2 exchange between water and air is a function of the difference in the partial pressure of carbon dioxide at the air–water interface and of the exchange processes in the sea and atmosphere. Partial pressure at the water surface is controlled by biological, chemical, and physical processes in the water, while the exchange processes in the atmosphere depend on the turbulence structure (e.g., wind speed, waves, and atmospheric stability). The main biogeochemical processes that need to be considered are depicted in Fig. 5.13. Phytoplankton

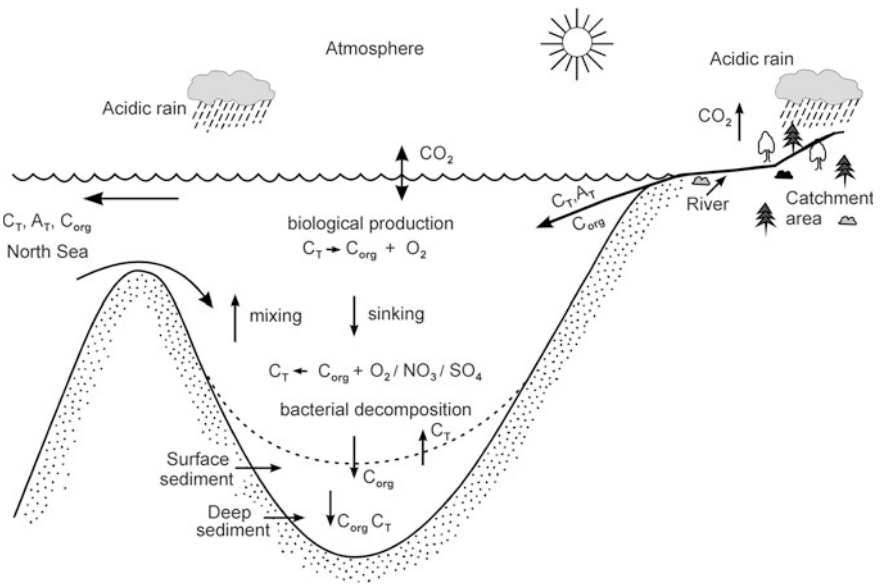

Fig. 5.13 Sketch of the processes modeled in the biogeochemical part of the PROBE-Baltic system (redrawn from Omstedt et al. 2009, based on an earlier sketch from Bernd Schneider)

growth, which depends on light and nutrient availability, forms the basis of the biological uptake of CO_2 in the surface water. Phytoplankton's exude dissolved organic matter and are grazed on by zooplankton; detritus forms from dead phytoplankton and zooplankton and from the fecal pellets of zooplankton. The dissolved organic matter mineralizes to carbon and nutrients. Nutrients, such as phosphate and nitrate, limit plankton growth and are involved in processes such as mixing, river runoff, and resuspension. Rivers may also transport large amounts of total inorganic and organic carbon into the surface water. River input of total inorganic carbon is a consequence of carbonate dissolution in the watershed area, which is reflected in the total alkalinity and associated uptake of atmospheric CO_2. In addition, water exchange with the surrounding seas may transport inorganic and organic carbon into the studied region.

5.4.2 Mathematical Formulation

Though mathematical formulation is kept as simple as possible, several aspects of the dynamics need to be included. The physical part of the model includes six equations for momentum (two equations), heat, salinity, turbulent kinetic energy, and dissipation of turbulent energy. The chemical part includes six equations for total alkalinity, total inorganic carbon, oxygen, nitrate, total ammonium, and phosphate. The biological part includes three different equations for depth- and time-dependent phytoplankton abundance, one equation for zooplankton, and three equations for detritus (i.e., C, N, and P). The first and third plankton equations treat species that are limited by both nitrogen and phosphorus availability, whereas the second treats species that can fix N_2 and thus are limited by phosphorus only. The dissolved CO_2 system is solved from the state variables, i.e., total alkalinity, A_T, and total inorganic carbon, C_T. Total inorganic carbon consists of dissolved CO_2 and the products formed by carbonic acid disassociation in water. The speciation is set by interaction with the total acid–base balance of seawater, source and sink terms associated with biogeochemical processes, and the air–sea exchange of CO_2. The full model including information about equations, constants, and numerical code is presented by Edman and Omstedt (2013) and Gustafsson (2012). The model version is called PROBE-Baltic 3.0 and is available as additional materials (see Appendix C).

As we have learned, all conservation equations in their one-dimensional, time-dependent form can be formally written as follows:

$$\frac{\partial \phi}{\partial t} + W\frac{\partial}{\partial z}\phi = \frac{\partial}{\partial z}\left(\Gamma_\phi \frac{\partial \phi}{\partial z}\right) + S_\phi \tag{5.24}$$

where the various terms represent the time changes in different variables (ϕ), vertical advection, and turbulent diffusion, as well as changes due to sources or sinks. In addition to the conservation equations, one must also consider the vertical

Table 5.2 Biogeochemical parameters in PROBE-Baltic version 3.2

Variables	Description	Units
$\rho_0 u$	x momentum	kg m^{-2} s^{-2}
$\rho_0 v$	y momentum	kg m^{-2} s^{-2}
$\rho_0 c_p T$	Heat	W m^{-2}
S	Salinity	-
k	Turbulent kinetic energy	m^2 s^{-3}
ε	Dissipation of turbulent kinetic energy	m^2 s^{-4}
${}^{pp_1}C$	Phytoplankton, group 1	mol kg^{-1} s^{-1}
${}^{pp_2}C$	Phytoplankton, group 2	mol kg^{-1} s^{-1}
${}^{pp_3}C$	Phytoplankton, group 3	mol kg^{-1} s^{-1}
${}^{zoo}C$	Zooplankton	mol kg^{-1} s^{-1}
${}^{DETC}C$	Detritus, carbon	mol kg^{-1} s^{-1}
${}^{DETN}C$	Detritus, nitrogen	mol kg^{-1} s^{-1}
${}^{DETP}C$	Detritus, phosphorus	mol kg^{-1} s^{-1}
${}^{C_T}C$	Total dissolved inorganic carbon	mol kg^{-1} s^{-1}
${}^{A_T}C$	Total alkalinity	mol kg^{-1} s^{-1}
${}^{NO_3}C$	Nitrate	mol kg^{-1} s^{-1}
${}^{NH_4}C$	Ammonium	mol kg^{-1} s^{-1}
${}^{PO_4}C$	Phosphate	mol kg^{-1} s^{-1}
${}^{O_2}C$	Dissolved oxygen gas	
Benthic variables		
SEDC	Benthic organic carbon	mol
SEDN	Benthic organic nitrogen	mol
SEDP	Benthic organic phosphorus	mol
BIP	Benthic inorganic phosphorus	mol

boundary conditions at the water–air and water–bottom interfaces as well as lateral boundary conditions. The lateral conditions in the outer sub-basin are given as temperature, salinity, nutrient, and carbon values representative of the Skagerrak and are prescribed only for the deep water inflows to the outer basin. The biogeochemical equations are listed in Table 5.2.

The boundary condition at the surface or the bottom relates the diffusion term to fluxes calculated from the forcing data of the model, as follows:

$$\frac{\partial}{\partial z}\left(\Gamma_\phi \frac{\partial \phi}{\partial z}\right)^{sur,bot} = F_\phi^{sur,bot} \tag{5.25}$$

where *sur* and *bot* indicate the flux conditions at the surface and bottom, respectively.

For the sediment–water interface, a zero-flux condition was applied to all variables. The accumulation and release of organic material and phosphorus from

sediments were calculated from mass balance considerations (Gustafsson 2012). Lateral boundary conditions in the model equations include inflow from rivers and from the Skagerrak. Inflow and outflow are modeled using various models of flow between the sub-basins (Sect. 5.2).

5.4.3 Details of Calculations

For the biogeochemical calculations, the PROBE-Baltic system can be run using `IBIO = 1` in `basin1.f`. The model is set up to simulate conditions observed from 1 November 1958 to the end of 2012. The biochemical model components are organized as individual subroutines, and in the subroutine `bio_model.f` they are labeled according to the model system used (`IBIO`) and the equation number (`J`). This subroutine reads:

```
SUBROUTINE BIO_MODEL(IYMDH)
      INCLUDE 'd:\probe_baltic\comp97.inc'
      INCLUDE 'd:\probe_baltic\biochempar.dat'
      INCLUDE 'd:\probe_baltic\comp_model.inc'
C
C-----COMPLETE BIOGEOCHEMICAL MODEL
      IF(IBIO.EQ.1)THEN
        IF(J.EQ.JPC1)CALL PLANKTON1
        IF(J.EQ.JPC2)CALL PLANKTON2
        IF(J.EQ.JPC3)CALL PLANKTON3
        IF(J.EQ.JZOO)CALL ZOOPLANKTON(IYMDH)
        IF(J.EQ.JCT)CALL TOTAL CARBON
        IF(J.EQ.JAT)CALL TOTAL ALKALINITY
        IF(J.EQ.JNO3)CALL NITRATE(IYMDH)
        IF(J.EQ.JNHT)CALL AMMONIUM(IYMDH)
        IF(J.EQ.JPO4)CALL PHOSPHATE(IYMDH)
        IF(J.EQ.JDC)CALL DETRITUS C
        IF(J.EQ.JDN)CALL DETRITUS N
        IF(J.EQ.JDP)CALL DETRITUS P
        IF(J.EQ.JO2)CALL OXYGEN
      ENDIF
C
C-----CONSTANT OXYGEN REMOVAL RATES
      IF(IBIO.EQ.3)THEN
        IF(J.EQ.JO2)CALL OXYGEN_CONST(IYMDH)
      ENDIF
C
      RETURN
      END
```

The coding of the various biochemical subroutines is given in subroutine `biology.for` and the corresponding constants are given in `biochempar.dat` and `biochempar2.dat`, where the interested reader can find more details.

5.4.4 Results

Figures 5.14 and 5.15 present some results for the central Baltic Sea. The surface water partial pressure of CO_2 displays a clear seasonal cycle, being below atmospheric values during plankton bloom and above them during winter convection. The atmospheric partial pressure of CO_2 displays both a seasonal cycle and a long-term increase. The calculated pH values are illustrated in Fig. 5.15.

It is generally believed that the surface pH of the ocean has declined by 0.1 pH units as a result of increases in atmospheric CO_2 levels since the advent of industrialization. In the future, we would expect an even greater reduction in pH. The sensitivity of the acid–base (pH) balance in the Baltic Sea is further explored by Omstedt et al. (2010, 2012).

Exercise 5.4
Investigate the spin-up time by assuming that the Baltic Sea inside the Drogden and Darss sills is filled with freshwater (i.e., salinity equals 0.5) and A_T, C_T, and nutrients all equal zero, while outside the sills these properties are at ocean levels. Run the model from 1 November 1700 to 2008. *Hint*: Use the reconstructed forcing field from 1700 to 2008 presented in Appendix C.

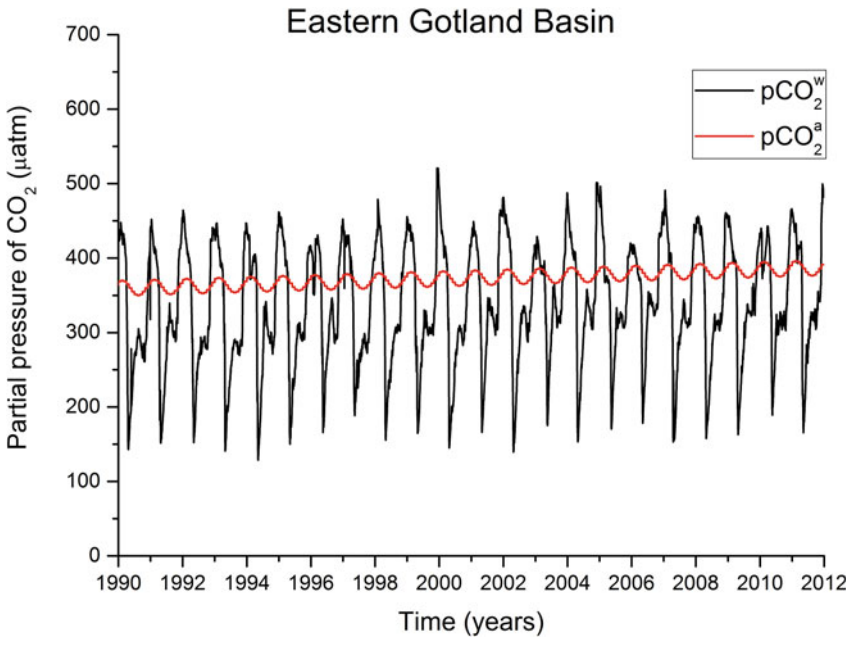

Fig. 5.14 Calculated surface pCO_2 in the central Baltic Sea

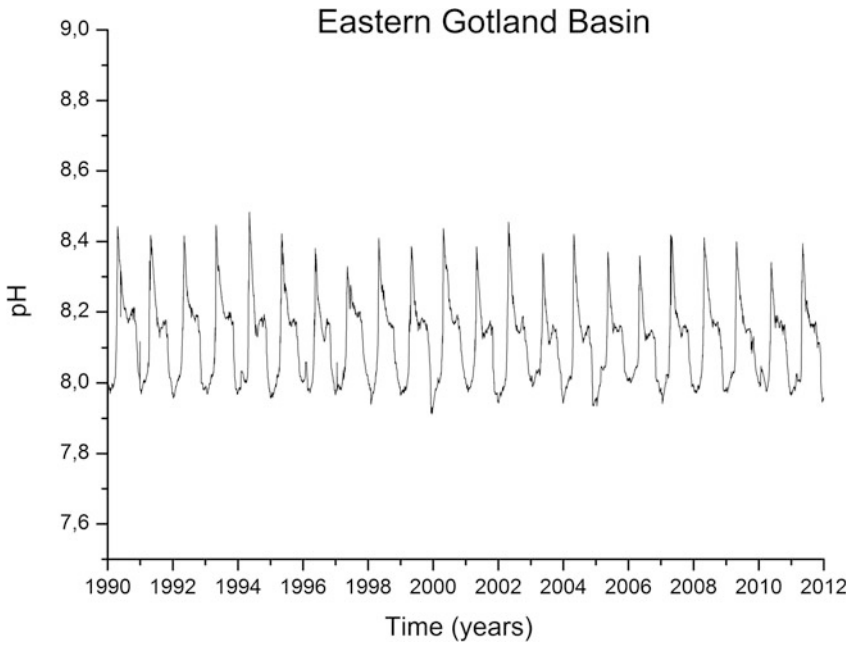

Fig. 5.15 Calculated surface pH in the central Baltic Sea

5.4.5 Discussion

The calculated surface water partial pressure of CO_2 displays low values in summer associated with large biological production of blue–green algae, which is limited only by phosphorus. By introducing the carbon dynamics, we obtain a model system that can address several threats to coastal seas, such as climate change, eutrophication, and changes in acid–base (pH) balance. A properly validated process-oriented model is indispensable for attributing observed changes to various sources or interventions (Omstedt et al. 2014). Some aspects of attributing the causes to observed changes by using models will be discussed in the next chapter.

5.5 Comments on Detection, Attribution, and Future Changes

5.5.1 Introduction

The major goals of climate assessments conducted by, for example, the IPCC and BACC are to detect changes and to attribute these changes to causes such as increased greenhouse concentrations or various human activities. These goals have

been developed within the IPCC where, for example, the detected increase in mean global temperature since the mid-twentieth century is attributed to human influence. Detection is formally a statistical test of the null hypothesis that recent climate changes are within the limits of natural variation. Attribution is formally a statistical fit, based on the assumption that the signal additively comprises the contributions of various influences (BACC I Authors Group 2008), for which models are often needed. In general, attribution is less powerful than is detection, as a best mix of contributions to the observed changes is determined within the model assumptions. For example, in coastal seas, we now discuss "cocktail effects," meaning that, while the individual load of each specific chemical component may not hurt the marine system, a combination of many such loads may threaten the system. Another example is the combination of acidification and warming variations in time and depth. As yet, few attribution studies are available on the regional scale (BACC I Authors Group and II Authors Group 2008, 2015), though those that do exist are of great importance for promoting successful management of the sea.

In regional studies we find a number of driving mechanisms, including human impacts, which change our environment. At the same time, the variability in many meteorological, hydrological, and ocean parameters is high on the regional scale and includes stochastic behavior. A typical stochastic time series, illustrated in Fig. 5.16, displays no trends, periodic oscillations, or regime shifts. In the figure, we have chosen to set the limits according to the maximum ice extent in the Baltic Sea

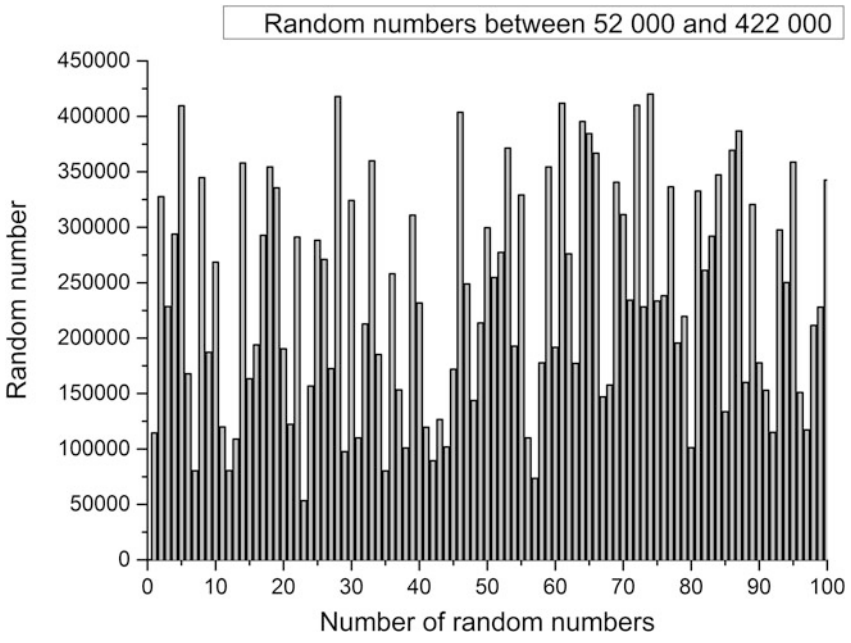

Fig. 5.16 Illustration of a stochastic time series with values that vary in the same range as the maximum ice extent in the Baltic Sea

(MIB), illustrated in Fig. 2.15d; the stochastic series displays great similarities to the MIB series, indicating that the MIB time series includes considerable noise. In the next sections, we will discuss some of the recent changes observed in the Baltic Sea and attribute these changes to causes.

5.5.2 *Recent Decline of Sea Ice in the Baltic Sea*

In Fig. 5.17, the MIB time series since 1900 is plotted together with a linear trend. The trend is significant at more than a 99 % level based on a simple *t*-test. We may therefore conclude that, over the past 100 years, the MIB has declined by 10 %; the next question is why.

A recent BACC II Authors Group (2015) assessment indicates that the annual mean Baltic Sea Basin temperature has increased by 0.11 °C/decade since 1870 north of latitude 60° and by 0.08 °C/decade south of latitude 60°. However, the seasonal temperature change varies greatly, with the strongest warming signal occurring during spring and a much smaller winter temperature change.

The relationship between temperature and Baltic Sea ice was analyzed by Omstedt and Hansson (2006a, b), who found an almost linear relationship between MIB and winter temperature. A winter temperature increase over the Baltic Sea of

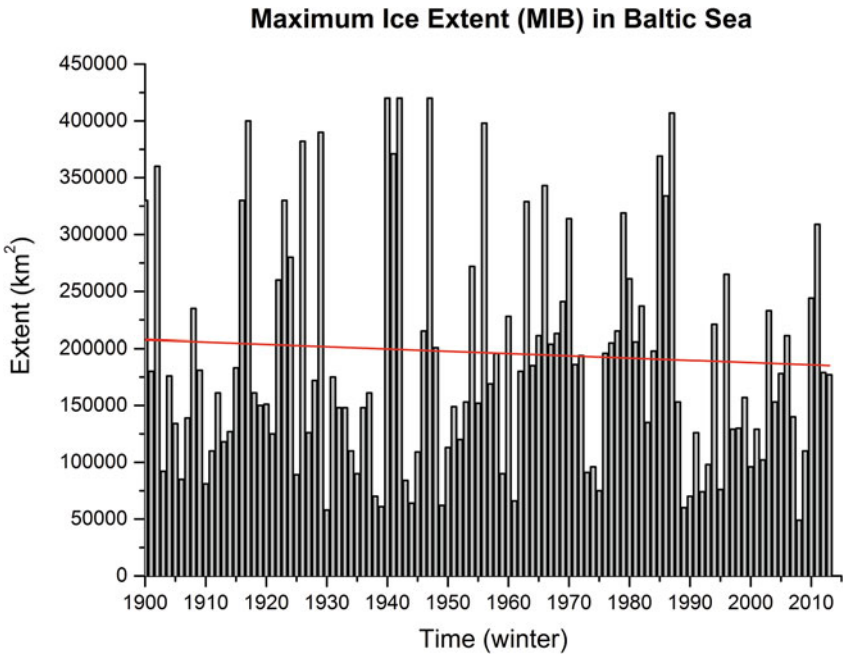

Fig. 5.17 Maximum ice extent in the Baltic Sea with a linear trend line (*red*)

less than approximately 1 °C over the past 100 years can explain a 10 % reduction in MIB, so we may then attribute the decline in ice extent to an air temperature increase. The reason for the temperature increase is more difficult to attribute, and relevant statements in BACC I Authors Group (2008) read:

- The Baltic Sea region is warming and the warming is virtually certain to continue through the 21st century.
- It is plausible that the warming is at least partly related to anthropogenic factors.
- So far, and as is likely to be the case for the next few decades, the signal is limited to temperature and directly related variables, such as sea ice conditions.

Future research efforts need to attribute the ongoing regional warming and include the effects of aerosols due to fossil fuel burning as well as improved air quality due to air pollution regulations in recent decades that may have influenced the air temperature.

5.5.3 Recent Increase of Hypoxia in the Baltic Sea

A major environmental concern in the Baltic Sea has been the spread of low-oxygen bottom water. The narrow entrance areas of the Baltic Sea and the large population in the Baltic Sea drainage basin have prompted debate about what is natural and what is caused by humans in this area. Scientists currently attribute increased hypoxia to an increase in total nutrient loads from atmospheric and terrestrial sources due to intensified agriculture with associated high fertilizer usage starting after the Second World War. For several decades, it has been discussed whether nitrogen or phosphorous emissions or both must be reduced to combat eutrophication. It has recently become clearer that, under anoxic conditions, sediment leaks phosphorus, constituting an internal load of considerable importance. The changes in anoxic and hypoxic waters are illustrated in Fig. 5.18 (Hansson et al. 2013), and it is easy to detect changes in hypoxic and anoxic conditions in recent decades.

Long-term variations in salinity and oxygen were examined by Hansson and Gustafsson (2011) by modeling the past 500 years using reconstructed forcing fields and PROBE-Baltic modeling. Their results indicate that anoxic conditions have occurred several times per century since 1500 (Fig. 5.19). However, since the mid twentieth century, increased oxygen deficiency in water below a depth of 125 m has probably been associated with increased nutrient load. The model study implies that contemporary severe oxygen conditions are unprecedented since 1500.

The nutrient dynamics have been studied by many scientists (e.g., Conley et al. 2002; Gustafsson et al. 2012; Savchuk 2013; Stigebrandt and Wulff 1987). Here we discuss some results of Gustafsson (2012), who has modeled the development of nutrient pools and sediment area covered with hypoxic water over the 1900–2009 period. The results of hindcast simulations with low external nutrient loads indicate that long-term climate change had no significant effects on hypoxic conditions or nutrient pools during the study period. Deteriorating oxygen conditions since the

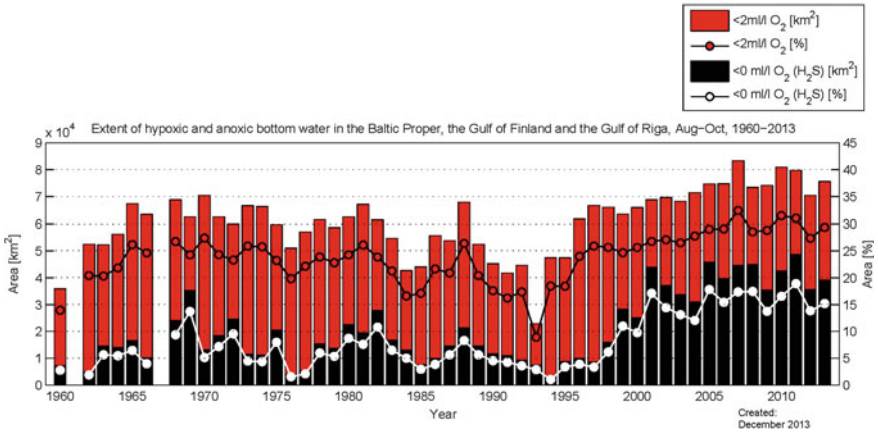

Fig. 5.18 Annual variation in hypoxic and anoxic areas in the Baltic Sea (*courtesy* of Lars Andersson, SMHI)

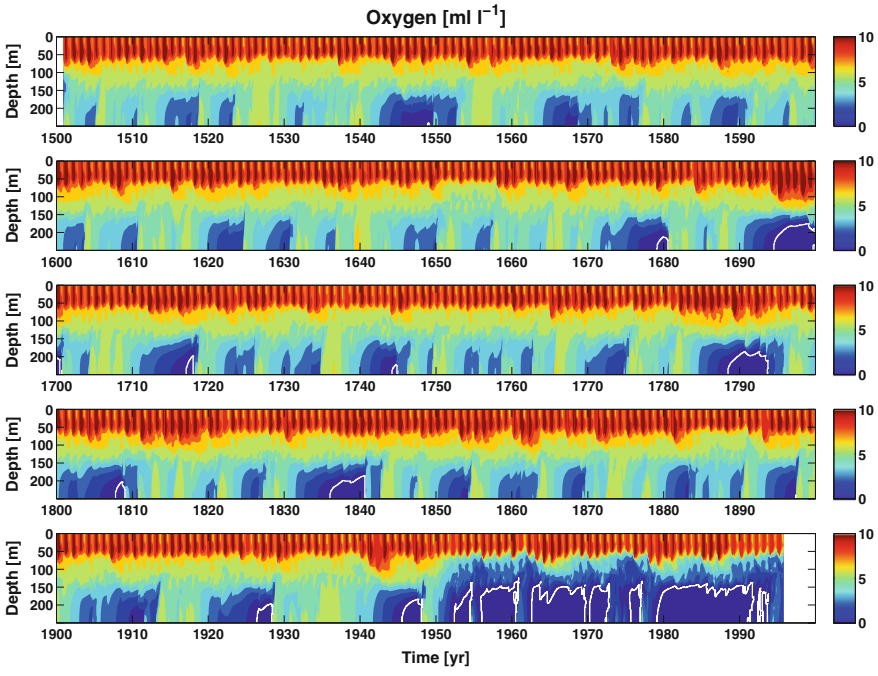

Fig. 5.19 Modeled oxygen concentration in the central part of the Baltic Sea from 1500 to the present (*courtesy* of Daniel Hansson)

1950s were related mainly to increased external nutrient loads in combination with internal nutrient feedback processes. The modeled pool of dissolved inorganic phosphorous more than doubled during the studied period. The reasons were partly due to increased load and partly due to the release of phosphorous from sediments under anoxic conditions. Another interesting implication of Gustafsson's (2012) model is that reducing both nitrogen and phosphorus loads would be more effective than reducing only the phosphorus load.

Ahtiainen et al. (2014) argued that at least three aspects need to be considered when reducing nutrient loads to the Baltic Sea: first, reducing the nitrogen load and reducing the phosphorus load have different eutrophication effects; second, the role of time and the lag between actions to reduce nutrient loads and perceived improvements; and third; the spatial dimension and roles of actions targeting the coastal and open sea environment and various sub-basins. An alternative or complement to nutrient load reduction could be to improve the deep water conditions by pumping oxygen into the Baltic Sea and reducing the internal leakage of phosphorus from anoxic sediments (Stigebrandt et al. 2014; Stigebrandt and Gustafsson 2007).

Many questions remain concerning the combating of eutrophication. However, it is clear that any eutrophication-reduction methods on land or in the sea need to be carefully evaluated using both observations and modeling.

5.5.4 Modeling Future Changes

What will happen to our lakes and coastal seas in the future? The only thing we can be sure of is that the future has a surprise or two in store for us. Is there an answer to the question, then? If we wish to say anything about the next hundred years, we should adopt a historical perspective. A time scale of a thousand years back in time immediately illustrates the uncertainty. However, the human impact on the environment has increased rapidly over the past 50 years, which may indicate that the changes seen today are unprecedented and that new ecosystem responses may cause effects outside present knowledge.

Efforts to estimate future changes due to anthropogenic climate change have been greatly developed within the IPCC process, and today many general circulation simulations are freely available for various emission scenarios. Each of these earth system models (ESMs) involves many sub-models of processes such as radiation, cloud formation, snow cover, ice cover, and ocean dynamics. Some of these process models are well tested and validated from observed forcing. However, in ESM systems they may generate large errors due to wrong forcing from other sub-models. In addition, they may generate large internal variability and are therefore also sensitive to initial conditions. The same ESM model will therefore give different projections due to different initial conditions. Instead of using just one future realization, several model realizations are used to create ensemble mean projections, which some regard as more reliable than individual projections. For example, one can study the Arctic Ocean sea ice extent and the possibility of this ocean becoming ice free during

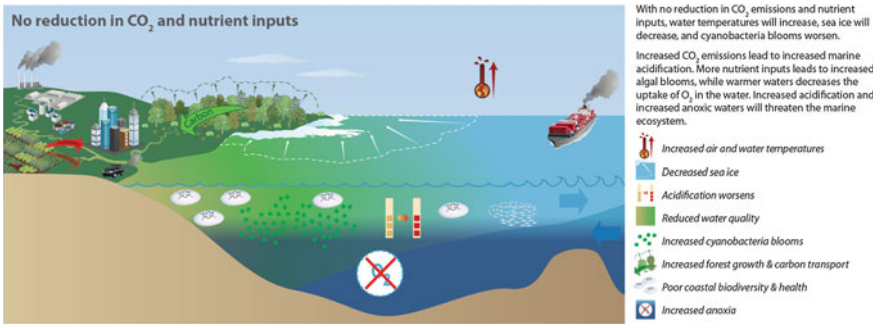

Fig. 5.20 Sketch of possible developments in the Baltic Sea without successful management efforts. Diagram created by the Integration and Application Network, University of Maryland Center for Environmental Science, USA, with guidance from Omstedt

this century. This exercise was discussed by the IPCC (2013, Chap. 12), which found great uncertainty between the models even for the same emission pathways. Reducing this uncertainty is a major research challenge, and a process-oriented approach and using less complex models could improve the progress.

Coastal seas and lakes face severe human-induced pressures, such as climate change, excess nutrient loads, pollution, ammunition dumping, overfishing, and various engineering-based modifications, including the strong growth of coastal settlement, hydro- and nuclear power plants, massive wind farms, and various bridge and tunnel crossings. At the same time, coastal seas and lakes are used for many purposes, such as intensive agriculture, shipping, and recreation. Ocean acidification has recently emerged as a key research priority for marine science. Only recently has this been addressed in the context of coastal seas. The combination of acidification and increasing anoxic waters associated with eutrophication severely stresses the marine environment. In Fig. 5.20, some of these changes are illustrated for a future Baltic Sea without successful management options, based on a study by Omstedt et al. (2012). Possible future changes were studied using a coupled catchment–sea model system and numerical experiments based on meteorological and hydrological forcing datasets and scenarios. The study demonstrates that substantial reductions in fossil-fuel burning are needed to minimize the coming pH decrease and that substantial reduction in nutrient loads are needed to reduce the coming increase in hypoxic and anoxic waters. Coastal models may allow the evaluation of future storylines, but they need to be well tested back in historical time. However, great uncertainties remain in correctly modeling the hydrological cycle on the regional scale (BACC II Author Group 2015). This is crucial in coastal areas where rivers bring large loads of nutrients and carbon into the sea and control the salinity. In addition, most ecosystem models are closed systems excluding dynamic aspects such as alien species or evolution. The modeling community thus has many interesting and difficult challenges that will require new research initiatives.

Chapter 6
Solutions Manual

6.1 Solutions to Exercises in Chapter 2

Exercise 2.1
The mean depth of the Baltic Sea is 54 m and its surface area is 3.9×10^5 km^2. How much would the level of the Baltic Sea increase over a year with river water inflow of 15,000 m^3 s^{-1} and no outflows? If the outflowing volume flow were 30,000 m^3 s^{-1}, how large would the inflowing volume flow need to be to keep the sea level unchanged? If the salinity of the inflowing water were 17 salinity units, what would the salinity be in the basin?

Answer:

The annual river runoff volume is 15,000 (m^3 s^{-1}) × 365 × 24 × 3600 (s) = 473 km^3. If this water volume were distributed over the whole area, the sea level change would be 473 (km^3)/3.9 × 10^5 (km^2) = 1.2 (m). The typical river runoff to the Baltic Sea thus corresponds to a height of 1 m; the corresponding value for net precipitation is 0.1 m.

From volume and salt conservation principles, we understand that:

$$Q_{out} = Q_{in} + Q_r$$
$$S_{in}Q_{in} = SQ_{out}$$

From the volume conservation principle, we find that $Q_{in} = 15,000\,\mathrm{m^3\,s^{-1}}$ and from the salt conservation principle we find that $S = 17 \times 15,000\,(\mathrm{m^3\,s^{-1}})/$

A. Omstedt, *Guide to Process Based Modeling of Lakes and Coastal Seas*,
Springer Praxis Books, DOI 10.1007/978-3-319-17990-2_6

$30,000\,(\mathrm{m}^3\,\mathrm{s}^1) = 7.5$. Thus, the salinity in the basin is 7.5, a typical result of the Knudsen theorem that has been frequently used in Baltic Sea research.

Exercise 2.2
Investigate the equation of state by plotting Eq. 2.5 for different temperatures and salinities. What are the typical densities in the Baltic and Mediterranean seas? What are the dominant factors that control the density in coastal seas? Compare Eq. 2.5 with the full equation of state given by Gill (1982, Appendix 3).

Answer:

The density equation, Eq. 2.5, is plotted in Fig. 6.1. Water densities in the Baltic Sea are typically 1000–1020 kg m^{-3}. Note the linear and nonlinear behavior with regard to salinity and temperature, respectively.

To evaluate the influence of temperature and salinity variations on density, one can derive the following relationship:

$$\Delta\rho \approx \frac{\partial\rho}{\partial T}\Delta T + \frac{\partial\rho}{\partial S}\Delta S = -2\alpha_1\left(T - T_{\rho m}\right)\Delta T + \alpha_2\Delta S \approx -10^{-4}\Delta T + 10^{-3}\Delta S$$

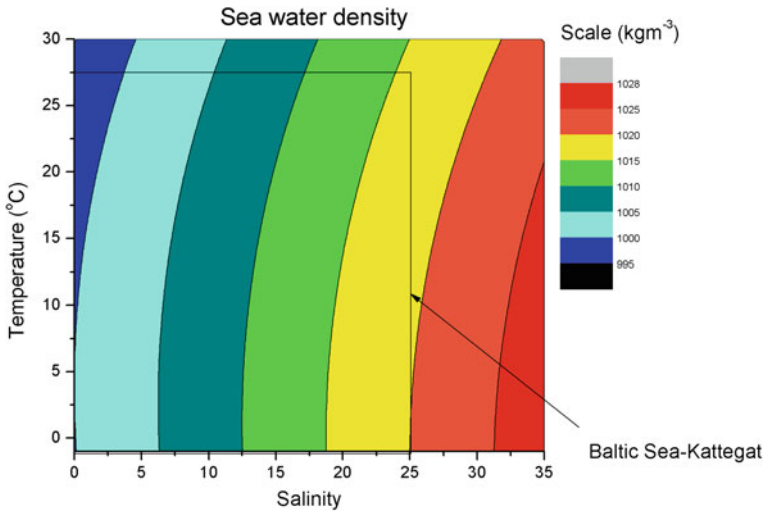

Fig. 6.1 Seawater density as a function of temperature and salinity

where we have used the following values: $T - T_{\rho m} \approx 10\,\alpha_1 = 5.10^{-6}$ ($^{\circ}C^{-2}$), and $\alpha_2 = 8.10^{-4}$. The results indicate that salinity variation often dominates density variation in the Baltic Sea. The rest of this exercise is left to the reader. *Hint*: A FORTRAN subroutine for density equations, `densty_diff.f`, is available in the `\process oriented\Ch3\All Files` directory.

Exercise 2.3
Some oceanographers imagine studying Earth's rotation by sitting in a bathtub and letting the water drain while they are passing over the Equator. Would Earth's rotation significantly affect the water flow when emptying a bathtub? Assume a horizontal scale of 1 m, a drainage rate in the order of 0.01 m s^{-1}, a motion time scale of 1000 s, and an ambient rotation rate of 7.3×10^{-5}.

Answer:

To investigate whether or not the effects of rotation can be ignored, we can compare the fluid motions with the time scale of rotation. We calculate two dimensionless Rossby numbers:

$$Ro_t = \frac{1}{\Omega T} = \frac{1}{7.310^{-5}1000} = 14$$

$$Ro = \frac{U}{\Omega L} = \frac{0.01}{7.310^{-5}1} = 137$$

As both the temporal Rossby number and the Rossby number are much greater than 1, we conclude that the effects of rotation can be ignored.

Exercise 2.4
A 60-m-deep surface layer with a salinity of approximately 7 characterizes the central Baltic Sea. Below the halocline, salinity is approximately 10. Using a value of 8×10^{-4} for the coefficient of salinity expansion, calculate the stratification or Brunt–Väisälä frequency. What is the horizontal scale at which rotation and stratification play comparable roles? *Hint*: Use the equation of state, i.e., $\rho = \rho_0(1 + \alpha_2 S)$, and assume that the density change takes place over 60 m.

Answer:

The horizontal scale at which rotation and stratification play comparable roles is given by the Rossby radius of deformation:

$$L = \frac{NH}{\Omega}$$
$$N^2 = \frac{-g\Delta\rho}{\rho_0 H} = \frac{g\alpha_2 \Delta S}{H}$$

Using the given value, we obtain:

$$N^2 = \frac{-g\Delta\rho}{\rho_0 H} = \frac{g\alpha_2 \Delta S}{H} = \frac{9.81810^{-4}3}{60} = 0.0003924$$
$$L = \frac{NH}{\Omega} = \frac{\sqrt{0.0003924} \times 60}{7.25 \times 10^{-5}} = 16.4 \text{ km}$$

At a scale of approximately 20 km, both the rotation and stratification processes need to be considered.

Exercise 2.5
Examine vorticity dynamics by assuming that the outflow from the Baltic Sea into the Kattegat conserves potential vorticity. What happens to the flow when the outflow enters the much deeper Skagerrak? Demonstrate how the relative vorticity might change.

Answer:

Outflow from the Baltic Sea passes through two channels and enters the Kattegat, a shallow sea. In the transition between the northern Kattegat and southern Skagerrak, there is a dramatic increase in depth. From the conservation of potential vorticity, we obtain:

$$\frac{d}{dt}\left(\frac{f+\zeta}{H}\right) = 0$$

We now assume that f is constant over the rather short distance between the northern Kattegat and southern Skagerrak and obtain:

$$\frac{d}{dt}\left(\frac{\zeta}{H}\right) = \frac{d}{dt}\left(\frac{\left(\frac{dV}{dx} - \frac{dU}{dy}\right)}{H}\right) \approx \frac{d}{dt}\left(\frac{\left(\frac{dV}{dx}\right)}{H}\right) \approx \frac{\Delta}{\Delta t}\left(\frac{\left(\frac{V_{coast} - V_{sea}}{\Delta x}\right)}{H}\right) \approx \frac{\Delta}{\Delta t}\left(\frac{V_{coast}}{H}\right) = 0$$

As H increases, the relative vorticity component must be positive and increase. This is associated with a strong positive current shear, which is only possible by forming a coastal current along the Swedish west coast.

Exercise 2.6
Calculate mean sea level variation in the Baltic Sea by examining the barotropic strait model given in Eq. 2.12. Assume that river runoff and net precipitation are constant and equal 15,000 and 1000 $m^3\ s^{-1}$, respectively. In addition, assume that the surface area is 3.9×10^5 km^2 and that the strait-specific constant, C_s, is typically 0.3×10^{-5} ($s^2\ m^{-5}$). Use sea level data from the Kattegat to force the model and compare the mean sea level with sea level variation in Stockholm (for the data needed, see Appendix C).

Answer:

Sea level data from 1980 to 2008 are contained in the data file, which includes dates, sea levels in the Kattegat (at the Viken Station), and sea levels in the Baltic Sea (at the Stockholm Station). Using Eq. 2.12, mean sea level variations in the Baltic Sea can be calculated and then compared with observations (see FORTRAN program in Appendix A). The calculations are illustrated in Fig. 6.2. Note the large variability in the Kattegat sea level and the damping of sea level variation in the Baltic Sea due to the narrow entrance area. In addition, the calculated Baltic Sea mean sea level closely follows the observed sea level at Stockholm. From the model, we can also derive statistics about inflowing and outflowing water volumes.

Exercise 2.7
Consider the Baltic Sea and its surface area of 3.9×10^5 km^2. Assume that the volume and heat content of the Baltic Sea do not change over time and that the exchange through the entrance area occurs via a two-layer flow. Assume that inflowing water and river water both equal 15,000 $m^3\ s^{-1}$ and that inflowing and outflowing water temperatures both equal 8 °C. If the river runoff temperature is 1 °C colder/warmer than the Baltic Sea surface temperature, what is the estimated heat exchange with the atmosphere?

Answer:

Assuming there is no time dependence, we can formulate the volume and heat conservation as:

$$Q_{out} = Q_{in} + Q_r$$
$$F_{loss} = F_{in} + F_r - F_{out}$$

From the volume conservation principle, we find that $Q_{out} = 30,000\ m^3\ s^{-1}$. The heat conservation can now be rewritten as:

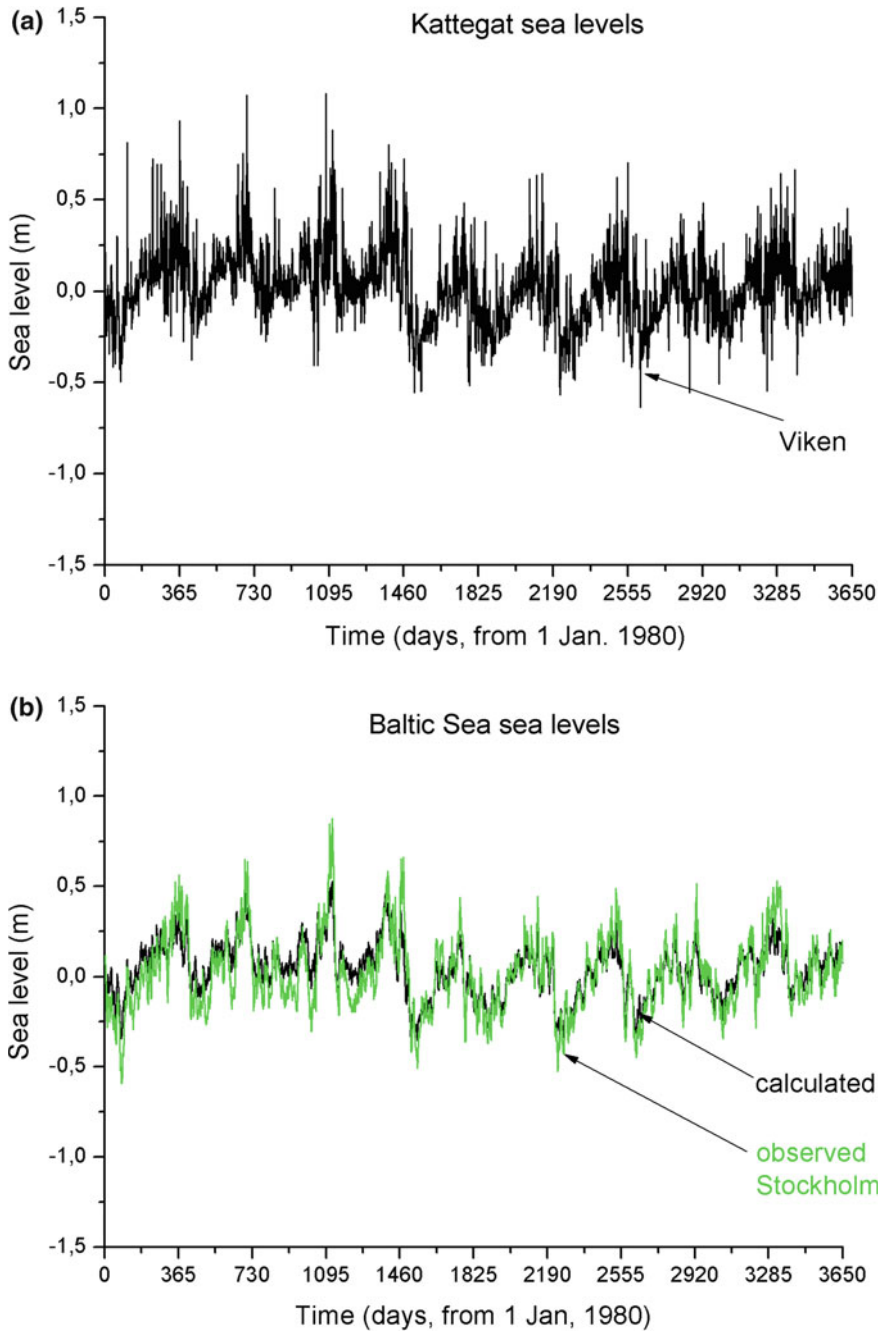

Fig. 6.2 Observed and calculated sea level variation in the Baltic Sea (**b**) based on forcing from the Kattegat sea level (**a**)

$$F_{loss}A_{sur} = \rho_0 c_p T_{in} Q_{in} + \rho_0 c_p T_r Q_r - \rho_0 c_p T Q_{out}$$
$$\approx \rho_0 c_p T Q_r + \rho_0 c_p T_r Q_r - \rho_0 c_p 2 T Q_r = \rho_0 c_p Q_r [T_r - T]$$

With a water density, ρ_0, of 1000 kg m^{-3}, a specific heat of water, c_p, of 4000 J/(kg^{-1} °C), and a river temperature 1 °C colder/warmer than the Baltic Sea temperature, the heat loss/gain becomes −0.15 and +0.15 Wm^{-2}, respectively. Thus, colder/warmer river water will be balanced by a heat gain/loss to the Baltic Sea that is less than 1 Wm^{-2} and therefore not easy to measure.

Exercise 2.8
Use P and N observations from the Baltic Sea and plot the surface properties of PO_4 and NO_3 for the last five years. Discuss the dynamics and discover what is controlling the primary production (for the data needed, see Appendix C).

Answer:

The required data are given in Fig. 6.3. Note the strong seasonal cycle and that the surface value of N is dramatically reduced due to the spring bloom. The ratio between winter N and P is less than 16, much as expected given the Redfield ratio

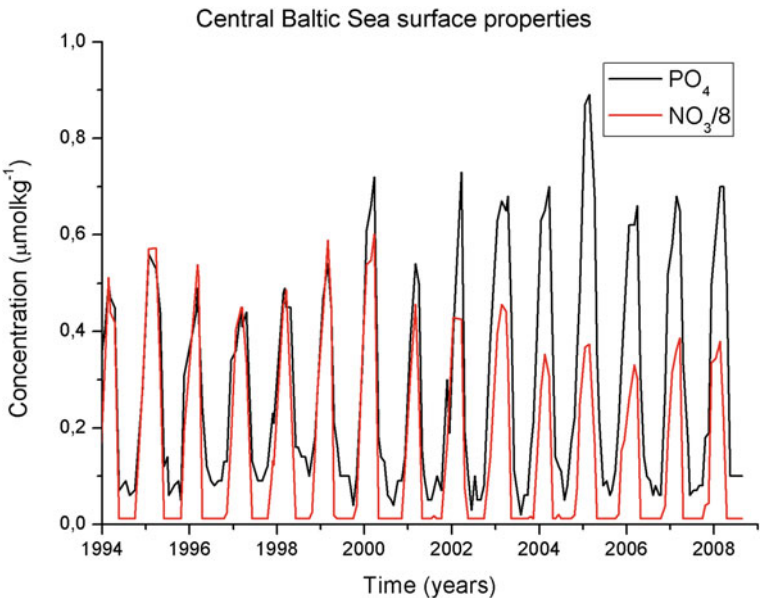

Fig. 6.3 Observed PO_4 and NO_3 surface concentrations at station BY15 in the Eastern Gotland Basin

associated with primary production. This also means that N is first reduced to minimum values while P is still available for further growth by blue-green algae that can use nitrogen from the air. In autumn, nutrient levels increase due to autumn and winter mixing that raises nutrients from deeper layers. The winter values are often used to indicate the amounts of nutrients available for biological production.

Exercise 2.9
Use pH observations from the Baltic Sea and plot the surface values. Discuss what controls seasonal and long-term variations of the acid–base balance (for the data needed, see Appendix C).

Answer:

Observed surface pH values from the Eastern Gotland Basin (Fig. 6.4) indicate a strong seasonal cycle. During the spring bloom, plankton builds up biological material using CO_2, thereby making the water more basic (i.e., increasing the pH). On the other hand, due to autumn and winter mixing, the surface water becomes

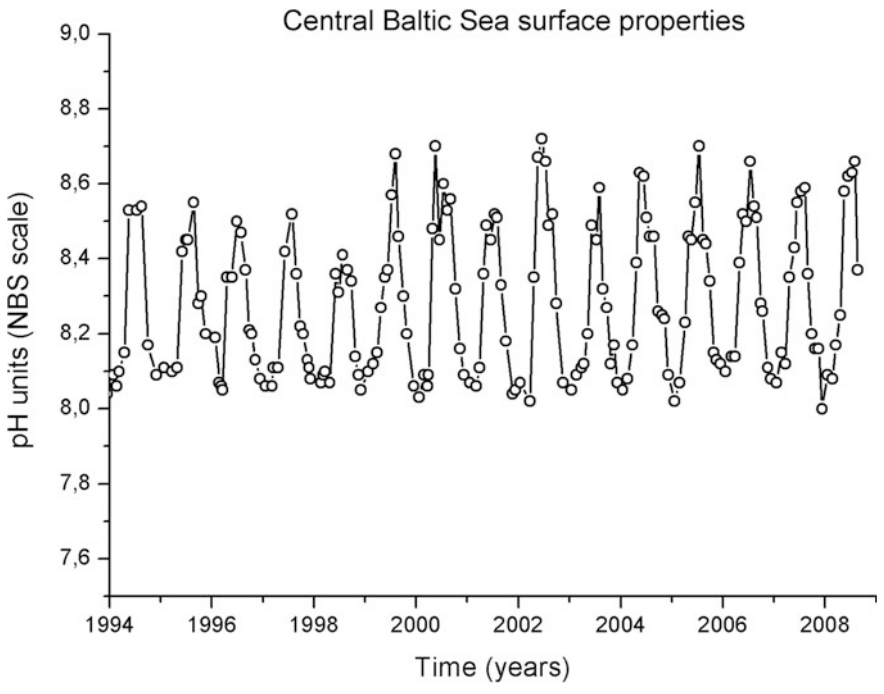

Fig. 6.4 Observed pH surface values at station BY15 in the Eastern Gotland Basin

more acid (the pH is reduced) due to the mineralization of biological material. From the figure, we note that the acid–base balance changes the pH by approximately ±0.3 pH units each year. The figure also indicates interannual variations but no trend.

Exercise 2.10
Investigate the climate variability and trend in Stockholm air temperature observations (for the data needed, see Appendix C). What determines the trend? What are the causes of the trend? Can trends tell us anything about the future?

Answer:

Annual air temperature (Fig. 6.5a) varies within a range of approximately 3–9 °C. If we define a typical climate period as 15 years (standard, 30 years), the running mean climate curve will considerably reduce variability. However, even using standard programs for smoothing data, we still need to determine the end points before calculating the trend. In Fig. 6.5a, we see that smoothing puts the weight on the last data points if the end points are not considered. This can create an artificial impression that there is a large climate trend. Before calculating the trend, we must remove the data representing half the climate period at the start and end points of the smoothed curve. In Fig. 6.5b, where we have removed the end point of the running mean and drawn a trend over the whole dataset, we estimate that temperature has increased 0.5 °C over almost 250 years. In Fig. 6.5c, where we have undertaken the same process, but considered only data starting from 1900, the temperature increase has become 0.6 °C. Residual temperature based on the smoothed time series is depicted in Fig. 6.5d. Typical climate variability (i.e., over a 15-year period) is about ±0.4 °C and recent temperatures are warmer by about a factor of 2 than those of the 1940s' warm period.

The time period considered thus determines the trend, though how we treat the end point values is also important. Trend analysis does not, however, let us determine the reasons for a trend, so we cannot tell what will happen in the future. Trends can be used in detection studies but not to attribute causes.

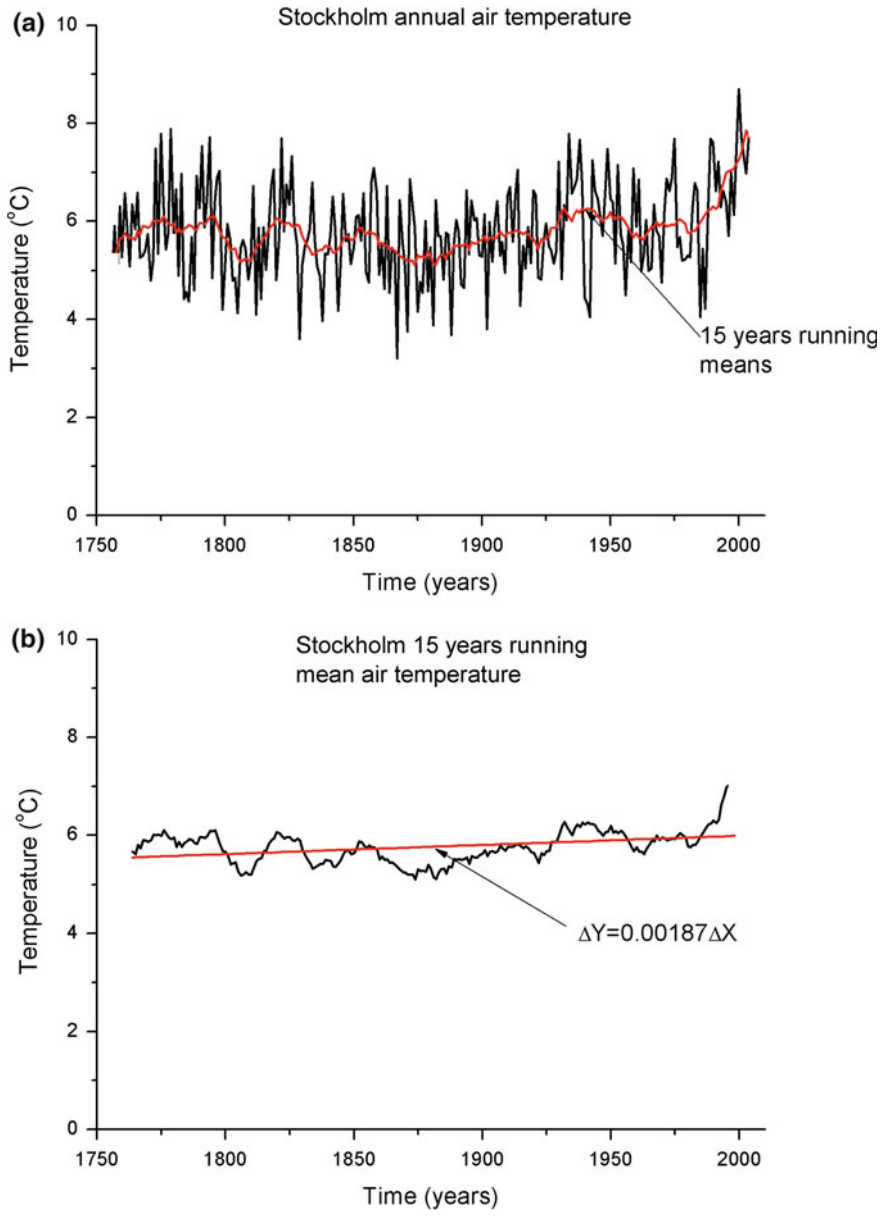

Fig. 6.5 The Stockholm annual air temperature with trend: **a** annual air temperature; **b** 15-year running mean air temperature; **c** 15-year running mean air temperature and **d** residual temperature from long-term trend

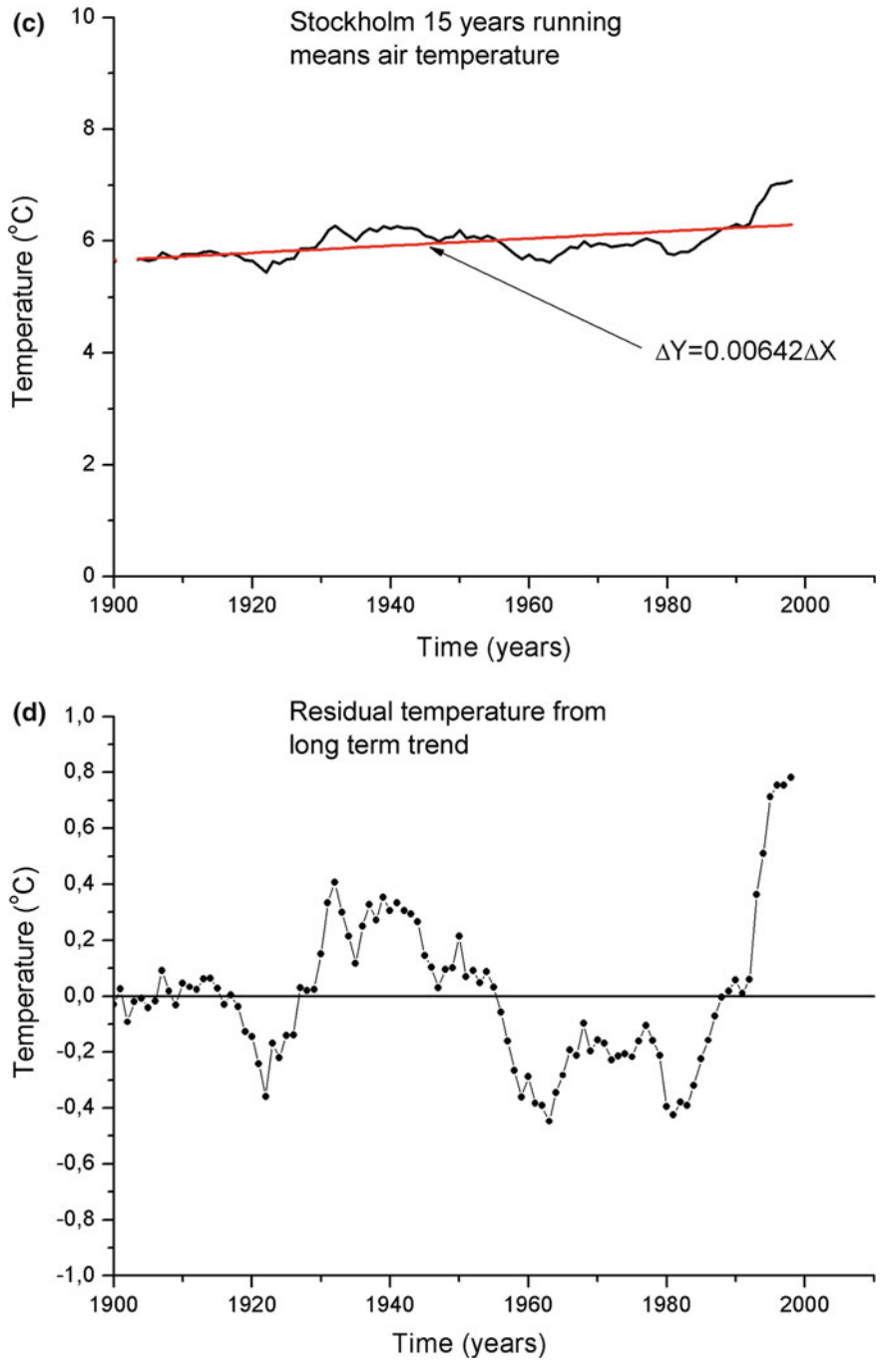

Fig. 6.5 (continued)

Exercise 2.11
Compare the Stockholm air temperature observations with the long-term variations in sea surface temperatures at Christianö, near Bornholm Island in the southern Baltic Sea (for the data needed, see Appendix C). Examine the trend of the 15-year running mean data for the period since 1900.

Answer:

The Christiansö data are plotted in Fig. 6.6a. The Figure presents a time series starting at approximately 1880 and including some data inhomogeneities. In Fig. 6.6b, climate properties are calculated by smoothing the dataset starting at 1900 using adjacent averaging. In addition, as the data stop at 2003 and the climate period considered is 15 years, the last eight years of smoothed data are omitted before a linear trend is calculated. The trend indicates a temperature increase, but the rate is less than half of the corresponding rate for Stockholm air temperatures. Residual smoothed Christiansö data are plotted in Fig. 6.6c, where we can see that the temperature change over the twentieth century is due to temperature oscillation over a typical time scale of several decades.

Exercise 2.12
Investigate Stockholm sea level variations relative to climate change (for the data needed, see Appendix C). Assume, as Ekman (2003) does, that the land uplift can be determined from the trend from 1774 to 1864.

Answer:

When dividing the dataset into two groups, i.e., 1774–1864 and 1865–2008, we find that the trends for the two datasets are $\frac{\Delta Y}{\Delta X} = -0.475$ (cm/year) and $\frac{\Delta Y}{\Delta X} = -0.374$ (cm/year), respectively. The difference is regarded as indicative of an increasing sea level due to climate change, which equals 0.1 cm year^{-1}. In Fig. 6.7a, the original data are plotted; in addition, the data are smoothed by averaging over 15 years to reveal the climate change signal more clearly. In Fig. 6.7b, 15-year running means are plotted. Note that the largest sea level change occurred at the end of the nineteenth century, probably associated with the ending of the Little Ice Age. By calculating the residual between the 15-year smoothed sea level variation and the trend for the last period, we obtain a signature of sea level variability, as depicted in Fig. 6.7c.

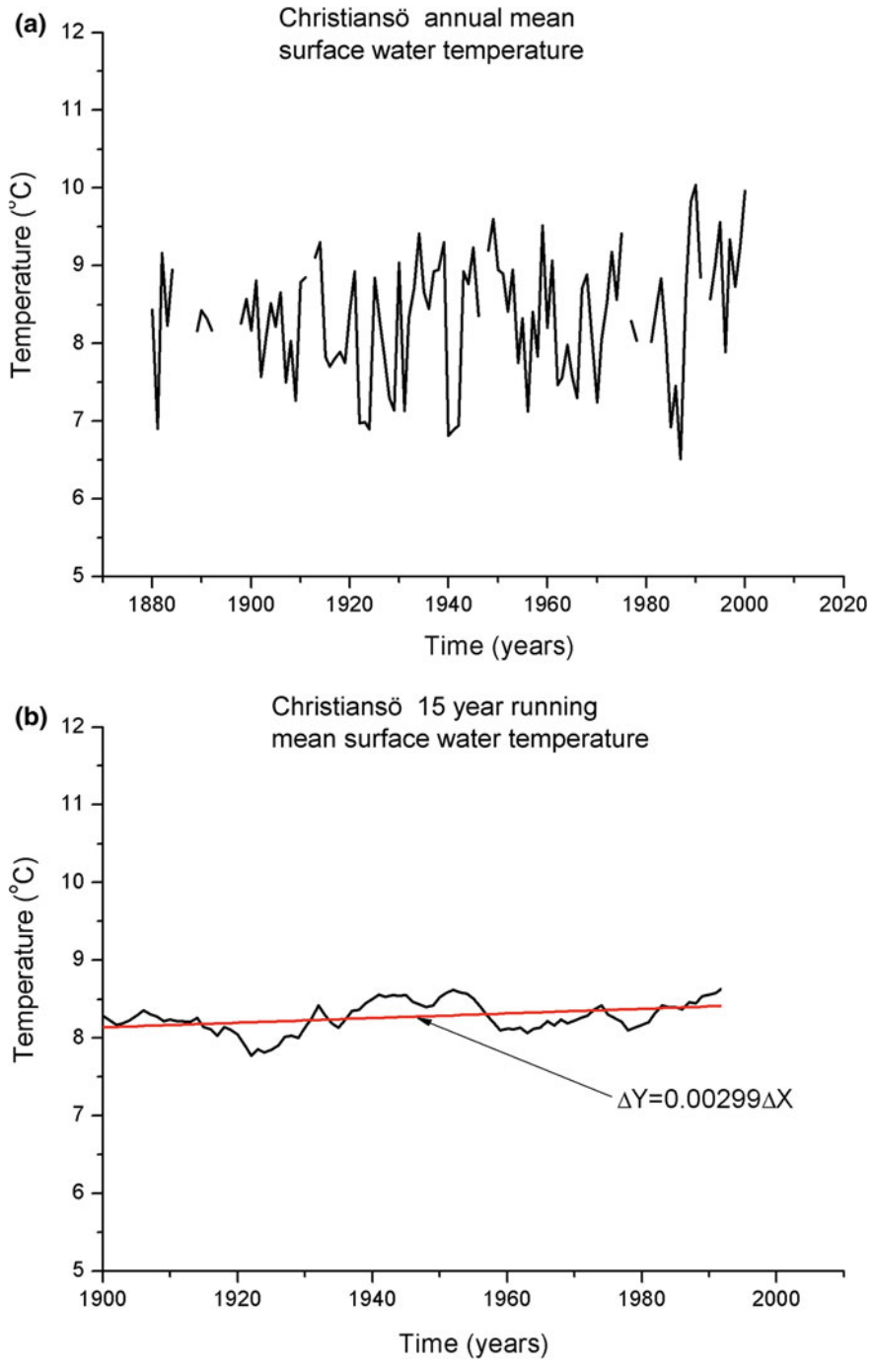

Fig. 6.6 The Christianö annual water temperature with trend: **a** annual mean surface water temperature; **b** 15-year running mean surface water temperature; **c** residual temperature from long-term trend

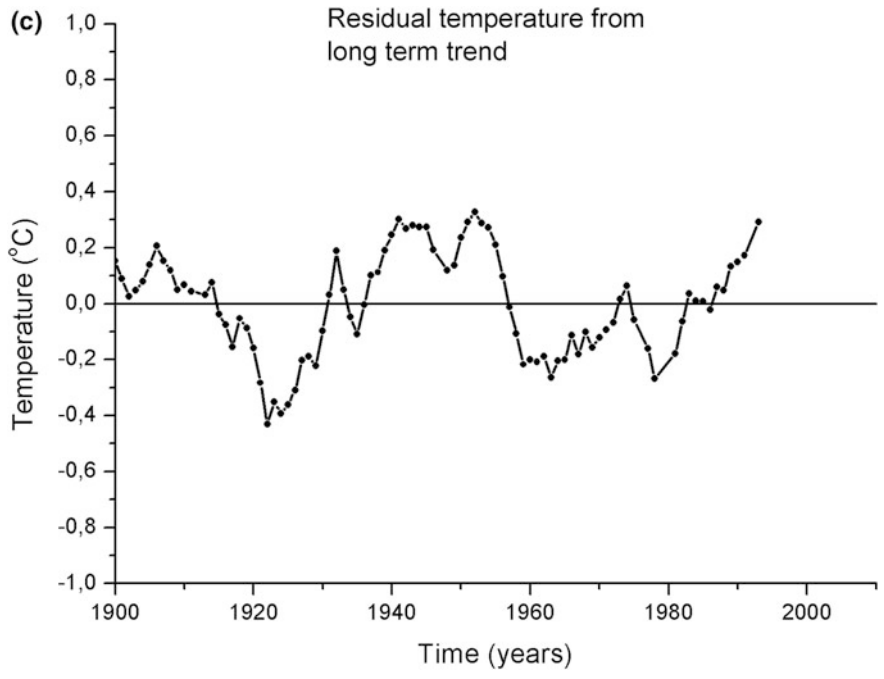

Fig. 6.6 (continued)

6.2 Solutions to Exercises in Chapter 3

Exercise 3.1
Run the Ekman boundary layer model until steady state is reached using the decay coefficient of Liljebladh and Stigebrandt (2000). Investigate grid and time-step independence: How many grid cells are needed? How large should the time step be? *Hint*: Link the main program `probe2002.f` with the `case_ex1.f` subroutine that defines the present application. Consult the *PROBE Manual* in Appendix D on how to use PROBE.

Answer:

In this exercise, we use the `case_ex1.f` subroutine, which is linked to the main program `probe2002.f`. The only changes needed are those made in

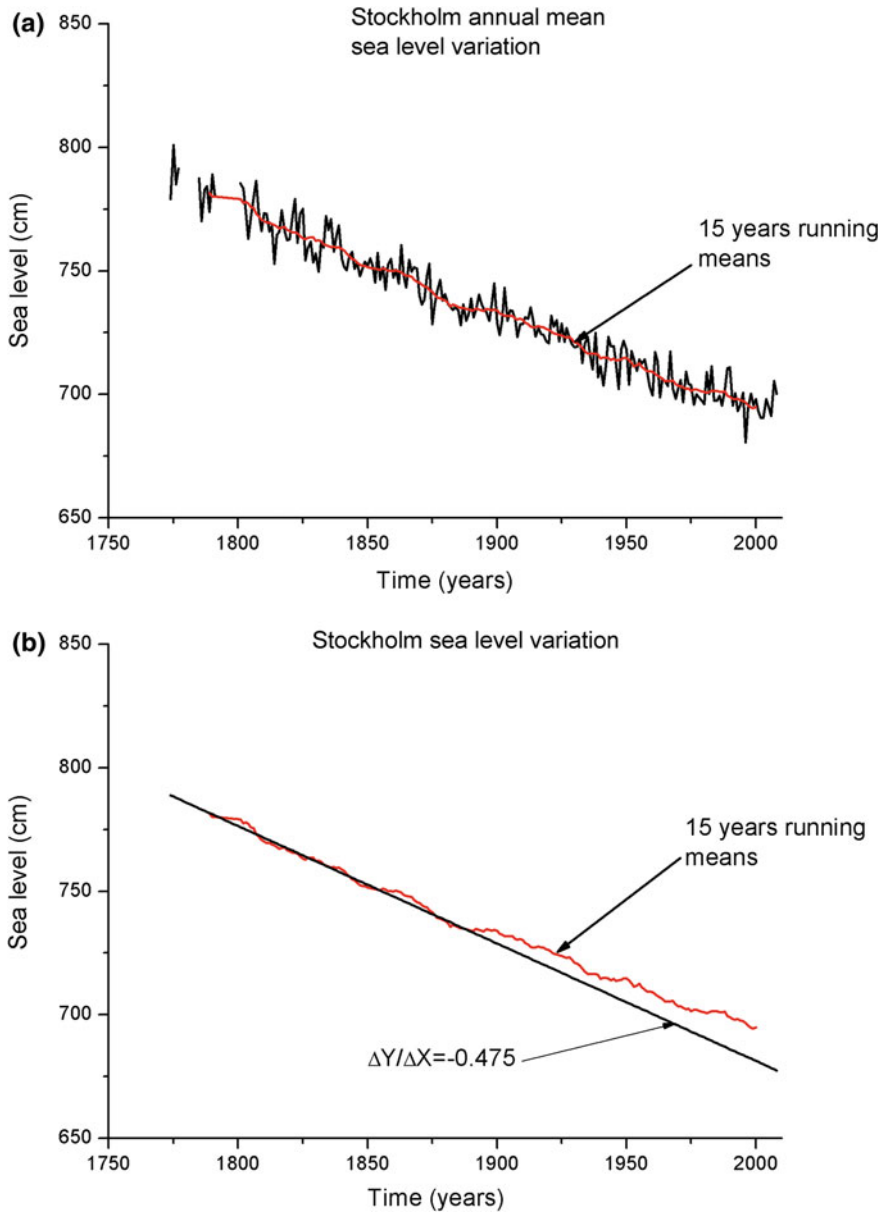

Fig. 6.7 Stockholm sea level variation with trends: **a** annual mean sea level variation and **b** 15-year running mean sea level variation

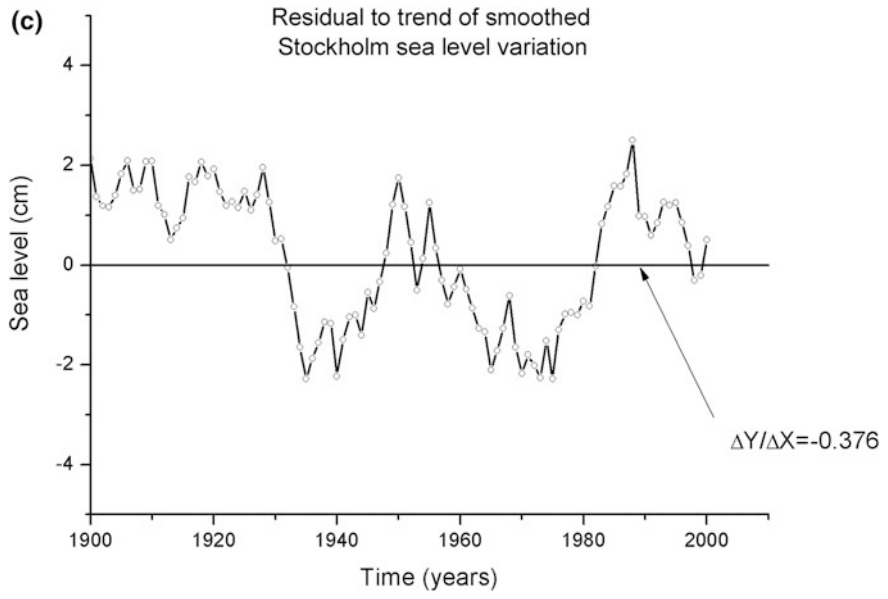

Fig. 6.7 (continued)

`case_ex1.f`. The number of grid cells is denoted N and the time step is denoted TFRAC(2). The number of grid cells available is `N-2` and the default value is 100 (consult Appendix D). If we do not change the default value, the number of grid cells available is 98. The results obtained using `N = 3`, `40`, and `100` are given in Fig. 6.8a. As already noted at `N = 3` (i.e., no vertical resolution), the solution agrees well with the results at higher vertical resolutions. The coarse vertical resolution damps the oscillation slightly but, compared with the uncertainties in the observations, this is of minor importance. The time resolution can be tested by changing TFRAC(2). The results obtained with a time resolution of 3600 s are depicted in Fig. 6.8b. A time resolution of one hour is inadequate, so it is recommended that a time resolution of 600 s be used instead.

Exercise 3.2
Compare the slab model with the vertically resolved models, and determine the typical lake depth at which the slab model can be used. Check heat conservation in the vertically resolved model.

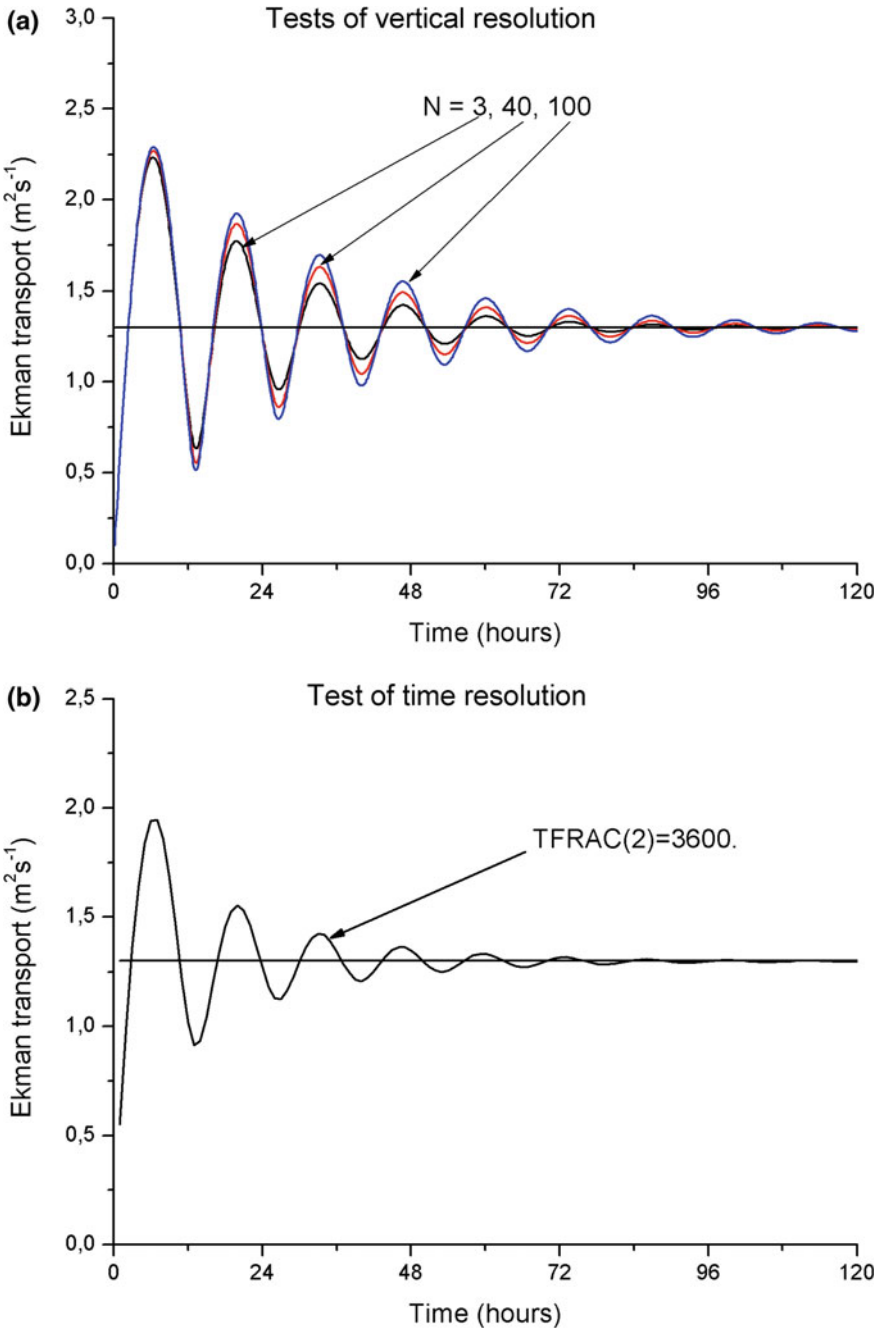

Fig. 6.8 Testing **a** grid resolution and **b** time resolution in an Ekman boundary layer

Answer:

Heat conservation is a major aspect to be investigated in all modeling efforts. If we have no inflows or outflows, the heat conservation depends only on air–sea fluxes. The numerical coding can be written as:

```
C------CONSERVATION CHECK
C1      BOUNDARY FLUXES
        FHAT=FHAT-(FLUXHZ(3)+FLXRAD)*AREA(NM1)*TFRAC(2)
C2      HEAT CONTENT
        HC=0.
        DO I=2,NM1
        HC=HC+F(I,JH)*DZCELL(I)*AREA(I)
        ENDDO
C3      CONSERVATION BUDGETS
        HC=HC-FHAT
C
```

where `FLUXHZ (3)` is net heat loss from the water and `FLXRAD` is the short-wave radiation from the Sun, both of which depend on latitude, time of the year, cloudiness, and ice. In the conservation budget, the two terms are the integrated heat content, `HC`, and the loss/gain, `FHAT`, during the whole run. Given the way we have programmed the heat conservation, `HC` should stay constant if the model conserves heat.

The results obtained using the numerically resolved lake model at a depth of 10 m are presented in Fig. 6.9. Careful study of the normalized heat content indicates that the model does not conserve heat and that the problem is associated with temperatures near zero. This problem occurs because we have not yet introduced ice into the lake model.

By running vertically resolved and slab models, it is evident that the slab model can do just as good a job as the vertically resolved model for lakes less than 10 m deep. However, this is only true for the forcing data currently used; under other forcing conditions (e.g., less wind), we need to reanalyze the problem.

Including pressure effects in a model of a very deep lake calls for some changes. (1) The default value for grid cells is 100, so the `NIM` values need to be changed in `comp2002.inc` and the storing size needs to be recalculated. (2) The equation for the temperature of maximum density needs to be calculated and, as this temperature

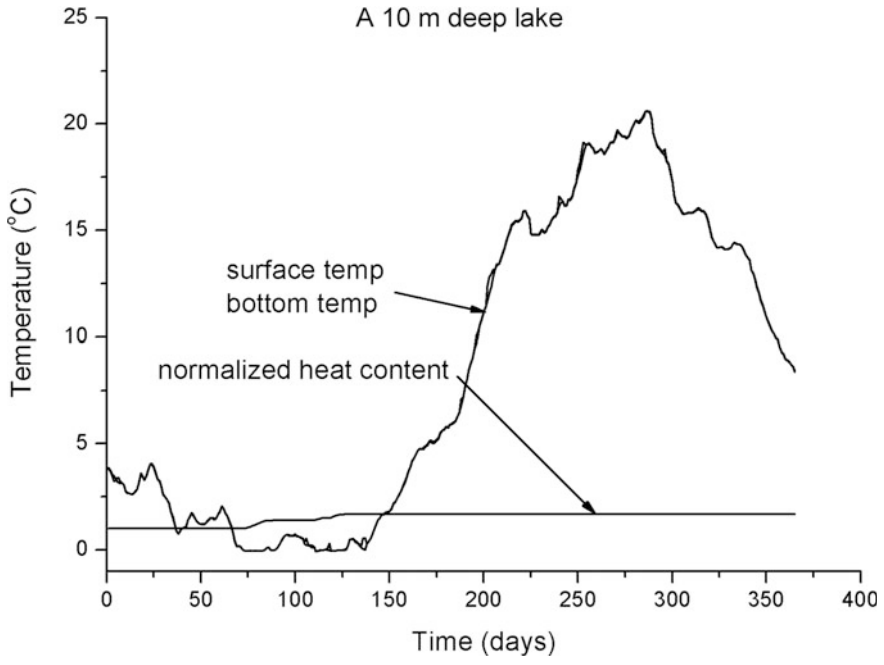

Fig. 6.9 Normalized heat content of a 10-m-deep lake (i.e., heat content/1.667 × 10^8), using the lake model

is now depth dependent, `TREF` must be changed to a vector—that is, `TRMAX(I)`. (3) `TREF` must be replaced with `TRMAX(I)` in `probe2002.f` and stored in the new include file `compao.inc`. All these settings are specified in the `case_ex2b.f` and `probe2002_1000.f` subroutines.

Exercise 3.3
Model estuarine circulation by adding river runoff (Q_r = 3000 m^3 s^{-1}) and a 3.5-times-greater inflow of more saline deep water to the model. Assume that inflows and outflows balance. What is the typical stratification spin-up time for the basin? For how long will the initial conditions influence the results? *Hint*: Use the *e*-folding time (i.e., the time needed for the salinity or temperature to increase or decrease by a factor of *e*) as an indication of the spin-up time.

Answer:

Estuarine circulation can be easily modeled by prescribing the inflows and outflows in subroutine `case_ex3.f`. The coding reads:

```
C-----IN AND OUT STORING-----------------------
      DO I=1,N
      QINFL(I)=0.0
      QOUTFL(I)=0.0
      ENDDO
C
C1-----FIRST FRESH WATER INPUT AT SURFACE
      NM2=N-2
      PHIIN(NM2,JH)=F(NM2,JH)
      PHIIN(NM2,JS)=0.
      QINFL(NM2)=QFBB
C2-----SECOND  OUTFLOW AT SURFACE
      QOUTFL(NM2)=QFBB+QDEEP
C
C3-----THIRD INFLOW OF DENSE BOTTOM WATER
      PHIIN(2,JH)=F(2,JH)
      PHIIN(2,JS)=4.3
      QINFL(2)=QDEEP
C
```

River runoff enters the surface grid cell with the properties of no salinity and a temperature equal to the surface temperature. The inflow of dense bottom water adds water of a given salinity (i.e., 4.3) and a temperature equal to the deep water temperature. According to conservation principles, inflows must equal outflows, which are modeled in this case as surface outflow.

The numerical simulation with QFBB = 3000 $m^3\ s^{-1}$ and QDEEP = 3.5 × QFBB $m^3\ s^{-1}$ and with an initial condition of zero salinity is depicted in Fig. 6.10. The *e*-folding time scale is determined by the time required for the amplitude to increase or decrease by a factor of *e*. The surface salinity used here is 3.4, and the spin-up time is defined from the salinity $3.4 - 3.4/e = 3.4 - 3.4/2.7 = 2.1$, which is reached after approximately two years.

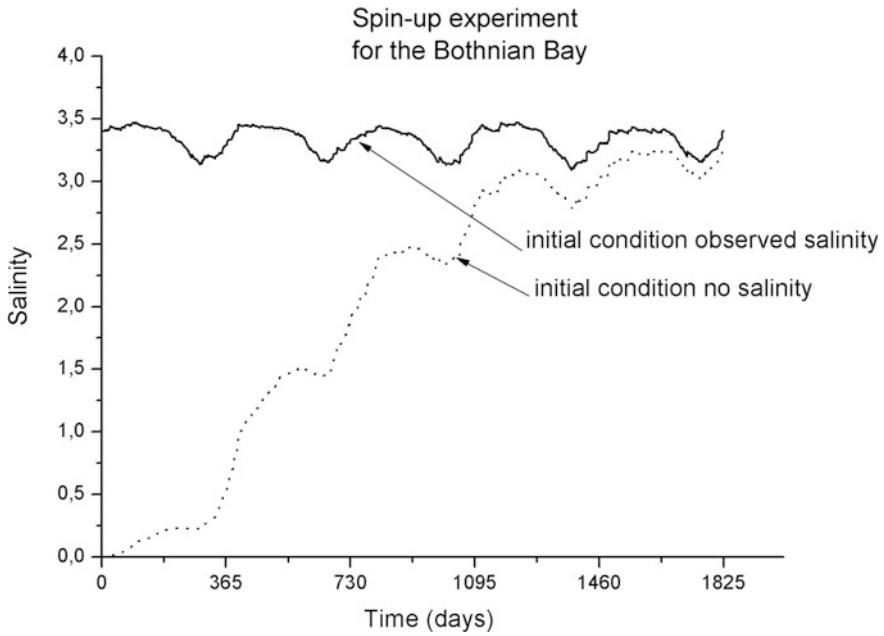

Fig. 6.10 Spin-up experiment for salinity in Bothnian Bay

Exercise 3.4
Examine the heat balance of an ice-covered water body. Run the model for a period of five years, and plot both the sensible and latent heat fluxes, net long-wave radiation, solar radiation, and the heat flow from water to ice. How does adding sea ice to the model alter the radiation balance?

Answer:

The various heat flux components are discussed below. Sensible flux, F_H, is calculated from the temperature difference between water and air and from wind speed. Latent heat flux, F_E, is calculated from the specific humidity at the sea surface and in the air and from wind speed; the net long-wave radiation is calculated from the sea surface and air temperature and from total cloudiness. Short-wave radiation to the open sea surface, F_{SW}, is calculated from latitude, time of year, cloudiness, and water albedo. When the sea is ice covered, short-wave radiation at the top of the ice/snow surface, F_{IT}, needs to be considered; this depends on latitude, time of year, cloudiness, and snow/ice albedo. Short-wave radiation that penetrates the snow/ice layers, F_{IB}, depends on snow and ice thicknesses and on heat flux from water to ice, F_W. The latter flux depends on heat stored under the ice and on mixing conditions.

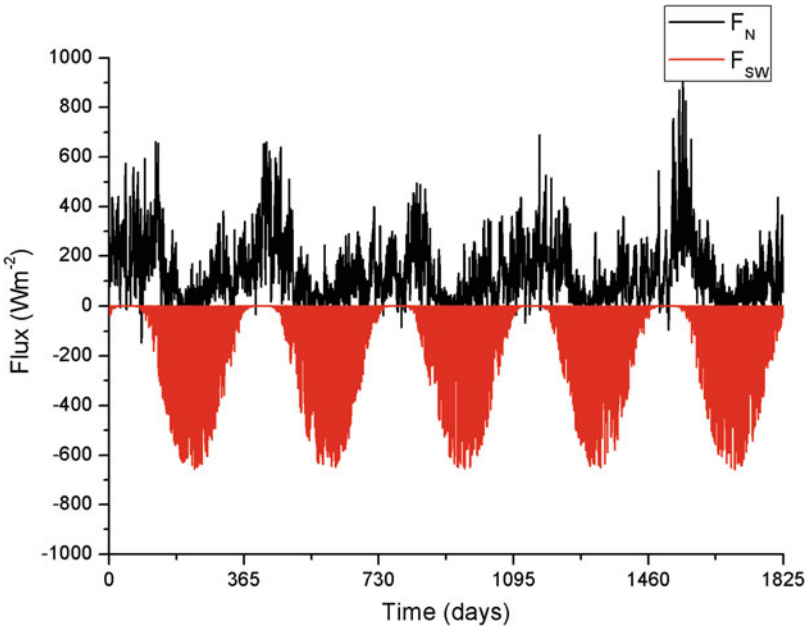

Fig. 6.11 Calculated net heat loss and short-wave radiation

Figure 6.11 depicts the net heat loss (i.e., $F_N = F_H + F_E + F_L$) and short-wave radiation into ice-free water, F_{SW}. From the figure we can see that net heat flux almost always cools the sea surface and that this heat loss is counteracted by sun radiation.

After the formation of ice, the sensible, latent, and net heat losses from the water surface have no effect on the heat balance. Instead, the heat flow from water to ice and short-wave radiation through the ice take control of the water heat balance. Ice thickness can be calculated from the difference in temperature between the water and air, the difference between the sun radiation to the top and bottom of the ice, and the heat flux from water to ice.

Figure 6.12 depicts major heat fluxes at the ice–water interface. At early stages of ice formation, solar radiation is small but the heat content in the water is still important. During the melting season, the solar radiation penetrating the ice increases, influencing the heat flux from water to ice. As can be seen in the figure, the modeling indicates that there are considerable heat fluxes beneath the ice.

Exercise 3.5
Test some of the turbulence models presented in this section and offered as options in the main PROBE program. Present the results produced by three of the turbulence formulations and state whether or not they could be used and, if so, when?

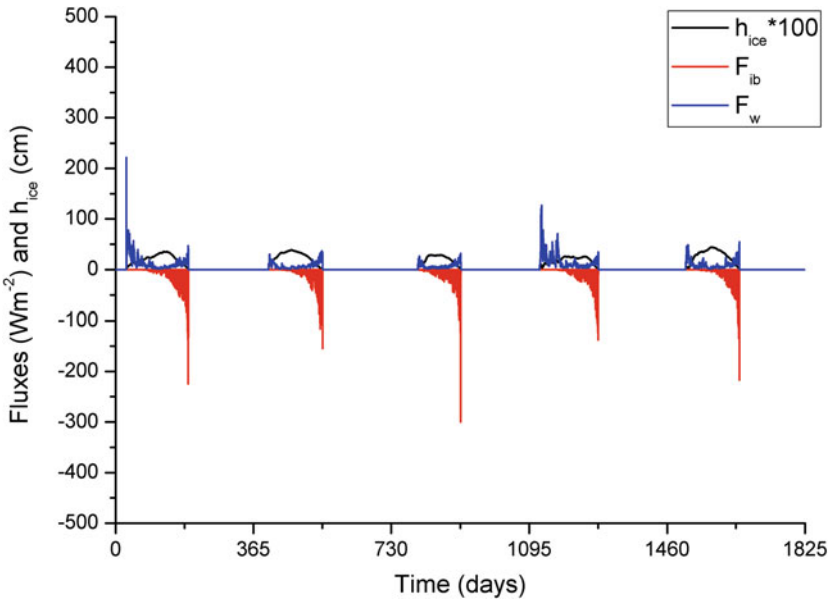

Fig. 6.12 Calculated ice thickness and sun radiation through ice and from water to ice

Answer:

In the modeling, we specify the turbulence model, i.e., `ITURBM` = 4, and write the code as a separate subroutine at the end of the case subroutine. However, when using the model of Axell and Liungman (2001), the built-in model `ITURBM` = 2 is used. In Fig. 6.13a–c, the zero-equation model of Svensson (1979) is compared with the one-equation model of Axell and Liungman (2001) and the two-equation model of Omstedt (1990a). Only the temperature structures are given in these calculations. The results indicate a close relationship between the models of Axell and Liungman (2001) and Omstedt (1990a). The first model, which ignores stratification effects, generates too much mixing and the whole water column becomes over mixed. We therefore conclude that the last two models can be used.

Exercise 3.6
Introduce tides into the model and estimate the tidal amplitude needed to destroy the density stratification caused by the estuarine circulation in Bothnian Bay in the northern Baltic Sea.

Hint: Tidal motions in Bothnian Bay are very small but we use this model setup to illustrate the importance of tidal mixing.

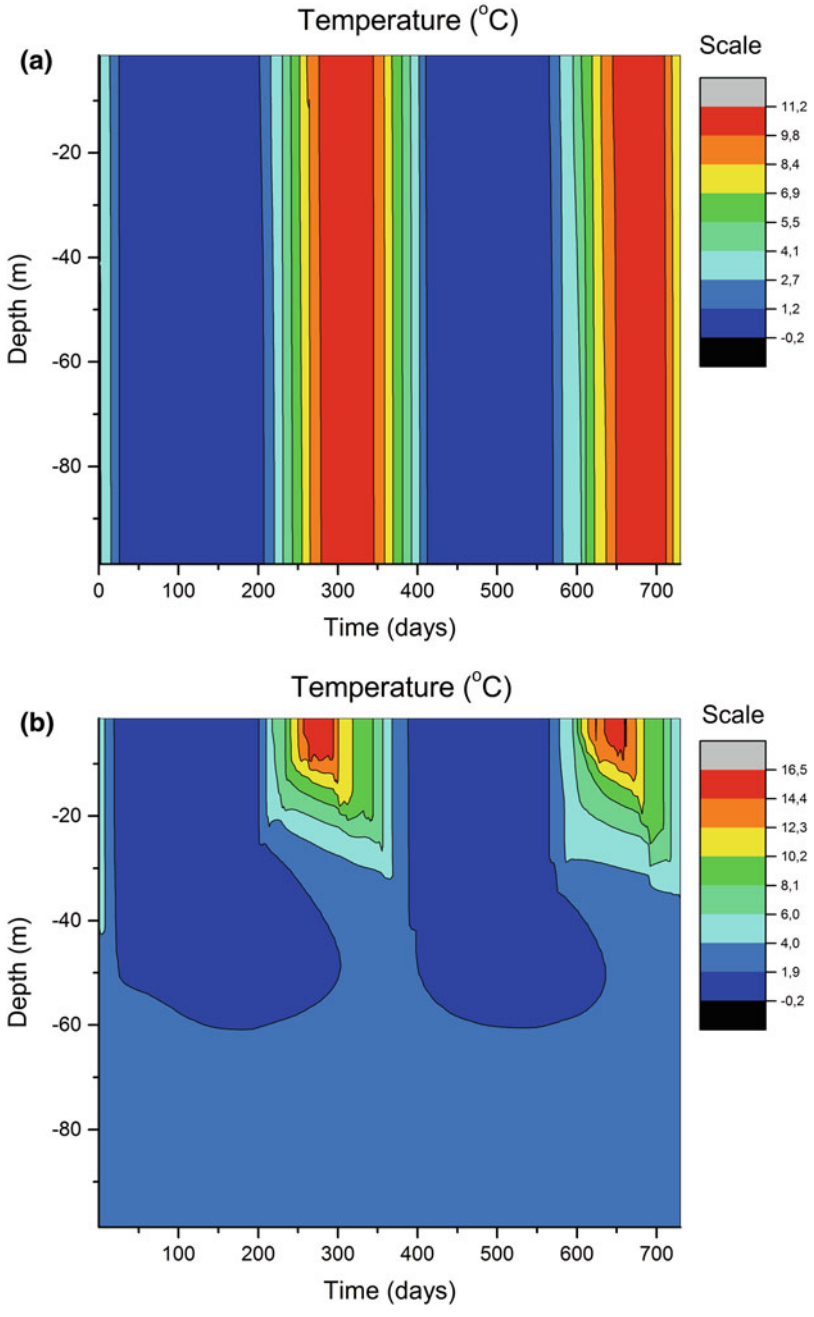

Fig. 6.13 Two-year simulations using the turbulence models of **a** Svensson (1979), **b** Axell and Liungman (2001), and **c** Omstedt (1990a)

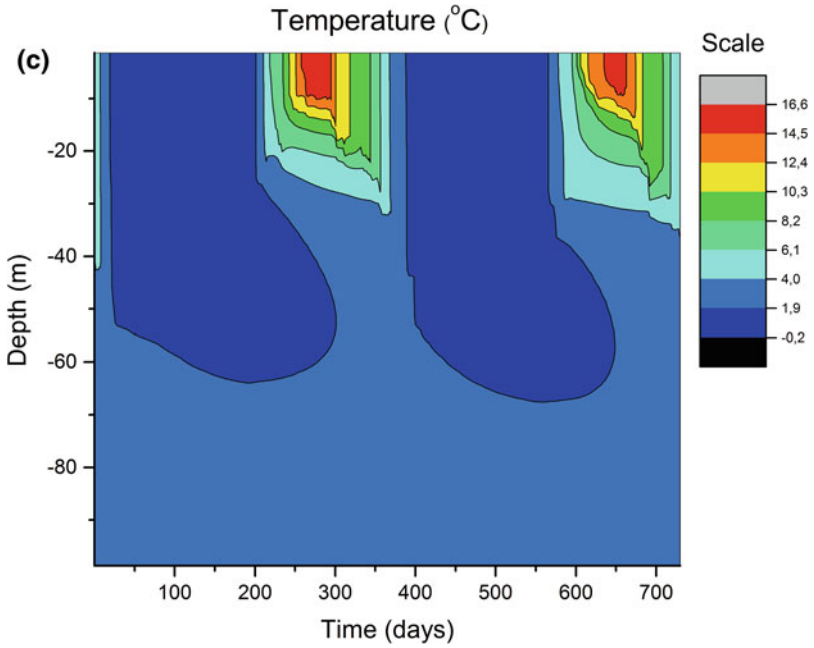

Fig. 6.13 (continued)

Answer:

Tidal motions are very small in the Baltic Sea and can often be neglected. Nevertheless, we will investigate tides in this system as a theoretical exercise. Stratification effects can be estimated by calculating the Richardson number, R_i:

$$R_i = \frac{\frac{-g}{\rho}\frac{\partial \rho}{\partial Z}}{\left[\left(\frac{\partial U}{\partial Z}\right)^2 + \left(\frac{\partial V}{\partial Z}\right)^2\right]}$$

When the Richardson number is small, typically less than 0.25, the velocity shear is considered sufficient to overcome stratification. From scale estimates, we obtain:

$$R_i \approx \frac{g\alpha_2 \frac{\Delta S}{H_s}}{\left(\frac{U_{tide}}{H_c}\right)^2} \leq 0.25 \text{ or } U_{tide} \geq H_c\sqrt{\frac{4g\alpha_2 \Delta S}{H_s}}$$

where H_c and H_s represent the typical length scale for the current shear and density stratification, respectively. In our example, we set *both* H_c and H_s to 10 m. With a salinity difference of 1, the estimated tidal velocity becomes nearly 0.6 m s^{-1}. We would now like to establish a relationship between tidal velocity and tidal

amplitude. From Eqs. 3.61 and 3.62, we assume a balance between acceleration and pressure according to:

$$\frac{\Delta\rho_0 V}{\Delta t} \approx \frac{\Delta P_w}{\Delta y} \approx \frac{\rho_0 g \Delta\eta}{\Delta y}$$

With a typical tidal time scale of 6 h and a length scale of 300 km, we obtain the following estimation:

$$\Delta V = \frac{\Delta t g}{\Delta y}\Delta\eta \approx \frac{6 \times 3,600 \times 9.81}{300,000}\Delta\eta = 0.7\Delta\eta$$

Thus, with a tidal amplitude of slightly less than 1 m, we should expect the stratification to vanish. We now investigate this in our numerical model by adding tidal forcing to the model described in Sect. 3.8. The result (Fig. 6.14) indicates that stratification breaks down when tidal amplitudes are less than 1 m but larger than 0.5 m.

6.3 Solutions to Exercises in Chapter 4

Exercise 4.1
Introduce estuarine circulation into the model by assuming that river inflow and deep water inflow both equal 15,000 $m^3\ s^{-1}$ and that the oxygen concentration in the inflowing deep water is of surface origin. Calculate oxygen variation over a five-year period. Introduce one extra equation for water age, assuming that it is zero at the surface. What is the typical age of the deep water? *Hint*: Set the source term in the equation for water age to equal 1/year = $3.17 \times 10^{-8}\ s^{-1}$.

Answer:

To model water age, we need to make some changes in subroutine `case_ex7.f`. First, a new equation needs to be added to Chap. 1 of the subroutine by writing `SOLVAR(8) = .TRUE.` The initial water age conditions need to be specified and can be set to zero assuming we consider only the age of the water from the start of the calculation. The source term, as outlined in the exercise, models the aging of the water. The boundary conditions only need to state that the value at the surface is zero or `IKBHZ(8) = 1`. This statement means that the boundary condition at the surface is a prescribed value with a default of zero. Finally, we need to consider the source term, which can be written in the subroutine `case_ex7.f` (Chap. 3 in the `subroutine case_ex7.f`) as:

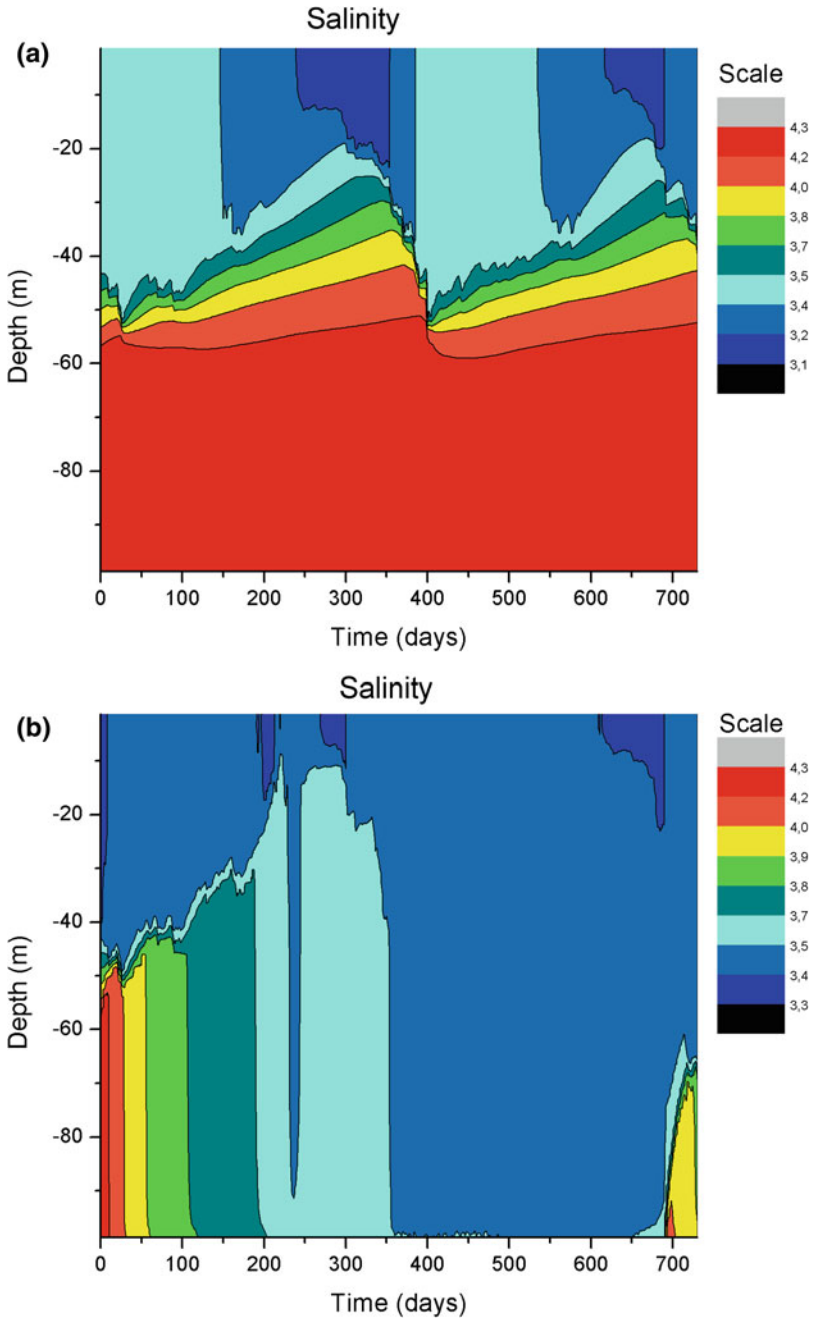

Fig. 6.14 Two-year simulation including estuarine circulation and tidal forcing with amplitudes of **a** 0.5 m and **b** 1 m

```
C      IF(J.EQ.8)THEN
C-----WATER AGE
          DO I=2,NM1
          SI(I)=1./(3600.*24.*365.)
          ENDDO
       RETURN
       ENDIF
```

The results are depicted in Fig. 6.15. As a result of the inflow of dense bottom water with high oxygen concentrations, bottom water is always rich in oxygen. Low oxygen concentrations are calculated below the halocline. The corresponding water age calculation indicates that the water just below the halocline is stagnant and of greater age.

Exercise 4.2
Examine the sensitivity of plankton growth by studying the importance of light penetration and Secchi depth. *Hint*: Assume that the extinction coefficient of short-wave radiation can be calculated from $\beta_w = \beta_{w1} + 0.4 \times 10^{6pp}C$ and Secchi depth from $Z_s = \frac{1.7}{\beta_w}$.

Answer:

Model results for surface plankton and oxygen concentrations are shown in Fig. 6.16. The extinction coefficient is now modeled as a vector in `subroutine case_ex8.f` together with Secchi depth (Chap. 2 of the subroutine):

```
C-----COMPUTE EXTINCTION COEFFICIENT AND SECCHI DEPTH
      DO I=2,NM1
        BETAP(I)=BETA+0.4*F(I,JPC)*1.E6
      ENDDO
C
      SECCIF=1.7
      SECCIZ=SECCIF/BETAP(NM2)
C
```

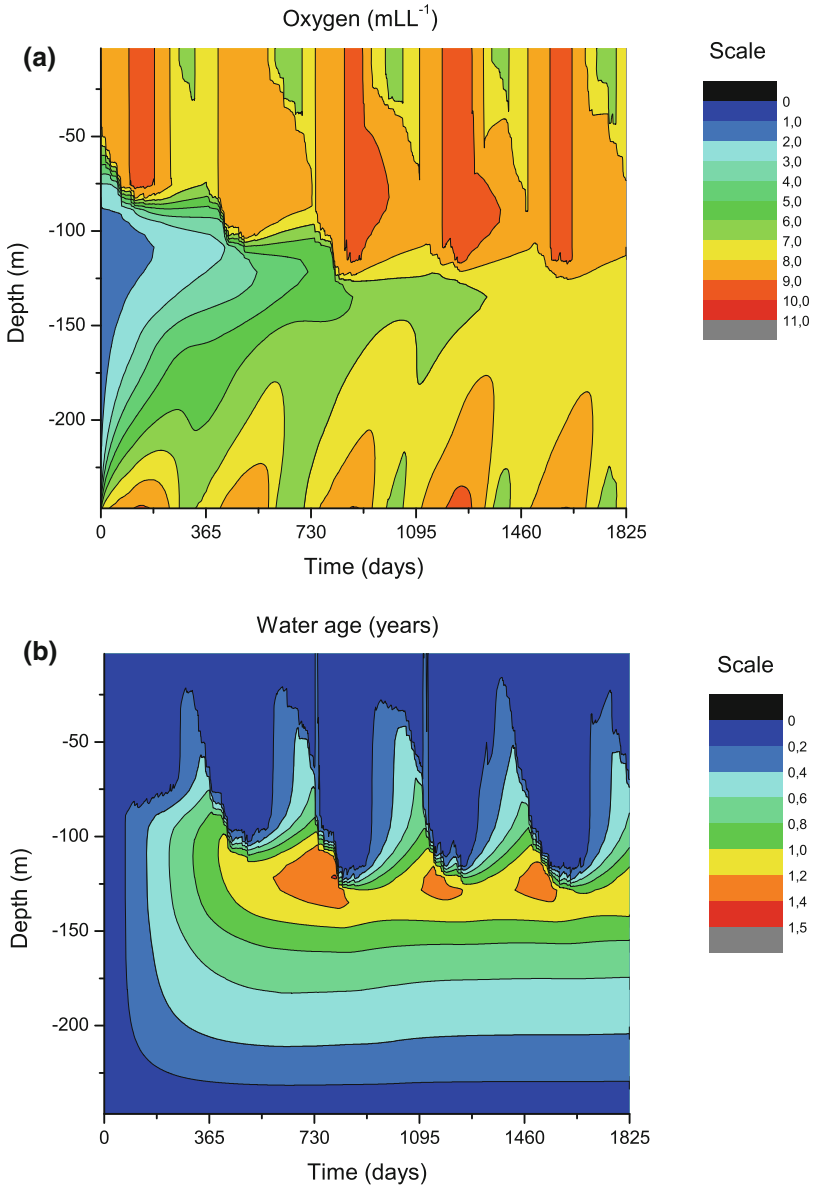

Fig. 6.15 Calculated **a** oxygen concentration (mL L–1) and **b** corresponding water age (years)

The dimension of `BETAP(I)` is given in the Chap. 1 of the subroutine, and in Chapter 3 of the subroutine we change BETA to `BETAP(I)`. Note that primary production is reduced when the extinction coefficient depends on plankton concentration as well. Plankton effectively shade each other and therefore limit their

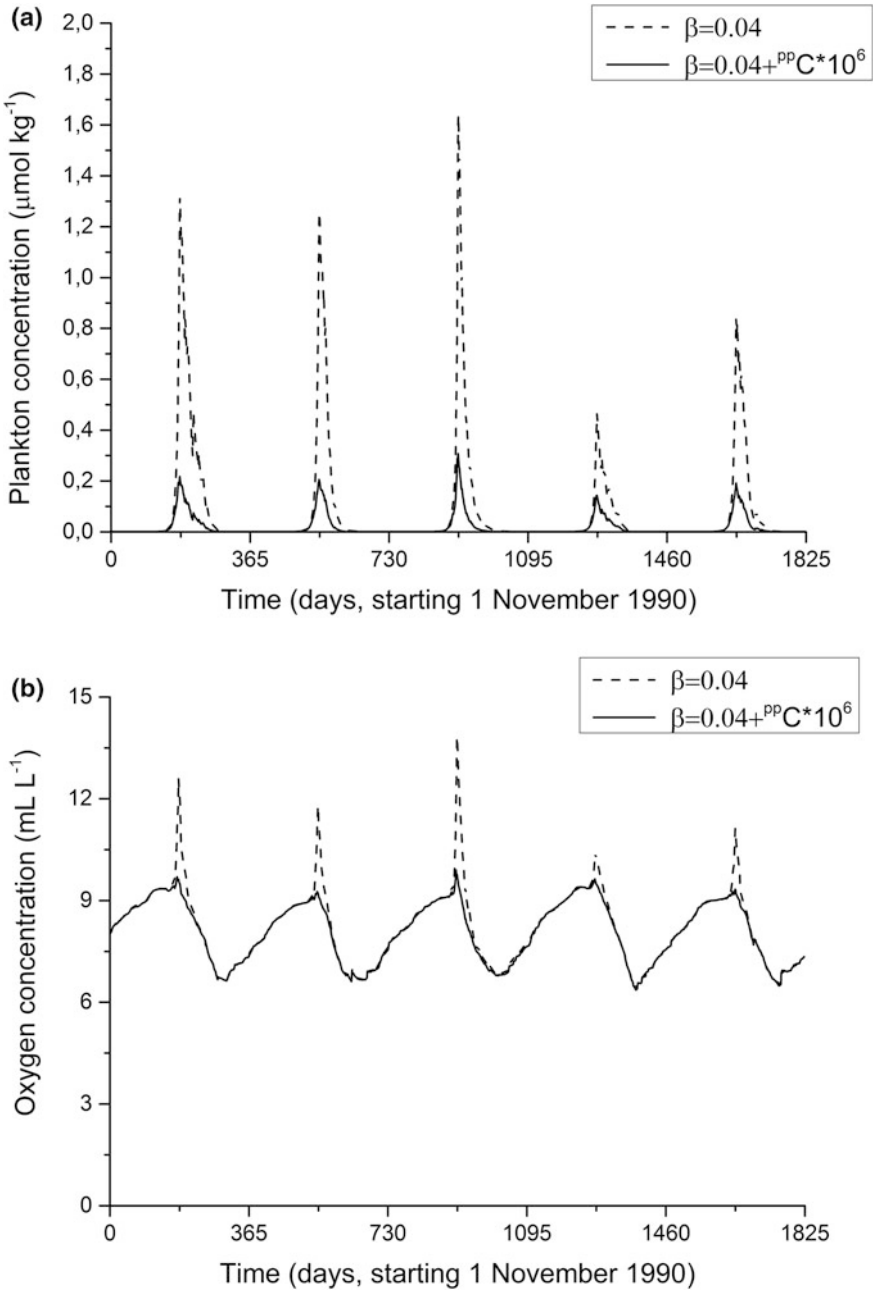

Fig. 6.16 Calculated plankton concentrations **a** without and **b** with light penetration parameterization that includes plankton concentration

own growth. This also damps the oxygen oversaturation during primary production. The Secchi depth in winter is controlled by `BETA` and is reduced during the summer plankton bloom, which is modeled in `BETAP(I)`.

Exercise 4.3
So far in our biogeochemical modeling of the sea, we have considered only one group of P-limited algae. In this exercise add another equation for nitrate. Model plankton dynamics using two plankton types, one for a group of P-limited and N-limited algae, and another for a group of blue–green algae limited only by *phosphorus*. The latter plankton group should also be assumed to be temperature and salinity limited. *Hint*: Look into subroutine `case_ex9b.f`

Answer:

Subroutine `case_ex9b.f` comes up with a model that has two nutrient and two plankton equations. For the nutrients, we now have one equation for nitrate, NO_3, and one for phosphate, PO_4. The two plankton models include one functional plankton type that is both nitrate and phosphate limited and a second type that is only phosphate limited. The river inputs of nitrate and phosphate are given as `PINPUT = 2.8E-6` and `NINPUT = 130.E-6`. The second functional algae type computes the concentration of blue–green algae. This type of algae can fix dissolved atmospheric nitrogen gas, N_2, and is of major concern in the Baltic Sea. These algae provide also extra nitrogen inputs to the sea surface and therefore strongly counteract nitrogen-reduction activity. Mineralization is assumed to take place below the thermocline. Temperature and salinity limitations are modeled together with the nutrient limitation for the first plankton type:

$$\mathtt{NUTLIM_1(I)} = \mathtt{MIN}\left[\frac{\mathtt{F(I,JNC)}}{(0.05 \times 10^{-6} + \mathtt{F(I,JNC)})}, \frac{\mathtt{F(I,JTN)}}{(1.5 \times 10^{-6} + \mathtt{F(I,JTN)})}\right]$$

For the second plankton type, we model the nutrient limitation as:

$$\mathtt{NUTLIM_2(I)} = \frac{\mathtt{F(I,JNC)}}{(0.05 \times 10^{-6} + \mathtt{F(I,JNC)})}\mathtt{TWLIM(I)SWLIM(I)}$$

The results are depicted in Fig. 6.17. In Fig. 6.17a, we see how the nitrate level declines with the advent of spring bloom. The nitrate is reduced to almost zero, but some phosphate remains, which can be used by the blue–green algae. The nutrient plot shows that the `N/P` ratio in winter is approximately 6, indicating that the situation is far from the Redfield ratio of 16/1. The dynamics of the two plankton types are illustrated in Fig. 6.17b.

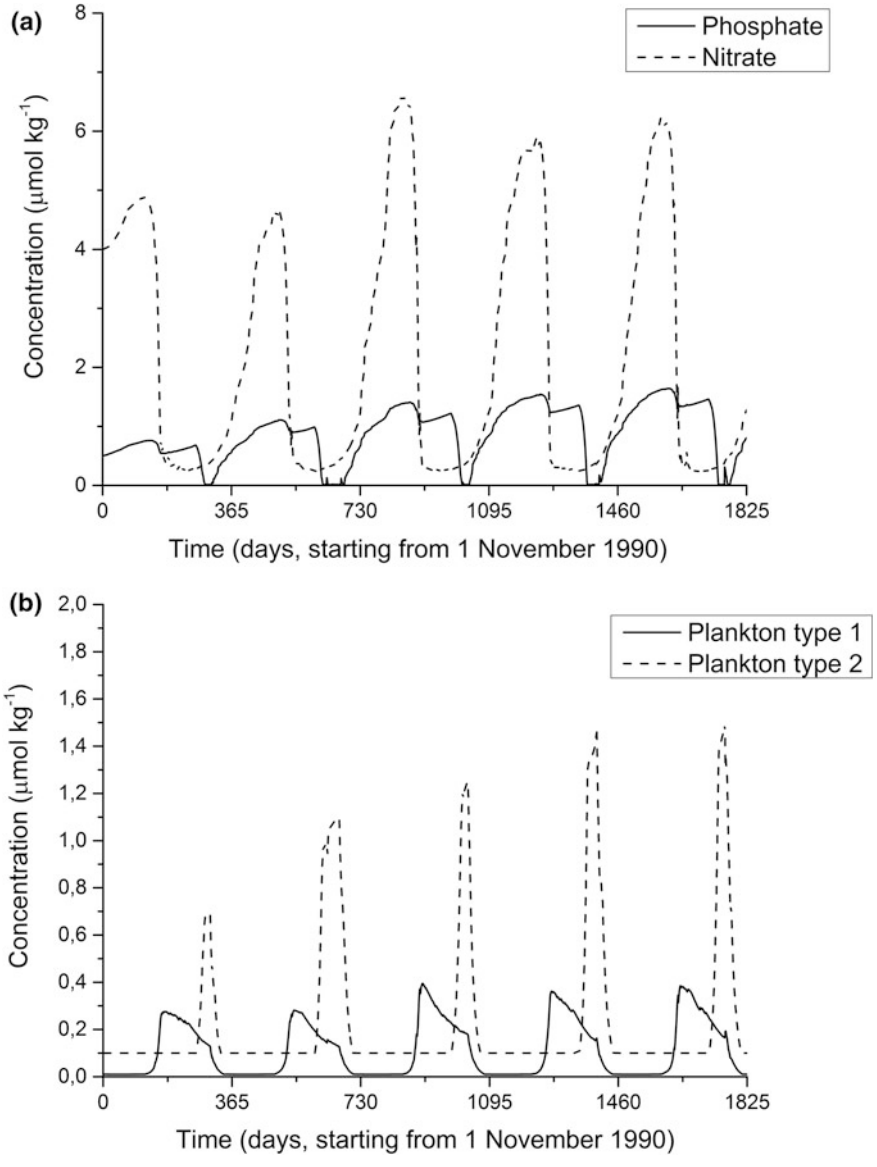

Fig. 6.17 Calculated **a** nutrient and **b** plankton dynamics with two plankton types

Exercise 4.4
The rivers entering the Baltic Sea are generally oversaturated with CO_2, typical concentrations being 1350 µatm (Humborg et al. 2009), and total alkalinity averages 1200 µmol kg^{-1}. Calculate the typical C_T and A_T concentrations in the Baltic Sea, assuming river runoff of 15,000 m^3 s^{-1} and an equally large inflow of saline water of 17 salinity units. Typical total alkalinity and total inorganic carbon concentrations in the inflowing water are equal to 2000 and 1800 µmol kg^{-1}, respectively. *Hint*: Assume steady state and apply conservation arguments.

Answer:

From volume and salt conservation principles and assuming steady state, we understand that:

$$Q_{out} = Q_{in} + Q_r$$
$$S_{in}Q_{in} = SQ_{out}$$

From C_T and A_T conservation, we obtain:

$$A_TQ_{in} + A_{Tr}Q_r = A_TQ_{out}$$
$$C_TQ_{in} + C_{Tr}Q_r = C_TQ_{out}$$

Now, using the given information, we can calculate the C_T and A_T concentrations in the sea:

$$A_T = [A_TQ_{in} + A_{Tr}Q]/Q_{out} = [2000 \times 15000 + 1200 \times 15000]/30000 = 1600\,\mu\text{mol kg}^{-1}$$
$$C_T = [C_TQ_{in} + C_{Tr}Q]/Q_{out} = [1800 \times 15000 + 1350 \times 15000]/30000 = 1575\,\mu\text{mol kg}^{-1}$$

The steady-state values are compared with a 15-year transient run in Fig. 6.18. The transient-run surface values approach the steady-state values after a several-year run.

Exercise 4.5
Observations from the central Baltic Sea indicate that the partial pressure of CO_2 in the water declines to nearly 150 µatm in summer. Several mechanisms may explain this, including the fact that nutrients are recycled more actively in the photic zone than is carbon. Explore this by letting the phosphorus recycle during primary production. *Hint:* Use `PFRAC` in `case_ex10b.f`. Include estuarine circulation, which generates oxygen-rich bottom water and inhibits phosphorus leakage from bottom sediments. Assume inflow values according to Exercise 4.4.

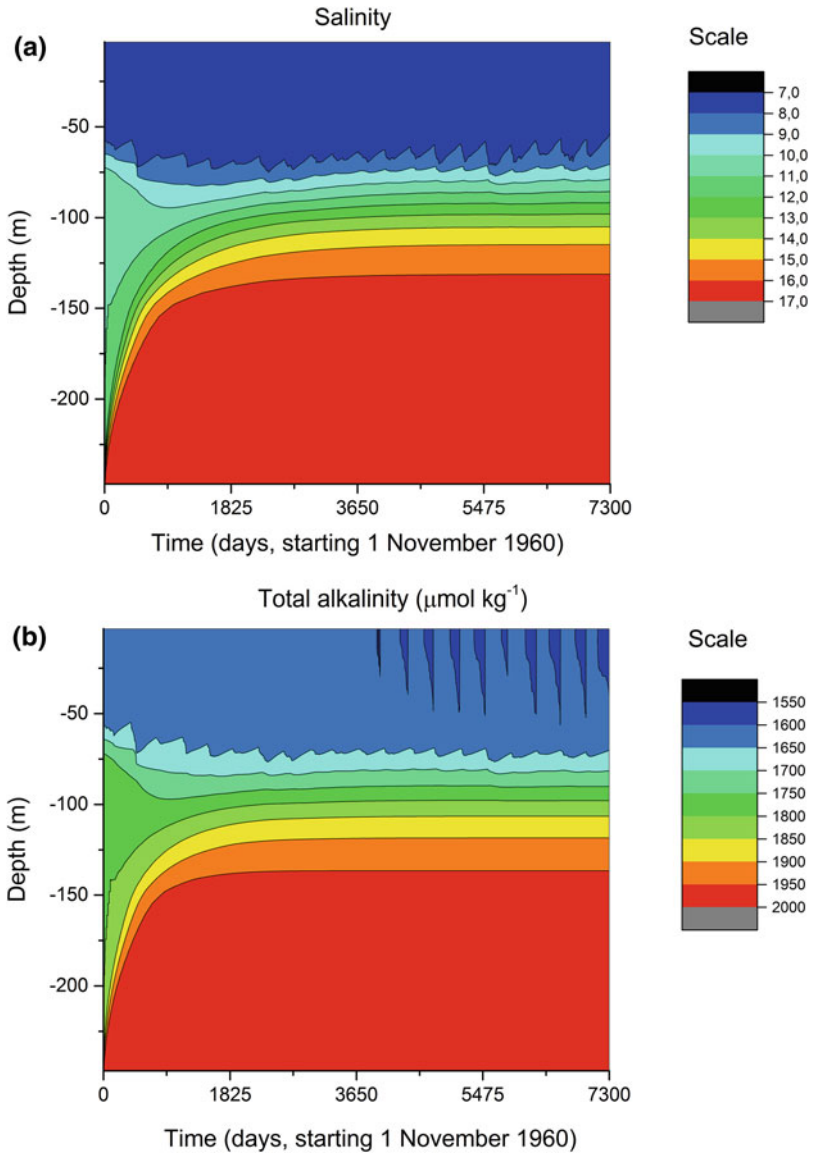

Fig. 6.18 Transient model calculations for **a** salinity, **b** total alkalinity (μmol kg^{-1}), and **c** total inorganic carbon (μmol kg^{-1}) using constant river and ocean inflows and values according to the exercise

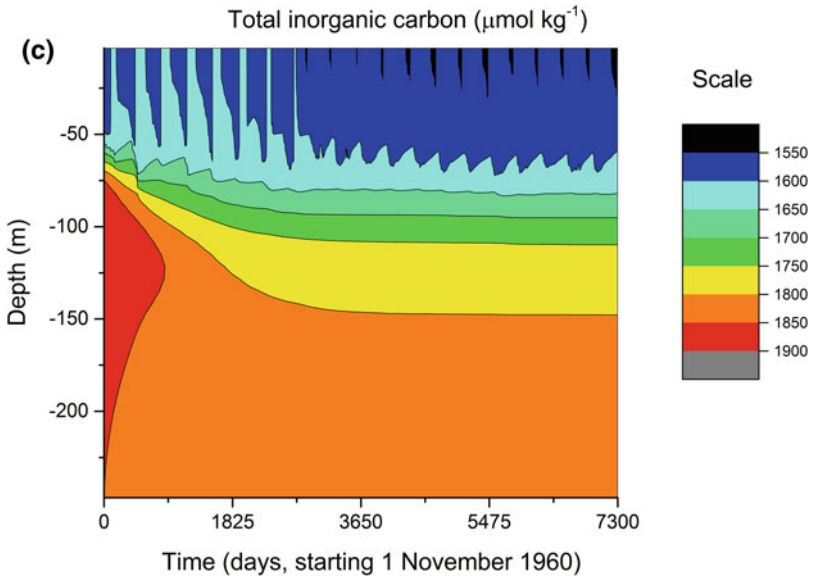

Fig. 6.18 (continued)

Answer:

In `case_ex10.fb`, we now set `PFRAC = 0.3`, which implies that the Redfield ratio between `C` and `P` is changed from 106:1 to 353:1. The results are depicted in Fig. 6.19 and indicate that the partial pressure in water is considerably reduced.

Exercise 4.6
When introducing the dynamics of CO_2 in a redox environment, models are developed that can be used for analyzing multiple factors stressing the marine ecosystem, for example, climate change, eutrophication, and marine acidification. Examine the surface pH change in a warmer atmosphere containing increased CO_2. Examine a 4 °C temperature increase with an atmospheric carbon dioxide partial pressure of 1000 µatm. Which is more important for the pH change, temperature increase or atmospheric CO_2 increase? *Hint:* Start from subroutine `case_ex10c.f` and change the air temperature and atmospheric carbon dioxide partial pressure one by one according to the exercise.

Answer:

Increase the air temperature in subroutine `case_ex10c.f` by 4 °C and pCO_2^a to 1000 µatm and run the model. If the atmospheric carbon dioxide partial pressure increases to 1000 µatm, the surface pH values are reduced by approximately 0.4 pH

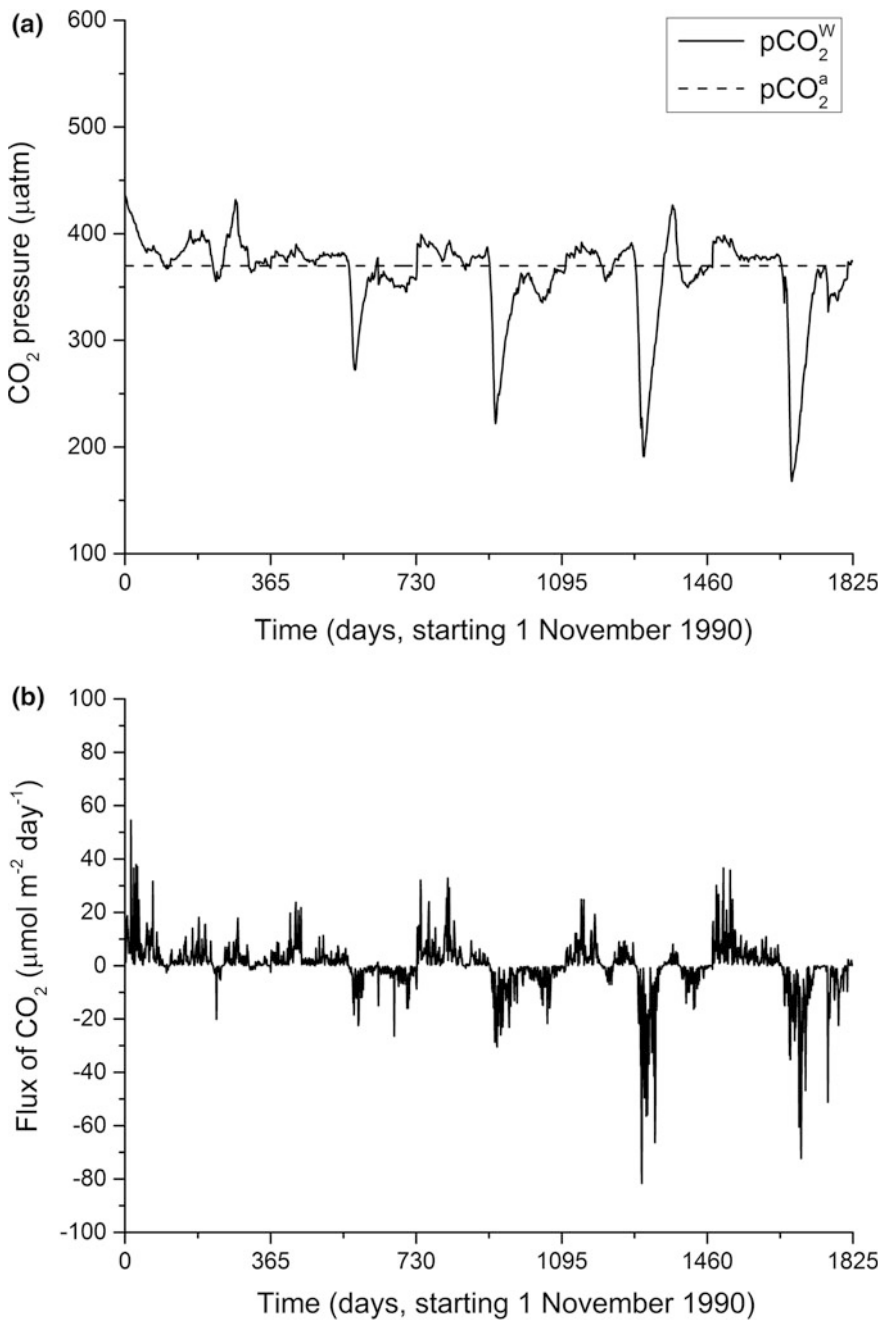

Fig. 6.19 Calculated **a** partial pressure and **b** flux of CO_2 in the water incorporating primary production and PFRAC = 0.3

units. The corresponding change for a warming of 4 °C is much smaller. To get confidence in the results, one can easily compare the results with Fig. 2.14 and the temperature effects with Fig. 3 in Omstedt et al. (2010).

6.4 Solutions to Exercises in Chapter 5

Exercise 5.1
Add a third basin and present the salinity variations for the new coupled system. *Hint*: Add a new inner basin to the two-basin model and assume river runoff of 5000 m^3 s^{-1} into the new basin. Assume a sill depth of 20 m between the outer and middle basins and of 30 m between the middle and inner basins.

Answer:

A third basin similar in size to the Gulf of Bothnia is added to the two-basin system. The area–depth distributions could be roughly modeled by changing `ZDIM`, `INDARE`, and `AREAHZ` in the three sub-basins. Typical surfaces in the basins are set according to 2.10^{10}, 2.710^{11}, and 1.10^{11} for the outer, middle, and inner sub-basins, respectively. Assume river runoff of 10,000 and 5000 m^3 s^{-1} to the middle and inner sub-basins, respectively. In the present case, a very simple model of strait flows is assumed, with constant inflows and outflows driven by the freshwater inflow to each of the basins. The resulting salinities are strongly influenced by the geometry of the sub-basins and sill depth, as depicted in Figs. 6.20a–c.

Exercise 5.2
Run the PROBE-Baltic model system for the 1958–2012 period, but only take physical aspects into consideration. Examine the calculated ice thickness in the Gulf of Riga over the 1960–2012 period. What is the typical calculated ice thickness in the Gulf?

Answer:

The fastest way of finding the solution is to set `IBIO = 2` in `basin1.f` and run the model from 1 November 1958 to 31 December 2012. In the `date.dat` file, set the start time to 1958110100. After running and gridding the data, the calculated ice thickness is available in directory `D:\probe_baltic\p13_70\ori_graph` and the Gulf of Riga file name is `gr_graph2.dat`. The various file names are as follows:

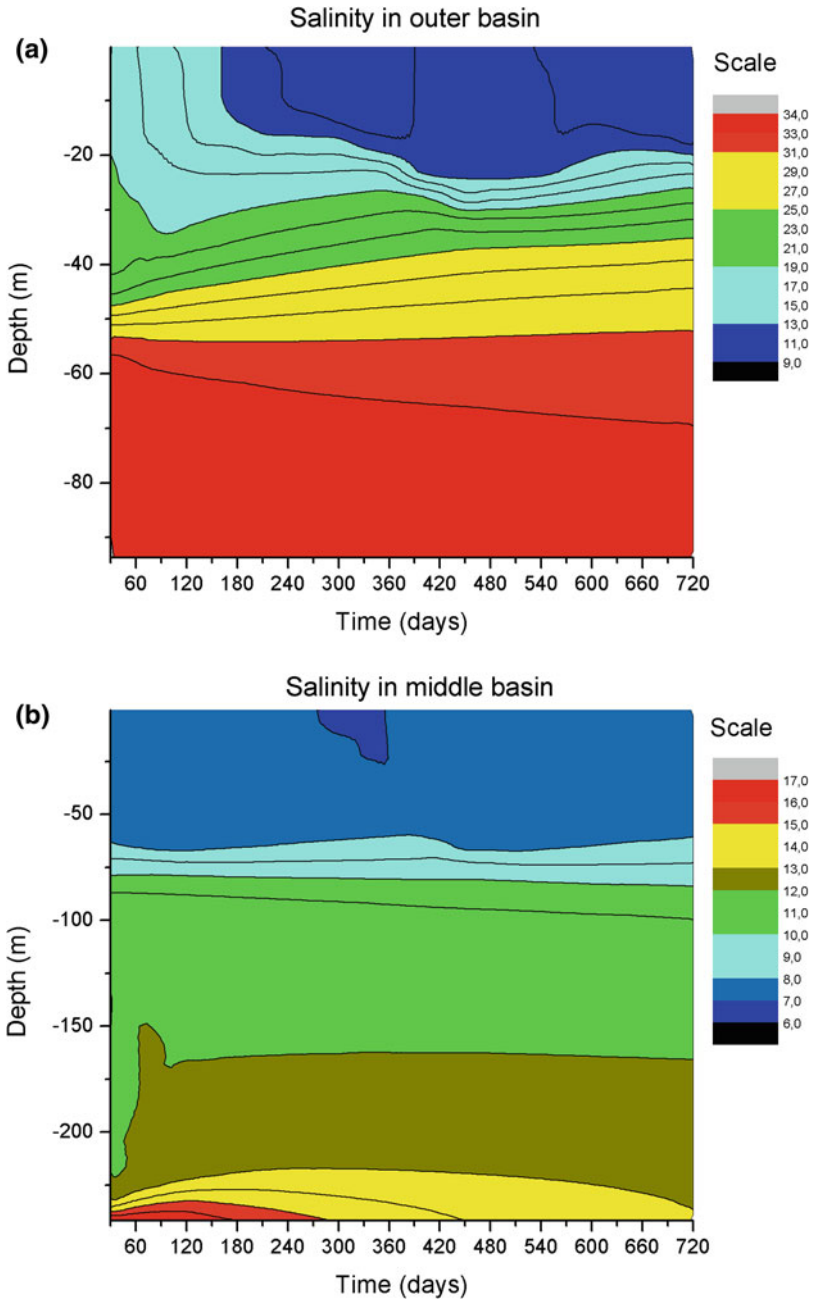

Fig. 6.20 Calculated salinity in the **a** outer basin, **b** middle basin, and **c** inner basin

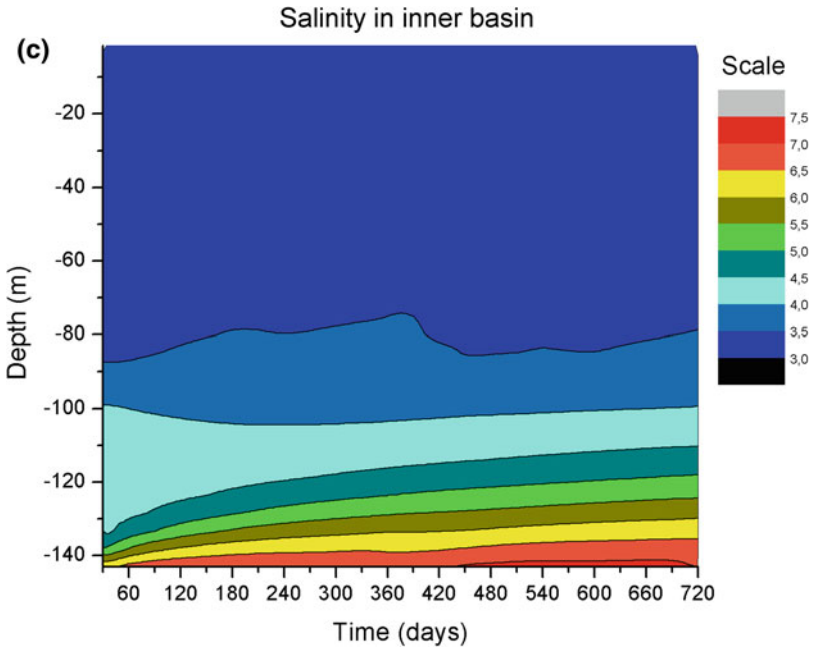

Fig. 6.20 (continued)

Sub-basin	Acronym	File name
Kattegat	ka	`ka_graph.dat, ka_graph2.dat`
Öresund	or	`or_graph.dat, or_graph2.dat`
Belt Sea	be	`be_graph.dat, be_graph2.dat`
Arkona Basin	ar	`ar_graph.dat, ar_graph2.dat`
Bornholm Basin	bh	`bh_graph.dat, bh_graph2.dat`
E Gotland Basin	go	`go_graph.dat. go_graph2.dat`
NW Gotland B.	nw	`nw_graph.dat, nw_graph2.dat`
Gulf of Riga	gr	`gr_graph.dat, gr_graph2.dat`
Gulf of Finland	gf	`gf_graph.dat, gf_graph2.dat`
Archipelago Sea	as	`as_graph.dat, as_graph2.dat`
Åland Sea	al	`al_graph.dat, al_graph2.dat`
Bothnian Sea	bs	`bs_graph.dat, bs_graph2.dat`
Bothnian Bay	bb	`bb_graph.dat, bb_graph2.dat`

The results are depicted in Fig. 6.21, indicating that, through most of the studied year, the Gulf of Riga is covered with ice, which is up to approximately 0.6 m thick during cold winters.

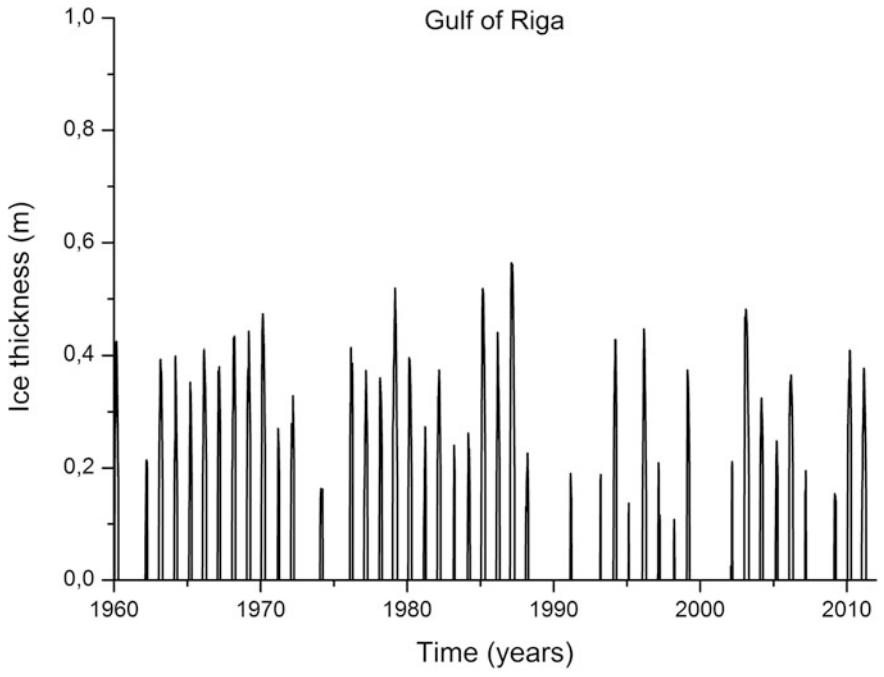

Fig. 6.21 Calculated ice thickness in the Gulf of Riga

Exercise 5.3
Run the PROBE-Baltic oxygen model and investigate the dynamics of salinity and oxygen over the 1960–2012 period. *Hint*: Compare the model results with the observed results presented in Fig. 5.10.

Answer:

After running and gridding the data, the salinity and oxygen profile data calculated are available in the directory `D:\probe_baltic\p13_70\ori_surf` and the file name for the central Baltic Sea is `go_surf.dat`. The various file names are as follows:

Sub-basin	Acronym	File name
Kattegat	ka	`ka_surf.dat`
Öresund	or	`or_surf.dat`
Belt Sea	be	`be_surf.dat`
Arkona Basin	ar	`ar_surf.dat`

(continued)

Sub-basin	Acronym	File name
Bornholm Basin	bh	bh_surf.dat
E Gotland Basin	go	go_surf.dat
NW Gotland B.	nw	nw_surf.dat
Gulf of Riga	gr	gr_surf.dat
Gulf of Finland	gf	gf_surf.dat
Archipelago Sea	as	as_surf.dat
Åland Sea	al	al_surf.dat
Bothnian Sea	bs	bs_surf.dat
Bothnian Bay	bb	bb_surf.dat

The results are depicted in Fig. 6.22. The structure of vertical salinity presented in Fig. 6.22a indicates both seasonal and long-term variations in upper surface layers. More dramatic changes, however, occur in deeper layers, as a result of water inflow and stagnation periods. The corresponding oxygen calculations are depicted in Fig. 6.22b, where deep water oxygen concentrations can be seen to be low, particularly from 1980 to 1992. These calculations are in good agreement with observed data (as indicated in Fig. 5.10). However, as the model run started on 1 November 1958, the results during the first decade are influenced by the initial conditions.

Exercise 5.4
Investigate the spin-up time by assuming that the Baltic Sea inside the Drogden and Darss sills is filled with freshwater (i.e., salinity equals 0.5) and A_T, C_T, and nutrients all equal zero, while outside the sills these properties are at ocean levels. Run the model from 1 November 1700 to 2008. *Hint*: Use the reconstructed forcing field from 1700 to 2008 presented in Appendix C.

Answer:

For longer time integrations, new forcing files need to be added (Appendix C) and the file names need to be changed in subroutine `bmain.f`. These changes are available in `bmain.f_ex5.4`.

New initial conditions need to be specified in the `in` directory. The physical conditions are available in `INIT_TABFSPI.DAT` and the chemical conditions in `INIT_TABBSPI.DAT`. In `D:\probe_baltic\p13_70\In\INIT`, the project `Finit.vfproj` needs to read the two initial tables and run the project. The new initial profiles then need to be copied to the correct directory. This is done by running the `copin_xx.bat` program in `D:\probe_baltic\p13_70\In`.

In addition, the correct start date needs to be specified in the `date.dat` file in directory `D:\probe_baltic\p13_70`. After the run is ready, interpolation should be done by running the Intel Fortran project `Finterpolering` at the `D:`

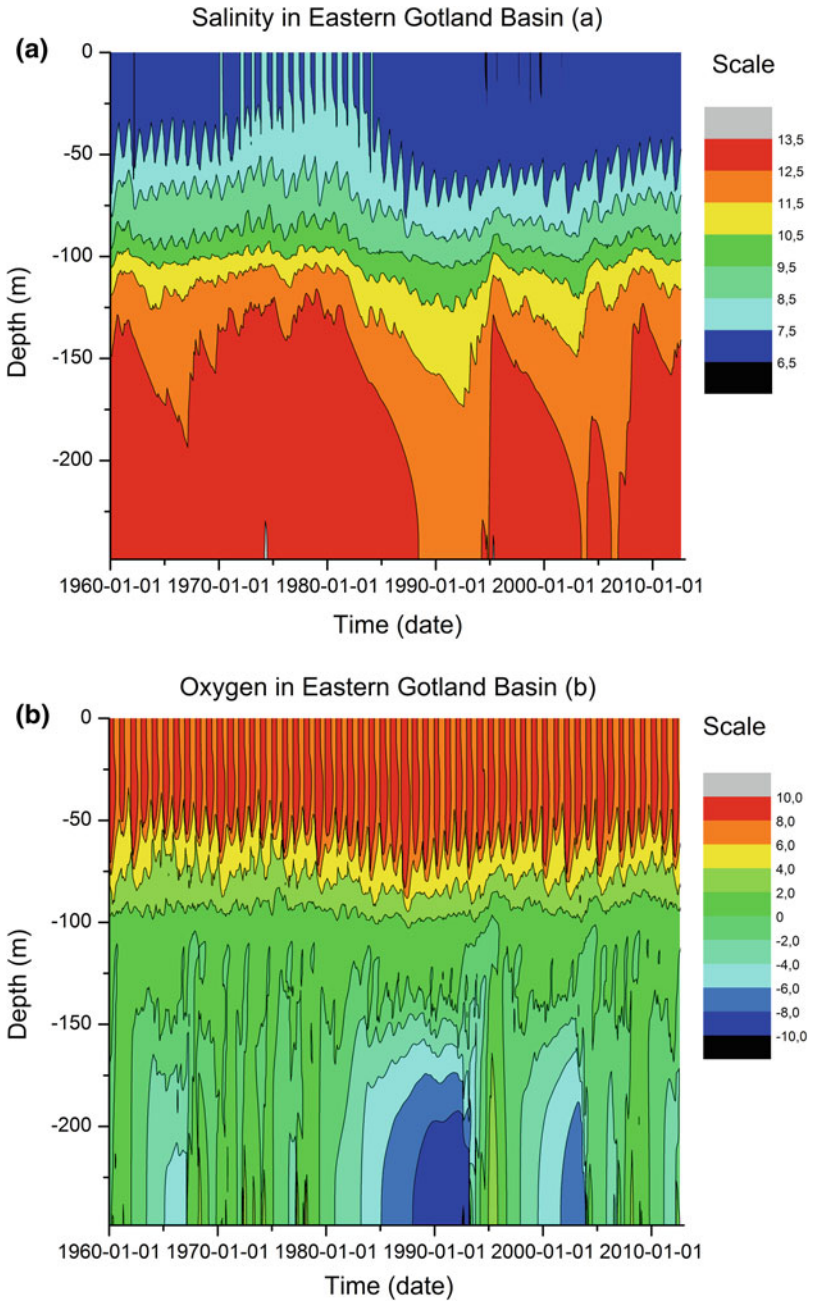

Fig. 6.22 Calculated **a** salinity and **b** oxygen dynamics in the Eastern Gotland Basin

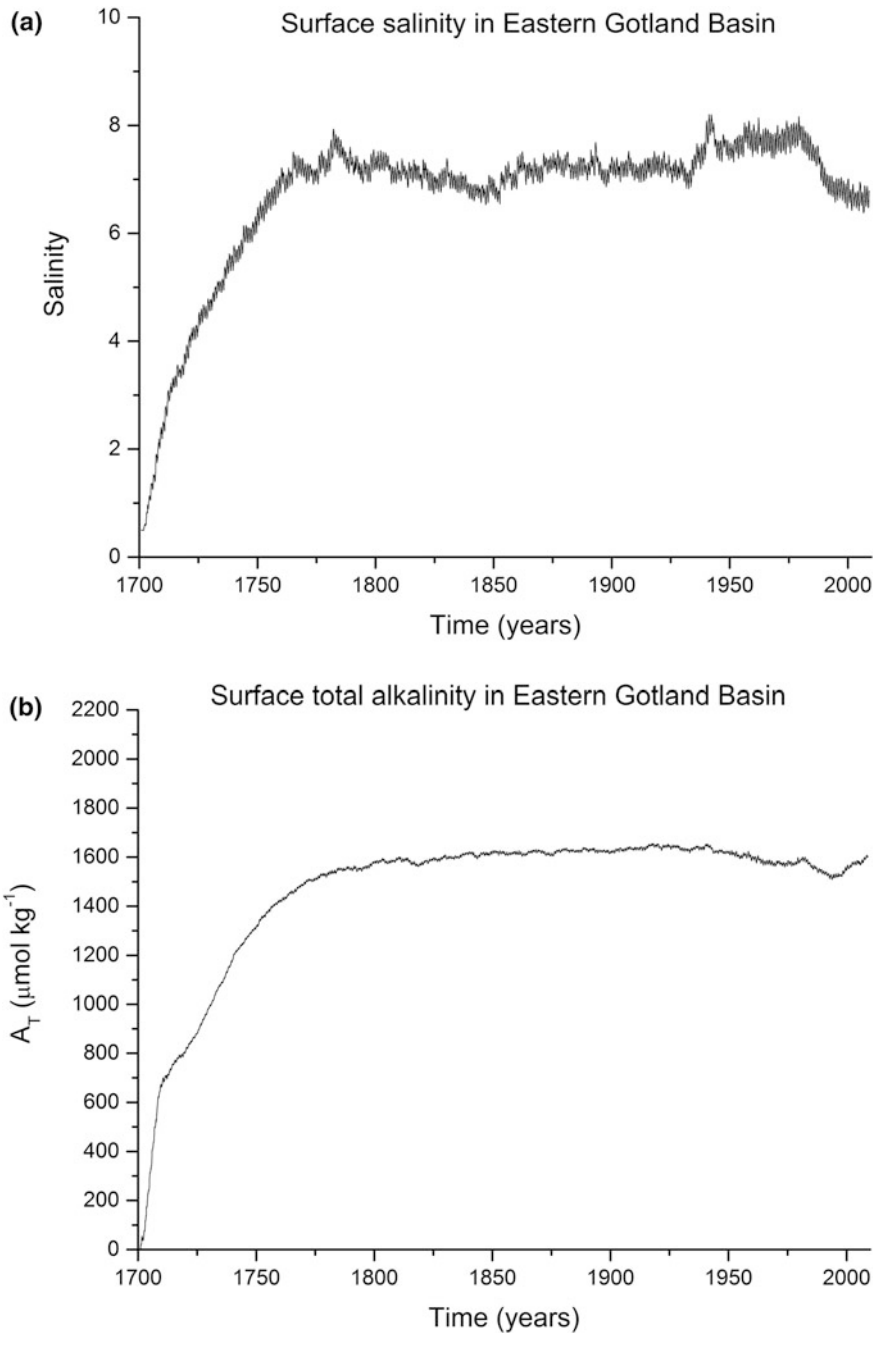

Fig. 6.23 Calculated spin-up of **a** surface salinity, **b** total alkalinity, and **c** surface pH in the Eastern Gotland Basin of the Baltic Sea

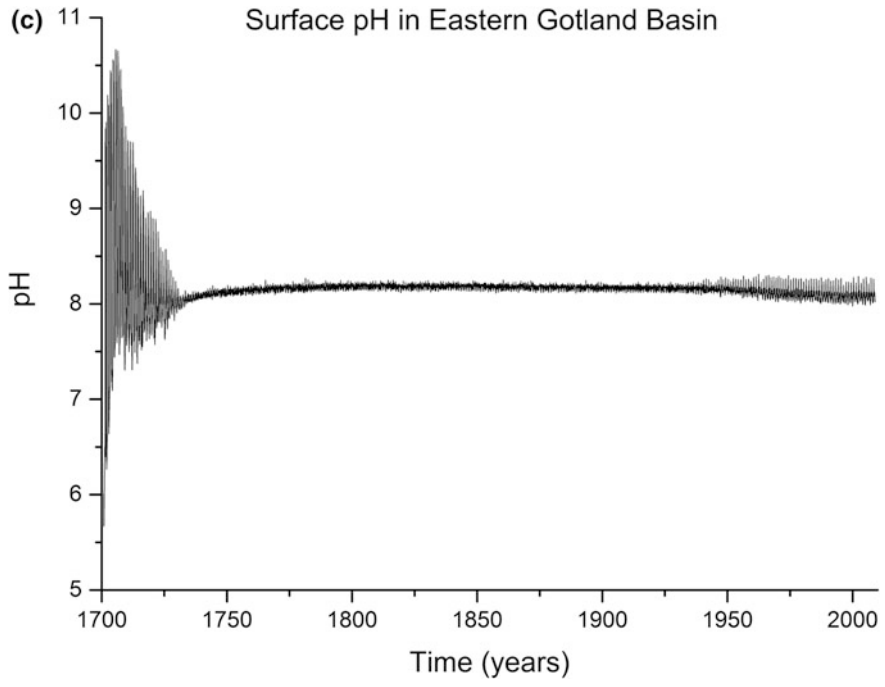

Fig. 6.23 (continued)

`\probe_baltic\Interpolering` directory after the start and stop dates are corrected in `to_surf_graph.for`.

The results are depicted in Fig. 6.23; note that total alkalinity (like salinity) has a typical spin-up time of several decades. The pH spin-up time seems faster, indicating a stronger atmospheric influence, but also displays much more variation during the spin-up phase. It can also be noted that the seasonal variations in pH increase after 1950, due to increased nutrient load to the Baltic Sea after the Second Word War. After about 50 years, the numerical solution is independent of the initial conditions and thus dependent only on boundary conditions.

Chapter 7
Summary and Conclusions

The intent of *Guide to Process-Based Modeling of Lakes and Coastal Seas* is to introduce its readers to the subject and provide them with a basic scientific understanding of and tools needed for aquatic studies. The book encourages the reader to solve geophysical problems using a systematic, process-based approach. This approach divides the studied water body into dynamically relevant parts or natural sub-basins and identifies the major processes involved in the water body. Based on field observations and simplifications, the dynamics of the water body are then expressed mathematically and tested carefully against relevant analytical solutions, extremes, and observations.

After an introduction to lake and coastal sea physics and biogeochemistry, the modeling started by addressing the Ekman ocean boundary layer. This gave the reader insight into numerical modeling and emphasized the importance of considering analytical solutions; we also learned how to test a solution for grid independence and time resolution. Section 3.4 considered the modeling of lakes. A simple slab model was developed for shallow lakes; for deep lakes we considered how to model the thermocline and for very deep lakes we considered the effects of pressure on the temperature of maximum density. We learned how to read meteorological data and calculate corresponding heat fluxes at the atmosphere–water interface. The first coastal sea model was then developed by adding the salinity equation to the lake model. Basin geometry and river runoff were then added to the model and the heat and salt conservation properties were investigated. The reader discovered that salt conservation was quite easily achieved; heat conservation, however, required that sea ice be included in the model. This was the topic of Sect. 3.6, which considered the modeling of sea ice with its new boundary conditions. The importance of turbulent modeling was studied in the Sect. 3.7. Various models, from zero-equation to two-equation models, were investigated. The reader learned the importance of employing good turbulent models and of considering deep water mixing. We then addressed how to include tides in the modeling by adding the horizontal pressure gradients modeled from tidal sea level variations.

The first biogeochemical application was to model the dynamics of oxygen, and the reader learned how to add one more equation to the physical equation system. Another equation for plankton growth and mineralization was added in Sect. 4.4. Oxygen concentration was related to plankton growth and mineralization, and the

A. Omstedt, *Guide to Process Based Modeling of Lakes and Coastal Seas*,
Springer Praxis Books, DOI 10.1007/978-3-319-17990-2_7

reader learned that understanding the dynamics of nutrients called for further equations. One nutrient equation, representing phosphate, was then added to the marine system and nutrient limitation was investigated. To learn more about the carbon system, we modeled the inorganic carbon dynamics in Sect. 4.6. The importance of introducing biological processes when modeling the CO_2 system was further investigated (Sect. 4.7) as was modeling the carbon system under anoxic conditions (Sect. 4.8).

The construction of nets of coupled sub-basins was then analyzed, and Sect. 5.1 addressed the modeling of two coupled basins. This exercise taught the reader to add an additional sub-basin to the system. The PROBE-Baltic marine modeling system was introduced, and its first application included only physical processes. Using this version, we were able to study several model aspects, such as turbulent mixing, dense bottom currents, heat and ice dynamics, water and heat budgets, and air–sea–land interactions. The second application, in Sect. 5.3, included oxygen concentrations as well, providing us with a tool for studying, for example, the interaction between inflow dynamics and oxygen reduction due to biological mineralization. In Sect. 5.4, the third PROBE-Baltic model application included physical–biogeochemical dynamics (in particular, the CO_2 system). This version allowed such aspects as the acid–base (pH) balance, biological production, and interaction with climate change to be studied. Comments on detection and attribution studies in coastal seas as well as future projections were then discussed in Sect. 5.5.

Various aspects of lakes and coastal seas were illustrated using a number of exercises, and their solutions were worked through in Chap. 6. The appendixes to the book touch on various matters, including a short introduction to FORTRAN, the nomenclature, data, and programs needed for the book, the *PROBE Manual*, and a discussion of how past aquatic conditions can be reconstructed.

With growing access to new observation platforms and data freely available on the Internet, it will become increasingly easy to analyze various water bodies, ranging from small lakes to coastal seas and ocean basins (e.g., Omstedt et al. 2014). Much can be learned using a process-based approach, and one of its strengths is that it focuses on process understanding rather than numerical methods. It is therefore my hope that this book will stimulate students and researchers to develop their modeling skills and make model codes and data transparently available to other research groups.

Appendix A
Introduction to FORTRAN

Introductions to the FORTRAN languages can be easily found on the Internet, for example, by searching for "FORTRAN77 for beginners" using Google. FORTRAN (FORmula TRANslation), introduced in 1956, was the first high-level language. It has since been revised several times. FORTRAN77 is widely used, and new versions such as Fortran 90 and Fortran 95 are also available.

The following program illustrates some FORTRAN77 commands. This program calculated the barotropic exchange through the entrance to the Baltic Sea by solving Eq. 2.12. Water exchange is driven by the sea level variations outside the entrance area and by freshwater inflow to the Baltic Sea. The sea level data file needed for this exercise is available in the supplementary material and is called `viken_sthlm_1980_2008d.dat`. The file needs to be rewritten according to the format used in the program below and renamed `zw.dat`.

```
C    PROGRAM: BAROTROP.FOR
C    NAME   : WATER BALANCE WITH BAROTROPIC EXCHANGE
C    BY     : ANDERS OMSTEDT
C    DATE   : 2009-12-14
C    COMMENTS:
C
C---DECLARATION
     IMPLICIT NONE
     REAL ASUR,QBAR,ZN,ZS,ZBA,ZVI,QF,CS,TSTEP,ZST,ZSTOBS,TIME
     INTEGER I,IYMD,IY,IM,ID
C
C---DEFINE FILES
     OPEN(21,FILE='D:\All files\
    1 zw.dat',FORM='FORMATTED',STATUS='OLD')
C
C---CONSTANTS
     ASUR=3.9E11
```


A. Omstedt, *Guide to Process Based Modeling of Lakes and Coastal Seas*,
Springer Praxis Books, DOI 10.1007/978-3-319-17990-2

```
      QF=16000.
      CS=0.3/10**5
      TSTEP=24.*3600.
C
C———INITIAL SEA LEVELS
      READ(21,*)IYMD,ZVI,ZSTOBS
      ZBA=ZSTOBS-12.503
      ZVI=ZVI-14.977
C
C———READ DATA NUMBERS OF DAYS AND CALCULATE
C     ZVI CALCULATED AROUND MEAN LEVEL
      DO I=1,365*18
         READ(21,*)IYMD,ZVI,ZSTOBS
         ZVI=ZVI-14.977
         ZS=ZVI
         ZN=ZBA
C————————SIGN POSITIVE WHEN INFLOW TO THE BALTIC
         QBAR=SIGN(SQRT(ABS(ZS-ZN)),(ZS-ZN))/CS
         ZBA=ZBA+TSTEP*(QBAR+QF)/ASUR
C
C———TIME
         IY=IYMD/10000
         IM=MOD(IYMD/100,100)
         ID=MOD(IYMD,100)
         TIME=I/(365.25)
C
C———WRITE ZST AROUND MEAN AND CORRECTED FOR LANDRISE
         ZST=ZSTOBS-12.503-0.00378*TIME
         WRITE(*,*)I,ZVI,ZBA,ZST,QBAR
         WRITE(11,*)I,TIME,ZVI,ZBA,ZST
      ENDDO
C
      END
```

The program starts with a header; the C at the beginning of the line indicates that this line is just for information. Then some variables are declared as real or integer numbers. After that, the program defines where the data are available (new users will need to check this), which, in the program, is given the unit number 21. Constants for the program are then given and the program reads the water level data to obtain the first initial value. After that, the main calculations are executed in a "do loop" and the data file is read for every day in the 18 years. Finally, the program writes the information we would like to analyze. The information is written in a free format both on the PC screen (*,*) and in unit 11, (11,*), the unit we use to plot the data.

In FORTRAN77, all statements must be contained in columns 7–72. Comment lines have a C in column 1 and continue lines are numbered in column 6. It is recommended that all variables be explicitly declared and that the statement

`IMPLICIT NONE` be put at the beginning of programs, functions, and subroutines. Otherwise, FORTRAN77 will treat all variables starting with a letter from I to N as integer numbers and the rest as real numbers. Arithmetic operators such as `+`, `−`, `*`, `/`, `**`, `sqrt`, `sin`, `cos`, `tan`, `asin`, `acos`, `atan`, `exp`, `log`, `min`, `max`, and `abs` return a result of the same type as that of the argument.

Typical control statements in FORTRAN are:

```
IF (CONDITION) THEN
STATEMENTS
ELSE
STATEMENTS
ENDIF

DO VAR=START, END
STATEMENTS
ENDDO
```

Functions and subroutines begin with subroutine `NAME(ARG1,ARG2,...)`. A subroutine ends with `RETURN` and `END`, which are called from another routine by `CALL NAME(ARG1,ARG2,...)`. A useful command is `INCLUDE 'd:\All files\compba.inc'`, where `compba.inc` given in the All Files directory contains a list of variables needed for communication between programs. The various exercises in the book will help the reader learn how to handle FORTRAN.

Appendix B
Nomenclature

Notation	Description	Unit
A	Area	m^2
A_i	Ice concentration	–
A_{sur}	Sea surface area	m^2
A_{sed}	Sediment area	m^2
A_T	Total alkalinity	mol kg^{-1}
α_1	Equation of state constant	$°C^{-2}$
α_2	Equation of state constant	–
α_{1s}	Sediment P leakage constant	mol kg^{-1} m^{-3}
α_{ip}	Ice strength coefficient	m^2 s kg^{-1}
B_T	Total boron	mol kg^{-1}
Br	Plankton respiration constant	–
b	Stanton number constant	
β_w	Extinction coefficient of short-wave radiation	–
β_{w1}	Extinction coefficient of short-wave radiation, pure water	–
C_{ice}	Ice strength constant	–
C_d^a	Air/sea drag coefficient	–
C_d^i	Ice/water drag coefficient	–
C_T	Total inorganic carbon	mol kg^{-1}
C_{decay}	Inertial wave drag coefficient	–
c_p	Specific heat of water	J kg^{-1} $°C^{-1}$
c_1	Constant	–
c_2	Constant	$°C^{-1}$
c_{bu}	Coefficient accounting for air bubbles in the water	–
c_g	Constant accounting for plankton growth	$°C^{-1}$
$C_{\varepsilon 1}$	Coefficient in dissipation equation	–
$C_{\varepsilon 2}$	Coefficient in dissipation equation	–
$C_{\varepsilon 3}$	Coefficient in dissipation equation	–
C_μ	Coefficient of the boundary condition for k	–

(continued)

A. Omstedt, *Guide to Process Based Modeling of Lakes and Coastal Seas*,
Springer Praxis Books, DOI 10.1007/978-3-319-17990-2

Notation	Description	Unit
c_p	Specific heat of seawater	J kg^{-1} K^{-1}
${}^{NH_4}C$	Ammonium	mol kg^{-1}
${}^{NO_3}C$	Nitrate	mol kg^{-1}
${}^{O_2}C$	Oxygen	mol kg^{-1}
${}^{PO_4}C$	Phosphate	mol kg^{-1}
${}^{pp1}C$	Spring/autumn algae concentration	mol kg^{-1}
${}^{pp2}C$	Blue-green algae concentration	mol kg^{-1}
d_1	Distance from boundary to near-boundary grid cell centre	m
D	Basin depth	m
E	Evaporation rate from water	m s^{-1}
Ek_h	Horizontal Ekman number	–
Ek_v	Vertical Ekman number	–
ε	Dissipation of turbulent kinetic energy	m^2 s^{-3}
f	Coriolis parameter	s^{-1}
f_*	Reciprocal Coriolis parameter	s^{-1}
f_{PO_4}	Phosphate release rate from sediments	mol m^{-2} s^{-1}
F_{loss}	Total heat loss from water to air	W m^{-2}
F_{CO_2}	Flux of CO_2	mol kg^{-1} m s^{-1}
F_e	Latent heat flux	W m^{-2}
F_h	Sensible heat flux	W m^{-2}
F_{ice}	Heat flux associated with ice advection	W m^{-2}
F_{net}	$F_h + F_e + F_{nl} + \eta F_s^w$	W m^{-2}
F_{nl}	Net long-wave radiation	W m^{-2}
F_s^w	Incoming short-wave radiation	W m^{-2}
F_{sb}	Short-wave radiation, bottom of ice surface	W m^{-2}
F_{st}	Short-wave radiation, top of ice surface	W m^{-2}
F_{salt}	Salt flux at the surface boundary	m s^{-1}
F_w	Heat flow at the ice-water interface	W m^{-2}
G_{max}	Temperature-dependent part of plankton growth	mol kg^{-1} s^{-1}
G_{pi}	Plankton growth of plankton group i	mol kg^{-1} s^{-1}
G_0	Plankton growth constant	mol kg^{-1} s^{-1}
g	Acceleration of gravity	m s^{-2}
H	Basin depth scale	m
h_i	Ice thickness	m
h_i^c	Columnar ice thickness	m
h_i^f	Frazil ice thickness	m
h_s	Snow thickness	m
I_{lim}	Light limitation for plankton growth	–
k	Turbulent kinetic energy	m^2 s^{-2}
k_i	Thermal conductivity of ice	W m^{-1} $°C^{-1}$

(continued)

Notation	Description	Unit
k_s	Thermal conductivity of snow	W m^{-1} °C^{-1}
k_w	Thermal conductivity of water	W m^{-1} °C^{-1}
$k_{n,1/2}$	Half-saturation value for nitrogen	–
$k_{p,1/2}$	Half-saturation value for phosphorus	–
k_{wCO_2}	CO_2 exchange velocity	m s^{-1}
κ	Coefficient of the boundary conditions for k and ε	–
L_e	Latent heat of evaporation	J kg^{-1}
L_i	Latent heat of ice	J kg^{-1}
L_{Ro}	Rossby radius of deformation	m
M_E	Ekman transport	m^2 s^{-1}
M_T	Total mineralization of organic matter	mol kg^{-1} s^{-1}
μ	Dynamic viscosity	kg m^{-1} s^{-1}
μ_{eff}	Effective dynamic turbulent viscosity	kg m^{-1} s^{-1}
μ_T	Turbulent dynamic turbulent viscosity	kg m^{-1} s^{-1}
N	Buoyancy frequency	s^{-1}
N_{denit}	Nitrogen sink due to denitrification	mol kg^{-1} s^{-1}
N_{limi}	Nutrient limitation, plankton group i	–
N_{nit}	Nitrification rate	mol kg^{-1} s^{-1}
η	Fraction of sun radiation absorbed in the surface	–
n_{frac}	Fractionation of nitrogen	–
ν	Kinematic viscosity	m^2 s^{-1}
ν_t	Kinematic turbulent viscosity	m^2 s^{-1}
V_T^d	Kinematic turbulent deepwater viscosity	m^2 s^{-1}
Ω	Frequency of Earth rotation	s^{-1}
P	Precipitation rate	m s^{-1}
P_i	Ice strength	N m^{-2}
P_a	Air pressure	N m^{-2}
P_w	Water pressure	N m^{-2}
P_{pi}	Plankton production of plankton group i	mol kg^{-1} s^{-1}
P_{sed}	Sediment release of phosphorus	mol kg^{-1} s^{-1}
P_b	Source-sink term due to buoyancy production/destruction	m^2 s^{-3}
P_s	Source term due to shear	m^2 s^{-3}
p_{frac}	Fractionation of phosphorus	–
p_{bind}	PO_4 sediment-binding rate constant	–
pCO_2^a	Partial pressure of CO_2 in air	atm
pCO_2^w	Partial pressure of CO_2 in water	atm
ϕ	Conservation property	
Q_f	River runoff	m^3 s^{-1}
Q_{in}	Inflow	m^3 s^{-1}
Q_{out}	Outflow	m^3 s^{-1}
R_i	Richardson number	–

(continued)

Notation	Description	Unit
R_o	Rossby number	–
R_{ot}	Temporal Rossby number	–
R_{pi}	Plankton respiration of plankton group i	mol kg^{-1} s^{-1}
ρ	Water density	kg m^{-3}
ρ_a	Air density	kg m^{-3}
ρ_0	Reference water density	kg m^{-3}
S	Water salinity	–
S_c	Schmidt number	–
S_{lim}	Salinity limitation in plankton growth	–
S_o	Ice-water interfacial salinity	–
S_{ref}	Reference salinity	–
S_{sur}	Surface water salinity	–
St_T	Stanton number for temperature	–
St_S	Stanton number for salinity	–
S_ϕ	Source term in conservation equation	
S_{CO_2}	Redfield ratio CO_2:P	–
S_N	Redfield ratio N:P	–
S_{O_2}	Redfield ratio O_2:P	–
S_P	Redfield ratio P:P	–
σ_L	Laminar Prandtl number	–
σ_{aC}	Turbulent Schmidt number for acid carbon	–
σ_{bC}	Turbulent Schmidt number for basic carbon	–
σ_{NH_4C}	Turbulent Schmidt number for ammonium	–
σ_{NO_3C}	Turbulent Schmidt number for nitrate	–
σ_{O_2C}	Turbulent Schmidt number for oxygen	–
σ_{PO_4C}	Turbulent Schmidt number for phosphate	–
σ_{ppC}	Turbulent Schmidt number for plankton	–
σ_ε	Turbulent Schmidt number for ε	–
σ_h	Turbulent Prandtl number for heat	–
σ_k	Turbulent Schmidt number for k	–
σ_s	Turbulent Schmidt number for salinity	–
T	Water temperature	°C
T_a	Air temperature	°C
T_f	Freezing temperature	°C
T_s	Surface temperature	°C
$T_{\rho m}$	Temperature of maximum density	°C
T_{lim}	Temperature limitation in plankton growth	–
t	Time	s
τ_1	Oxygen-dependent constant	s^{-1}
τ_2	Oxygen-dependent constant	s^{-1}
τ_x^a	Air stress in the x direction	kg m^{-1} s^{-2}

(continued)

Notation	Description	Unit
τ_x^b	Water/bottom stress in the *x* direction	kg m^{-1} s^{-2}
τ_x^i	Ice/water stress in the *x* direction	kg m^{-1} s^{-2}
τ_y^a	Air stress in the *y* direction	kg m^{-1} s^{-2}
τ_y^b	Water/bottom stress in the *y* direction	kg m^{-1} s^{-2}
τ_y^i	Ice/water stress in the *y* direction	kg m^{-1} s^{-2}
u_*	Friction velocity	m s^{-1}
U	Mean velocity in the *x* direction	m s^{-1}
U^a	Mean air velocity in the *x* direction	m s^{-1}
U_i, i = x, y, z	Velocity vector	m s^{-1}
U^i	Ice drift in the *x* direction	m s^{-1}
U_{free}^i	Free ice drift in the *x* direction	m s^{-1}
u_*	Friction velocity	m s^{-1}
V	Mean velocity in the *y* direction	m s^{-1}
V^a	Mean air velocity in the *y* direction	m s^{-1}
V^i	Ice drift in the *y* direction	m s^{-1}
U_i^{free}	Free ice drift in the *y* direction	m s^{-1}
V_0	Water volume	m^3
ΔV	Volume at depth *z*	m^3
ΔV_{in}	Volume associated with inflow	m^3
ΔV_{out}	Volume associated with outflow	m^3
v_{O_2}	Oxygen exchange velocity	m s^{-1}
W	Vertical velocity	m s^{-1}
W^i	Ice drift vector	m s^{-1}
w_{denit}	Denitrification rate	s^{-1}
w_{min}	Mineralization rate	mol kg^{-1} s^{-1}
w_{nit}	Nitrification rate	s^{-1}
w_p	Plankton sinking velocity	m s^{-1}
w_{psed}	Phosphate sediment release rate	mol kg^{-1} s^{-1}
W^a	$\text{Wind speed}\left(=\left[(U^a)^2+(V^a)^2\right]^{1/2}\right)$	m s^{-1}
x	Horizontal coordinate, positive in east direction	m
X_d	Size of sub-basin	m
X_f	Ice front position	
y	Horizontal coordinate, positive in north direction	m
Z_s	Secchi depth	m
z	Vertical coordinate, positive upward	m
z_o	Roughness length	m

Appendix C
Data and Programs Needed for the Exercises

The following learning aids can be downloaded from http://extras.springer.com. The supplementary material is designed to help the reader succeed at process-based modeling. Data and programs are organized in three directories:

1. Forcing fields, 1500–2008
2. Process oriented
3. Reconstructions

Within each directory, the following information is given:

1. Forcing fields 1500–2008

data	`All files` needed for long runs

2. Process oriented

ch2	Data
ch3	`All files`
	Exercise 3.1
	Exercise 3.2
	Exercise 3.3
	Exercise 3.4
	Exercise 3.5
	Exercise 3.6
ch4	`All files`
	Exercise 4.1
	Exercise 4.2
	Exercise 4.3
	Exercise 4.4
	Exercise 4.5
	Exercise 4.6
ch5	`All files`
	Exercise 5.1
	`probe_baltic`

A. Omstedt, *Guide to Process Based Modeling of Lakes and Coastal Seas*,
Springer Praxis Books, DOI 10.1007/978-3-319-17990-2

3. Reconstructions

   BALTEX Bridge water and heat cycles
   Baltic Sea model results 1958–2012
   Maximum ice extent in the Baltic Sea
   Mean salinity and temperature
   Net precipitation
   River runoff

To get under way, the user should copy the `process oriented` directory to her/his own computer under unit `D`. This is also the case for the `probe_baltic` programs in Chap. 5. If unit `D` is not available on the PC, all addresses in the program need to be changed (see the `INCLUDE` statements that can be found in all FORTRAN programs). In the directories, modeling is made ready by means of the Intel Visual Fortran compiler (http://software.intel.com/en-us/forums/intel-visual-fortran-compiler-for-windows/). If another compiler is used, the programs given in `All files` should be used. Advice on installing PROBE and how to use it is given in Appendix D.

The reader should consult the *PROBE Manual* (Appendix D) and then reproduce some of the figures from Chap. 3 to check that the compiler used has been given correct FORTRAN77 commands.

Appendix D
The PROBE Manual

PROBE

Program for Boundary Layers in the Environment
(system description and manual)
Updated version 2014

Urban Svensson,[1] *Lars Axell*,[2] *Jörgen Sahlberg*,[2] *and Anders Omstedt*[3]

D.1 Introduction

D.1.1 Purpose of the Manual

This manual is intended to provide users of the PROBE computer code with the necessary background information and assistance for successful use. The user is supposed to have some knowledge of the field of computational fluid dynamics (i.e., fluid dynamics, numerical analysis, and computer programming). However, the structure of PROBE allows users to develop their understanding of the code and computational fluid dynamics in a gradual manner. PROBE in conjunction with its manual are thus suitable as teaching aids.

After studying the manual and running a few applications from the exercises in this book it is believed that the user will be in a position to carry out new applications. The reader without prior experience of computational fluid dynamics should, however, be aware that numerical prediction of fluid flow phenomena rarely is simple or standard. This is a consequence of nonlinearities in the basic equations

[1]Computer-aided Fluid Engineering AB, Frankes väg 3, SE-371 65 Lyckeby, Sweden.
[2]SMHI, Folkborgsvägen 1, SE-601 76 Norrköping, Sweden.
[3]Department of Earth Sciences, University of Gothenburg, Box 460, SE-405 30 Göteborg, Sweden.

A. Omstedt, *Guide to Process Based Modeling of Lakes and Coastal Seas*,
Springer Praxis Books, DOI 10.1007/978-3-319-17990-2

and boundary conditions. Although the material in this book can assist the user in getting a good result, the intelligence and insight of the user are more important in most situations.

D.1.2 The General Features of PROBE

PROBE (Program for Boundary Layers in the Environment) can be classified as an "equation solver for one-dimensional transient or two-dimensional steady-state boundary layers." Typical examples of such boundary layers are the Ekman layer and channel flows as they develop. A major difficulty with these kinds of flows is to characterize turbulent mixing in mathematical terms. PROBE embodies a two-equation turbulence model (the $k-\varepsilon$ model), which calculates mixing coefficients. Together with two momentum equations the turbulence model forms the basis for the hydrodynamical part of the mathematical model. In the basic version six additional variables are allowed for: heat energy, salinity, and four concentrations. The number of concentrations can, of course, be easily increased as and when needed.

PROBE has been structured in such a way so as to facilitate easy and safe use. The user will only be concerned with one subroutine, called `CASE`; so, the rest of the program should not be modified in any way. Many applications will only require the insertion of about 15 FORTRAN statements in `CASE`. PROBE is written in standard FORTRAN 77 and requires very little memory. This makes the code suitable for both PCs and mainframe computers. All units are from the SI system.

D.1.3 What PROBE Can Do

As already mentioned, boundary layers are the class of flows considered. This may seem to be a rather narrowly restricted class of flows. However, the number of applications presently carried out reveal the opposite to be the case. For environmental flows and idealized flows, one-dimensional analysis can often provide good insight and understanding of a new problem. The very name PROBE indicates that one-dimensional analysis can be a preliminary sensor to more complex (three-dimensional) analysis. To give a foretaste of what PROBE can do, a few examples will be discussed briefly.

The entrainment experiment by Kantha, Phillips, and Azad (1977)
This laboratory experiment deals with the rate of deepening of an initially two-layered fluid suddenly exposed to shear on the surface—see Fig. D.1a. A racetrack-shaped flume ensures that the experiment is one-dimensional. Predicted and measured deepening is shown in the figure.

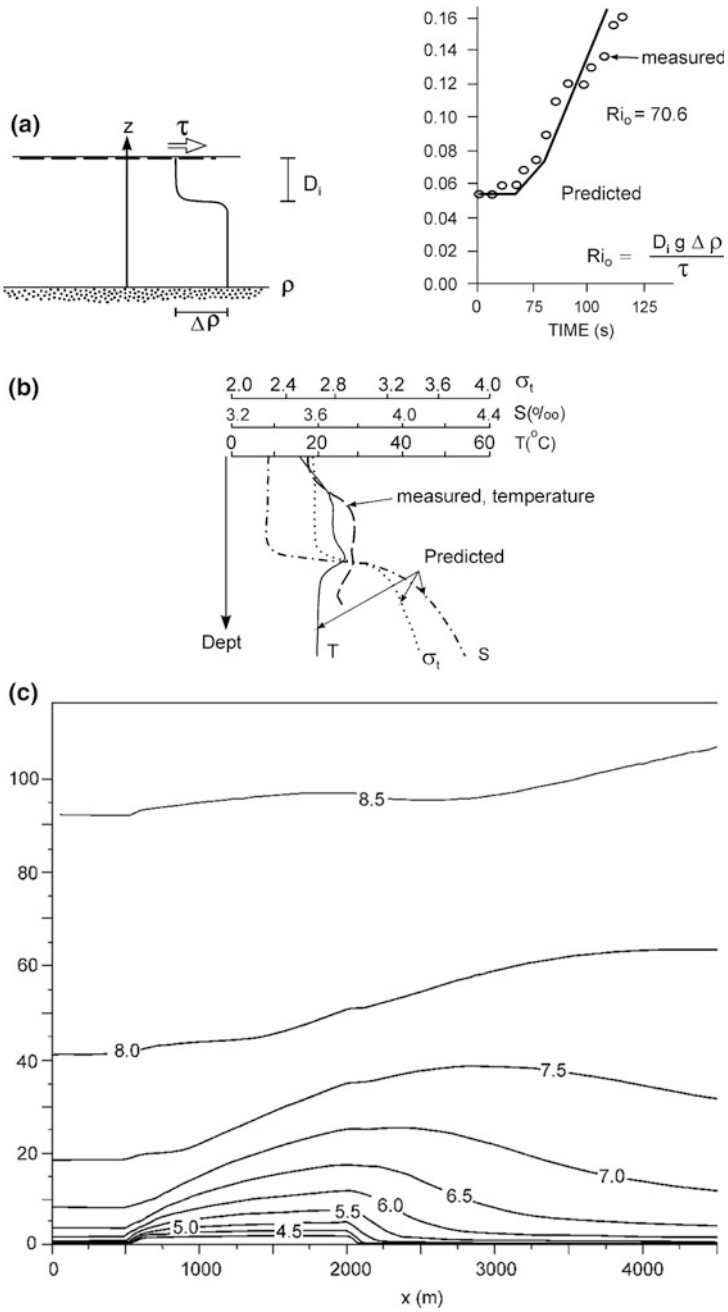

Fig. D.1 **a** The entrainment experiment. **b** Autumn cooling of the coastal sea. **c** The atmospheric boundary layer. The horizontal velocity distribution (m/s) of air flows from left to right across a flat island extending from x = 500 m to x = 2000 m

Autumn cooling of the ocean
The ocean's Ekman layer, stratified with respect to both temperature and salinity, has been analysed using PROBE (see Omstedt et al. 1983). Unexpected phenomena, like local temperature maxima, are found both in field measurements and predictions—see Fig. D.1b.

The adiabatic atmospheric boundary layer
An example of a two-dimensional steady-state situation is given in Fig. D.1c, where the flow of air over an island is shown (from Nordblom 1997).

Hopefully, these three examples will give the reader an impression of the kinds of flows that lend themselves to application by PROBE.

D.1.4 The History and Future of PROBE

The first version of PROBE, even though it had no name at the time, was presented by Svensson (1978). That version was designed for studies of the seasonal thermocline, but it was found that other applications could also be carried out. In fact, it was the range of possible applications that motivated the construction of the present more general version of PROBE.

The first version was released in 1984 and has now been successfully applied to a wide range of different problems. The 1986 version was developed to cover many important aspects: for example, a series of interacting runs can be performed, a moving free surface can be simulated, and more flexibility can be provided in terms of the number of equations, cells, etc. The 1997 version extended the capabilities of PROBE by including two-dimensional steady-state boundary layers into the class of flows that can be analyzed using PROBE. The present version, PROBE 2002, is still coded in FORTRAN 77 and includes, among other things, the latest developments in the field of turbulence modeling.

The direction of future developments is closely related to the kinds of applications that will predominate—there are several possibilities that spring to mind including

- *Dispersed and layered two-phase flows*. This is a difficult task to simulate and should only be undertaken if development work can be supported and motivated as part of a major project.
- *Rewriting the code using object-oriented techniques*. The present version does not employ modern concepts regarding code construction and coding itself. When PROBE is integrated with other code systems, it may prove necessary to rewrite the code.

D.1.5 Outline of the Manual

A brief description of the basic differential equation and its finite difference counterpart are given in Sect. D.2. Section D.3 outlines the general features of the code. Instructions on the use of PROBE are given in Sect. D.4. Advice on how to get the most out of PROBE can be found in Sect. D.5. In Sect. D.6 some concluding remarks are given. Details of the differential equations and finite difference equations employed in the manual are given in Sects. D.9, D.10, and D.11, respectively.

D.2 Brief Description of Basic Equations and Techniques

D.2.1 The General Differential Equation

All differential equations can be formally written as:

$$\underbrace{\frac{\partial \phi}{\partial t}}_{\text{Change in time}} + \underbrace{\frac{\partial}{\partial x_i} u_i \phi}_{\text{Advection}} = \underbrace{\frac{\partial}{\partial z}\left(\Gamma_\phi \frac{\partial \phi}{\partial z}\right)}_{\text{Diffusion}} + \underbrace{S_{\phi'}}_{\text{Source/sink}} \tag{D.1}$$

where ϕ is the dependent variable; t is time; z is a vertical coordinate; x is a horizontal coordinate; u is horizontal velocity; Γ_ϕ is the exchange coefficient; and S_ϕ are source and sink terms. For one-dimensional cases the advection term is not active and for two-dimensional steady-state cases the transient term is absent. The equation is formulated in the Cartesian coordinate system shown in Fig. D.2a. When ϕ, for example, is heat energy, the source term will contain terms describing the penetration of short-wave radiation, while for momentum the pressure gradient is a typical source term. Advection along the vertical space coordinate is included to account for vertical transport in a reservoir as a result of inflows and outflows.

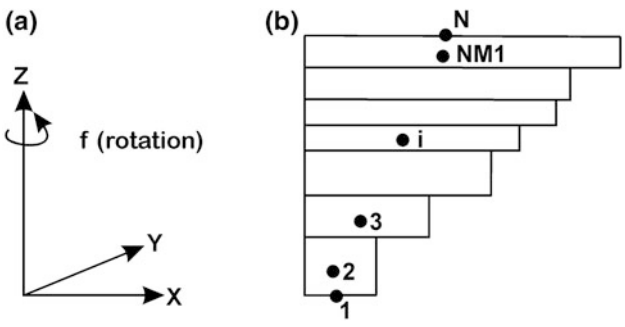

Fig. D.2 **a** Coordinate system. **b** Grid cell arrangement

However, despite not being fully developed for general application, the term is formally included in the source term. A complete discussion of all differential equations is given in Sect. D.8.

Boundary conditions may be specified in two ways: either the value or the flux of the variable in question is given. For example, if wind stress on a water surface is prescribed, it is the flux alternative that is chosen in this case.

D.2.2 Numerical Methods Employed

The general differential equation can be integrated over a specified volume—a grid cell—with the following result:

$$\phi_i(D_i + S_i') = \phi_{i+1}A_i + \phi_{i-1}B_i + S_i \tag{D.2}$$

where D_i, A_i, and B_i are coefficients; and S_i and S_i' are source terms. The grid arrangement is shown in Fig. D.2b. It is seen that variables are stored in N locations. As two of these are on the boundaries, it follows that the number of cells is $N - 2$. Equation (D.2) shows that the value of grid cell i, ϕ_i, is related to the values in the neighboring cells ϕ_{i+1} and ϕ_{i-1}. The strength of the connection is given by the coefficients A_i and B_i, which, on closer inspection, are found to represent transport effects. A detailed derivation of finite difference equations is given in Sects. D.9 and D.10.

D.3 Description of the Code

In this section PROBE's structure and how the different subroutines function will be explained. The reader is advised, while reading the following sections, to cross-refer of the list of PROBE commands given in the PROBE 2002 FORTRAN program available in the extra material, see Appendix C.

D.3.1 Flow Diagrams

A flow diagram is shown in Fig. D.3. As can be seen, the code is divided into two parts: the user section and the general section. In terms of FORTRAN lines the user subroutine `CASE` will only take up a few percent of the total code, amounting to about 1500 lines including all comment statements. The diagram shows four links between the general section and the user section. It should be noted that three of these are within the `DO` loop in `MAIN`, which is responsible for time advancement

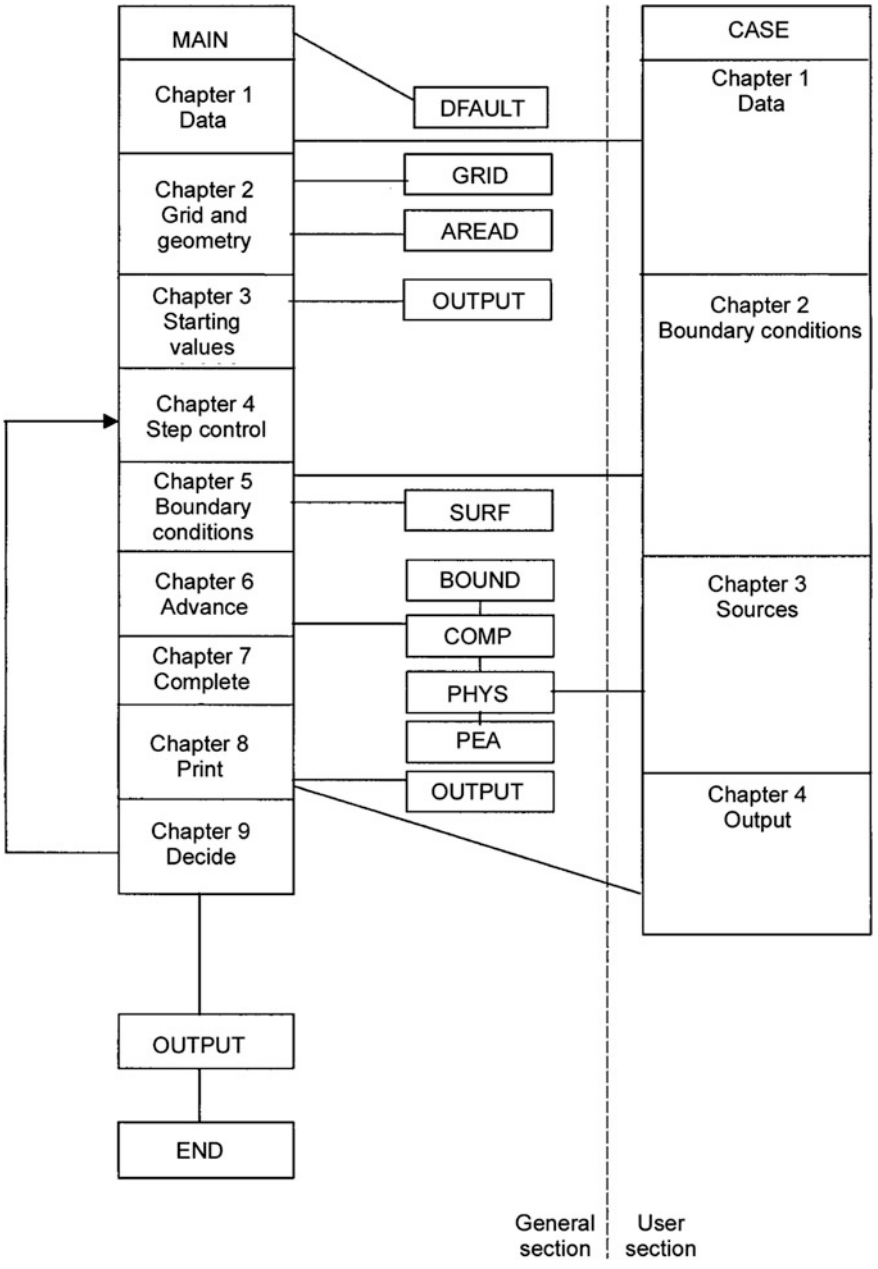

Fig. D.3 Flow diagram

(or space in a 2D steady-state calculation). This DO loop runs from chapters 4 to 9 of MAIN, as indicated. This arrangement makes it possible to interact with calculations in a simple way. An example of when this is needed is given by the boundary condition at the water surface for dissolved oxygen. If it is assumed that oxygen content has reached its saturation value, we have to prescribe this value as a function of temperature, which is a calculated variable. Continuous interaction is thus needed.

The flow diagram in Fig. D.4 shows the special arrangements that are made for linked runs (NPROBE>1). In this mode PROBE may be thought of as an empty shell, which can only be filled by the contents of common blocks. The subroutine STORE has the task of storing common blocks and is thus called when it is time to read/write a new common block.

D.3.2 General Section Subroutines

MAIN

To simplify the description of the main features of this subroutine, the special calls and loops for linked runs (NPROBE>1) have not been explained. However, the reader is referred to Fig. D.4 and Sect. D.5.1 for further details of use.

The subroutine that arranges and controls the calculation is called MAIN. In order to facilitate understanding, the different chapters in MAIN and their interaction with other subroutines are shown in the flow diagram. MAIN's chapter 1 provides input data initially set by DFAULT. Some of these data are modified by the user in subroutine CASE's chapter 1, which is the first subroutine called. The grid and the geometry are specified in DFAULT and CASE, and any necessary calculations using these data are done in the subroutines GRID and AREAD, which are called from chapter 2 of MAIN. MAIN's chapter 3 initializes dependent variables and other variables that are functions of dependent variables. The main DO loop starts in MAIN's chapter 4 at statement number 400. In this chapter of MAIN a new time step is calculated according to the information given in CASE. MAIN's chapter 5 specifies time-dependent boundary conditions. The CALL CASE(2) statement gives a link to CASE's chapter 2, where transient boundary conditions can be found. MAIN's chapter 6 is where the COMP subroutine is called—this is where solution of the equations is carried out. When leaving chapter 6 of MAIN, the calculation has thus advanced one time step. Then, in chapter 7 of MAIN, density, temperature, and eddy viscosity are updated. Tests are also made to ensure that turbulent kinetic energy k and its dissipation rate ε are positive. The reason for this is that negative values may be generated during the calculation because of strong buoyancy forces. A small positive value is then prescribed. Chapter 8 of MAIN is where subroutine OUTPUT

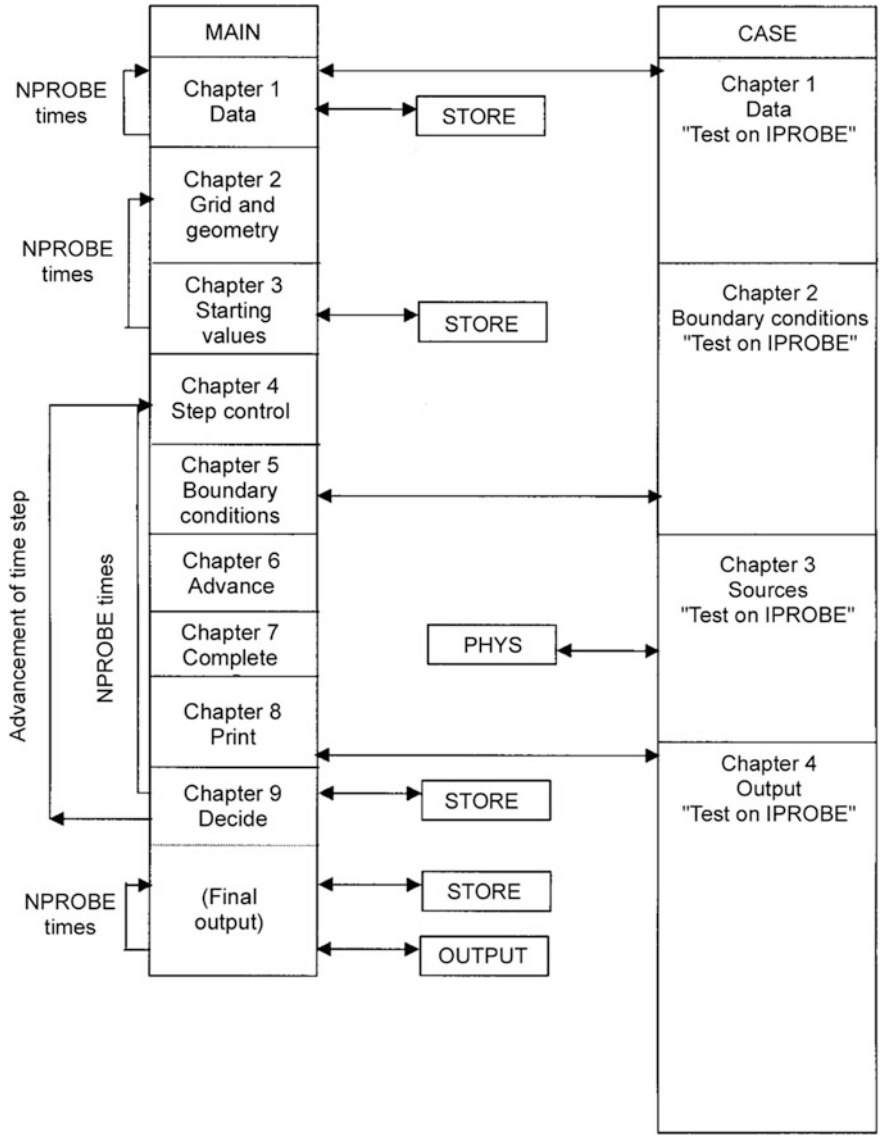

Fig. D.4 Flow diagram showing how linked runs (`NPROBE>1`) are performed

and CASE (4) are called—this is where user-specific output may be generated. In MAIN's chapter 9 tests are run to decide whether to continue or to terminate the calculation. If it is continued, a jump back to chapter 4 of MAIN is made.

DFAULT

This subroutine contains the default values of all data of concern to the user. A detailed discussion of this subroutine is given in Sect. D.4 of the manual.

GRID

The computational grid can be arranged in various ways (uniform, expanding, etc.) and necessitates calculation of grid cell sizes, distances, etc. This is done in GRID.

AREAD

The horizontal area of lakes and reservoirs varies with depth. Idealized area distributions can be generated from CASE and calculated in the subroutine AREAD.

OUTPUT

This subroutine, as the name indicates, is responsible for printout in various forms. Options, which are set in CASE, control the frequency of output in the form of integral parameters or profiles.

STORE

When linked runs (NPROBE>1) are performed, all information from a specific run is contained in common blocks. The subroutine STORE is used to store common blocks that are not presently active.

SURF

Necessary changes to the grid, when a moving surface is present, are done in this subroutine.

PHYS

As discussed in Sect. D.2, all equations may be presented in the general form:

$$\frac{\partial \phi}{\partial t} + \frac{\partial}{\partial x_i} u_i \phi = \frac{\partial}{\partial z}\left(\Gamma_\phi \frac{\partial \phi}{\partial z}\right) + S_{\phi'}$$

To identify a variable we have to specify the transport coefficient, Γ_ϕ, and the source term, S_ϕ. This is done in subroutine PHYS. In Chapter A in the subroutine program, eddy viscosity for grid nodes F(I,JEMU), Prandtl/Schmidt number PRSCNU (I), and effective viscosity EMU(I) for cell boundaries are calculated. Also, a reference transport coefficient DIFREF(I), which is the coefficient for momentum, is calculated. In Chapter B we can determine which variable is considered, and which transport coefficients and source terms are supplied in the relevant chapter. Two new subroutine calls have been added at the end of Chapters F and G, to include parameterizations of the effects of internal waves and Langmuir circulations on turbulence. By default, these new features are turned off.

COMP

In this subroutine forward steps are performed. COMP is the subroutine used for each dependent variable at each time or space step. In order to save computer time the F-array, which is the two-dimensional array where all variables are stored, is converted into a one-dimensional array. Necessary changes to indices are made in Chapter A. The results of subroutine PHYS are linked to COMP in Chapter B, which also includes the transport coefficients at the boundaries. The finite difference coefficients derived in Sect. D.10 are calculated in Chapter C, and the equation is then solved in Chapter D. Depending on the type of boundary condition the flux or the value of the variable at a boundary is then calculated in Chapter E.

BOUND

Transport coefficients close to the boundaries are calculated assuming logarithmic or linear profiles. When using these profile assumptions, information about the length of hydrodynamic roughness is needed. This information is given in CASE by specifying ROULLZ and ROULHZ. The transport laws for heat, salinity, and concentration include a Stanton number for the variable in question. These numbers are specified in CASE in the array STANTN.

PEA

This subroutine contains the code of the partial elimination algorithm (see Spalding 1976). The algorithm helps to make solutions for strongly coupled equations more stable. In the present context it is the Coriolis force that is responsible for the coupling.

D.3.3 User Section Subroutine

Only one subroutine, CASE, can be modified by the user. Going back to the flow diagram we see that CASE is divided into four chapters, each one having a specific purpose. Instructions on the use of CASE will be given in Sect. D.4.

From the flow diagram in Fig. D.4 we can see that the information given in CASE has to be selective for linked runs. This is done by a test ("an if statement") on IPROBE, which is the running index for linked runs.

D.4 How to Use PROBE

Let us now suppose that PROBE has been installed on the user's computer and some cases have been run for test purposes. The user is now ready to set up a new problem, and the best way of doing this is to follow the steps outlined in this section.

D.4.1 Analysis of the Problem Considered

The first question to address is whether the case considered is in the class of flows that PROBE can solve. If not, can a meaningful approximation be made? If PROBE is believed to be applicable, the next step is to characterize the problem in terms of equations and boundary conditions. It is further recommended that an analysis of length and time scales is carried out. This will be helpful when the grid size in space and time is selected. If something like a sine wave can be identified, we may, as a rule of thumb, need 10 grid cells or time steps to resolve it. This should always be followed up by making a more careful examination of grid size and time step independence.

To summarize, careful analysis of the problem backed up by expected behavior of the process that is well founded will significantly simplify the computational task.

D.4.2 Modification of Default Data

In this section the groups in DFAULT are explained and discussed. The values given in this subroutine are called the default values and are the values that will enter the calculation if they have not been reset in CASE. The user is recommended to make notes about the modifications in each group that are needed for the case to be set up. The modifications will later be a part of the content of CASE. It should be emphasized that DFAULT belongs to the general section and should never be subject to direct changes.

Group 0

```
C*****GROUP 0. TYPE OF FLOW
C      ITYPEF=INDEX FOR TYPE OF FLOW
C        =1 GIVES 1-D TRANSIENT FLOW (DEFAULT)
C        =2 GIVES 2-D PARABOLIC FLOW
       ITYPEF=1
```

The index `ITYPEF` is 1 for 1D transient flows and 2 for 2D parabolic steady-state flows.

Group 1

```
C*****GROUP 1. GRID IN SPACE AND TIME
C———N=NUMBER OF GRID CELLS PLUS 2. MAXIMUM=NIM.
      N=NIM
      TIME=0.
      TLAST=1.E15
      LSTEP=10
C———GRID DISTRIBUTION IN SPACE
C———IGRID=INDEX FOR GRID
C        =1 GIVES UNIFORM GRID
C        =2 GIVES EXPANDING GRID FROM LOW Z
C        =3 GIVES EXPANDING GRID FROM HIGH Z
C        =4 INDICATES THAT THE GRID IS SPECIFIED IN CASE
C———SEE MANUAL FOR DETAILS OF THE EXPANDING GRID
      IGRID=1
      CEXPG=1.1
      DO 11 IJK=1,NIM
      DZCELL(IJK)=0.
     11 CONTINUE
C———TIME STEP VARIATION
C      A VARIABLE TIME STEP IS SPECIFIED BY THE TFRAC FIELD
C      TFRAC/10.,1.,200.,2.,16*0./ GIVES A TIME STEP OF 1.0 S
C      THE FIRST 10 STEPS FOLLOWED BY 200 OF 2.0 S.
C      A CONSTANT TIME STEP IS OBTAINED BY SPECIFYING TFRAC(2)
C       IN CASE.
      DO 12 IJK=1,20
      TFRAC(IJK)=0.
     12 CONTINUE
      TFRAC(1)=1.E8
```

The maximum number of grid points that can be specified is `NIM`, which is a number that can be set by the user in a parameter statement (see Sect. D.5.5) and has a standard value of 100. The actual number of grid points is called `N`. This means (see Fig. D.2) that the standard number of grid cells is 98. A calculation can be terminated when one of two criteria occurs: if the maximum number of time

steps, LSTEP, is reached or if the integration time, TIME, has reached the maximum time, TLAST.

The expanding grid system is based on the geometrical series. The expansion factor, CEXPG, is the ratio between the height of the two neighboring cells. Guidance on how to choose CEXPG is given by the following formulas:

Size of first cell in expansion = ZDIM * (CEXPG − 1)/($\mathrm{CEXPG}^{N-2} - 1$

Size of last cell in expansion = CEPG^{N-3} * ZDIM * (CEPG − 1)/($\mathrm{CEXPG}^{N-2} - 1$

where ZDIM is the physical dimension in the Z-direction.

The index ITYPEF is 1 for 1D transient flows and 2 for 2D parabolic steady-state flows.

Group 2

```
C*****GROUP 2. PHYSICAL DIMENSIONS
      XDIM=1.E10
      YDIM=1.E10
      ZDIM=1.E10
C———————VERTICAL AREA DISTRIBUTION
C
C———————INDARE=INDEX FOR AREA-DISTRIBUTION
C——————— =1 INDICATES UNIFORM AREA
C——————— =2 INDICATES LINEAR DISTRIBUTION
C——————— =3 INDICATES NON-LINEAR DISTRB.,SEE MANUAL
C——————— =4 DISTR. SPECIFIED IN CASE
      INDARE=1
      AREAHZ=1.0
      CEXPA=2.
```

The physical dimensions of the computational domain are given by ZDIM, XDIM, and YDIM. ZDIM should always be reset in CASE, while XDIM and YDIM will only be modified for special cases like lakes and reservoirs.

Nonlinear area distribution is generated by:

$$\mathrm{AREA(I)} = (\mathrm{Z(I)}/\mathrm{Z(N)}) ** \mathrm{CEXPA} * \mathrm{AREAHZ}$$

CEXPA is the expansion factor and has typical values from −0.5 to 2.0. The default value 2.0 is typical for Swedish lakes. Linear distribution is obtained, if INDARE is set at 2. CEXPA will then automatically be set at 1.0, and the above expression will then generate the linear distribution.

Group 3

```
C*****GROUP 3. DEPENDENT VARIABLES
C     F(I,JRHOU)=X-DIRECTION MOMENTUM
C     F(I,JRHOV)=Y-DIRECTION MOMENTUM
C     F(I,JH)=HEAT-ENERGY
C     F(I,JS)=SALINITY
C     F(I,JK)=TURBULENT KINETIC ENERGY
C     F(I,JD)=DISSIPATION OF TURBULENT KINETIC ENERGY
C     F(I,JC1)=CONCENTRATION NO.1
C     F(I,JC2)=CONCENTRATION NO.2
C     F(I,JC3)=CONCENTRATION NO.3
C     F(I,JC4)=CONCENTRATION NO.4
C     F(I,10+(NJM-10))=ADDITIONAL VARIABLES ACTIVATED FOR
      NJM>10.
C     F(I,JEMU)=DYNAMICAL EDDY VISCOSITY
C     F(I,JTE)=TEMPERATURE
      JRHOU=1
      JRHOV=2
      JH=3
      JS=4
      JK=5
      JD=6
      JC1=7
      JC2=8
      JC3=9
      JC4=10
      DO 31 IJK=1,NJM
      SOLVAR(IJK)=.FALSE.
     31 CONTINUE
      JEMU=NJMP1
      JTE=NJMP2
```

PROBE solves as many as 30 dependent variables in the standard setup. If more dependent variables are needed, a parameter statement (see Sect. D.5.5) has to be reset. `NJM` (equal to 30 in the standard setup) defines the number of variables accounted for. Two more variables—dynamical eddy viscosity and temperature—are stored in the `F` array. It should be emphasized that when heat energy is the dependent variable, temperature is calculated from heat energy by dividing it by density and specific heat. Similarly, when momentum is the dependent variable, then velocity is calculated from momentum by dividing it by density. `SOLVAR` is the logical array that selects the variables to be solved. As can be seen, all its variables are set at `FALSE`, which means that `SOLVAR` always needs to be reset in the `CASE` file.

Group 4

```
C*****GROUP 4. PROPERTIES
      CPHEAT=4190.
      RHOREF=1000.
      EMULAM=0.0013
      DO 41 IJK=1,NJM
      PRL(IJK)=1.
     41 CONTINUE
      PRL(3)=9.5
      PRL(4)=1000.
      AGRAV=9.81
```

Specific heat (CPHEAT), reference density (RHOREF), and dynamical laminar viscosity (EMULAM), all have default values that are suited for freshwater at 10 °C. Modifications are thus needed when air or seawater is considered or if some other average water temperature is needed. The laminar Prandtl/Schmidt number (PRL) is the array that covers NJM-dependent variables. Once again alterations may be needed when default values are not suitable. The acceleration due to gravity (AGRAV) may, however, be treated as a constant.

Group 5

```
C——GROUP 5. EQUATION OF STATE
C——IEQSTATE=INDEX FOR EQUATION OF STATE
C     =1 GIVES SIMPLIFIED FORMULA:
C      RHO=RHOREF*(1.-C1RHO*(T-TREF)**2+C2RHO*S
C      +C3RHO*JC1+C4RHO*JC2+C5RHO*JC3+C6RHO*JC4)
C     =2 GIVES UNESCO'S FORMULA (GILL, 1982)
C      WITHOUT PRESSURE EFFECTS
C————————————————————————————————————————————
    IEQSTATE=1
    C1RHO=7.18E-6
    C2RHO=8.E-4
    TREF=3.98
    C3RHO=0.
    C4RHO=0.
    C5RHO=0.
    C6RHO=0.
```

The default value is IEQSTATE=1, which means that the equation of state employed is based on quadratic dependence on temperature and linear dependence on salinity and concentrations. It should be mentioned that all variables used in the equation of state will influence turbulence intensity, since the production/destruction terms due to buoyancy are sensitive to density gradients. If the influence of temperature needs to be linear, it is recommended that one of the concentration equations is used for heat energy.

For NJM > 10, variables with indices greater than 10 are assumed not to influence density. If buoyancy effects are required, variables should be chosen from the first four concentration equations.

If IEQSTATE=2 is chosen, density and its gradients regarding the vertical coordinate, temperature, and salinity are all calculated according to the UNESCO formula (Gill 1982, p. 599). However, the pressure effects on density are neglected.

Group 6

```
C———GROUP 6. TURBULENCE MODEL
C———ITURBM: INDEX FOR TURBULENCE MODEL
C     =1 GIVES CONSTANT VALUE (=EMUCON)
C     =2 GIVES ONE-EQUATION K MODEL
C     =3 GIVES TWO-EQUATION K-EPSILON MODEL
C     =4 INDICATES THAT F(I,JEMU) IS SPECIFIED IN CASE
C———IPRSC: INDEX FOR TURBULENT PRANDTL/SCHMIDT NUMBER.
C     USED FOR HEAT, SALINITY, AND CONCENTRATIONS.
C     =1 CONSTANT PRANDTL NUMBERS ARE USED (GIVEN BELOW)
C     =2 BUOYANCY-DEPENDENT PRANDTL NUMBERS (LAUNDER, 1975).
C      NOTE:SHOULD ONLY BE USED WITH ITURBM EQUAL TO 2 OR 3
C     =3 BUOYANCY-DEPENDENT PRANDTL NUMBERS
C      (AXELL & LIUNGMAN, 2001).
C      NOTE:SHOULD ONLY BE USED WITH ITURBM EQUAL TO 2 OR 3
C     =4 FULL STABILITY FUNCTIONS (AXELL & LIUNGMAN, 2001).
C      NOTE:SHOULD ONLY BE USED WITH ITURBM EQUAL TO 2 OR 3
C———IIWE: INDEX FOR INTERNAL WAVE ENERGY (IWE) MODEL
C     =0 NO IWE
C     =1 CONSTANT ENERGY FLUX TO IWE FIELD (AXELL, 2002)
C     =2 WIND-DEPENDENT ENERGY FLUX TO IWE FIELD (AXELL, 2002)
C———ILC INDEX FOR LANGMUIR CIRCULATION (LC) MODEL
C     =0 NO LC
C     =1 LC ACCORDING TO AXELL (2002)
C———————————————————————————————————————————————
    ITURBM=3
    IPRSC=2
    IIWE=0
    ILC=0
    EMUCON=0.
    DO 61 IJK=1,NJM
    PRT(IJK)=1.
   61 CONTINUE
    PRT(5)=1.0
    PRT(6)=1.08
C———CONSTANTS IN TURBULENCE MODEL. SHOULD NOT BE CHANGED.
    CMU0=0.5562
    CMU03=CMU0**3
    CMU04=CMU0**4
```

```
DO I=1,NIM
 CMU(I)=CMU04
ENDDO
C1=1.44
C2=1.92
DO I=1,NIM
 CEPS3(I)=0.0     ! INITIALIZE CEPS3(I)
 CB(I)=0.35       ! INITIALIZE CB(I)
ENDDO
```

ITURBM allows some different turbulence models to be selected. If the flow considered is laminar, we should set SOLVAR for k and ε at FALSE; the specified laminar exchange coefficients will then be responsible for diffusion.

When ITURBM=1 constant eddy diffusivity is used and takes its value from EMUCON. When ITURBM=2 the simple one-equation k model of Axell and Liungman (2001) is used as it can handle convection, neutral flows, and stably stratified flows. When ITURBM=3 the more complex two-equation $k-\varepsilon$ model is used as it too can handle convection, neutral flows, and stably stratified flows. For a comparison between the k model and the $k-\varepsilon$ model see Axell and Liungman (2001). Finally, when ITURBM=4 turbulence needs to be specified in the CASE file.

Several alternatives are given for turbulent Prandtl/Schmidt numbers. If IPRSC is set at 1, constant Prandtl/Schmidt numbers are used as specified by the vector PRT. If IPRSC is set at 2 or 3, the numbers will depend on stratification according to Launder (1975) or Axell and Liungman (2001), respectively. Finally, if IPRSC is set at 4, the full stability functions of Axell and Liungman (2001) are employed. For reasons of backward compatibility, IPRSC=2 by default. Further details about the physical basis and mathematical formulation are given in Sect. D.10. Note that constants in the turbulence model should not be changed by the user.

This version of PROBE already includes an internal wave model that can be accessed by setting IIWE=1 or 2. The first choice gives a constant energy flux to the pool of internal wave energy, whereas the second choice gives a wind-dependent energy flux. These two options may be tried to prevent layers outside the surface mixed layer from becoming stagnant (see Axell 2002 for details). The model has only been tested in ocean and lake applications, but should work with IIWE=1 for the atmosphere as well. However, energy flux may have to be tuned for this case. The default setting is IIWE=0, which turns off the internal wave module.

Another new feature is the possibility to include simple parameterization of Langmuir circulations in the ocean mixed layer. This option (ILC=1) may be used in order to increase near surface mixing in ocean and lake models (see Axell 2002 for more details). By default, ILC=0, which turns off the Langmuir circulation module.

Group 7

```
C*****GROUP 7. SOURCE TERMS
C
C------CORIOLIS PARAMETER
     CORI=1.E-4
C------PRESSURE GRADIENTS
C    INDPX=INDEX FOR PRESSURE GRADIENTS IN X-DIRECTION
C     =1 GIVES PRESCRIBED CONSTANT PRESSURE
C      GRADIENTS,DPDXP.
C     =2 GIVES PRESCRIBED MASS FLOW,RHOUP. ONLY
C      RELEVANT FOR STEADY STATE PROBLEMS.
C     =3 GIVES PRESSURE GRADIENT DEVELOPMENT ACCORDING TO
C      HORIZONTAL EXTENT OF WATER BODY. ONLY RELEVANT TO
C      LAKES AND RESERVOIRS.
C     =4 INDICATES THAT THE PRESSURE GRADIENTS ARE TO BE
C      READ FROM SEPARATE FILE AS A TIME SERIES.
C     =-1,-2,-3 OR -4 AS ABOVE,BUT WITH BUOYANCY DAMPING
C      OF PRESSURE GRADIENTS(EFFECT OF TILTED THERMOCLINE).
C    INDPY=SAME FOR Y-DIRECTION
     RHOUP=0.
     RHOVP=0.
     DPDXP=0.
     DPDYP=0.
     PFILT=1.
     INDPX=1
     INDPY=1
C------IN- AND OUTFLOWS.
C------SEE MANUAL FOR INSTRUCTIONS ON USE
     DO 71 IJK=1,NIM
     QZ(IJK)=0.
     QINFL(IJK)=0.
     QOUTFL(IJK)=0.
     DO 72 IKJ=1,NJM
     PHIIN(IJK,IKJ)=0.
    72 CONTINUE
    71 CONTINUE
C------SHORT-WAVE RADIATION
C     ASSUMED TO PENETRATE THE WATER BODY.
C     FLXRAD=SHORT-WAVE RADIATION.
C     RADFRA=FRACTION ASSUMED TO BE A BOUNDARY FLUX
C     BETA=EXTINCTION COEFFICIENT
      FLXRAD=0.0
      RADFRA=0.5
      BETA=0.1
```

The technique used to calculate pressure gradients is detailed in Sect. D.8. When the option `INDPX` (or `INDPY`) = 2 is used, we may get a solution that never reaches a steady state. The user must then reduce the time step and the factor `PFILT`, which produces an under relaxation of the development of the pressure gradients.

Unfortunately a trial-and-error procedure must be carried out to find the optimum values for the time step and PFILT. When INDPX (or INDPY) =3, or −3, a non-unity PFILT has another implication. The pressure gradient formula for lakes and reservoirs simulates seiches with periods based on the dimensions of the water body. Often the period is of the order of minutes, which requires a time step of the order of 10 s (one-tenth of the seiche period). If PFILT is set at 0.2, for example, the seiche period will be fivefold longer, and a more economical time step may have to be used. It should be noted that the main effects of pressure gradients will still be present. Test calculations should be performed to establish whether this filtering of pressure significantly affects the overall behavior of seasonal stratification, for example.

Volume flux and the properties of inflows and outflows can be specified from CASE. Volume fluxes are specified in QINFL(I) and QOUTFL(I) for inflows and outflows, respectively. These flows generate volume flux that is vertical and that can be calculated by applying the continuity equation cell by cell. Properties only need to be specified for inflows and are given in PHIIN (I, J). If QINFL ≠ QOUTFL, when integrated over the depth, the moving surface option needs to be activated (see Group 13).

Incoming short-wave radiation varies during the day and should therefore be specified in chapter 2 of CASE. Examples of how this is done can be found in the CASE reports on thermocline development.

Group 8

```
C*****GROUP 8. INITIAL DATA
      DO 81 IJK=1,NIM
      DPDX(IJK)=0.
      DPDY(IJK)=0.
      FW(IJK)=0.
      DO 82 IKJ=1,NJMP2
      F(IJK,IKJ)=0.
     82 CONTINUE
     81 CONTINUE
C-----INITIALISE DEPENDENT VARIABLES
C     ISTPR=INDEX FOR STARTING PROFILES
C      =1 PROFILES ARE SPECIFIED WITH VST1(1-NJM)-ZST2(1-NJM)
C       SEE MANUAL.
C      =2 PROFILES ARE SPECIFIED IN CASE WITHOUT THE USE
C       OF VST1(1-NJM)-ZST2(1-NJM).
C-----NOTE: DEFAULT VALUE FOR ALL VARIABLES IS 0.0.
      ISTPR=1
      DO 83 IJK=1,NJM
      VST1(IJK)=0.
      VST2(IJK)=0.
      ZST1(IJK)=0.
      ZST2(IJK)=0.
     83 CONTINUE
```

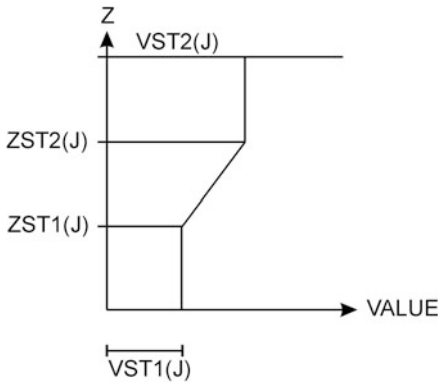

Fig. D.5 Specification of the intial pro-files of dependent variables

All variables in the F array are here given the default value 0.0. Two alternatives are available for the specification of non-zero initial profiles. If ISTPR=1, the profiles are specified according to Fig. D.5, while ISTPR=2 indicates that the profiles are specified directly in the F array.

Only dependent variables (such as momentum, heat, salt, or nutrient concentrations) should be initialized; density, temperature, eddy viscosity, etc. are calculated as functions of the dependent variables in the MAIN subroutine. In this context it is important to remember that momentum and heat energy are the dependent variables—not velocity and temperature.

Group 9

```
C*****GROUP 9. BOUNDARY CONDITIONS
C
C———————ITYPEH=INDEX FOR TYPE OF BOUNDARY AT HIGH Z
C       =1 GIVES SOLID WALL(STATIONARY OR MOVING)
C       =2 GIVES SYMMETRY LINE
C       =3 GIVES SOLID WALL BUT NO-FLUX CONDITION ON K, AND
C        EPSILON=CMU0**3*K**1.5/CAPPA/DZ
         (BURCHARD ET AL., 1998).
C       =4 GIVES SOLID WALL BUT NO-FLUX CONDITIONS ON K AND EPS.
C      ITYPEL=SAME FOR LOW Z BOUNDARY
C
C———————IKBHZ(J)=INDEX FOR KIND OF BOUNDARY CONDITION FOR
C      VARIABLE J AT HIGH Z BOUNDARY
C       =1 GIVES PRESCRIBED VALUE
C       =2 GIVES PRESCRIBED FLUX
C      IKBLZ(J)=SAME FOR LOW Z BOUNDARY
C———————ITRHZ(J)=INDEX FOR TIME DEPENDENCE OF BOUNDARY FOR
C      VARIABLE J
C       =1 GIVES STATIONARY CONDITIONS
C       =2 GIVES TRANSIENT CONDITIONS SPECIFIED FROM CASE-
C        SUBROUTINE.SEE MANUAL FOR INSTRUCTIONS ON USE.
C       =3 GIVES TRANSIENT CONDITIONS READ FROM FILE
C      ITRLZ(J)=SAME FOR LOW Z BOUNDARY
```

```
C------IKBOT(J)=INDEX FOR KIND OF BEHAVIOR AT BOTTOM FOR
        VARIABLE J
C      ONLY RELEVANT FOR CASES WITH VERTICAL AREA-DISTRIB.
C       =1 GIVES "CONSERVATIVE" CONDITION.SEE MANUAL.
C       =2 GIVES "NON-CONSERVATIVE" CONDITION.SEE MANUAL.
C------SPECIFICATION FOR STATIONARY BOUNDARY CONDITIONS
C
C------SPECIFICATION FOR TRANSIENT CONDITIONS(ITRHZ OR
        ITRLZ=2).SEE MANUAL
C
C------SPECIFICATION OF WALL-FKN PARAMETERS.
C     ITYPEH=1
      ITYPEL=1
      DO 91 IJK=1,NJM
      IKBHZ(IJK)=2
      IKBLZ(IJK)=2
      ITRHZ(IJK)=1
      ITRLZ(IJK)=1
      IKBOT(IJK)=1
      FLUXHZ(IJK)=0.
      FLUXLZ(IJK)=0.
      V1HZ(IJK)=0.
      V2HZ(IJK)=0.
      V3HZ(IJK)=0.
      V4HZ(IJK)=0.
      V5HZ(IJK)=0.
      V1LZ(IJK)=0.
      V2LZ(IJK)=0.
      V3LZ(IJK)=0.
      V4LZ(IJK)=0.
      V5LZ(IJK)=0.
      STANTN(IJK)=1.E-3
     91 CONTINUE
      IKBOT(1)=2
      IKBOT(2)=2
      IKBOT(5)=2
      IKBOT(6)=2
      STANTN(1)=1.
      STANTN(2)=1.
      STANTN(3)=0.05
      STANTN(5)=1.
      STANTN(6)=1.
      CAPPA=0.4
      C3B=9.
      ROULHZ=0.
      ROULLZ=0.
```

If ITYPEH is set at 1, a wall is assumed to be present at the high Z boundary. This will activate the wall functions in subroutine BOUND. Symmetry line conditions (ITYPEH=2) can be used when a zero-flux condition prevails at the boundary in question. The same applies for ITYPEL at the lower boundary. If the internal wave model is employed (IIWE=1 or 2), it is recommended to set ITYPEL=3 or 4 in order to prevent laminar conditions in the lowest grid cell. The default settings are ITYPEL=ITYPEH=1.

Transient boundary conditions can be specified for all dependent variables according to the following instructions (see Fig. D.6).

The user must, of course, have made a decision about whether the boundary condition should be specified as a value or a flux when the above values are given. Alternatively, the user may specify transient boundary conditions in chapter 2 of CASE.

When a variable horizontal area is specified, the index IKBOT has to be considered. If IKBOT is set at 1, a conservative condition is assumed, which means zero flux through the bottom area for all cells (see Fig. D.7). This may be suitable for heat and salinity, when momentum in bottom contact is lost; this indicates that IKBOT should be set at 2 for momentum equations. Section D.9 explains this point further.

Wall functions require information about the roughness of surfaces. This is specified in ROULHZ and ROULLZ, which are the roughness lengths z at high and low Z. A zero value indicates that the surface is hydrodynamically smooth. Heat, salinity, and concentrations at the wall are assumed to obey the following transport law:

$$\texttt{FLUX}(\phi) = \texttt{STANTIN}(\phi) U_* \Delta\phi$$

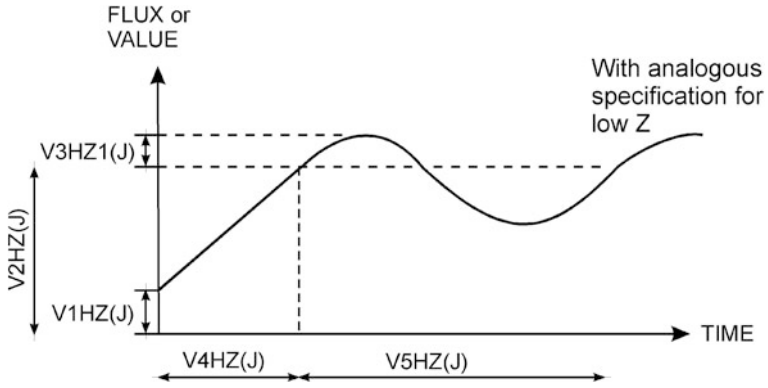

Fig. D.6 Specification of transient boundary conditions

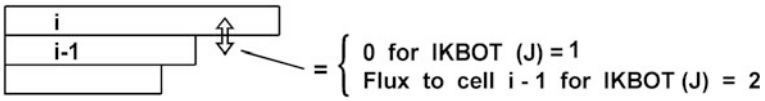

Fig. D.7 Meaning of IKBOT

where STANTN(ϕ) is the Stanton number for variable ϕ; $\Delta\phi$ is the difference in ϕ between the boundary and the first cell; and U_* is friction velocity.

Group 10

```
C*****GROUP 10. LIMITS AND NUMBERS
      EMTMIN=1.E-6
      FKMIN=1.E-15
      FDMIN=1.E-15
      TAUMIN=1.E-3
      KINDAV=1
```

These numbers are the minimum values that ensure the variables considered never become negative. Normally, they should not be changed.

Group 11

```
C*****GROUP 11. PRINT OUT
C------PRINT CONTROL
C     -SET ITPLOT=2 FOR CROSS-STREAM PLOT, =1 FOR NO PLOT
      ITPLOT=1
C     -SET NSTAT,NPROF,NPLOT TO NUMBER OF STEPS BETWEEN OUTPUT
C     OF STATION VALUES,PROFILES AND CROSS-STREAM PLOTS
      RESPECTIVELY
     NSTAT=10
     NPROF=50
     NPLOT=100
C     -SET INIOUT .FALSE. FOR NO INITIAL OUTPUT
      INIOUT=.TRUE.
C
C------SELECT PROFILES TO BE PRINTED AND PLOTTED.
C------U,V,T,S,1C,2C,3C,4C,K,E,EMU,SIGM,DPDX,DPDY,W,PRSCN,
       RIF,N,UW,VW
C      1,2,3,4,5,6,7,8,9,10,11,12,13,14,15,16,17,18,19,20
C------PRINTED
C------PLOTTED
      DO 111 IJK=1,20
      PRPROF(IJK)=.FALSE.
      PLPROF(IJK)=.FALSE.
     111 CONTINUE
C
C------PARTICLE TRACKING.SEE MANUAL.
C------INDPT=INDEX FOR PARTICLE TRACKING
C       =0 GIVES NO TRACKING
C       =1-4 ONE TO FOUR PARTICLES ARE TRACKED
C
       INDPT=0
       ILEVEL(1)=0
       ILEVEL(2)=0
       ILEVEL(3)=0
       ILEVEL(4)=0
       IPSAVE=1000
```

PRPROF is a logical array that selects variables for the printing of profiles. The particle-tracking routine is activated by setting INDPT at 1–4, when one to four particles are to be tracked. ILEVEL, which is an array dimensioned to four, also needs to be considered. If, for example, ILEVEL(2)=30, particle number 2 will be on level Z(30). IPSAVE specifies an interval in which coordinates are to be saved. If IPSAVE=10, then coordinates will be stored every tenth time step. The maximum number of steps that can be stored is 500. Examples on how to use the particle- tracking routine can be found in CASE reports.

Group 12

```
C*****GROUP 12.LINKED RUNS.
      DO 121 IJK=1,NPM
      NSTPDT(IJK)=1
     121 CONTINUE
      NPROBE=1
```

For linked runs, NPROBE is the number of runs to be made. NSTPDT(J) provides a means of having different time steps in different runs. One run should have NSTPDT=1, which indicates that this run should have the specified time step, DT. If another run has, for example, NSTPDT(5)=4, it gives a time step of DT/4 for run number 5. Note that it is not recommended to specify different time steps in different runs directly by TFRAC(2), due to pre-arranged interactions between runs and the formulation of output sequences.

Group 13

```
C*****GROUP 13. MOVING FREE SURFACE.
      MOVE=.FALSE.
      ZSSTRT=0.
      PREEVA=0.
```

MOVE is a logical command that is set to true if a moving free surface is present. PREEVA represents precipitation and evaporation and is given in meters per second; it is positive along the vertical space coordinate. Rain on a lake surface is thus specified in meters per second and has a negative value. ZSSTRT means "*Z*-surface start" and gives the initial water surface level. This value needs to be smaller than ZDIM, which is the maximum surface level that is to be considered.

D.4.3 The CASE Subroutine

All modifications of default values are held in chapter 1 of CASE. Chapter 2 of CASE provides a link to the MAIN subroutine. The link is intended for the supply of transient boundary conditions, which cannot be handled by prepared functions. An

example is meteorological data obtained from field measurements, which in this chapter of CASE should be read from a separate file and included as transient boundary conditions. Additional source terms should be supplied in chapter 3 of CASE, which provides a link to the PHYS subroutine. A call is made from every dependent variable, and the user has to select the appropriate variable to be supplied with extra source terms. The following example shows a typical coding sequence:

```
      IF (J.NE.JC1) RETURN
      DO 10 I=2,NM1
      FJCIN=F(I+1,JC1)*WSED
      FJCIS=F(I,JC1)*WSED
      IF(I.EQ.2) FJCIS=0.0
      IF(I.EQ.NM1) FJCIN=0.0
 10   SI(I)=SI(I)-(FJCIN-FJCIS)/DZCELL(I)
      RETURN
```

A source term for variable C1, which describes sedimentation at a settling velocity specified by WSED, is thus added. Further examples can be found in CASE reports.

Additional output can be generated from chapter 4 of CASE. The call to this chapter once again comes from MAIN, but this time from the position where standard output is called for. This ensures that generated output is at the same integration time as standard output. Extra output may be useful; for example, when the dependent variables are requested in non-dimensional form. For linked runs we need, as mentioned earlier, to select the correct run (test on IPROBE) when providing information in the CASE subroutine.

D.4.4 Test Calculation

It is advisable to use LSTEP=10 so that preliminary checking and test calculations can be made. Assuming that compilation errors have been eliminated and that numbers are produced, the user should proceed by means of the following steps:

- Check the section PRINCIPAL DATA USED. Is everything as expected?
- Check grid and initial profiles in the profile output called INITIAL PROFILES.
- Is the output generated after 10 steps according to expectations?

If no objections have been raised to the results produced, it is time to proceed with a longer run. However, if the output shows unrealistic or unexpected behavior, we have to go through the process of analyzing and coding once again.

D.5 Advice on Effective Use

D.5.1 Grid Independence in Space and Time

A coarse grid (i.e., few cells and large time steps) needs less computer time and should be used during the preliminary stages of calculations. However, only a grid-independent solution, in space and time, represents the true implication of differential equations. Systematic refinement of the grid must always therefore be carried out, if a claim regarding solution of differential equations is to be made. It is thus recommended that a coarse grid, which typically could be 15 grid cells in both directions, be used in the preliminary stage and a grid refinement study be carried out before final calculations are performed.

D.5.2 Use of Integral Checks

Integral checks for heat and salinity are supplied by PROBE. These should always be studied, as they may indicate errors in boundary conditions or in the stability of the numerical solution. Note that the available integral checks are not valid if extra source or sink terms are added to the equations for heat and salinity.

When concentration equations need to be solved, the user is advised to make estimates of integral balances whenever possible.

D.5.3 Verification Studies

In order to gain confidence in predicted results, some form of verification is needed. Some or all of the following steps may then be considered:

- Is it possible to idealize the situation in such a way that an analytical solution can be obtained? If so, we could set up PROBE to solve the same situation and any resultant agreement would only be limited by grid dependence. We should, of course, never expect more than 5–6 correct figures, due to computer limitations.
- Are there any laboratory experiments that can be used to consider the basic physical processes? If so, these may be very useful for verification studies, as boundary conditions, initial conditions, and the quality of recording such processes are normally known with good accuracy.
- Are there any other model predictions for the problem considered? If there are, we could consider repeating them, as long as they can be regarded as well established and accepted.
- The final test is, of course, application to the environmental problem itself. This is the most difficult part with transient and often incomplete boundary conditions. This often makes it hard to judge the degree of success when comparing predicted and measured behavior.

D.5.4 Causes of Diverging Solutions

A diverging solution is normally easy to detect: integral checks are not fulfilled and unrealistic profiles are predicted. Assuming that the user has checked that the problem specification is correct—by studying `CASE` and the initial output—we may consider the following points:

- Has it been firmly established that a solution to the problem, as defined, exists? We should, in this context, be particularly observant of prescribed boundary conditions.
- Have all length and time scales in the problem been identified? If a typical period in space or time can be found, we may need 10–20 grid cells or time steps to resolve the process.
- If a lake or reservoir is considered, the seiche period will enter through the pressure gradient formula. Once again a time step of the order of one-tenth of the seiche period is needed.
- If a sedimentation process is considered, we should estimate the time step required for settling velocity. The time it takes for particles to travel across a grid cell may be used as an estimate of the time step required.

D.5.5 Some Advice on Installing PROBE

Test installations of the present version of PROBE have been carried out on VAX 8600, UNIVAC 1108, CRAY, SUN and PCs. The experience gained from these installations can be summarized as:

- The inclusion of parameter statements and common blocks need to be arranged according to the computer used.
- The unlabeled common block `IA1` in subroutine `STORE` needs to be dimensioned to `NSTR1` (and not 1) on some computers. Note that the code needs to be recompiled when the maximum number of cells, equations, or runs are reset.
- Of the two common blocks included in most subroutines one is unlabeled. This one corresponds to `IA1` in subroutine `STORE`. It may be necessary on some computers to label these two common blocks and then, as mentioned above, give `IA1` the dimension `NSTR1` as well.
- `TFRAC(1)` is the number of `TFRAC(2)` time steps. `TFRAC(1)` is converted into an integer in the code. The default value 10^8 may be too large for some computers (especially PCs) to convert into an integer. If this is the case, then reset `TFRAC(1)` in chapter 1 of `CASE`.

When the code has been installed and found to reproduce results from test cases, the user may wish to change the pre-set maximum number of cells, equations, or linked runs. This is done in the parameter statements that precede the common blocks.

When any of these values (NIM, NJM, or NPM) is reset, we also need to reset NSTOR1 (for the first common block) and NSTORE (the size of both common blocks, NSTOR1+108). NSTOR1 is calculated according to:

$$\texttt{NSTOR1} = (32 * \texttt{NIM} + 27 * \texttt{NJM} + \texttt{NIM} * (\texttt{NJM} + 2) + \texttt{NIM} * \texttt{NJM} + \texttt{NPM} + 64)$$

which is equal to 10,304 for pre-set values.

D.6 Concluding Remarks

As remarked earlier, computational fluid dynamics seldom becomes standard or simple. It is therefore not possible nor has it been the objective to write a manual that guarantees effective use of PROBE. Instead, it is hoped that it will assist potential users. Ultimately, though, their own insight and intelligence will be critical to its use.

D.7 Nomenclature

The following glossary of FORTRAN variable names is arranged with reference to the GROUPS in the subroutine DFAULT.

Group	*Name*	*Type*	*Meaning*
1	N	Integer	Number of grid points
1	TIME	Real	Integration time
1	TLAST	Real	Maximum integration time
1	LSTEP	Integer	Maximum number of time steps
1	IGRID	Integer	Index for grid
1	CEXPG	Real	Expansion factor for grid
1	DZCELL(NIM)	Real array	Vertical dimension of cells
1	TFRAC(20)	Real array	Specification of time step
1	ITYPEF	Integer	Type of flow, 1D or 2D
2	ZDIM	Real	Physical dimension in z-direction
2	XDIM	Real	Physical dimension in x-direction
2	YDIM	Real	Physical dimension in y-direction
2	INDARE	Integer	Index for area distribution

(continued)

Group	*Name*	*Type*	*Meaning*
2	AREAHZ	Real	Horizontal area of top cell
2	CEXPA	Real	Expansion factor for area distribution
3	F(NIM, NJM+2)	Real array	Dependent variables
3	SOLVAR (NJM)	Logical array	Select variables to be solved for
4	CPHEAT	Real	Specific heat
4	RHOREF	Real	Reference density
4	EMULAM	Real	Laminar viscosity
4	PRL(NJM)	Real array	Laminar Prandtl/Schmidt numbers
4	AGRAV	Real	Acceleration due to gravity
5	C(1-5)RHO	Real	Coefficient in equation of state
5	TREF	Real	Temperature of maximum density
6	ITURBM	Integer	Index for turbulence model
6	IPRSC	Integer	Index for Prandtl/Schmidt number
6	EMUCON	Real	Constant turbulence viscosity
6	PRT(NJM)	Real array	Turbulent Prandtl/Schmidt numbers
6	CD-CKSURF	Real	Constants in turbulence model
7	CORI	Real	Coriolis parameter
7	INDPX	Integer	Index for pressure gradients
7	INDPY	Integer	Index for pressure gradients
7	RHOUP	Real	Prescribed mass flow
7	RHOVP	Real	Prescribed mass flow
7	DPDXP	Real	Prescribed pressure gradient
7	DPDYP	Real	Prescribed pressure gradient
7	PFILT	Real	Pressure filtering coefficient
7	QZ(NIM)	Real array	Vertical volume flux
7	QINFL(NIM)	Real array	Inflow
7	QOUTFL(NIM)	Real array	Outflow
7	PHIIN(NIM, NJM)	Real array	Properties of inflow
7	FLXRAD	Real	Short-wave radiation
7	RADFRA	Real	Fraction of FLXRAD absorbed at the surface
7	BETA	Real	Extinction coefficient
8	F(NIM, NJM+2)	Real array	See Group 3
8	DPDX(NIM)	Real array	Pressure gradient, x-direction
8	DPDY(NIM)	Real array	Pressure gradient, y-direction
8	ISTPR	Integer	Index for starting profiles
8	VST1(NJM) VST2 (NJM)	Real array	Values for starting profiles

(continued)

Group	*Name*	*Type*	*Meaning*
8	ZST1(NJM) ZST2 (NJM)	Real array	Z-levels for starting profiles
9	ITYPEH	Integer	Index for boundary at high Z
9	ITYPEL	Integer	Index for boundary at low Z
9	IKBHZ(NJM)	Integer array	Index for boundary conditions at high Z
9	IKBLZ(NJM)	Integer array	Index for boundary conditions at low Z
9	ITRHZ(NJM)	Integer array	Index for time dependence at high Z
9	ITRLZ(NJM)	Integer array	Index for time dependence at low Z
9	IKBOT(NJM)	Integer array	Index for behavior at bottom
9	FLUXHZ(NJM)	Real array	Flux at high Z
9	FLUXLZ(NJM)	Real array	Flux at low Z
9	V1HZ(NJM) V5LZ (NJM)	Real array	Specify transient boundary conditions
9	STANTN(NJM)	Real array	Stanton number
9	CAPPA	Real	Von Karman's constant
9	C3B	Real	Constant in wall function
9	ROULHZ	Real	Roughness length at high Z
9	ROULLZ	Real	Roughness length at low Z
9	EMTMIN	Real	Minimum value for eddy viscosity
10	FKMIN	Real	Minimum value for turbulent energy
10	FDMIN	Real	Minimum value for dissipation
10	TAUMIN	Real	Minimum shear for wall functions
10	KINDAV	Integer	Index for harmonic or arithmetic averaging of diffusion coefficient
11	NSTAT	Integer	Steps between station values
11	NPROF	Integer	Steps between profiles
11	PRPROF(20)	Logical array	Selected printed profiles
11	INDPT	Integer	Index for particle tracking
11	ILEVEL(4)	Integer array	Levels for tracking
11	IPSAVE	Integer	Steps between saved coordinates
11	INIOUT	Logical	Controls initial output
12	NSTPDT(NPM)	Integer array	Numbers of steps on each time step for each run

(continued)

Group	*Name*	*Type*	*Meaning*
12	NPROBE	Integer	Number of linked runs
13	MOVE	Logical	Activates moving surface mode
13	ZSSTRT	Real	Initial water surface level
13	PREEVA	Real	Precipitation/Evaporation

D.8 Mathematical Formulation

D.8.1 Basic Assumptions

Most assumptions are related to one-dimensional treatment of the situations considered. All gradients in horizontal directions can then be neglected. It will further be assumed that turbulent mixing processes can be described by turbulent exchange coefficients. This description is based on Reynold's averaging of Navier–Stokes equations, which accordingly is assumed to be valid. The introduction of exchange coefficients and gradient laws exclude the proper treatment of counter-gradient fluxes. Internal absorption of short-wave radiation is assumed to follow an exponential decay law. Gravitational effects are assumed to obey the Boussinesq approximation, and the effect of the rotation of the Earth is described by the Coriolis parameter.

Vertical advection as a result of inflows and outflows at different levels in a reservoir can be accounted for in PROBE. However, since the treatment is not general (e.g., advective momentum transport across boundaries is not allowed), the advective term will not be included in the general treatment of the equations, but will be considered as a source/sink term in the special case mentioned above.

In the 1997 version of PROBE an option for two-dimensional steady-state parabolic flows was introduced. In the presentation below the set of equations for this option can be obtained by replacing the time derivative $(\partial\phi/\partial t)$ with an advective term $(\partial\phi u/\partial x)$. A full account of the two-dimensional option is given in Nordblom (1997).

D.8.2 Momentum Equations

Within the assumptions made, the momentum equations are:

$$\frac{\partial(\rho u)}{\partial t} = -\frac{\partial p}{\partial x} + \frac{\partial}{\partial z}\left(\nu_{\text{eff}}\frac{\partial(\rho u)}{\partial z}\right) + f\,\rho v \tag{D.3}$$

$$\frac{\partial(\rho v)}{\partial t} = -\frac{\partial p}{\partial y} + \frac{\partial}{\partial z}\left(v_{\text{eff}}\frac{\partial(\rho v)}{\partial z}\right) - f\,\rho u \tag{D.4}$$

where t is the time coordinate; x and y are horizontal space coordinates; z is the vertical space coordinate; u and v are horizontal velocities in the x-direction and the y-direction, respectively; p is pressure; f is the Coriolis parameter; and ρ is density. The kinematic effective viscosity v_{eff} is the sum of turbulent viscosity v_t and laminar viscosity v. Pressure gradients may be treated in several ways, depending on the problem considered:

(a) *Prescribed*.
(b) *Calculated with respect to prescribed total mass flux*. The formula employed is iterative of the following type:

$$\frac{\partial p^{i+1}}{\partial x} = \frac{\partial p'}{\partial x} + \texttt{PFILT} * (\overline{\rho u} - \overline{\rho u_p}) \tag{D.5}$$

where i is an iteration step; PFILT is a constant; $\overline{\rho u}$ is total mass flux; and $\overline{\rho u_p}$ is prescribed total mass flux. The formula produces a pressure gradient, which in the steady state gives $\overline{\rho u}$ equal to $\overline{\rho u_p}$. From the formula it can be understood that the value of PFILT will not affect the converged solution.
(c) *Pressure formula for lakes and reservoirs*. In Svensson (1978) (see also Svensson and Sahlberg 1989) pressure formulas for lakes and reservoirs were derived simulating the effect of the limited horizontal extent of a water body:

$$\frac{\partial}{\partial t}\left(\frac{\partial p}{\partial x}\right) = \rho g\frac{\pi^2 \bar{u} \times D}{L_x^2} \tag{D.6}$$

$$\frac{\partial}{\partial t}\left(\frac{\partial p}{\partial y}\right) = \rho g\frac{\pi^2 \bar{v} \times D}{L_y^2} \tag{D.7}$$

where g is acceleration due to gravity; D is depth; $\bar{u}$ and $\bar{v}$ are mean velocities; $\pi = 3.1416$; and L_x and L_y are the horizontal dimensions of the water body.

It is, however, necessary to include the effect of stratification on pressure gradients (as illustrated in Fig. D.8). The tilted thermocline shown has been observed both in lakes and in the laboratory. Realizing that the effect of the tilt is to eliminate pressure gradients below the interface, we may formulate the following expressions:

$$\frac{\partial p^{i+1}}{\partial x} = \left[\frac{\partial p^i}{\partial x} + \frac{\Delta t + \rho g \pi^2 \times \bar{u} D}{L_x^2}\right] \times \frac{T - T_{\text{bottom}}}{T_{\text{surface}} - T_{\text{bottom}}} \tag{D.8}$$

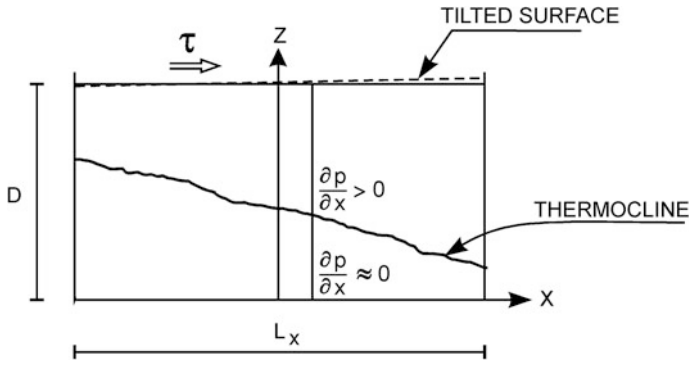

Fig. D.8 Illustration of stratification effects on pressure gradients

$$\frac{\partial p^{i+1}}{\partial y} = \left[\frac{\partial p^{i}}{\partial y} + \frac{\Delta t + \rho g \pi^2 \times \bar{v} D}{L_y^2}\right] \times \frac{T - T_{\text{bottom}}}{T_{\text{surface}} - T_{\text{bottom}}} \tag{D.9}$$

where i is the time level; and Δt is a time step. Thus, Formulas (D.5) and (D.6)—with the time derivative expressed as a finite difference—are the basic equations. From the formulas it is evident that the effects of stratification will be that pressure gradients are zero close to the bottom, since T then equals T_{bottom}, and that they will be unaffected close to the surface, since T then equals T_{surface}. These implications are qualitatively correct. The formulas do not, however, contain any mechanism for the generation or description of internal oscillations. It should be mentioned that Formulas (D.6)–(D.9) are tentative and have not yet been fully tested.

D.8.3 Heat Energy Equation

The heat energy equation is given by

$$\frac{\partial}{\partial t}(\rho c_p T) = \frac{\partial}{\partial z}\left(\nu'_{\text{eff}} \frac{\partial}{\partial z}(\rho c_p T)\right) + \beta_w F_s^w (1-\eta) e^{-\beta_w (D-Z)} \tag{D.10}$$

where temperature is denoted by T; c_p is specific heat; ν'_{eff} is the sum of eddy diffusivity ν'_t and the laminar diffusivity for heat; F_s^w is incoming short-wave radiation; η is the fraction of F_s^w absorbed at the surface; and β_w is the extinction coefficient.

D.8.4 Salinity and Concentration Equations

These equations can be expressed in the general form:

$$\frac{\partial \phi}{\partial t} = \frac{\partial}{\partial z}\left(\nu'_{\text{eff}} \frac{\partial \phi}{\partial z}\right) + S_\phi \tag{D.11}$$

where ϕ stands for salinity S or one of the concentrations c_1, c_2, c_3, or c_4. No source terms are provided for these variables. The user thus has to supply them explicitly, when it has been established which source and sink terms are constituents of the concentration equation considered.

D.8.5 Turbulence Model

PROBE has two different turbulence models: a one-equation turbulence model (the k model of Axell and Liungman 2001) and a two-equation turbulence model (the $k-\varepsilon$ model). A detailed description of the derivation and application of the latter model is given by Rodi (1980).

In the k model, kinematic eddy viscosity ν and kinematic eddy diffusivity ν'_t are calculated from turbulent kinetic energy k and the turbulent length scale l by the Kolmogorov-Prandtl relation:

$$\nu_t = c_\mu k^{1/2} l \tag{D.12}$$

$$\nu'_t = c'_\mu k^{1/2} l \tag{D.13}$$

where c_μ and c'_μ are stability functions (see Sect. D.8.6). In the $k-\varepsilon$ model, ν_t and ν'_t are calculated as

$$\nu_t = c_\mu \left(c_\mu^0\right)^3 \frac{k^2}{\varepsilon} \tag{D.14}$$

and

$$\nu'_t = c'_\mu \left(c_\mu^0\right)^3 \frac{k^2}{\varepsilon} \tag{D.15}$$

respectively.

The equation for turbulent kinetic energy k can be derived from the Navier–Stokes equations and thereafter modeled to the following form:

$$\frac{\partial k}{\partial t} = \frac{\partial}{\partial z}\left(\frac{v_t}{\sigma_k}\frac{\partial k}{\partial z}\right) + P_s + P_b - \varepsilon \tag{D.16}$$

where

$$P_s = v_t\left[\left(\frac{\partial_u}{\partial_z}\right)^2 + \left(\frac{\partial v}{\partial z}\right)^2\right] \tag{D.17}$$

is the production of shear as a result of turbulence, and

$$P_b = v_t^{'}\frac{g}{\rho_0}\frac{\partial \rho}{\partial z} \tag{D.18}$$

is the production or destruction of turbulent kinetic energy due to buoyancy.

In the k model, the dissipation rate ε is calculated according to

$$\varepsilon = (c_\mu^0)^3\frac{k^{3/2}}{l} \tag{D.19}$$

where $c_\mu^0 = 0.5562$ is a constant. When stratification is stable, the turbulent length scale l is calculated as

$$\frac{1}{l^2} = \frac{1}{l_g^2} + \frac{N^2}{c_b^2 k} \tag{D.20}$$

In (D.20), the first term on the right-hand side is the correction necessary to account for upper and lower boundaries, calculated as

$$\frac{1}{l_g^2} = \frac{1}{(\kappa d_1)^2} + \frac{1}{(\kappa d_2)^2} \tag{D.21}$$

where $\kappa = 0.4$ is von Karman's constant; and d_1 and d_2 are distances to the upper and lower boundaries, respectively. Further, $c_b = 0.35$ is a constant; and N^2 is calculated as

$$N^2 = -\frac{g}{\rho_0}\frac{\partial \rho}{\partial z} \tag{D.22}$$

When stratification is unstable, the turbulent length scale is calculated according to

$$l = l_g[1 - (c_\mu^0)^6 c_b^{-2} R_t]^{1/2} \tag{D.23}$$

where R_t is a turbulent Richardson number calculated as

$$R_t = \frac{k^2 N^2}{\varepsilon^2} \tag{D.24}$$

(see Axell and Liungman 2001 for further details).

In the $k-\varepsilon$ model, the dissipation rate ε is calculated as

$$\frac{\partial \varepsilon}{\partial t} = \frac{\partial}{\partial z}\left(\frac{\nu_t}{\sigma_\varepsilon}\frac{\partial \varepsilon}{\partial z}\right) + \frac{\varepsilon}{k}\left(c_{\varepsilon_1} P_s + c_{\varepsilon_3} P_b - c_{\varepsilon_2}\varepsilon\right) \tag{D.25}$$

where $c_{\varepsilon_1} = 1.44$ and $c_{\varepsilon_2} = 1.92$ are constants in the turbulence model, and the value of c_{ε_3} depends on the stability of the fluid and on the properties of turbulence (as described in Axell, 2002).

D.8.6 Turbulent Prandtl Numbers and Stability Functions

There are several options available to correct for the effect of stratification on the turbulent fluxes of momentum, heat, salt, and other scalars. First, when `IPRSC=1`, Prandtl/Schmidt numbers are given constant values specified by the user. Second, when `IPRSC=2`, the Prandtl number formulation of Launder (1975) is used. Third, when `IPRSC=3`, Prandtl numbers are calculated according to Axell and Liungman (2001). Finally, when `IPRSC=4`, the full stability functions of Axell and Liungman (2001) are used. The default setting is `IPRSC=2`.

Prandtl numbers are calculated according to

$$\sigma_t = \frac{c_{pr_1} + c_{pr_2} R_t}{1 + c_{pr_3} R_t} \tag{D.26}$$

The values of the coefficients in Eq. (D.26) are

$$(c_{pr_1}, c_{pr_2}, c_{pr_3}) = (0.63;\ 0.13;\ 0.063) \tag{D.27}$$

if `IPRSC=2` (Launder 1975), and

$$(c_{pr_1}, c_{pr_2}, c_{pr_3}) = (1.00;\ 0.193;\ 0.0302) \tag{D.28}$$

if `IPRSC=3` (Axell and Liungman 2001). c_μ and c'_μ are then calculated as

$$c_\mu = c_\mu^0 \tag{D.29}$$

with c_μ^0 being the neutral value of c_μ, and

$$c'_\mu = \frac{c_\mu}{\sigma_t} \tag{D.30}$$

If `IPRSC` is set to 4, full stability functions are used and calculated as

$$c_\mu = \frac{0.566 + 0.108R_t}{1 + 0.308R_t + 0.00837\,R_t^2} \tag{D.31}$$

$$c'_\mu = \frac{0.566}{1 + 0.277R_t} \tag{D.32}$$

The structural form of (D.31)–(D.32) was suggested by Launder (1975), but the values of the coefficients were suggested by Axell and Liungman (2001) to agree with more recent data.

D.8.7 Boundary Conditions

For momentum, heat energy, salinity, and concentrations, boundary conditions can be applied in two different ways: either the flux of the variable or the value of the variable at the boundary is given. Shear stress at a water surface, for example, is a "flux condition", while zero velocity at the bottom is a "value condition".

The boundary conditions for k and ε are somewhat different. In the default setting `(ITYPEL=1, ITYPEH=1)`, k and ε are specified close to the boundaries in relation to momentum and buoyancy fluxes. Details can be found in Svensson (1978) and Rodi (1980). When shear or bouyancy flux are absent, k and ε must be calculated in some other way to prevent laminar conditions near the walls. With `ITYPEL=3 (ITYPEH=3)`, k is calculated with a no-flux condition (i.e., zero gradient), and ε is calculated using the law of the wall at the lower (upper) boundary. Finally, with `ITYPEL=4 (ITYPEH=4)`, both k and ε are calculated using no-flux boundary conditions at the lower (upper) boundary.

D.8.8 Equation of State

In the default setting (`IEQSTATE=1`), the equation of state assumes a quadratic relationship between temperature and density and a linear relationship between salinity and concentration, thus:

$$\rho = \rho_0\left(1 - \alpha_1(T - T_r)^2 + \alpha_2 S + \alpha_3 C_1 + \alpha_4 C_2 + \alpha_5 C_3 + \alpha_6 C4\right) \quad \text{(D.33)}$$

where ρ_0 is a reference density; T_r is the temperature of maximum density; and α_1–α_6 are coefficients. In order to obtain maximum accuracy it may be necessary to tune T_r and the coefficients. For example, it is necessary to choose T_r with respect to the salinity interval under consideration.

It is also possible to select the UNESCO formula for the equation of state (`IEQSTATE=2`) (see, e.g., Gill 1982). This formula is more precise than Eq. (D.33) and its coefficients do not need tuning. However, the pressure effects on density are not included.

D.9 Finite Difference Equations for the One-Dimensional Transient Option

D.9.1 Introduction

There are several ways of deriving the finite difference form of differential equations. In this section they will be derived by integrating the differential equations over control volumes. The general outline of the technique follows from Spalding (1976) or Patankar (1980).

D.9.2 The Grid Arrangement and the General Differential Equation

All the differential equations given in Sect. D.8 may be presented in the general form:

$$\frac{\partial \phi}{\partial t} = \frac{\partial}{\partial z}\left(\Gamma_\phi \frac{\partial \phi}{\partial z}\right) + S_\phi \quad \text{(D.34)}$$

where ϕ stands for ρu when x-direction momentum is considered; and ρcT when heat energy is considered, etc. The source term for the variable ϕ is denoted by S_ϕ; and Γ_ϕ is a transport coefficient defined by:

$$\Gamma_\phi = \frac{\mu_{\text{eff}}}{\rho \sigma_{\text{eff},\phi}} \quad \text{(D.35)}$$

where $\sigma_{\text{eff},\phi}$ is the effective Prandtl/Schmidt number for the variable ϕ.

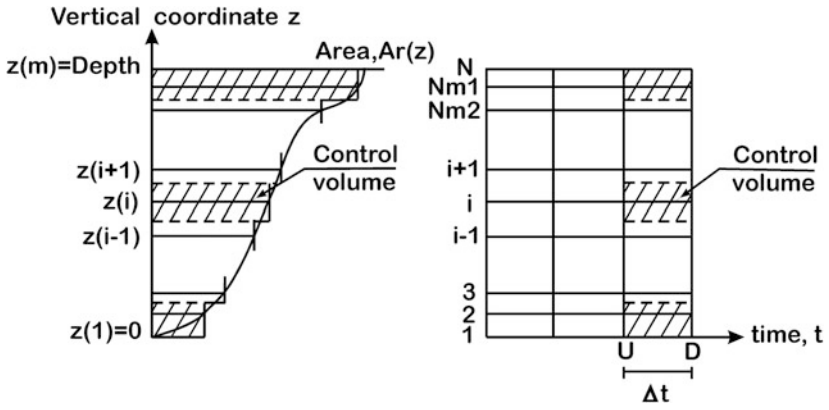

Fig. D.9 Illustration of grid and control volumes

This general equation is to be integrated over the control volume with index i (see Fig. D.9). This figure demonstrates vertical variation of a horizontal area, $Ar(z)$. This variation will be considered in a stepwise manner (as illustrated).

Time will be denoted by t. When we consider control volumes, U stands for up and D for down along the time axis. N is the number of grid lines in the vertical direction. `NM1` means $N - 1$ and `NM2` means $N - 2$, etc.

D.9.3 Integration Over a Control Volume

Equation (D.34) is to be integrated over a horizontal area, a vertical distance, and time. This will be done for the general control volume *i.* Thus:

$$\int_0^{Ar(i)} \int_{z(i-1/2)}^{z(i+1/2)} \int_U^D \left[\underbrace{\frac{\partial \phi}{\partial t}}_{(a)} = \underbrace{\frac{\partial}{\partial z}\left(\Gamma_\phi \frac{\partial \phi}{\partial z} \right)}_{(b)} + \underbrace{S_\phi}_{(c)} \right] dt\, dz\, dAr \tag{D.36}$$

Let us integrate this equation term by term:

$$\text{Term (a):} \quad \int_0^{Ar(i)} \int_{z(i-1/2)}^{z(i+1/2)} \int_U^D \frac{\partial \phi}{\partial t}\, dt\, dz\, dAr = \Delta z(i)\, Ar(i)\, (\phi_D(i) - \phi_U(i)) \tag{D.37}$$

$$\text{Term (b):} \quad \int_0^{Ar(i)} \int_U^D \int_{z(i-1/2)}^{z(i+1/2)} \left(\frac{\partial}{\partial z} \left(\Gamma_\phi \frac{\partial \phi}{\partial z} \right) \right) dz\, dt\, dAr$$

$$= \int_0^{Ar(i)} \int_U^D \left[\left(\Gamma_\phi \frac{\partial \phi}{\partial z} \right)_{i+1/2} - \left(\Gamma_\phi \frac{\partial \phi}{\partial z} \right)_{i-1/2} \right] dt\, dAr \tag{D.38}$$

$$= \Delta t \left[\left(Ar \Gamma_\phi \frac{\partial \phi}{\partial z} \right)_{1+1/2,t^*} - \left(Ar \Gamma_\phi \frac{\partial \phi}{\partial z} \right)_{1-1/2,t^*} \right]$$

where t^* is some time between U and D. To increase the numerical stability of the scheme, time level D will be used for t^* whenever possible. With this choice the numerical solution technique is of the fully implicit kind. In the above expression $Ar\left(i+\frac{1}{2}\right)$ and $Ar\left(i-\frac{1}{2}\right)$ are used. The stepwise specification of Ar is, however, discontinuous at these locations, and the question then arises as to which Ar should be used. To settle this, we look at the physical significance of (D.38) (see Fig. D.10).

The term $\left(Ar\Gamma_\phi \frac{\partial \phi}{\partial z}\right)_{i-1/2}$ represents a loss (assume $\frac{\partial \phi}{\partial z} > 0$) for control volume i at the lower boundary due to diffusive transport. It also represents a gain for control volume $i - 1$ at the upper boundary. If there is no loss associated with bottom contact, we will require all flux leaving control volume i to enter control volume $i - 1$. An example of such a variable is heat energy, as it is well known that only a negligible part of vertical heat flux will be stored in bottom sediments. The correct area at $i - \frac{1}{2}$ is thus $Ar(i - 1)$ and—using the same argument—$Ar(i)$ will be the appropriate area $i + \frac{1}{2}$. This area specification should be used for all variables that exhibit such a "conservative" nature in contact with the bottom. If, on the other hand, the variable in question experiences losses in contact with the bottom, it is clear from Fig. D.10 that the flux leaving control volume $i - \frac{1}{2}$ is not the same as that entering control volume $i - 1$ at the upper boundary. Momentum is an example of such a "non-conservative" variable. This is brought about by losses at the bottom

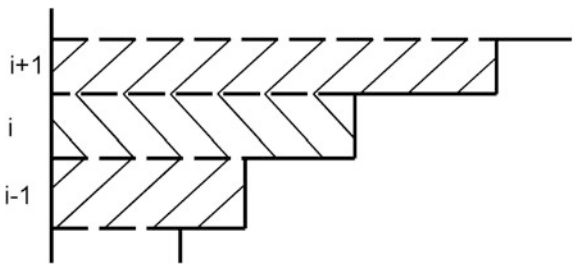

Fig. D.10 Detail of the control volumes

due to friction. For all "non-conservative" variables the most reasonable choice is $Ar(i)$ for both $i+\frac{1}{2}$ and $i-\frac{1}{2}$ when studying control volume i. This is the area specification normally used for all hydrodynamical variables, whereas heat energy, salinity, and concentrations will normally be treated as "conservative".

These conclusions will now be introduced into Eq. (D.38) through the definitions:

$$T_+ = Ar(i)\Gamma_\phi\left(i+\frac{1}{2}\right)/\Delta z\left(i-\frac{1}{2}\right) \tag{D.39}$$

$$T_- = \begin{cases} Ar(i)\Gamma_\phi\left(i-\frac{1}{2}\right)/\Delta z\left(i-\frac{1}{2}\right) & \text{if } \phi \text{ is not "conservative"} \\ Ar(i-1)\Gamma_\phi\left(i-\frac{1}{2}\right)/\Delta z\left(i-\frac{1}{2}\right) & \text{if } \phi \text{ is not "conservative"} \end{cases} \tag{D.40}$$

With these expressions we may write (D.38) as:

$$\Delta t[T_+(\phi_D(i+1)-\phi_D(i)) - T_-(\phi_D(i-1))] \tag{D.41}$$

$$\text{Term (c):} \quad \int_0^{Ar(i)} \int_{z(i-1/2)}^{z(i+1/2)} \int_U^D S_\phi \, dt \, dz \, dAr = Ar(i)\,\Delta z(i) S_{\phi,t^*}\,\Delta t \tag{D.42}$$

The source term will be divided into two parts, one of which contains the variable itself. Thus:

$$S_{\phi,t^*} = S(i) + S'(i)\phi_D \tag{D.43}$$

With this definition (D.42) becomes:

$$Ar(i)\Delta z(i)\Delta t(S(i)+S'(i)\phi_D) \tag{D.44}$$

By collecting terms (D.37), (D.41), and (D.44) we obtain:

$$\begin{aligned} \Delta z(i)Ar(i)(\phi_D(i)-\phi_U(i)) = {} & \Delta t[T_+(\phi_D(i+1)-\phi_D(i)) - T\_(\phi_D(i)-\phi_D(i-1))] \\ & + Ar(i)\Delta z(i)\Delta t[S(i)+S'(i)\phi_D] \end{aligned} \tag{D.45}$$

Which may be rearranged to:

$$\begin{aligned} \phi_D(i)[Ar(i)\Delta z(i) + \Delta t(T_+ + T_-) - Ar(i)\Delta z(i)\Delta t S'(i)] + \phi_D(i+1)(-\Delta t T_+) \\ + \phi_D(i-1)(-\Delta t T_-) + \phi_U(i)(-Ar(i)\Delta z(i)) \\ - Ar(i)\Delta z(i)\Delta t S(i) = 0 \end{aligned} \tag{D.46}$$

or

$$D(i)\phi_D(i) = A(i)\phi_D(i+1) + B(i)\phi_D(i-1) + C(i) \tag{D.47}$$

where:

$$A(i) = T_+/Ar(i) \tag{D.48}$$

$$B(i) = T_-/Ar(i) \tag{D.49}$$

$$C(i) = \phi_U(i)\Delta z(i)/\Delta t + \Delta z(i)S(i) \tag{D.50}$$

$$\begin{aligned} D(i) &= \Delta z(i)/\Delta t + (T_+ + T_-)/Ar(i) - \Delta z(i)S'(i) \\ &= A(i) + B(i) + \Delta z(i)/\Delta t - \Delta z(i)S'(i) \end{aligned} \tag{D.51}$$

Equation (D.47) is in a form that is easily solved using a tri-diagonal matrix algorithm. For a presentation of such an algorithm see Spalding (1976).

D.9.4 Coefficients for Control Volumes at Boundaries

Background

Transport coefficients often vary steeply close to boundaries. Special attention must therefore be paid to coefficients in these regions. In PROBE, coefficients are calculated using special wall functions, which are based on logarithmic and linear laws.

In this section we will show how coefficients are incorporated into finite differential formulation. Two different cases may be distinguished, depending on whether the value of ϕ or the flux of ϕ is prescribed.

The value of ϕ is prescribed

For this boundary condition all we need do is introduce new boundary coefficients:

$$B(2) = TB/Ar(2) \tag{D.52}$$

$$A(N) = TS/Ar(\texttt{NM1}) \tag{D.53}$$

where *TB* and *TS* are transport coefficients at the bottom and surface, respectively.

The flux of ϕ is prescribed

For the surface:

$$Ar(\texttt{NM1})\gamma_\phi = TS(\phi_D(\texttt{NM1}) — \phi_D(\texttt{N})) \tag{D.54}$$

where γ_ϕ is the flux of ϕ per unit area and time. From (D.54):

$$\phi_D(\mathtt{N}) = \gamma_\phi Ar(\mathtt{NM1})/TS + \phi_D(\mathtt{NM1}) \tag{D.55}$$

As a result of this, substitute ϕ_N in Eq. (D.47) with $i = \mathtt{NM1}$

$$\begin{aligned} D(\mathtt{NM1})\phi_D(\mathtt{NM1}) = TS/Ar(\mathtt{NM1})[-\gamma_\phi Ar(\mathtt{NM1}/Ts + \phi_D(\mathtt{NM1})] \\ + B(\mathtt{NM1})\phi_D(\mathtt{NM2}) + C(\mathtt{NM1}) \end{aligned} \tag{D.56}$$

which may be written as:

$$D'(\mathtt{NM1})\phi_D(\mathtt{NM1}) = A'(\mathtt{NM1})\phi_D(N) + B(\mathtt{NM1})\phi(\mathtt{NM2}) + C'(\mathtt{NM1}) \tag{D.57}$$

where

$$D'(\mathtt{NM1}) = D(\mathtt{NM1}) - TS/Ar(\mathtt{NM1}) \tag{D.58}$$

$$C'(\mathtt{NM1}) = C(\mathtt{NM1}) - \gamma_\phi \tag{D.59}$$

$$A'(\mathtt{NM1}) = 0.0 \tag{D.60}$$

This is the set of coefficients to be used when the flux of ϕ at the surface is prescribe. Expressions for the bottom boundary are analogous.

D.10 Finite Difference Equations for Two-Dimensional Steady-State Options (From Nordblom 1997)

Before deriving the finite difference equations needed for PROBE, we have to decide the order in which they are to be solved. It is assumed here that the first equation solved at each new integration step is the horizontal momentum equation. Thereafter, the vertical velocity component is calculated from the continuity equation. Then, the heat equation, the turbulent kinetic energy equation, and the dissipation rate equation are solved, one after the other. Thus, after the horizontal momentum equation has been solved and the vertical velocity component has been obtained from the continuity equation, the velocity field can be regarded as known when the remaining equations are solved. This fact will be referred to in what follows.

While the numerical scheme used in PROBE for the one-dimensional transient case can be characterized as fully implicit, the finite difference equations are derived here for the general case where the level between the fully explicit and the fully implicit scheme is expressed by a weighting factor. It is then easy to select a specific scheme (e.g., of Crank–Nicholson type or of fully implicit type), simply by adjusting the weighting factor.

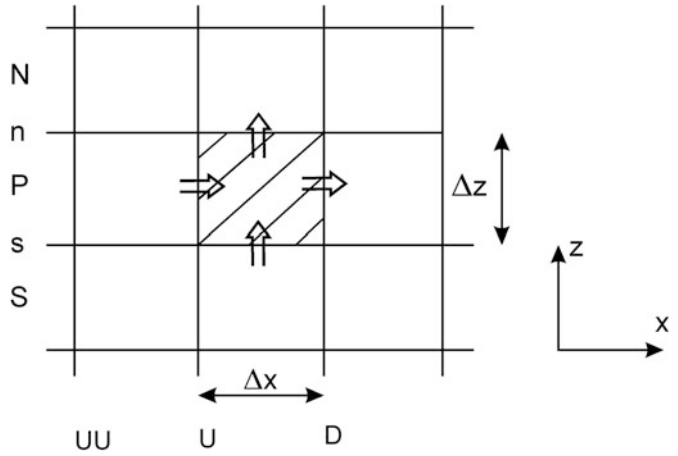

Fig. D.11 Part of the finite difference mesh

The starting point in the derivation is the general differential equation for two-dimensional parabolic steady flows, here written with all the terms on the left:

$$\frac{\partial}{\partial x}(u\phi) + \frac{\partial}{\partial z}(w\phi) - \frac{\partial}{\partial z}\left(\Gamma \frac{\partial \phi}{\partial z}\right) - S = 0 \qquad \text{(D.61)}$$

In this equation, we get the horizontal momentum equation when $\phi = \rho u$; and we get the heat equation, the turbulent kinetic energy equation, and the dissipation rate equation when $\phi = \theta, \phi = k$ and $\phi = \varepsilon$, respectively. S denotes the source term; and Γ denotes the vertical exchange coefficient, corresponding to the variable ϕ.

In the Cartesian coordinate system used in PROBE, the horizontal axis is denoted by x and the vertical axis by z. The calculation domain is divided into a rectangular mesh (a part of this is shown in Fig. D.11). The horizontal distance between grid cells Δx is assumed to be constant while the vertical distance Δz can vary.

Equation (D.61) is to be integrated over the dashed grid cell shown in Fig. D.11. The direction of flow is assumed to be from left to right. With reference to Fig. D.11, the letters U and D stands for Up and Down and are the limits of integration in the horizontal direction; UU denotes the x-coordinate one integration step upstream of $x = U$; the lowercase letters s and n refer to the z-coordinate of the lower and upper boundaries of the grid cell, respectively, and are the limits of integration in the vertical direction; P stands for the z-coordinate at the center of the dashed grid cell; and S and N refer to the z-coordinate at the center of the adjacent grid cells below (South) and above (North) the grid cell considered. Arrows indicate the actual locations where velocities are calculated (vertical velocity is here arbitrarily directed upward). The different terms in the differential equation are divided into three groups that are integrated separately. Group I is the horizontal convection

term, Group II is the vertical convection and diffusion terms (handled together), and Group III is the source term.

Group I The horizontal convection term

When integrating over the vertical extent of the grid cell, it is assumed that $u\phi$ is constant at z and equal to the center point value $(u\phi)_P$. By making this assumption, we get

$$\int_z \int_x \frac{\partial}{\partial x}(u\phi)\, dx\, dz = \int_z (u\phi)_D - (u\phi)_U\, dz = \Delta z[u_{P,D}\phi_{P,D} - u_{P,U}\phi_{P,U}] \quad \text{(D.62)}$$

where the coefficients $u_{P,D}$ and $u_{P,U}$ denote the horizontal wind speeds in the cell walls at $x = D$ and $x = U$, respectively.

The coefficients $u_{P,D}$ and $u_{P,U}$ will be determined in different ways depending on whether $\phi = \rho u$ or not. If ϕ is any of the variables θ, k, or ε, both $u_{P,D}$ and $u_{P,U}$ can be regarded as known since the horizontal wind speed can be determined from the horizontal momentum equation before the other variables are solved. On the other hand, when $\phi = \rho u$, $u_{P,D}$ is unknown and must be approximated.

One way of approximating $u_{P,D}$ is to set it equal to $u_{P,U}$, where $u_{P,U}$ is known from the previous integration step. The error term resulting from this approximation can be determined by setting $u_{P,D} = u_{P,U} + \Delta u$, where Δu is the change in horizontal wind speed between $x = U$ and $x = D$. Inserting the relation $u_{P,D} = u_{P,U} + \Delta u$ in Expression (D.62), we get

$$\Delta z[u_{P,U}\phi_{P,D} - u_{P,U}\phi_{P,U} + \Delta u\phi_{P,D}]$$

Thus, the error introduced by replacing $u_{P,D}$ by $u_{P,U}$ is $\Delta z \Delta u \phi_{P,D}$, which is equal to $\Delta z \Delta u \rho u \phi_{P,D}$ (since $\phi = \rho u$ when the momentum equation is solved). A smaller error term can, however, be achieved if both $u_{P,D}$ and $u_{P,U}$ are replaced by the upstream values $u_{P,U}$ and $u_{P,UU}$, respectively. To see this, we write $u_{P,D}$ and $u_{P,U}$ in terms of the upstream values and the change over the horizontal grid distance Δx is:

$$u_{P,U} = u_{P,UU} + \Delta u_1$$
$$u_{P,D} = u_{P,U} + \Delta u_2$$

If the horizontal grid distance is constant, the change in horizontal wind speed from $x = U$ to $x = D$ will be nearly the same as the change from $x = UU$ to $x = U$ (i.e., $\Delta u_2 \approx \Delta u_1 = \Delta u$). Inserting the relations $u_{P,U} = u_{P,UU} + \Delta u$ and $u_{P,D} = u_{P,U} + \Delta u$ in Expression (D.62), we can see that $\Delta u(\phi_{P,D} - \phi_{P,U}) = \rho \Delta u(u_{P,D} - u_{P,U}) = \rho(\Delta u)^2$ and we get:

$$\Delta z[u_{P,U}\phi_{P,D} - u_{P,UU}\phi_{P,U} + \rho(\Delta u)^2]$$

In this case, provided that $\Delta u_1 = \Delta u_2$, the resulting error term is $\Delta z \rho (\Delta u)^2$. Comparing the two error terms, we can see that the error is reduced by the factor $\Delta u / u_{P,D}$, which is a significant improvement since the change in u over the grid distance Δx is only a small fraction of the absolute value of u (i.e., $\Delta u / u_{P,D} \ll 1$).

If the coefficients $u_{P,D}$ and $u_{P,U}$ in Expression (D.62) are replaced by C_D and C_U, respectively, and the error term above is dropped, we get the following final expression for the integrated horizontal convection term:

$$\Delta z [C_D \phi_{P,D} - C_U \phi_{P,U}] \tag{D.63}$$

where $C_D = u_{P,U}$ and $C_U = u_{P,UU}$ if $\phi = \rho u$; and $C_D = u_{P,D}$ and $C_U = u_{P,U}$ otherwise. (When $x = 0$ and $\phi = \rho u$, we must set $C_D = C_U = u_{P,U}$, where $u_{P,U}$ is the prescribed velocity at the upstream boundary.)

Group II Horizontal Convection and Diffusion Terms

When integrating over the horizontal extent of the grid cell, it is assumed that all terms are constant at x and equal to a representative value of $x = x^* \in [U, D]$. By making this assumption, we get:

$$\int_x \int_z \frac{\partial}{\partial z}(w\phi) - \frac{\partial}{\partial z}\left(\Gamma \frac{\partial \phi}{\partial z}\right) dz\, dx = \int_x (w\phi)_n - \left(\Gamma \frac{\partial \phi}{\partial z}\right)_n - \left((w\phi)_s - \left(\Gamma \frac{\partial \phi}{\partial z}\right)_s\right) dx$$

$$= \Delta x \left[(w\phi)_{n,x^*} - \left(\Gamma \frac{\partial \phi}{\partial z}\right)_{n,x^*} - \left((w\phi)_{s,x^*} - \left(\Gamma \frac{\partial \phi}{\partial z}\right)_{s,x^*}\right)\right]$$

For convenience, the index x^* is temporarily dropped here, but will be included later in the derivation. The expression then takes the following form

$$\Delta x \left[w_n \phi_n - \Gamma_n \left(\frac{\partial \phi}{\partial z}\right)_n - \left(w_s \phi_s - \Gamma_s \left(\frac{\partial \phi}{\partial z}\right)_s \right)\right] \tag{D.64}$$

The value and gradient of ϕ at the lower and upper boundary of the grid cell can now be expressed in terms of ϕ_S, ϕ_P and ϕ_N. This will, however, require knowledge of how ϕ varies with z, which is of course unknown since variation of ϕ in the x-direction and z-direction is the outcome of the numerical solution. Instead, we must use approximate relations for w_n $\left(\frac{\partial \phi}{\partial z}\right)_n$, w_s, and $\left(\frac{\partial \phi}{\partial z}\right)_s$. They are expressed in the grid point values ϕ_S, ϕ_P, and ϕ_N.

In Patankar (1980) several methods are discussed. The so-called "upwind scheme" is the simplest approach to the problem, while more advanced methods are variants of the so-called "exponential scheme". These schemes are presented below.

The upwind scheme

In the upwind scheme, the value of ϕ at a cell wall is replaced by the upwind value, and the gradient of ϕ is calculated from a central difference approximation. Using the FORTRAN operator `MAX[]` which returns the greater of its arguments, the convective terms $w_n\phi_n$ and $w_s\phi_s$ can be written in compact form as:

$$w_n\phi_n = \phi_P \,\mathtt{MAX}[w_n\, 0] - \phi_N \,\mathtt{MAX}[-w_n, 0]$$
$$w_s\phi_s = \phi_S \,\mathtt{MAX}[w_s, 0] - \phi_P \,\mathtt{MAX}[-w_s, 0]$$

These expressions will always assign the upwind value to ϕ at a cell wall, regardless of flow direction.

Diffusive flux at the upper cell wall and the lower cell wall is calculated from a central difference approximation as:

$$\Gamma_n\left(\frac{\partial\phi}{\partial z}\right)_n = \frac{\Gamma_n}{z_N - z_P}\,(\phi_N - \phi_P)$$
$$\Gamma_s\left(\frac{\partial\phi}{\partial z}\right)_s = \frac{\Gamma_s}{z_P - z_S}\,(\phi_P - \phi_S)$$

Introducing the variables $\mathtt{DIF}_n$ for $\frac{\Gamma_n}{z_N - z_P}$ and $\mathtt{DIF}_s$ for $\frac{\Gamma_s}{z_P - z_S}$, Expression (D.64) takes the following form:

$$\Delta x[(\mathtt{MAX}[w_n, 0] + \mathtt{DIF}_n + \mathtt{MAX}[-w_s, 0] + \mathtt{DIF}_s)\phi_P - (\mathtt{MAX}[-w_n, 0] + \mathtt{DIF}_n)\phi_N - (\mathtt{MAX}[w_s, 0] + \mathtt{DIF}_s)\phi_S)]$$

Setting $A = \mathtt{MAX}[-w_n, 0] + \mathtt{DIF}_n$ and $B = \mathtt{MAX}[w_s, 0] + \mathtt{DIF}_s$, we get the final expression for the integrated convection and diffusion terms for the upwind scheme:

$$\Delta x[(w_n - w_s + A + B)\phi_P - A\phi_N - B\phi_S] \tag{D.65}$$

The exponential scheme and variants

In the exponential scheme, we can derive an exact expression showing the extent to which ϕ varies with z for an idealized convection-diffusion flow: a one-dimensional stationary flow without source terms and with constant density ρ and a constant diffusion coefficient Γ. The differential equation for this situation reads:

$$w\frac{\partial\phi}{\partial z} - \Gamma\frac{\partial^2\phi}{\partial z^2} = 0 \quad \text{or} \quad \frac{\partial^2\phi}{\partial z^2} - \frac{w}{\Gamma}\frac{\partial\phi}{\partial z} = 0$$

Since this is a linear ordinary differential equation with constant coefficients, the equation is easily solved by analytical methods. (Note that it is not only Γ that is constant here, w is also constant in a one-dimensional flow with constant density,

for continuity reasons.) The solution in the interval $[z_P, z_N]$, subject to the boundary conditions $\phi(z_P) = \phi_P$ and $\phi(z_N) = \phi_N$ becomes:

$$\phi(z) = \phi_P + (\phi_N - \phi_P)\frac{\exp\left(\frac{w}{\Gamma}(z - z_P)\right) - 1}{\exp\left(\frac{w}{\Gamma}(z_N - z_P)\right) - 1}, \quad z \in [z_P, z_N] \tag{D.66}$$

By differentiating this function, we get

$$\frac{\partial \phi}{\partial z}(z) = (\phi_N - \phi_P)\frac{w}{\Gamma}\frac{\exp\left(\frac{w}{\Gamma}(z - z_P)\right)}{\exp\left(\frac{w}{\Gamma}(z_N - z_P)\right) - 1}, \quad z \in [z_P, z_N] \tag{D.67}$$

The functional relationships for the value and gradient of ϕ in the interval $[z_S, z_P]$ will be analogous—all indices N are simply replaced by P and P by S.

Since the actual flow is two-dimensional and has a non-zero source term (in general) and a variable diffusion coefficient, we do not expect the analytical functions to be exact for the flow considered. However, from these functions we can probably make the best assumption possible regarding the value and gradient of ϕ at the cell walls.

Thus, we insert functions (D.66) and (D.67) for a z-coordinate in the interval $[z_P, z_N]$ and the corresponding functions for a z-coordinate in the interval $[z_S, z_P]$ in Expression (D.64). After some manipulations, we get:

$$\Delta x\left[w_n\left(\phi_P + \frac{\phi_P - \phi_N}{\exp\left(P_n/\rho_n\right) - 1}\right) - w_s\left(\phi_S + \frac{\phi_S - \phi_P}{\exp\left(P_s/\rho_S\right) - 1}\right)\right] \tag{D.68}$$

where P_n and P_s are Péclet numbers at the upper wall and lower wall of the grid cell, respectively. Péclet numbers express the relative strength of convection and diffusion at cell walls and are defined as:

$$P_n = \frac{\rho_n w_n (z_N - z_P)}{\Gamma_n} = \frac{\rho_n w_n}{\mathtt{DIF}_n}$$
$$P_s = \frac{\rho_s w_s (z_P - z_S)}{\Gamma_s} = \frac{\rho_s w_s}{\mathtt{DIF}_s}$$

where, as before, the variables $\mathtt{DIF}_n$ and $\mathtt{DIF}_s$ stand for $\frac{\Gamma_s}{z_S - z_P}$ and $\frac{\Gamma_s}{z_N - z_S}$, respectively.

By factoring out ϕ_P, ϕ_N, and ϕ_S in Expression (D.68), we get:

$$\Delta x\left[\left(w_n + \frac{w_n}{\exp(P_n/\rho_n) - 1} + \frac{w_s}{\exp(P_s/\rho_s) - 1}\right)\phi_P - \left(\frac{w_n}{\exp(P_n/\rho_n) - 1}\right)\phi_N - \left(w_s + \frac{w_s}{\exp(P_s/\rho_s) - 1}\right)\phi_S\right]$$

The above expression can be simplified to (D.65) by defining coefficients A and B as:

$$A = \frac{w_n}{\exp(P_n/\rho_n) - 1} = \mathtt{DIF}_n \frac{P_n/\rho_n}{\exp(P_n/\rho_n) - 1}$$
$$B = w_s + \frac{w_s}{\exp(P_s/\rho_s) - 1} = \mathtt{DIF}_s \left(P_s/\rho_s + \frac{P_s/\rho_s}{\exp(P_s/\rho_s) - 1} \right)$$

As a result of these definitions, the integrated convection and diffusion terms for the exponential scheme become:

$$\Delta x[(w_n - w_s + A + B)\phi_P - A\phi_N - B\phi_S]$$

Following Patankar (1980), A and B will now be approximated by polynomial functions. There are two reasons for doing so: polynomials are considerably easier to compute than exponentials, and they are well defined and equal the limit value of A and B at the point $P/\rho = 0$. From these approximate functions, we get the so-called "hybrid scheme" and "power-law scheme" (Patankar 1980).

In the hybrid scheme, A and B are approximated by piecewise linear functions as:

$$A = \mathtt{DIF}_n \cdot \mathtt{MAX}\left[-P_n/\rho_n,\, 1 - \frac{P_n/\rho_n}{2},\, 0 \right] = \mathtt{MAX}\left[-w_n,\, \mathtt{DIF}_n - \frac{w_n}{2},\, 0 \right]$$
$$B = \mathtt{DIF}_s \cdot \mathtt{MAX}\left[P_s/\rho_s,\, 1 + \frac{P_s/\rho_s}{2},\, 0 \right] = \mathtt{MAX}\left[-w_s,\, \mathtt{DIF}_s + \frac{w_s}{2},\, 0 \right]$$

In the power-law scheme, A and B are approximated by a 5th-degree polynomial for $P/\rho \in [-10,\, 10]$ and linear functions outside this interval. The definitions read:

$$\begin{aligned} A &= \mathtt{DIF}_s \cdot \left(\mathtt{MAX}\left[(1 - 0.1 \cdot |P_n/\rho_n|)^5, 0 \right] + \mathtt{MAX}[-P_n/\rho_n,\, 0] \right) \\ &= \mathtt{MAX}[\mathtt{DIF}_n (1 - 0.1 \cdot |w_s/\mathtt{DIF}_n|)^5, 0] + \mathtt{MAX}[-w_n,\, 0] \end{aligned} \tag{D.69}$$

$$\begin{aligned} B &= \mathtt{DIF}_s \cdot \left(\mathtt{MAX}\left[(1 - 0.1 \cdot |P_s/\rho_s|)^5, 0 \right] + \mathtt{MAX}[P_s/\rho_s,\, 0] \right) \\ &= \mathtt{MAX}[\mathtt{DIF}_s (1 - 0.1 \cdot |w_s/\mathtt{DIF}_s|)^5, 0] + \mathtt{MAX}[w_s,\, 0] \end{aligned} \tag{D.70}$$

To sum up, it is recognized that the difference between the schemes presented lies in the coefficients A and B. In the upwind scheme, A and B have the simplest form. The exponential scheme and its variants are somewhat more complicated, but are believed to perform better than the upwind scheme. As pointed out in Patankar (1980), for high lateral flow (i.e., large Péclet numbers), the gradient of ϕ will become very small, making diffusive flux negligible. For this case, the upwind scheme has the drawback of overestimating diffusion since it always calculates diffusion from a central difference approximation. In the other schemes where the coefficients A and B are functions of the Péclet number, the influence from diffusion at large Péclet numbers is reduced automatically. It is true that all schemes will produce the same result when the grid distance is made small enough since a finer grid will also reduce the Péclet number. From a computational point of view, we

should however choose a method that produces reasonable results using a coarse grid as well. Thus, the scheme of choice here is the hybrid scheme or the power-law scheme. It is probably arbitrary which one is chosen. Following the recommendation in Patankar (1980), the power-law scheme will be used, with A and B from Eqs. (D.69) and (D.70).

Now, re-introducing the index $x^* \in [U, D]$ that was dropped earlier, Expression (D.65) (valid for all schemes) becomes:

$$\Delta x \lfloor (w_n - w_s + A + B)\phi_{P,x^*} - A\phi_{N,x^*} - B\phi_{S,x^*} \rfloor \tag{D.71}$$

The value of ϕ at $x = x^*$ will now be expressed in terms of the old value from the previous integration step at $x = U$ and the new value from the current integration step at $x = D$ according to the linear relation $\phi_{x^*} = (1-f)\phi_U + f\phi_D$. When $f = 0$, we get the so-called fully explicit scheme, while $f = 0.5$ leads to the Crank–Nicholson scheme and $f = 1$ leads to the fully implicit scheme.

Inserting the relation $\phi_{x^*} = (1-f)\phi_U + f\phi_D$. in Expression (D.71), we get the following final expression for the integrated convection/diffusion term:

$$\begin{aligned}\Delta x[(w_n - w_s + A + B)[(1-f)\phi_{P,U} + f\phi_{P,D}] \\ - A[(1-f)\phi_{N,U} + f\phi_{N,D}] - B[(1-f)\phi_{S,U} + f\phi_{S,D}]]\end{aligned} \tag{D.72}$$

Group III The source term

When integrating over the vertical extent of the grid cell, it is assumed that the source term S is constant at z and equal to the center point value S_P. When integrating over the horizontal extent of the grid cell, it is assumed that S_P is constant at x and equal to a representative value S_{P,x^*} at $x = x^* \in [U, D]$. Moreover, to prepare for situations where the source term is a function of ϕ, we use a linear expression for this dependence according to $S_P = \mathtt{SI} + \mathtt{SIP}\phi_{P,x^*}$, where `SI` and `SIP` are coefficients. By making these assumptions, we get:

$$\int_x \int_z S\, dz\, dx = \Delta z \int_x S_P\, dx = \Delta x \Delta z S_{P,x^*} = \Delta x \Delta z(\mathtt{SI} + \mathtt{SIP}\phi_{P,x^*})$$

Inserting the relation $\phi_{x^*} = (1-f)\phi_U + f\phi_D$ in the expression above, we get:

$$\Delta x \Delta z(\mathtt{SI} + \mathtt{SIP}[(1-f)\phi_{P,U} + f\phi_{P,D}]) \tag{D.73}$$

Now, adding Expressions (D.63), (D.72), and (D.73) together, we arrive at the final finite difference equation for two-dimensional parabolic flows. The equation reads:

$$\left[\frac{\Delta z}{\Delta x}C_D + (w_n - w_s + A + B)f - \Delta z\texttt{SIP}f\right]\phi_{P,D}$$
$$= Af\phi_{N,D} + Bf\phi_{S,D} + \left[\frac{\Delta z}{\Delta x}C_U\phi_{P,U} - (w_n - w_s + A + B)(1-f)\phi_{P,U}\right.$$
$$+ A(1-f)\phi_{N,U}$$
$$\left. + B(1-f)\phi_{S,U} + \Delta z(\texttt{SI} + \texttt{SIP}(1-f)\phi_{P,U}\right]$$

or

$$D'\phi_{P,D} = A'\phi_{N,D} + B'\phi_{S,D} + C' \tag{D.74}$$

where

$$D' = \left[\frac{\Delta z}{\Delta x}C_D + (w_n - w_s + A + B)f - \Delta z\texttt{SIP}f\right]$$
$$A' = Af$$
$$B' = Bf$$

and

$$C = \left[\frac{\Delta z}{\Delta x}C_U\phi_{P,U} - (w_n - w_s + A + B)(1-f)\phi_{P,U} + A(1-f)\phi_{N,U}\right.$$
$$\left. + B(1-f)\phi_{S,U} + \Delta z(\texttt{SI} + \texttt{SIP}(1-f)\phi_{P,U}\right]$$

Calculation of vertical velocity

Vertical velocity at cell boundaries is obtained from the continuity equation applied to each grid cell after the horizontal momentum equation has been solved, thus giving horizontal velocities. By referring to the dashed grid cell in Fig. D.9 and assuming constant density, the continuity equation gives:

$$\Delta x(w_n - w_s) = \Delta z(u_{P,U} - u_{P,D})$$

Solving vertical velocity at the upper wall of the grid cell, w_n, we get:

$$w_n = w_s + \frac{\Delta z}{\Delta x}(u_{P,U} - u_{P,D}) \tag{D.75}$$

At a solid wall, vertical velocity is known and is equal to zero. Assuming a solid wall at the lower boundary, the vertical velocity at the upper wall of each grid cell in the finite difference mesh can be determined by iterating Equation (D.75) through all the grid cells from bottom to top.

D.11 Acknowledgments

The basic philosophy, structure and features of PROBE have much in common with the two fluid dynamic codes GENMIX and PHOENICS developed by Spalding (1977) and Spalding et al. (1983). There are two basic reasons for this. First, these codes are very well structured and written and therefore well suited to be good examples that merit follow-up. Second, PHOENICS is in use at the Swedish Meteorological and Hydrological Institute (SMHI). Moreover, it is beneficial to users that general features and variable names are the same in both codes.

Anders Omstedt, Jörgen Sahlberg, and Ola Nordblom at SMHI have made major contributions to the development of PROBE. Their assistance in developing, testing, and refining the program is acknowledged with thanks.

D.12 References

D.12.1 Literature References for the Manual

Axell, L.B. (2002). "Wind-driven internal waves and langmuir circulations in a numerical ocean model of the southern Baltic Sea," *J. Geophys. Res.*, **107**(C11), 3204, doi: 10.1029/2001JC000922,2002.

Axell, L.B.; and Liungman, O. (2001). "A one-equation turbulence model for geophysical applications: Comparison with data and the k–ε model," *Environ. Fluid Mech.*, **1**, 71–106.

Gill, A.E. (1982). *Atmosphere–Ocean Dynamics* (International Geophysics Series, Vol. 30), Academic Press.

Kantha, L.H.; Phillips, O.M.; and Azad, R.S. (1977). "On turbulent entrainment at a stable density interface," *J. Fluid Mech*., **79**(4), 753.

Launder, B.E. (1975). "On the effects of a gravitational field on the transport of heat and momentum," *J. Fluid Mech*., **67**(3), 569.

Nordblom, O. (1997). "Numerical simulation of the atmospheric surface layer," Master's thesis, Lulea University of Technology.

Omstedt, A.; Sahlberg, J.; and Svensson, U. (1983). "Measured and numerically simulated autumn cooling in the Bay of Bothnia," *Tellus*, **35A**, 231–240.

Patankar, S.V. (1980). *Numerical Heat Transfer and Fluid Flow*, Hemisphere Publishing, Washington, D.C.

Rodi, W. (1980). *Turbulence Models and Their Application in Hydraulics: A State of the Art Review*, International Association for Hydraulic Research (IAHR).

Spalding, D.B. (1976). *Basic Equations of Fluid Mechanics and Heat and Mass Transfer, and Procedures for Their Solution* (Heat Transfer Section, Report HTS/76/6), Imperial College London.

Spalding, D.B. (1977). *GENMIX: A General Computer Program for Two-dimensional Parabolic Phenomena* (Mech. Eng. Dept., Report No. HTS/77/9), Imperial College London.

Spalding, D.B.; Gunton, M.C.; Rosten, H.J.; and Tatchel, D.G. (1983). *PHOENICS. An Instruction Manual* (Report CHAM TR/75), Concentration, Heat and Momentum Ltd. (CHAM), London.

Svensson, U. (1978). *A Mathematical Model of the Seasonal Thermocline* (Dept. of Water Res. Eng., Report No. 1002), Lund Institute of Technology, Lund, Sweden.

Svensson, U.; and Sahlberg J. (1989). "Formulae for pressure gradients in one-dimensional lake models," *J. Geophys. Res*., **94**(C4), 4939–4946.

D.12.2 Papers and Reports Based on the Use of PROBE

Andreasson, P. (1992). "Energy conversions in turbulent wind-induced countercurrent flow," *Journal of Hydraulic Research*, **30**(6), 783–799.

Andreasson, P.; and Svensson, U. (1989). "A mathematical simulation of energy conversions in a fully developed channel flow," *Journal of Hydraulic Research*, **27**(3), 401–416.

Andreasson, P.; and Svensson, U. (1992). "A note on a generalized eddy-viscosity hypothesis," *Journal of Fluids Engineering*, **114**, 463–466.

Axell, L.B. (2002). "Wind-driven internal waves and langmuir circulations in a numerical ocean model of the southern Baltic Sea," *J. Geophys. Res.*, **107**(C11), 3204, doi: 10.1029/2001JC000922.

Axell, L.B.; and Liungman, O. (2001). "A one-equation turbulence model for geophysical applications: Comparison with data and the k–ε model," *Environ. Fluid Mech.,* **1**, 71–106.

Blenckner, T.; Omstedt, A.; and Rummukainen, M. (2002). "A Swedish case study of contemporary and possible future consequences of climate change on lake function," *Aquat. Sci.,* **64**, 171–184

Broman, B. (1984). *Consequences of Heat Extraction by the Heat Pump Method in Lake Drevviken,* Swedish Meteorological and Hydrological Institute, Norrköping, Sweden.

Broström, G. (1997). "Interaction between mixed layer dynamics, gas exchange and biological production in the oceanic surface layer with application to the northern North Atlantic," PhD thesis, Department of Oceanography, Göteborg University, Gothenburg, Sweden.

Broström, G. (1998). "A note on the C/N and C/P ratio of biological production in the Nordic seas," *Tellus,* **50B**, 93–109.

Broström, G.; and Rodhe, J. (1996). "Velocity shear and vertical mixing in the Ekman layer in the presence of a horizontal density gradient," *Continental Shelf Research,* **16**, 1245–1257.

Edman, M. (2008). "Modelling light attenuation in the Baltic Sea," M.Sc thesis (ISSN 1400-3821), Earth Sciences Centre, Göteborg University, Gothenburg Sweden.

Edman, A.; Sahlberg, J.; Hjerdt, N.; Marmefelt, E.; and Lundholm, K. (2007). *HOME Vatten i Bottenvikens vattendistrikt. Integrerat modellsystem för vattenkvalitetsberakningar* (SMHI Oceanografi Rapport Nr. 89). Swedish Meteorological and Hydrological Institute, Norrköping, Sweden [in Swedish].

Edman, M.; and Omstedt, A. (2013). "Modeling the dissolved CO_2 system in the redox environment of the Baltic Sea," *Limnol. Oceanogr.,* **58**(1), 74–92.

Eidner, G.; Utnes, T.; and McClimans, T.A. (1984). *On Wind Mixing of a Stratified Shear Flow,* Norwegian Hydrodynamic Laboratories, Trondheim, Norway.

Elo, A.-R.; and Vavrus S. (2000). "Ice modelling calculations, comparision of models PROBE and LIMNOS," *Verein Int. Limnol.,* **27**, 2816–2819.

Elo, A.-R. (1994). *Application of a PROBE Temperature Model for Deep Lake Preliminary Results,* University of Szczecinski Materialy Konferencje Nr. 2, pp. 7–16.

Elo, A.-R. (1994, 1995). "A sensitivity analysis of a temperature model of a lake examining components of the heat balance," *Geophysica,* **30**(1/2), 79–92.

Elo, A-R. (1995). "Some lake temperature simulations considering optical properties," in K. Pulkkinen (Ed.), *Proceedings of the Second Finnish–Estonian Seminar on Underwater Optics with Applications* (University of Helsinki, Department of Geophysics, Report Series of Geophysics No. 32, pp. 101–111).

Elo, A.-R. (1998). "Lake temperature modelling using long climate series," in R. Lemmela and N. Helenius (Eds.), *Proceedings of the Second International Conference on Climate and Water, Espoo, Finland, August 17–20* (Vol II, pp. 597–604).

Elo, A-R. (1999). "Physically based lake modelling," in A. Reinart and M.-J. Lilover (Eds.), *Fourth Workshop on Physical Processes in Natural Waters, September 13–17, Roosta, Estonia* (Estonian Marine Institute, Report Series No, 10, Tallinn, pp. 34–38).

Elo, A.-R. (2000). "Long term modelling of water temperature of Lake Constance," in S. Semovski (Ed.), *Fifth Workshop on Physical Processes in Natural Waters. August 23–29, Irkutsk. Russian Academy of Sciences Siberian Branch* (Limnological Institute Preprint No. 4, Irkutsk, pp. 32–35. ISBN 5-94115-003-2).

Elo, A.-R. (2001). "Long-term thermal modeling of morphologically different lakes," in J. Kajander (Ed.), *Northern Research Basins 13th International Symposium and Workshop, Saariselkä Finland Murmansk Russia Proceedings, Edita, Helsinki* (pp. 131–140).

Elo, A.-R. (2002). "Effects of climate change on the thermal conditions of lakes," in Å. Killingtveit (Ed.), *XXII Nordic Hydrological Conference, Røros, Norway, August 4–7* (Nordic Hydrological Programme NHP Report No. 47, pp. 589–596).

Elo, A.-R. (2005). "Modelling of summer stratification of morphologically different lakes," *Nordic Hydrology*, **36**(3), 281–294.

Elo, A.-R. (2006). "Long-term modelling of winter ice for morphologically different lakes," *Nordic Hydrology*, **37**(2), 107–119.

Elo, A-R. (2007). *Effects of Climate and Morphology on Temperature Conditions of Lakes* (Report Series in Geophysics 51, p. 56). Yliopistopaino, Helsinki, http://ethesis.helsinki.fi.

Elo, A-R. (2007). "Effects of lake size on the energy balance and vertical thermal structure of two small boreal lakes during the summer season," *Boreal Env. Res*, **12**, 585–600.

Elo, A.-R.; Huttula T.; Peltonen A.; and Virta J. (1998). "The effects of climate change on the temperature conditions of lakes," *Boreal Env. Res*., **3**, 137–150.

Engqvist, A.; and Omstedt, A. (1992). "Water exchange and density structure in a multi-basin estuary," *Continental Shelf Research*, **12**(9), 1003–1026.

Gustafsson, N.; Nyberg, L.; and Omstedt, A. (1998). "Coupling high resolution atmosphere and ocean models for the Baltic Sea," *Monthly Weather Review*, **126**, 2822–2846.

Gustafsson, E.O.; and Omstedt, A. (2008). "Sensitivity of Baltic Sea deep water salinity and oxygen concentrations to variations in physical forcing," *Boreal Environmental Research*, **14**, 18–30. Available at http://www.borenv.net/

Hansson, D.; and Omstedt, A. (2008). "Modelling the Baltic Sea ocean climate on centennial time scales: Temperature and sea ice," *Climate Dynamics*, **30**(7/8), 763–778, doi: 10.1007/ s00382-007-0321-2.

Hennemuth, B.; Rutgersson, A.; Bumke K.; Clemens, M.; Omstedt, A.; Jacob, D.; and Smedman A-S. (2003). "Net precipitation over the Baltic Sea for one year using models and data-based methods," *Tellus*, **55A**, 352–367.

Hjerdt, N.; Sahlberg, J.; Marmefelt, E.; and Lundholm, K. (2007). *HOME Fatten i Bottenhavets vattendistrikt: Integrerat modellsystem för vattenkvalitetsberäkningar* (SMHI, Oceanografi Rapport Nr. 90), Swedish Meteorological and Hydrological Institute, Norrköping, Sweden [in Swedish].

Huttula T. (1992). "Modelling resuspension and settling in lakes using a one dimensional vertical model," *Aqua Fennica*, **22**, 1.

Huttula T.; and Krogerus, K. (1991). "One-dimensional vertical resuspension model for lakes," *IAHR Symposium on Sediment Transport and Modelling, September, Florence* (Univ. degli Studi di Firenze, Dip. di Ingegneria Civile, pp. 647–664).

Huttula, T.; Peltonen, A.; Bilaletdin, Ä.; and Saura, M. (1992). "The effects of climatic change on lake ice and water temperature," *Aqua Fennica*, **22**, 2.

Huttula, T.; Peltonen, A.; and Kaipainen, H., (1996). "Effects of climatic changes on ice conditions and temperature regime in Finnish lakes (sensitivity analysis of wind forcing and other climatic variables)," in J. Roos (Ed.), *The Finnish Research Programme on Climatic Change: Final Report* (Publications of the Academy of Finland 4/96, pp. 167–172).

Jutterström, S.; Andersson, H.C.; Omstedt, A.; and Malmaeus, J.M. (2014). "Multiple stressors threatening the future of the Baltic Sea-Kattegat marine ecosystem: Implications for policy and management actions," *Marine Pollution Bulletin*, in press.

Kallio, K.; Huttula, T.; and Lehtinen, K. (1996). "Climate change and the eutrophication of a shallow, agriculturally loaded lake," in J. Roos (Ed.), *The Finnish Research Programme on Climate Change: Final Report* (Publications of the Academy of Finland 4/96, pp. 141–145).

Kauppi, L.; Frisk, T.; Forsius, M.; Huttula, T.; Posch, M.; Bilaletdin, Ä.; Kämäri, J.; Kallio, K.; Peltonen, A.; and Saura, M. (1992). "Effects of climatic change, air pollutants and land use on lake ecosystems," in M. Kanninen and P. Anttila (Eds.), *The Finnish Reasearch Programme for Climate Change: Progress Report* (Publications of the Academy of Finland 3/92, pp. 126–136).

Koponen, J.; Alasaarela, E.; Lehtinen, K.; Sarkkula, J.; Simbirowitz, V.H.; and Virtanen, M. (1992). *Modelling the Dynamics of Large Sea Areas* (Publications of Water and Environment Research Institute, No. 7), National Board of Water and the Environment.

Larsson, R.; and Svensson, U. (1980). "A one-dimensional numerical model study of some basic features of the flow in ice-covered lakes," *J. of Hydraulic Res.,* **18**(3), 251–267.

Leppäranta, M.; and Omstedt, A. (1990). "Dynamic coupling of sea ice and water for an ice field with free boundaries," *Tellus,* **42A**, 482–495.

Leppäranta, M.; Haapala, J.; Elo, A.-R.; and Herlevi, A. (1994). "Development of a Baltic Sea ice climate model," in M. Kanninen and P. Heikinheimo (Eds.), *The Finnish Research Programme on Climate Change: Second Progress Report* (Publications of the Academy of Finland 1/94, Edita, Helsinki, pp. 165–170).

Ljungemyr, P.; Gustafsson, N.; and Omstedt, A. (1996). "Parameterization of lake thermodynamics in a high resolution weather forecasting model," *Tellus,* **48A**(5), 608–621.

Malve, O.; Huttula, T.; and Lehtinen, K. (1991). "Modelling of eutrophication and oxygen depletion in Lake Lappajärvi," in *First Int. Conference on Water Pollution, Southampton, September* (ISBN 1-85166-697-4, pp. 111–124).

Marmefelt, E.; Sahlberg, J.; and Bergstrand, M. (2007). *HOME Vatten i södra Östersjöns vattendistrikt: Integrerat modellsystem för vattenkvalitetsberäkningar* (SMHI, Oceanografi Rapport Nr. 87), Swedish Meteorological and Hydrological Institute, Norrköping, Sweden [in Swedish].

Marmefelt, E.; Olsson, H.; Lindow, H.; and Svensson, J. (2004). *Integrerat kustzonssystem för Bohusläns skärgård* (SMHI Oceanografi Rapport Nr. 76), Swedish Meteorological and Hydrological Institute, Norrköping, Sweden [in Swedish].

Norman, M.; Rutgersson, A.; and Sahlée, E. (2013). "Impact of improved air-sea gas transfer velocity on fluxes and water chemistry in a Baltic Sea model," *J. Mar. Syst.*, **111–112**, 175–188.

Omstedt, A. (1983). "On autumn cooling in the Gulf of Bothnia," *Geophysica,* **20**(1), 27–40.

Omstedt, A. (1984). *A Forecast Model for Water Cooling in the Gulf of Bothnia and Lake Vänern* (SMHI Reports, No. RHO 36), Swedish Meteorological and Hydrological Institute, Norrköping, Sweden.

Omstedt, A. (1985a). "On supercooling and ice formation in turbulent sea water," *Journal of Glaciology,* **31**(109), 263–271.

Omstedt, A. (1985b). "Modelling frazil ice and grease ice formation in the upper layers of the ocean," Cold Regions Science and Technology, **11**, 87–98.

Omstedt, A. (1987a). "Forecasting water cooling in the Kattegat, the Öresund, the Belt Sea and the Arkona Basin," *Nordic Hydrology,* **18**, 247–258.

Omstedt, A. (1987b). "Water cooling in the entrance of the Baltic Sea," *Tellus,* **38A**, 254–265.
Omstedt, A. (1990). "A coupled one-dimensional sea ice–ocean model applied to a semi-enclosed basin," *Tellus,* **42A**, 568–582.
Omstedt, A. (1990a). "Modelling the Baltic Sea as thirteen sub-basins with vertical resolution," *Tellus,* **42A**, 286–301.
Omstedt, A. (1990b). *Real-time Modelling and Forecasting of Temperatures in the Baltic Sea* (SMHI Reports, RO 12, pp. 1–28), Swedish Meteorological and Hydrological Institute, Norrköping, Sweden.
Omstedt, A. (1994). "Numerical simulation of frazil ice," in S.F. Daly (Ed.), *Report on Frazil Ice* (CRREL Special Report 94–23), U.S. Army Cold Regions Research and Engineering Laboratory, Hanover, NH.
Omstedt, A.; and Axell, L.B. (1998). "Modeling the seasonal, interannual and long-term variations of salinity and temperature in the Baltic proper," *Tellus,* **50A**, 637–652.
Omstedt, A.; and Axell, L. (2003) "Modeling the variations of salinity and temperature in the large gulfs of the Baltic Sea," *Continental Shelf Research,* **23**, 265–294.
Omstedt, A.; Carmack, E.C.; and Macdonald, R.W. (1994). Modelling the seasonal cycle of salinity in the Mackenzie shelf/estuary," *J. Geophys. Res.*, **99**(C5), 10011–10021.
Omstedt, A.; and Chen, D. (2001). "Influence of atmospheric circulation on the maximum ice extent in the Baltic Sea," *J. Geophys. Res.*, **106**(C3), 4493–4500.
Omstedt, A.; Chen, Y.; and Wesslander, K. (2005). "A comparison between the ERA40 and the SMHI gridded meteorological databases as applied to Baltic Sea modelling," *Nordic Hydrology*, **36**(4), 369–380.
Omstedt, A.; Elken, J.; Lehmann, A.; Leppäranta, M.; Meier, H.E.M.; Myrberg, K.; and Rutgersson, A. (2014). "Progress in physical oceanography of the Baltic Sea during the 2003–2014 period," *Progress in Oceanography*, doi: 10.1016/j.pocean.2014.08.010.
Omstedt, A.; Gustafsson, E.; and Wesslander, K. (2009). "Modelling the uptake and release of carbon dioxide in the Baltic Sea surface water," *Continental Shelf Research*, **29**, 870–885, doi: 10.1016/j.csr.2009.01.006.
Omstedt, A.; and Hansson, D. (2006a). "The Baltic Sea ocean climate system memory and response to changes in the water and heat balance components," *Continental Shelf Research*, **26**, 236–251, doi: 10.1016/j.csr.2005.11.003.
Omstedt, A.; and Hansson, D. (2006b). Erratum to: "The Baltic Sea ocean climate system memory and response to changes in the water and heat balance components," *Continental Shelf Research*, **26**, 1685–1687, doi: 10.1016/j.csr.2006.05.011.
Omstedt, A.; Humborg, C.; Pempkowiak, J.; Pertillä, M.; Rutgersson, A.; Schneider, B.; and Smith, B. (2014). "Biogeochemical control of the coupled CO_2–O_2 system of the Baltic Sea: A review of the results of Baltic-C," *Ambio*, **43**, 49–59, doi: 10.1007/s13280-013-0485-4.
Omstedt, A.; Meuller, L.; and Nyberg, L. (1997). "Interannual, seasonal and regional variations of precipitation and evaporation over the Baltic Sea," *Ambio*, **26**(8), 484–492.
Omstedt, A.; and Nohr, C. (2004). Calculating the water and heat balances of the Baltic Sea using ocean modelling and available meteorological, hydrological and ocean data," *Tellus*, **56A**, 400–414.
Omstedt, A.; Nyberg, L.; and Leppäranta, M. (1994). *A Coupled Ice–Ocean Model Supporting Winter Navigation in the Baltic Sea, Part 1: Ice Dynamics and Water Levels* (SMHI Reports, RO 17, 17 pp.), Swedish Meteorological and Hydrological Institute, Norrköping, Sweden
Omstedt, A.; and Nyberg, L. (1995). *A Coupled Ice–Ocean Model Supporting Winter Navigation in the Baltic Sea, Part 2: Thermodynamics and Meteorological Coupling* (SMHI Reports, RO 21), Swedish Meteorological and Hydrological Institute, Norrköping, Sweden.
Omstedt, A.; and Nyberg, L. (1996). "Response of Baltic Sea ice to seasonal, inter-annual forcing and to climate change," *Tellus*, **48A**(5), 644–662.
Omstedt, A.; Nyberg, L.; and Leppäranta, M. (1996). "On the ice–ocean response to periodic forcing," Tellus, **48A**, 593–606.

Omstedt, A.; and Rutgersson, A. (2000). "Closing the water and heat cycles of the Baltic Sea," *Meteorol. Z.*, **9**, 57–64.

Omstedt, A.; and Sahlberg, J. (1982). *Vertical Mixing and Restratification in the Bay of Bothnia during Cooling* (SMHI, RHO 32), Swedish Meteorological and Hydrological Institute, Norrköping, Sweden.

Omstedt, A.; Sahlberg, J.; and Svensson, U. (1983). "Measured and numerically simulated autumn cooling in the Bay of Bothnia," *Tellus*, **35A**, 231–240.

Omstedt, A.; and Svensson, U. (1984). "Modelling super cooling and ice formation in a turbulent Ekman layer," *J. Geophys. Res.*, **89**(C1), 735–744.

Omstedt, A.; and Svensson, U. (1991). "On the melt rate of drifting ice heated from below," *Cold Regions Science and Technology*, **21**, 91–100.

Omstedt, A.; and Svensson, U. (1992). "On the melt rate of drifting ice heated from below," *Cold Regions Science and Technology*, **21**, 91–100.

Omstedt, A.; and Wettlaufer, J.S. (1992). "Ice growth and oceanic heat flux: Models and measurements," *J. Geophys. Res.*, **97**(C6), 9383–9390.

Omstedt, A.; Gustafsson, B.; Rodhe, B.; and Walin, G. (2000). "Use of Baltic Sea modelling to investigate the water and heat cycles in GCM and regional climate models," *Climate Research,* **15**, 95–108.

Omstedt, A.; Elken, J.; Lehmann, A.; and Piechura, J. (2004). "Knowledge of Baltic Sea physics gained during the BALTEX and related programmes," *Progress in Oceanography,* **63**, 1–28.

Omstedt, A.; Edman, M.; Anderson, L.G.; and Laudon, H. (2010). "Factors influencing the acid–base pH balance in the Baltic Sea: A sensitivity analysis," *Tellus,* **62B**, 280–295, doi: 10.1111/j.1600-0889.2010.00463.x.

Rahm, L-A.; and Svensson, U. (1986). "Dispersion of marked fluid elements in a turbulent Ekman layer," *J. Phys. Oceanogr.,* **16**, 2084–2096.

Rahm, L-A.; and Svensson, U. (1989). "Dispersion in a stratified benthic boundary layer," *Tellus,* **41A**, 148–161.

Rahm, L-A.; and Svensson, U. (1989). "On the mass transfer properties of the benthic boundary layer with an application to oxygen fluxes," *Netherlands Journal of Sea Research,* **24**(1), 27–35.

Rahm, L-A.; and Svensson, U. (1993). "Note on dispersion in an ocean surface Ekman layer due to variable wind forcing," *Deutsche Hydrogr. Z.,* **45**.

Roos, J. (1996). *The Finnish Research Programme on Climate Change* (Publications of the Academy of Finland 4/96). In this report a number of lake applications can be found.

Rutgersson, A.; Omstedt, A.; and Chen, Y. (2005). "Evaluation of the heat balance components over the Baltic Sea using four gridded meteorological data bases and direct observations," *Nordic Hydrology,* **36**(4), 381–396.

Rutgersson, A.; Omstedt, A.; and Räisänen, J. (2002). "Net precipitation over the Baltic Sea during present and future climate conditions," *Climate Research,* **22**, 27–39.

Rutgersson, A.; Smedman, A.-S.; and Omstedt A., (2001). "Measured and simulated latent and sensible heat fluxes at two marine sites in the Baltic Sea," *Boundary Layer Meteorology,* **99**, 53–84.

Rummukainen, M.; Räisänen, J.; Bringfelt, B.; Ullerstig, A.; Omstedt, A.; Wille'n, U.; Hansson, U.; and Jones, C. (2001). "A regional climate model for northern Europe: Model description and results from the downscaling of two GCM control simulations," *Climate Dynamics,* **17**, 339–359.

Sahlberg, J. (1983). "A hydrodynamical model for calculating the vertical temperature profile in lakes during cooling," *Nordic Hydrology,* **14**(4), 239–254.

Sahlberg, J. (1984). *A Hydrodynamical Model for Heat Contents Calculations on Lakes at the Ice Formation Date* (Document D4:1984), Swedish Council for Building Research,

Sahlberg, J. (1988). "Modelling the thermal regime of a lake during the winter season," *Cold Regions Science and Technology,* **15**, 151–159.

Sahlberg, J. (2003). "Physical modeling of the Akkajaure Reservoir," *Hydrology and Earth System Sciences,* **7**(3), 268–282.

Sahlberg, J. (2009). *The Coastal Zone Model* (SMHI Oceanography No. 98), Swedish Meteorological and Hydrological Institute, Norrköping, Sweden.

Sahlberg, J.; and Rahm, L. (2005). "Light limitation of primary production in high latitude reservoirs," *Hydrology and Earth System Sciences,* **9**(2).

Sahlberg, J.; Marmefelt, E.; Brandt, M.; Hjerdt, N.; and Lundholm, K. (2008). *HOME Vatten Norra Östersjöns vattendistrikt: Integrerat modellsystem för vattenkvalitetsberäkningar* (SMHI, Oceanografi Rapport Nr. 93), Swedish Meteorological and Hydrological Institute, Norrköping, Sweden [in Swedish].

Saura, M.; Bilaletdin, Ä.; Frisk, T.; and Huttula, T. (1995). "The effects of climate change on a small polyhumic lake," in P. Heikinheimo and J. Roos (Eds.), *Climate Change and Waters in the Boreal Zone* (Publications of the Academy of Finland 7/95:49).

Shaltout, M.; and Omstedt, A. (2012). "Calculating the water and heat balances of the Eastern Mediterranean Basin using ocean modelling and available meteorological, hydrological, and ocean data," *Oceanologia*, **54**(2), 199–232. doi: 10.5697/oc.54-2.199.

Shaltout, M.; and Omstedt, A. (2014). "Modelling the water and heat balances of the Mediterranean Sea using a two-basin model and available meteorological, hydrological and ocean data," *Submitted Oceanologia*.

Spalding, D.B.; and Svensson, U. (1977). "The development and erosion of the thermocline," in D. B. Spalding, and N. Afgan (Eds.), *Heat Transfer and Turbulent Buoyant Convection, Studies and Applications for Natural Environment Buildings, and Engineering Systems*, Hemisphere Publishing, Washington, D.C.

Svensson, U. (1978). *A Mathematical Model of the Seasonal Thermocline* (Dept. of Water Resources Eng., Report No. 1002), University of Lund, Sweden.

Svensson, U. (1978). "Examination of summer stratification," *Nordic Hydrology*, **9**, 105–120.

Svensson, U. (1979). "The structure of the Ekman layer," *Tellus*, **31**, 340–350.

Svensson, U. (1980). "On the numerical prediction of vertical turbulent exchange in stratified flows," in *Second IAHR Symposium on Stratified F/ows, Trondheim, NorWay, June.*

Svensson, U. (1981). "On the influence of buoyancy on the turbulent Ekman layer," in *Proc. Third Symposium on Turbulent Shear Flows, University of California Davis.*

Svensson, U. (1982). *Modelling the Turbulence Structure of the Adiabatic Atmospheric Boundary Layer* (Water Resources Eng., Report TULEA), University of Luleå, Sweden.

Svensson, U. (1984). "PROBE: A computer code for lake water quality modelling," paper presented at *Nordic Hydrological Conference, Nyborg, Denmark*.

Svensson, U. (1985). "Applications of a two-equation turbulence model to geophysical boundary layers," paper presented at *IUTAM Symposium on Mixing in Stratified Fluids, Margaret River, Western Australia.*

Svensson, U. (1998). *PROBE Program for Boundary Layers in the Environment: System Description and Manual* (SMHI Report Oceanography, No. 24, 100 pp.), Swedish Meteorological and Hydrological Institute, Norrköping, Sweden.

Svensson, U.; and Omstedt, A. (1990). "A mathematical model of the boundary layer under drifting melting ice," *Journal of Physical Oceanography*, **20**(2), 161–171.

Svensson, U.; and Omstedt, A. (1994). "Simulation of supercooling and size distribution in frazil ice dynamics," *Cold Regions Science and Technology*, **22**, 221–233.

Svensson, U.; and Omstedt, A. (1998). "Numerical simulation of frazil ice dynamics in the upper layer of the ocean," *Cold Regions Science and Technology*, **28**, 29–44.

Svensson, U.; and Rahm, L. (1988). "Modeling the near-bottom region of the benthic boundary layer," *J. Geophys. Res.*, **93**(C6), 6909–6915.

Svensson, U.; Axell, L.; Sahlberg, J.; and Omstedt, A. (2002). *PROBE Program for Boundary Layers in the Environment: System Description and Manual*, updated version available from Anders Omstedt (Anders.Omstedt@gvc.gu.se) or Jörgen Sahlberg (Jorgen.Sahlberg@smhi.se).

Virta, J.; Elo, A.-R.; and Pulkkinen, K. (1992). "Effect of climatic change on the temperature of lakes," in M. Kanninen and P. Anttila (Eds.), *The Finnish Research Programme on Climate Change: Progress Report* (Publications of the Academy of Finland 3/92, Edita, Helsinki, pp. 109–114).

Virta, J.; Elo, A.-R.; and Pulkkinen, K. (1994). "Application of lake temperature model for predicting the effect of climatic change," in M. Kanninen and P. Heikinheimo (Eds.), *The Finnish Research Programme on Climate Change: Second Progress Report* (Publications of the Academy of Finland 1/94, Edita, Helsinki, pp. 134–139).

Virta, J.; Elo, A.-R.; and Pulkkinen, K. (1996). "Effects of climate change on the temperature conditions of lake," in J. Roos (Ed.), *The Finnish Reseach Programme on Climate Change: Final Report* (Publications of the Academy of Finland 4/96, Edita, Helsinki, pp. 185–189).

Wåhlström, I.; Omstedt, A.; Björk, G.; and Anderson, A.G. (2012). "Modelling the CO_2 dynamics in the Laptev Sea, Arctic Ocean: Part 1," *Journal of Marine Systems*, **102–104**, 29–38.

Wåhlström, I.; Omstedt, A.; Björk, G.; and Anderson, A.G. (2013). "Modelling the CO_2 dynamics in the Laptev Sea, Arctic Ocean: Part II sensitivity of fluxes to changes in the forcing," *Journal of Marine Systems*, **111–112**, 1–10.

Appendix E
Reconstructions of Past Aquatic Conditions

Ocean and lake modeling provide us with interesting tools for learning more about the past and future. Regarding the past, we may speak about reconstructions and, regarding the future, about scenarios or storylines. In this appendix, we will briefly present some reconstructions of past climatic conditions and how to develop them. When we endeavor to learn something about the aquatic conditions in the past but do not have enough data, we could establish a statistical relationship such as:

$$Y = \mathrm{f}(X_1, X_2 \ldots X_\mathrm{N}) \tag{E.1}$$

where Y is the output variable or predictand that we would like to study and X_i, where $i = 1 \ldots n$, is the input variables or predictors. Methods for linking variables associated with the large scale and variables that represent the small scale have been developed in meteorology; they are called downscaling methods (Benestad et al. 2008). There are two basic approaches to downscaling: dynamic or empirical-statistical. Dynamic downscaling, which uses models, is a method often used in climate research when regional climate models are used to downscale larger-scale climate models. Empirical-statistical downscaling instead uses a combination of observations and large-scale predictors. Typical large-scale predictors are air pressures and air temperatures extracted from gridded datasets or climate models. In all downscaling, it is important to use predictors that represent strong underlying physical mechanisms in the problem. For example, Chen (2000) used monthly circulation climatology to study winter temperatures in Sweden. Other studies often use the North Atlantic Oscillation index; however, as this is just one number that often poorly characterizes the complex atmospheric circulation, a better method is to use the whole air pressure field. This method was introduced by Eriksson et al. (2007) when characterizing the European Sub-Arctic winter climate (Fig. E.1). The connection between air pressure and wind is through the geostrophic wind relationship:

A. Omstedt, *Guide to Process Based Modeling of Lakes and Coastal Seas*,
Springer Praxis Books, DOI 10.1007/978-3-319-17990-2

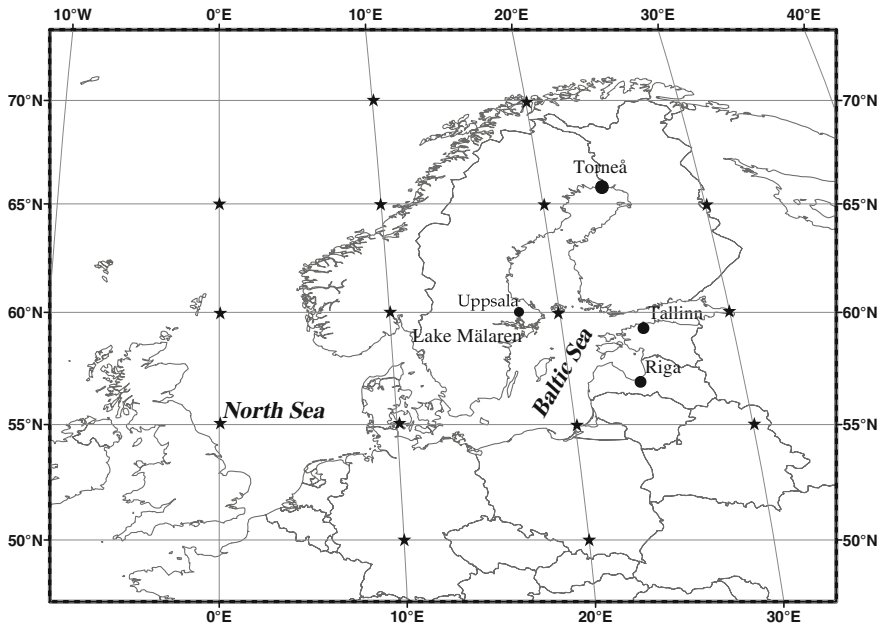

Fig. E.1 The Baltic Sea and Skagerrak region where the stars indicate the pressure points used when calculating the atmospheric circulation indices (Eriksson et al. 2007)

$$\begin{cases} f\rho V_0 = \frac{\partial P}{\partial x} \\ f\rho U_0 = -\frac{\partial P}{\partial y} \end{cases} \tag{E.2}$$

From the pressure gradients, we can calculate any large-scale wind that does not include frictional effects. We may then decompose the linearized vector field into five basic components by considering a two-dimensional vector field, $\mathbf{V}_h = (U\mathbf{i}, V\mathbf{j})$, as a function of time and of horizontal coordinates, $\mathbf{r} = (x\mathbf{i}, y\mathbf{j})$. The vector field near point $\mathbf{r}_0 = (x_0\mathbf{i}, y_0\mathbf{j})$ can be expressed by means of the Taylor expansion, in which only the linear part is considered:

$$\mathbf{V}_h = \mathbf{V}_0 + \mathbf{r} \cdot \nabla \mathbf{V}_h \tag{E.3}$$

The velocity $\mathbf{V}_0 = (U_0\mathbf{i}, V_0\mathbf{j})$ is the velocity at the origin position, $\mathbf{r}_0$, and $\nabla \mathbf{V}_h$ is the velocity gradient tensor. The velocity gradient tensor and its transpose, $\nabla \mathbf{V}_h^T$, can be written in explicit form as follows:

$$\nabla \mathbf{V}_h = \begin{bmatrix} \frac{\partial U}{\partial x} & \frac{\partial V}{\partial x} \\ \frac{\partial U}{\partial y} & \frac{\partial V}{\partial y} \end{bmatrix}, \quad \nabla \mathbf{V}_h^T = \begin{bmatrix} \frac{\partial U}{\partial x} & \frac{\partial U}{\partial y} \\ \frac{\partial V}{\partial x} & \frac{\partial V}{\partial y} \end{bmatrix} \tag{E.4}$$

with the introduction of this identity:

$$\nabla \mathbf{V}_h = \frac{1}{2}\left(\nabla \mathbf{V}_h - \nabla \mathbf{V}_h^T\right) + \frac{1}{2}\left(\nabla \mathbf{V}_h + \nabla \mathbf{V}_h^T\right) \tag{E.5}$$

The explicit form of the equations, after some rearrangements of the various components, reads:

$$\begin{aligned}\mathbf{V}_h &= \mathbf{V}_0 + \mathbf{r} \cdot \nabla \mathbf{V}_h \\ &= (U_0\mathbf{i}, V_0\mathbf{j}) + \frac{1}{2}(\zeta(-y\mathbf{i} + x\mathbf{j}) + \varepsilon(x\mathbf{i} + y\mathbf{j}) + \delta_1(y\mathbf{i} + x\mathbf{j}) + \delta_2(x\mathbf{i} - y\mathbf{j}))\end{aligned} \tag{E.6}$$

where

$$\varepsilon = \frac{\partial U}{\partial x} + \frac{\partial V}{\partial y},\ \zeta = \frac{\partial V}{\partial x} - \frac{\partial U}{\partial y},\ \delta_1 = \frac{\partial U}{\partial y} + \frac{\partial V}{\partial x},\ \delta_2 = \frac{\partial U}{\partial x} - \frac{\partial V}{\partial y}.$$

By adopting new notation, we can divide horizontal velocity into five distinct components:

$$\begin{aligned}\mathbf{V}_h &= \mathbf{V_0} + \mathbf{R} + \mathbf{E} + \mathbf{D}_1 + \mathbf{D}_2 \\ \mathbf{V}_0 &= (U_0\mathbf{i}, V_0\mathbf{j}) \\ \mathbf{R} &= 1/2\zeta(-y\mathbf{i} + x\mathbf{j}) \\ \mathbf{E} &= 1/2\varepsilon(x\mathbf{i} + y\mathbf{j}) \\ \mathbf{D}_1 &= 1/2\delta_1(y\mathbf{i} + x\mathbf{j}) \\ \mathbf{D}_2 &= 1/2\delta_2(x\mathbf{i} - y\mathbf{j})\end{aligned} \tag{E.7}$$

The first term represents translation (or zonal) and meridional geostrophic winds,$\mathbf{V}_0$; the second term represents rotation **R**, associated with either positive values as cyclonic rotation or with negative values as anti-cyclonic circulation. The third term captures convergence and divergence in the expansion velocity component, **E**. Finally, the two deformation velocity fields represent the torque exerted on the velocity field due to shear, $\mathbf{D}_1$, and normal deformation, $\mathbf{D}_2$, respectively.

Gridded pressure data are needed to calculate the velocity components. Figure E.2 provides an example in which a grid of 16 pressure points is designed over the North Sea-Baltic Sea area. Using gridded pressure data and calculating the full velocity field, one gains access to five predictors (i.e., advection, rotation, expansion, and two deformation velocity fields) associated with strong underlying physical mechanisms. With point 1 defined as the pressure point in the south-western corner, the zonal, U_0, and meridional, V_0, wind components can be calculated from:

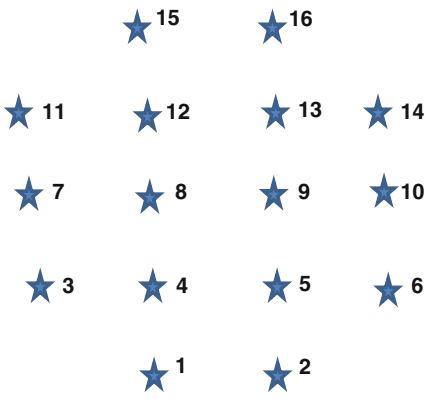

Fig. E.2 A 16-point grid designed for the Baltic Sea and Skagerrak region with a 5° × 10° (latitude × longitude) horizontal resolution

$$\begin{aligned} U_0 &= \frac{1}{f\rho\Delta y}[P(12) + P(13) - P(4) - P(5)] \\ V_0 &= \frac{1}{f\rho\Delta x}[P(5) + 2P(9) + P(13) - P(4) - 2P(8) - P(12)] \end{aligned} \tag{E.8}$$

Note that we average over two points. Rotation can be calculated in a similar manner:

$$\begin{aligned} \frac{\Delta U_0}{\Delta y} &= \frac{1}{f\rho\Delta y}[(P(15) + P(16) - P(8) - P(9)) - (P(8) + P(9) - P(1) - P(2))] \\ \frac{\Delta V_0}{\Delta x} &= \frac{1}{f\rho\Delta x}[(P(6) + 2P(10) + P(14) - P(5) - 2P(9) - P(13)) \\ &\quad - (P(4) + 2P(8) + P(12) - \mathrm{P}(3) - 2\mathrm{P}(7) - \mathrm{P}(11))] \end{aligned} \tag{E.9}$$

And expansion as:

$$\begin{aligned} \frac{\Delta U_0}{\Delta x} &= \frac{1}{f\rho\Delta y}[(P(14) + P(13) - P(6) - P(5)) - (P(12) + P(11) - P(4) - P(3))] \\ \frac{\Delta V_0}{\Delta y} &= \frac{1}{f\rho\Delta x}[(P(9) + P(2) - P(8) - P(1)) - (P(16) + P(9)) - P(15) - P(8))] \end{aligned} \tag{E.10}$$

Finally, we need to calculate the two deformation velocity fields:

$$\begin{aligned} \delta_1 &= \frac{\Delta U_0}{\Delta y} + \frac{\Delta V_0}{\Delta x} \\ \delta_2 &= \frac{\Delta U_0}{\Delta x} - \frac{\Delta V_0}{\Delta y} \end{aligned} \tag{E.11}$$

Here, we can use the relationship already developed above (Eqs. E.9 and E.10).

Using multi-regression methods, one can then derive a linear regression to fit the predictors to the predictands. This method computes a linear relationship using least square estimates. If one uses the five predictors and divides the velocity field into zonal and meridional components, the multiple regression procedure will estimate a linear equation of the form:

$$Y = a_0 + a_1 U_0 + a_2 V_0 + a_3 \zeta + a_4 \varepsilon + a_5 \delta_1 + a_6 \delta_2 \tag{E.12}$$

where a_i, i = 0.6, represents the constants to be determined. To choose which predictor is the most important, we can use stepwise regression (Draper and Smith 1966); by applying an F-test after each step, the model ensures that a newly added predictor does not reduce the importance of all the previous chosen predictors, lowering the best fit.

The empirical-statistical approach then uses available data for the predictand, dividing it into a calibration part and a validation part. This can be done by either dividing the available dataset into two equally large parts or sorting them into groups (e.g., dividing the predictands into even and uneven years). Data from the first group can then be used for calibration and data from the second for validation.

Data often lack good time resolution and are often available on only annual or seasonal scales. To overcome this, we train our datasets using high-resolution data from shorter time periods. Hansson and Omstedt (2008) used gridded data from ECMWF (ERA40) for the 1 January 1971 to 31 December 2000 period to increase the time resolution of a gridded dataset covering the past 500 years compiled by Luterbacher et al. (2002). The predictand Y was then calculated as follows:

$$Y = X^{season} + \left(X_{ERA40} - X^{season}_{ERA40}\right) \tag{E.13}$$

with a time resolution of six hours; X^{season} represents gridded seasonal data from Luterbacher et al. (2002) and X_{ERA40} and X^{season}_{ERA40} represent ERA40 data with 6-h and seasonal resolutions, respectively. The idea underlying this was that climate variations would be captured in the slow variations, X^{season}, while high-resolution fluctuations, $\left(X_{ERA40} - X^{season}_{ERA40}\right)$, would be captured by variations on time scales smaller than seasons.

Empirical-statistical downscaling has been used in various applications (Benestad et al. 2008). Omstedt and Chen (2001) compared the dynamic and statistical downscaling of large-scale circulation in relation to the maximum ice extent of the Baltic Sea (MIB). Later, Ericsson (2009) developed a statistical model of MIB over the past 500 years, while Hansson and Omstedt (2008) calculated how MIB has varied over last 500 years using a combination of dynamic and statistical methods. Hansson et al. (2010) examined the modeling of river runoff to the Baltic Sea by dividing the area into three drainage basins and developing statistical models for each one. Omstedt et al. (2009) used 500 years of forcing fields to model the uptake and release of carbon dioxide in the Baltic Sea before and after the start of

industrialization. Hansson and Gustafsson (2011) and Gustafsson (2012) modeled the development of hypoxia in the Baltic Proper in recent centuries. Some of these reconstructions are provided as supplementary data (Appendix C provides information on how to download them).

References

Aken, H.M. van: The Oceanic Thermohaline Circulation: An Introduction. Atmospheric and Oceanographic Sciences Library, no. 39. Springer, Berlin, New York (2007)

Anderson, L.G., Turner, D.R., Wedborg, M., Dyrssen, D.: Determination of total alkalinity and total dissolved inorganic carbon. In: Kremling, K., Ehrhards, M. (eds.) Methods of Seawater Analysis, 3rd edn, pp. 127–148. VCH, Weinheim, Germany (1999)

Ahtiainen, H., Artell, J., Elmgren, R., Hasselström, L., Håkansson, C.: Baltic Sea nutrient reductions—What should we aim for? J. Environ. Manage. **145**, 9–23 (2014)

Axell, L.B.: On the variability of Baltic Sea deepwater mixing. J. Geophys. Res. **103**(C10), 21667–21682 (1998)

Axell, L.B., Liungman, O.: A one-equation turbulence model for geophysical applications: comparison with data and the k–ε model. Environ. Fluid Mech. **1**, 71–106 (2001)

BACC I Author Team: The BALTEX Assessment of Climate Change for the Baltic Sea basin. Regional Climate Studies. Springer, Berlin, New York (2008). ISBN: 978-3-540-72785-9

BACC II Author Team: The BALTEX Assessment of Climate Change for the Baltic Sea basin (2015). In Press

Benestad, R., Hanssen-Bauer, E.I., Chen, D.: Empirical-Statistical Downscaling. World Scientific Publishing, Singapore (2008)

Björk, G.: The relation between ice deformation oceanic heat flux and the ice thickness distribution in the Arctic Ocean. J. Geophys. Res. **102**(C8), 18681–18698 (1997)

Björk, G., Söderkvist, J.: Dependence of the Arctic Ocean ice thickness distribution on the poleward energy flux in the atmosphere. J. Geophys. Res. **107**(C10), (2002). doi:10.1029/2000JC000723

Broström, G., Rodhe, J.: Velocity shear and vertical mixing in the Ekman layer in the presence of a horizontal density gradient. Cont. Shelf Res. **16**, 1245–1257 (1996)

Burchard, H.: Applied Turbulence Modeling in Marine Waters. Lecture Notes in Earth Sciences, 100. Springer, Berlin (2002)

Carmack, E.C., Weiss, R.F.: Convection in Lake Baikal: an example of thermobaric instability. In: Chu P.C., Gascard J.C. (eds.) Deep Convection and Deep Water Formation in the Oceans. Elsevier Oceanography Series, no. 57, pp. 215–228. Elsevier Science Publishers, Amsterdam (1991)

Carstensen, J., Andersen, J.H., Gustafsson, B.G., Conley, D.J.: Deoxygeneration of the Baltic Sea during the last century. PNAS Early Edition (2014). www.pnas.org/cgi/doi/10.1073/pnas.1323156111

Chen, D.: A monthly circulation climatology for Sweden and its application to a winter temperature case. Int. J. Climatol. **20**, 1067–1076 (2000)

Conley, D.J., Humborg, C., Rahm, L., Savchuk, O.P., Wulff, F.: Hypoxia in the Baltic Sea and basin-scale changes in phosphorus niogeochemistry. Environ. Sci. Technol. **36**, 5315–5320 (2002)

A. Omstedt, *Guide to Process Based Modeling of Lakes and Coastal Seas*,
Springer Praxis Books, DOI 10.1007/978-3-319-17990-2

Crowley, T.J.: Causes of climate change over the past 1000 years. Science **289**(5477), 270–277 (2000). doi:10.1126/science.289.5477.270

Cushman-Roisin, B., Becker, J.-M.: Introduction to Geophysical Fluid Dynamics: Physical and Numerical Aspects, vol. 101, 2nd edn. In the International Geophysics Series. Academic Press, Elsevier, Waltham (2011)

Diaz, R.J., Rosenberg, R.: Spreading dead zones and consequences for marine ecosystems. Science **321**, 926–929 (2008). doi:10.1126/science.1156401

Dickson, A.G., Sabine, C.L., Christian, J.R. (eds.): Guide to best practices for ocean CO_2 measurements. PICES Special Publication, no. 3. North Pacific Marine Science Organization, P.O. Box 6000, Sidney, BC V8L 4B2, Canada (2007)

Donelan, M.A., Wanninkhof, R.: Gas transfer and water surfaces: concepts and issues. In: Doneland M.A., Drenman W.M., Saltzman E.S., Wanninkhof R. (eds.) Gas Transfer at Water Surfaces, pp. 1–10. Geophysical Monograph, no. 127. American Geophysical Union, Washington, DC (2002)

Draper, N.R., Smith, H.: Applied Regression Analysis. Wiley, New York (1966)

Dyrssen, D., Sillén, L.G.: Alkalinity and total carbonate in sea water: a plea for *p-T*-independent data. Tellus **XIX**(1), 113–121 (1967)

Edman, M., Omstedt, A.: Modeling the dissolved CO_2 system in the redox environment of the Baltic Sea. Limnol. Oceanogr. **58**(1), 74–92 (2013)

Eilola, K.: Development of a spring thermocline at temperatures below the temperature of maximum density with application to the Baltic Sea. Geophys. Res. **102**(C4), 8657–8662 (1997)

Ekman, V.W.: On the influence of the earth's rotation on ocean currents. Ark f Mat Astron och Fysik **2**(11), 1–53 (1905)

Ekman, M.: The world's longest sea level series and a winter oscillation index for Northern Europe, 1774–2000. Small Publications in Historical Geophysics, no. 12. Gävle, Sweden: Winter Office for Geodynamics, Brändströmsgatan, Gävle, Sweden (2003)

Emeis, K.-C., Struck, U., Leipe, T., Pollehne, F., Kunzendorf, H., Christiansen, C.: Changes in the C, N, P burial rates in some Baltic Sea sediments over the last 150 years: relevance to P regeneration rates and the phosphorus cycle. Marine Geology. **167**, 43–59 (2000)

Engqvist, A., Omstedt, A.: Water exchange and density structure in a multi-basin estuary. Cont. Shelf Res. **12**(9), 1003–1026 (1992)

Engqvist, A., Stenström, P.: Archipelago strait exchange processes: An overview. Deep-Sea Res. Pt II **51**(4-5), 371–392 (2004)

Eriksson, C.: Characterizing and reconstructing 500 years of climate in the Baltic Sea Basin. Ph.D. dissertation. A125 by Bengt Christin Eriksson. Earth Sciences Centre, University of Gothenburg, Sweden

Eriksson, C., Omstedt, A., Overland, J.E., Percival, D.B., Mofjeld, H.O.: Characterizing the European sub-Arctic winter climate since 1500 using ice, temperature, and atmospheric circulation time series. J. Clim. **20**, 5316–5334 (2007). doi:10.1175/2007JCLI1461.1

Erlandsson, C.: The vertical transport of particulate organic matter regulated by fjord topography. J. Geophys. Res. **113**, G01008 (2008). doi:10.1029/2006JG000375

Fennel, W., Neumann, T.: Introduction to the modelling of marine ecosystems. Elsevier Oceanography Series, no. 72. Elsevier Sciences, Amsterdam (2004)

Gill, A.E.: Atmosphere-ocean dynamics. International Geophysics Series, vol. 30. Academic Press, New York (1982)

Gordon, D.C., Jr., Boudreau, P.R., Mann, K.H., Ong, J.-E., Silvert, W.L., Smith, S.V., Wattayakorn, G., Wulff, F., Yanagi, T.: LOICZ biogeochemical modelling guidelines. LOICZ/R&S/95-5, VI +96 pp. TEXEL, LOICZ, The Netherlands (1996)

Green, M.J.A.: Dynamics of the upper coastal ocean with special reference to the inshore-offshore water exchange. Ph.D. dissertation. A89, Department of Earth Sciences: Oceanography, University of Gothenburg, Sweden (2004)

Green, M.J.A., Liljebladh, B., Omstedt, A.: Physical oceanography and water exchange in the Northern Kvark Strait. Cont. Shelf Res. **26**, 721–732 (2006). doi:10.1016/j.csr.2006.01.012

Gustafsson, B.G.: Time-dependent modelling of the Baltic entrance area. 1. Quantification of circulation and residence times in the Kattegat and the straits of the Baltic sill. Estuaries **232**, 231–252 (2000)

Gustafsson, B.G.: Time-dependent modelling of the Baltic entrance area. 2. Water and salt exchange of the Baltic Sea. Estuaries **232**, 253–266 (2000)

Gustafsson, T., Kullenberg, B.: Untersuchungen von Trägheitsströmungen in der Ostsee [English translation of title here]. Svenska Hydrogr-Biol Komm Skr Ny Ser Hydrogr 13, Lund, pp. 1–28 (1936)

Gustafsson, E.: Modelled long-term development of hypoxic area and nutrient pools in the Baltic Proper. J. Mar. Syst. **94**, 120–134 (2012)

Gustafsson, E., Omstedt, A.: Sensitivity of Baltic Sea deep water salinity and oxygen concentration to variations in physical forcing. Boreal Environ. Res. **14**, 18–30 (2009)

Gustafsson, B.G., Schenk, F., Blenckner, T., Eilola, K., Meier, H.E.M., Muller-Karulis, B., Neumann, T., Ruoho-Airola, T., et al.: Reconstructing the development of Baltic Sea eutrophication 1850–2006. AMBIO **41**, 534–548 (2012)

Gustafsson, E., Wällstedt, T., Humborg, C., Mörth, C.-M., Gustafsson, B.G.: External total alkalinity loads versus internal generation: the influence of nonriverine alkalinity sources in the Baltic Sea. Global Biogeochem. Cycles, 1358–1370 (2014). doi:10.1002/2014GB004888

Hansson, D., Omstedt, A.: Modelling the Baltic Sea ocean climate on centennial time scales: Temperature and sea ice. Clim. Dyn. **30**(7–8), 763–778 (2008). doi:10.1007/s00382-007-0321-2

Hansson, D., Gustafsson, E.: Salinity and hypoxia in the Baltic Sea since A.D. 1500. J. Geophys. Res. **116**(C03027), 1–9 (2011). doi:10.1029/2010JC006676

Hansson, D., Eriksson, C., Omstedt, A., Chen, D.: Reconstruction of river runoff to the Baltic Sea, AD 1500–1995. Int. J. Climatol. (2010). doi:10.1002/joc.2097

Hansson, M., Andersson, L., Axe, P., Szaron, J.: Oxygen Surveys in the Baltic Sea 2012—Extent of Anixia and Hypoxia, 1960–2012. Report Oceanography 46, Swedish Meteorological and Hydrological Institute, Norrköping, Sweden (2013)

Hibler III, W.D.: A dynamic thermodynamic sea ice model. J. Phys. Oceanogr. **9**, 815–846 (1979)

Hjalmarsson, S., Wesslander, K., Anderson, L.G., Omstedt, A., Perttilä, M., Mintrop, L.: Distribution, long-term development and mass balance calculations of total alkalinity in the Baltic Sea. Cont. Shelf Res. **28**(4–5), 593–601 (2008)

Humborg, C., Mörth, C.-M., Sundbom, M., Borg, H., Blenckner, T., Gleisler, R., Ittekkot, V.: CO_2 supersaturation along the aquatic conduit in Swedish watersheds as constrained by terrestrial respiration, aquatic respíration and weathering. Glob. Change Biol. (2009). doi:10.1111/j.1365-2486.2009.02092.x

IPCC: Climate change 2013: the physical science basis. In: Stocker, T.F., Qin, D., Plattner, G.-K., Tignor, M., Allen, S.K., Boschung, J., Nauels, A., Xia, Y., Bex, V., Midgley, P.M. (eds.) Contribution of Working Group I to the Fifth Assessment Report of the Intergovernmental Panel on Climate Change, 1535 pp. Cambridge University Press, Cambridge (2013)

IPCC: Climate change 2007: the physical science basis. In: Houghton et al. (eds.) Contribution of Working Group I to the Third Assessment Report of the Intergovernmental Panel on Climate Change, 881 pp. Cambridge University Press, Cambridge (2001)

Jones, P.D., Briffa, K.R.: Unusual climate in Northwest Europe during the period 1730–1745 based on instrumental and documentary data. Climatic Change **79**, 361–379 (2006). doi:10.1007/s10584-006-9078-6

Kuli´nski, K., Schneider, B., Hammer, K., Machulik, U., Schulz-Bull, D.: The influence of dissolved organic matter on the acid-base system of the Baltic Sea. J. Mar. Syst. **132**, 106–115 (2014). doi:10.1016/j.jmarsys.2014.01.011

Kotov, S., Harff, J.: A comparison of Greenland ice and Baltic Sea sediment record: a contribution to climate change analysis. Math. Geol. **38**(6), 721–733 (2006). doi:10.1007/s11004-006-9047-7

Launiainen, J., Cheng, B., Uotila, U., Vihma, T.: Turbulent surface fluxes and air-ice coupling in the Baltic Air-Sea-Ice Study (BASIS). Ann. Glaciol. **33**, 237–242 (2001)

Leppäranta, M.: The Drift of Sea Ice, 2nd edn. Chichester, UK/Berlin-Heidelberg-New York: Praxis Publishing/Springer, Springer-Praxis Books in Geophysical Sciences (2011)

Leppäranta, M., Myrberg, K.: Physical oceanography of the Baltic Sea. Chichester, UK/Berlin-Heidelberg-New York: Praxis Publishing/Springer-Verlag, Springer-Praxis Books in Geophysical Sciences (2009)

Liljebladh, B., Stigebrandt, A.: The contribution from the surface layer via internal waves to the energetics of deepwater mixing in the Baltic Sea. In: Experimental Studies of Some Physical Oceanographic Processes. Ph.D. dissertation. A56 by Bengt Liljebladh. Earth Sciences Centre, University of Gothenburg, Sweden (2000)

Ljungemyr, P., Gustafsson, N., Omstedt, A.: Parameterization of lake thermodynamics in a high-resolution weather forecasting model. Tellus **48A**, 608–621 (1996)

Luterbacher, J., Xoplaki, E., Dietrich, D., Rickli, R., Jacobeit, J., Beck, C., Gyalistras, D., Schmutz, C., Wanner, H.: Reconstruction of sea level pressure fields over Eastern North Atlantic and Europe back to 1500. Clim. Dyn. **18**, 545–561 (2002). doi:10.1007/s00382-001-0196-6

Marmefelt, E., Arheimer, B., Lagner, J.: An integrated biogeochemical model system for the Baltic Sea. Hydrobiologia **393**, 45–56 (1999)

Mattsson, J.: Some comments on the Barotropic flow through the Danish Straits and the division of the flow between the Belt and the Öresund. Tellus **48**, 456–471 (1996)

McPhee, M.: Air-Sea-Ocean Interaction: Turbulent Ocean Boundary Layer Exchange Processes. Springer, New York (2008)

McPhee, M.G., Maykut, G.A., Morrison, J.H.: Dynamics and thermodynamics of the ice/upper ocean system in the marginal ice zone of the Greeenland Sea. J. Geophys. Res. **92**, 7017–7031 (1987)

Millero, F.J.: Freezing point of sea water. In: Eight Report of the Joint Panel on Oceanographic Tables and Standards. UNESCO Tech. Pap. Mar. Sci. No. 28, Annex 6. UNESCO, Paris (1978)

Millero, F.J., Perron, G., Desnoyers, J.E.: Heat capacity of seawater solution from 5 to 35 °C and 0.5 to 22 % chlorinity. J. Geophys. Res. **78**, 4499–4507 (1973)

Moberg, A., Bergström, H., Krigsman, J.R., Svanered, O.: Daily air temperature and pressure series for Stockholm 1756–1998. Clim. Change **53**, 171–212 (2002)

Norman, M., Rutgersson, A., Sahlée, E.: Impact of improved air-sea gas transfer velocity on fluxes and water chemistry in a Baltic Sea model. J. Mar. Syst. 111–112, 175–188 (2013)

Omstedt, A.: On autumn cooling in the Gulf of Bothnia. Geophysica **20**, 27–40 (1983)

Omstedt, A.: A forecast model for water cooling in the Gulf of Bothnia and Lake Vänern. SMHI Reports, RHO 36. SMHI, Norrköping, Sweden (1984)

Omstedt, A.: Water cooling in the entrance of the Baltic Sea. Tellus **38A**, 254–265 (1987)

Omstedt, A.: Forecasting water cooling in the Kattegat, the Öresund, the Belt Sea, and the Arkona Basin. Nord. Hydrol. **18**, 247–258 (1987)

Omstedt, A.: Modelling the Baltic Sea as thirteen sub-basins with vertical resolution. Tellus **42A**, 286–301 (1990a)

Omstedt, A.: Real-time modelling and forecasting of temperatures in the Baltic Sea. SMHI Reports of Oceanography, RO 12. SMHI, Norrköping, Sweden (1990b)

Omstedt, A.: A coupled one-dimensional sea ice–ocean model applied to a semi-enclosed basin. Tellus **42A**, 568–582 (1990c)

Omstedt, A.: Freezing estuaries and semi-enclosed basins. In: Leppäranta, M. (ed.) Physics of Ice-Covered Seas, vol. 2, pp. 483–516. Available at Department of Geophysics, University of Helsinki, P.O. Box 4 (Fabianinkatu 24 A), FIN-00014 University of Helsinki, Finland (1998)

Omstedt, A., Nyberg, L.: Response of Baltic Sea ice to seasonal, interannual forcing and to climate change. Tellus **48A**, 644–662 (1996)

Omstedt, A., Axell, L.: Modeling the seasonal, interannual, and long-term variations of salinity and temperature in the Baltic proper. Tellus **50A**, 637–652 (1998)
Omstedt, A., Axell, L.: Modeling the variations of salinity and temperature in the large gulfs of the Baltic Sea. Cont. Shelf Res. **23**, 265–294 (2003). doi:10.1016/S0278-4343(02)00207-8
Omstedt, A., Rutgersson, A.: Closing the water and heat cycles of the Baltic Sea. Meteorol. Z. **9**, 57–64 (2000)
Omstedt, A., Chen, D.: Influence of atmospheric circulation on the maximum ice extent in the Baltic Sea. J. Geophys. Res. **106**(C3), 4493–4500 (2001)
Omstedt, A., Nohr, C.: Calculating the water and heat balances of the Baltic Sea using ocean modelling and available meteorological hydrological, and ocean data. Tellus **56**(A), 400–414 (2004)
Omstedt, A., Hansson, D.: The Baltic Sea ocean climate system memory and response to changes in the water and heat balance components. Cont. Shelf Res. **26**, 236–251 (2006a). doi:10.1016/j.csr.2005.11.003
Omstedt, A., Hansson, D.: Erratum: the Baltic Sea ocean climate system memory and response to changes in the water and heat balance components. Cont. Shelf Res. **26**, 1685–1687 (2006b). doi:10.1016/j.csr.2006.05.011
Omstedt, A., Sahlberg, J., Svensson, U.: Measured and numerically simulated autumn cooling in the Bay of Bothnia. Tellus **35A**, 231–240 (1983)
Omstedt, A., Carmack, E.C., Macdonald, R.W.: Modelling the seasonal cycle of salinity in the Mackenzie shelf/estuary. J. Geoph. Res. **99**(C 5), 10011–10021 (1994)
Omstedt, A., Meuller, L., Nyberg, L.: Interannual, seasonal, and regional variations of precipitation and evaporation over the Baltic Sea. Ambio **26**, 484–492 (1997)
Omstedt, A., Gustafsson, B., Rodhe, B., Walin, G.: Use of Baltic Sea modelling to investigate the water and heat cycles in GCM and regional climate models. Clim. Res. **15**, 95–108 (2000)
Omstedt, A., Elken, J., Lehmann, A., Piechura, J.: Knowledge of the Baltic Sea physics gained during the BALTEX and related programmes. Prog. Oceanogr. **63**, 1–28 (2004). doi:10.1016/j.pocean.2004.09.001
Omstedt, A., Gustafsson, E., Wesslander, K.: Modelling the uptake and release of carbon dioxide in the Baltic Sea surface water. Cont. Shelf Res. **29**, 870–885 (2009). doi:10.1016/j.csr.2009.01.006
Omstedt, A., Edman, M., Anderson, L.G., Laudon, H.: Factors influencing the acid-base (pH) balance in the Baltic Sea: a sensitivity analysis. Tellus **62B**, 280–295 (2010). doi:10.3402/tellusb.v64i0,19586
Omstedt, A., Edman, M., Claremar, B., Frodin, P., Gustafsson, E., Humborg, C., Mörth, M., Rutgersson, A., Schurgers, G., Smith, B., Wällstedt, T., Yurova, A.: Future changes of the Baltic Sea acid-base (pH) and oxygen balances. Tellus B, 64, 19586 (2012). doi:10.3402/tellusb.v64i0,19586
Omstedt, A., Humborg, C., Pempkowiak, J., Pertillä, M., Rutgersson, A., Schneider, B., Smith, B.: Biogeochemical control of the coupled CO_2–O_2 System of the Baltic Sea: a review of the results of Baltic-C. Ambio **43**, 49–59 (2014). doi:10.1007/s13280-013-0485-4
Omstedt, A., Elken, J., Lehmann, A., Leppäranta, M., Meier, H.E.M., Myrberg, K., Rutgersson, A.: Progress in physical oceanography of the Baltic Sea during the 2003–2014 period. Prog. Oceanogr. (2014). doi:10.1016/j.pocean.2014.08.010
Overland, J.E., Pease, C.: Modeling ice dynamics in coastal seas. J. Geophys. Res. **93**, 15619–15637 (1988)
Pacanowski, R.C., Philander, S.G.: Parameterization of vertical mixing in numerical models of tropical oceans. J. Phys. Oceanogr. **11**, 1443–1451 (1981)
Piechura, J., Beszczynska-Möller, A.: Inflow waters in the deep regions of the southern Baltic Sea: transport and transformations. Oceanologia **461**, 113–141 (2004)
Pielke Jr, R.A.: The honest broker: Making sense of science in policy and politics. Cambridge University Press, Cambridge (2007)

Pielke Sr, R.A.: Heat storage within the earth system. Bull. Am. Meteorol. Soc. **84**, 331–335 (2003)

Rasmussen, B., Gustafsson, B.G., Aerteberg, G., Lundsgaard, C.: Oxygen concentration and consumption at the entrance to the Baltic Sea from 1975 to 2000. J. Mar. Syst. **42**, 13–30 (2003)

Rodhe, J.: Wind mixing in the turbulent surface layer in the presence of a horizontal density gradient. J. Phys. Oceanogr. **21**, 1080–1083 (1991)

Rodi, W.: Examples of calculation methods for flow and mixing in stratified flows. J. Geophys. Res. **92**, 5305–5328 (1987)

Rutgersson, A., Omstedt, A., Räisänen, J.: Net precipitation over the Baltic Sea during present and future climate conditions. Clim. Res. **22**, 27–39 (2002)

Rutgersson, A., Smedman, A.-S., Omstedt, A.: Measured and simulated latent and sensible heat fluxes at two marine sites in the Baltic Sea. Bound. Layer Meteorol. **99**, 53–84 (2001)

Sahlberg, J.: Modelling the thermal regime of a lake during the winter season. Cold Reg. Sci. Technol. **15**, 151–159 (1988)

Sahlberg, J.: The coastal zone model. SMHI Oceanography, no. 98/2009. SMHI, Norrköping, Sweden (2009)

Saloranta, M.T.: Snow and snow ice in sea ice thermodynamic modeling. Report Series in Geophysics, no. 39. Department of Geophysics, University of Helsinki, Finland (1998)

Sarmiento, J.L., Gruber, N.: Ocean Biogeochemical Dynamics. Princeton University Press, Princeton (2006)

Savchuk, O.P.: Large-scale dynamics of hypoxia in the Baltic sea. In: Yakushev E.V. (ed.) Chemical Structure of Pelagic Redox Interfaces: Observation and Modeling, vol. 22, pp. 137–160. Hdb Env. Chem. Springer, Berlin, Published online: 19 Feb 2010, (2013). doi:10.1007/698_2010_53

Savchuk, O.P., Wulff, F.: Modeling the Baltic Sea eutrophication in a decision support system. Ambio **36**, 141–148 (2007)

Schneider, B., Kaitala, S., Manula, P.: Identification and quantification of plankton bloom events in the Baltic Sea by continuous pCO_2 and chlorophyll *a* measurements on a cargo ship. J. Mar. Syst. **59**, 238–248 (2006)

Schneider, B., Nausch, G., Pohl, C.: Mineralization of organic matter and nitrogen transformations in the Gotland Sea deep water. Mar. Chem. **119**, 153–161 (2010)

Shaltout, M., Omstedt, A.: Calculating the water and heat balances of the Eastern Mediterranean Basin using ocean modelling and available meteorological, hydrological, and ocean data. Oceanologia **54**(2), 199–232 (2012). doi:10.5697/oc.54-2.199

Shaltout, M., Omstedt, A.: Modelling the water and heat balances of the Mediterranean Sea using a two-basin model and available meteorological, hydrological and ocean data. Submitted Oceanologia (2014)

Sokolov, A., Andrejev, O., Wulff, F., Medina, M.R.: The data assimilation for data analysis in the Baltic Sea. Systems Ecology Contributions, no. 3. Department of Systems Ecology, Stockholm University, Sweden (1997)

Speziale, C.G.: Modeling of turbulent transport equations. In: Gatski, T.B., Hussaini, M.Y., Lumley, J.L. (eds.) Simulation and Modeling of Turbulent Flows, Chapter 5. ICASE/LaRC Series in Computational Science and Engineering. Oxford University Press, New York (1996)

Stigebrandt, A.: A model for the exchange of salt and water between the Baltic and the Skagerrak. J. Phys. Oceanogr. **13**, 411–427 (1983)

Stigebrandt, A.: A model for the vertical circulation of the Baltic deep water. J. Phys. Oceanogr. **17**, 1772–1785 (1987)

Stigebrandt, A.: Computations of oxygen fluxes through the sea surface and the net production of organic matter with application to the Baltic and adjacent seas. Limnol. Oceanogr. **36**(3), 444–454 (1991)

Stigebrandt, A.: Physical oceanography of the Baltic Sea. In: Wulff, F., Rahm, L., Larsson, P. (eds.) System Analysis of the Baltic Sea, Chapter 2. Ecological Studies, vol. 148. Springer, Berlin (2001)

Stigebrandt, A.: A model for the vertical circulation of the Baltic Deep water. J. Phys. Oceanogr. **17**(10), 1772–1785 (1987)

Stigebrandt, A., Wulff, F.: A model for the dynamics of nutrients and oxygen in the Baltic proper. J. Mar. Res. **45**, 729–759 (1987)

Stigebrandt, A., Gustafsson, B.G.: Improvement of Baltic proper water quality using large-scale ecological engineering. Ambio **26**(2–3), 280–286 (2007). doi:10.1029/2006JG000304

Stigebrandt, A., Rahm, L., Viktorsson, L., Ödalen, M., Hall, P., Liljebladh, B.: A new phosphorous paradigm for the Baltic proper. Ambio. AMBIO **2014**(43), 634–643 (2014). doi:10.1007/s13280-013-0441-3

Stommel, H.M., Farmer, H.J.: Control of salinity in an estuary by transition. J. Mar. Res. **12**, 13–20 (1953)

Svensson, U.: A mathematical model of the seasonal thermocline. Report no. 1002. Department of Water Resources Engineering, University of Lund, Sweden (1978)

Svensson, U.: The structure of the Ekman layer. Tellus **31**, 340–350 (1979)

Svensson, U., Omstedt, A.: A mathematical model of the ocean boundary layer under drifting melting ice. J. Phys. Oceanogr. **202**, 161–171 (1990)

Svensson, U., Rahm, L.: Modeling the near-bottom region of the Benthic Boundary Layer. J. Geophys. Res. **93**(C6), 6909–6915 (1988)

Versteeg, H.K., Malalasekera, W.: An Introduction to Computational Fluid Dynamics: The Finite Method. Addison Wesley Longman, Harlow (1995)

von Storch, H., Zorita, E., Jones, J.M., Dimitriev, Y., González-Rouco, F., Tett, S.F.B.: Reconstructing past climate from noisy data. Science **306**(5696), 679–682 (2004)

Wanninkhof, R., Asher, W.E., HO, D.T., Sweeney, C., MCGillis, W.R.: Advances in quantifying air-sea gas exchange and environmental forcing. Annu. Rev. Mar. Sci. **1**, 213–244 (2009). doi:10.1146/annurev.marine.010908.163742

Weiss, R.T.: The solubility of nitrogen, oxygen and argon in water and sea water. Deep-Sea Res. **17**, 721–735 (1970)

Wesslander, K., Omstedt, A., Schneider, B.: On the carbon dioxide air-sea flux balance in the Baltic Sea. Cont. Shelf Res. **30**, 1511–1521 (2010). doi:10.1016/j.csr.2010.05.014

Winsor, P., Rodhe, J., Omstedt, A.: Baltic Sea ocean climate: an analysis of 100 yr of hydrographic data with focus on the freshwater budget. Clim. Res. **18**, 5–15 (2001)

Winsor, P., Rodhe, J., Omstedt, A.: Erratum: Baltic Sea ocean climate: an analysis of 100 yr of hydrographical data with focus on the freshwater budget. Clim. Res. **18**, 5–15 (2003)

Wotton, T.J., Pfister, C.A., Forester, J.D.: Dynamic patterns and ecological impacts of declining ocean pH in a high-resolution multi-year dataset. PNAS **105**(48), 18848–18853 (2008)

Wåhlström, I., Omstedt, A., Björk, G., Anderson, A.G.: Modelling the CO_2 dynamics in the Laptev Sea, Arctic Ocean: part II sensitivity of fluxes to changes in the forcing. J. Mar. Syst. **111-112**, 1–10 (2013)

Wåhlström, I., Omstedt, A., Björk, G., Anderson, A.G.: Modelling the CO_2 dynamics in the Laptev Sea, Arctic Ocean: part 1. J. Mar. Syst. **102–104**, 29–38 (2012)

Yaglom, A.M., Kader, B.A.: Heat and mass transfer between a rough wall and turbulent fluid flow at high Reynolds and Peclet numbers. J. Fluid. Mech. **62**, 601–623 (1974)

Zeebe, R.E., Wolf-Gladrow, D.: CO_2 in seawater: equilibrium, kinetics, isotopes. Elsevier Oceanography Series, no. 65. Elsevier Science Publishers, Amsterdam (2001)

Index

A. Omstedt, *Guide to Process Based Modeling of Lakes and Coastal Seas*,
Springer Praxis Books, DOI 10.1007/978-3-319-17990-2